AN ABSRACT OF THE THESIS OF

Suchithra Narayanan for the degree of Doctor of Philosophy in Civil Engineering presented on April 2, 1999. Title: Experimental Analysis of a Nonlinear Moored Structure.

Abstract approved: Redacted for privacy

Solomon C.S. Yim, Ph.D.

Complex nonlinear and chaotic responses have been observed and demonstrated in various compliant ocean systems characterized by a nonlinear mooring restoring force and a coupled fluid-structure interaction exciting force. Such floating structures and compliant systems have caused considerable concerns for the designer because the dynamics are inherently nonlinear in nature. An experimental mooring system with two configurations is chosen for this study. The first configuration, a single-degree-of-freedom (SDOF) (horizontal or surge motion only), consists of a sphere moored by linear elastic wires, with vertical displacement restricted by a horizontal rigid rod passing through its center. In the second configuration, corresponding to the multi-degree-of-freedom (MDOF) case (both horizontal and vertical (heave) motions), the restraining rod is removed, thus allowing motion in the vertical direction. Both configurations exhibit nonlinear behavior due to geometric (large mooring line angles) and complex hydrodynamic excitations.

Three alternative multiple-input/single-output models -- nonlinear-structure linearly-damped (NSLD) model, nonlinear-structure coupled hydrodynamically-damped (NSCHD) model, and nonlinear-structure nonlinearly-damped (NSND) model -- distinguished by the different inputs and outputs used are derived for the SDOF system

and a Reverse Multiple-Input/Single-Output (R-MI/SO) technique is adapted to determine the most suitable analytical model. The NSND model developed and validated for the SDOF configuration is extended to the MDOF system and it is found that the identified system parameters simulate a response that matches the experimental data.

A sensitivity analysis reveals that the effects of system parameters on the responses become more significant with an increase in wave excitation amplitude. For the SDOF system, the identified nonlinear structural damping coefficient varies among the tests whereas all the other system parameters remain relatively constant. With the rod restricting the vertical motion of the sphere, the horizontal motion amplitude for the SDOF system is smaller than that of the corresponding MDOF system without vertical constraint.

Applying the R-MI/SO technique with the inertia coefficient, C_m varying within a wide range shows that the identified natural frequency remains constant, but other system parameters increase with increasing C_m. Also, the subharmonic response decreases with increasing values of the inertia coefficient. Since inertia effects dominate the total forces, the response is found to be insensitive to the hydrodynamic drag coefficient, C_d.

Experimental Analysis of a Nonlinear Moored Structure

by

Suchithra Narayanan

A THESIS

submitted to

Oregon State University

in partial fulfillment of
the requirements for the
degree of

Doctor of Philosophy

Presented April 2, 1999
Commencement June 1999

Doctor of Philosophy thesis of Suchithra Narayanan presented on April 2, 1999

APPROVED:

Redacted for privacy

Major Professor, representing Civil Engineering

Redacted for privacy

Head of the Department of Civil, Construction and Environmental Engineering

Redacted for privacy

Dean of Graduate School

I understand that my thesis will become part of the permanent collection of Oregon State University libraries. My signature below authorizes release of my thesis to any reader upon request.

Redacted for privacy

Suchithra Narayanan, Author

ACKNOWLEDGEMENTS

I would like to express my most sincere appreciation to Dr. Solomon Yim for his guidance, suggestions, and encouragement with my research and during my stay lasting four years at Oregon State University. I would also like to thank Dr. Robert Hudspeth for his expertise and invaluable advice during my course of study. I would like to thank Dr. Sollitt for his suggestions and input into my research. Also, I wish to express my appreciation to my committee members, Drs. William McDougal, Satish Reddy and Clayton Paulson for their advice toward the completion of the thesis.

The financial support from the United State of Naval Research Grant No. N00014-92-J-1221 is gratefully acknowledged. I wish to express my sincere gratitude to Dr. Huan Lin for his input and ideas in my research. Thanks also to the office staff, Linda Rowe and Anita Vaughn.

The support from all the family members and friends is greatly acknowledged. I would like to express my gratefulness to Amutha and Pugal for their friendship and support. I would like to express my deep gratitude to my parents, sisters and my husband for their never-ending support, patience, motivation, and belief in my pursuit of the doctoral degree.

TABLE OF CONTENTS

TABLE OF CONTENTS (Continued)

LIST OF FIGURES

LIST OF FIGURES (Continued)

LIST OF FIGURES (Continued)

LIST OF FIGURES (Continued)

LIST OF TABLES

LIST OF APPENDICES

LIST OF APPENDIX FIGURES

LIST OF SYMBOLS

a	dominant wave amplitude
a_1, a_2, a_3	linear, quadratic and cubic stiffness coefficients
A_p, $\forall$	projected area and volume of the sphere respectively
b_1, b_3	linear and cubic stiffness coefficients
C_a, C_m, C_d	added mass, inertia and drag coefficients respectively
C_s, C_d'	linear and nonlinear damping coefficients, SDOF system in surge
$C_{s1,3}, C_{d1,3}'$	linear and nonlinear damping coefficients, MDOF system in surge and heave
D	diameter of the sphere
h	water depth
k	wave number
K	spring constant
$l_{1,2}$	spring lengths
l_c	initial spring length
$R(x(t))$	actual restoring force
$R'(x(t))$	approximate restoring force
Re, KC	Reynolds and Keulegan-Carpenter number respectively
s	distance of the instantaneous sphere center from the bottom
S_{xx}	spectral density of response
$S_{\eta\eta}$	spectral density of wave
T, T_o	periods of oscillation of water particle and structure respectively
$u(t)$, $\dot{u}(t)$	water particle velocity and acceleration respectively
$u_{1,3}(t)$, $\dot{u}_{1,3}(t)$	water particle velocity and acceleration in surge and heave
$V(x(t)$	potential function
$x(t), \dot{x}(t), \ddot{x}(t)$	sphere displacement, velocity and acceleration respectively
$x_{1,3}(t), \dot{x}_{1,3}(t), \ddot{x}_{1,3}(t)$	sphere displacement, velocity and acceleration in surge and heave
η	wave displacement
ζ	structural damping ratio, SDOF system in surge
$\zeta_{1,3}$	structural damping ratio, MDOF system in surge and heave
ξ	zero-mean delta correlated white noise
ρ	mass density
ω	angular velocity
υ	viscosity of the fluid

Dedicated to my parents

EXPERIMENTAL ANALYSIS OF A NONLINEAR MOORED STRUCTURE

1. INTRODUCTION

1.1 Background

The highly nonlinear responses of compliant ocean structures characterized by a large-geometry restoring force and a coupled fluid-structure interaction excitation (for example data collection buoys, ships, barges, semi-submersibles, and tension-leg platforms) are of great interest to ocean engineers and naval architects. An understanding of the nonlinear responses including coexisting periodic (primary, subharmonic and superharmonic resonance) and aperiodic (quasi-periodic and chaotic) phenomena is essential to ensure sound engineering design and safe operation of these structures. To analyze these nonlinear phenomena, deterministic analysis theories and numerical prediction techniques have been developed for single-point mooring systems (Thompson *et al* 1984, Gottlieb *et al* 1992), ships (Bishop and Virgin 1988), and multi-point mooring systems (Bernitsas and Chung 1990, Gottlieb and Yim 1992, 1993). Stochastic extensions of these analysis techniques have also been developed by Lin and Yim (1996a & b, 1997) to provide guidelines for interpreting field and experimental observations where randomness cannot be neglected.

To calibrate the prediction capability of these techniques, a number of experiments have been conducted (Thompson and Stewart 1987, Isaacson and Phadke 1994, Lin and Yim 1998, Lin *et al* 1998). In order to compare analytical predictions to experimental results, the system parameters employed in the analytical techniques need to be identified.

Because the system is nonlinear, conventional system identification techniques based on linear system theory (Bendat and Piersol 1993) are not applicable.

In 1988, Rice and Fitzpatrick proposed a spectral approach to the identification of single-degree-of-freedom (SDOF) systems under random excitations, incorporating the effects of stiffness and damping nonlinearities. Applicability of the method was illustrated using numerically simulated random inputs (Rice and Fitzpatrick 1988). The method performs the nonlinear operations in the time domain and the linear operations in the frequency domain. This approach was later validated by Esmonde *et al* (1990) by modeling and identifying the dynamic parameters associated with a highly nonlinear experimental system using measured data.

Over the past decade, Bendat has independently developed a Reverse Multiple-Input/Single-Output (R-MI/SO) technique to determine amplitude and frequency dependent properties of various nonlinear systems, including the Duffing and Van der Pol types, subjected to broad band excitation inputs (Bendat *et al* 1992). Numerically simulated random excitations were used to verify the technique.

For ocean engineering applications of Bendat's MI/SO methods, both Direct and Reverse methods have been applied to identify nonlinear system response properties of a naval frigate and a barge using measured field data (Bendat 1998). In demonstrating the applicability of the techniques, since the hydrodynamic force on the moving body excited by the waves was not directly measured, linear equivalent wave input was used as an approximation.

However, in general, the nonlinear wave forces on an offshore structure are evaluated using the Morison formulation, Froude-Krylov theory or diffraction theory depending on the

relative length scales of the waves and the structure. The Morison equation is applied when the wavelength is large with respect to the longitudinal dimension and the wave height is a small fraction of the wavelength (Sarpkaya and Isaacson 1981).

An experiment has been performed at the O. H. Hinsdale Wave Laboratory at Oregon State University (OSU) on a multi-point moored submerged sphere subject to wave excitations (Lin *et al* 1998). In this study, the wave input and the system responses measured during the test are employed for parameter identification. Three mathematical models -- nonlinear-structure linearly-damped (NSLD) model, nonlinear-structure coupled hydrodynamically-damped (NSCHD) model, and nonlinear-structure nonlinearly-damped (NSND) model -- are derived to depict the physics of the fluid-structure interaction of the SDOF, symmetric spherical mooring system submerged in ocean waves. A detailed study is conducted on the different reverse dynamic models to arrive at the most physically representative model for the ocean mooring system considered. Using the identified properties from each model, numerical predictions of the dynamic response from each model are compared with the experimental results in both time and frequency domains to select the most suitable model for the system. The R-MI/SO technique is also used to evaluate the effects of variations in hydrodynamic coefficients on the system parameters and the associated system responses.

Parameter identification of MDOF systems has been of great interest in the last several years. Modal superposition and spectral techniques based on the assumption of orthogonality of the normal modes of the system and the subsequent decoupling of the equations using modal vectors are widely used for the analysis and identification of general MDOF systems (Edwins 1984). However, as pointed out by Rice and Fitzpatrick (1991),

these techniques are limited to linear systems only and not applicable when the systems have significant modal coupling due to damping and/or nonlinearity.

The nonlinear identification technique based on the inversion approach of spectral analysis for SDOF systems discussed earlier (Rice and Fitzpatrick 1988) was extended to the identification of nonlinear parameters of MDOF systems (Rice and Fitzpatrick 1991). Bendat *et al* (1992) independently developed the Reverse Multiple-Input/Single-Output (R-MI/SO) technique and applied it to several MDOF systems incorporating nonlinear damping as well as nonlinear stiffness (see also Bendat and Piersol (1993)).

Additional experiments have been conducted at the O. H. Hinsdale Wave Laboratory at Oregon State University (OSU) on a multi-point moored submerged sphere with the MDOF configuration subject to wave excitations. In this study, the nonlinear-structure nonlinearly-damped (NSND) model developed and validated for the SDOF constrained experimental system is extended to the MDOF system.

The NSND model requires the knowledge of inertia and drag coefficients, C_m and C_d respectively for the evaluation of hydrodynamic force on the sphere. A vast library of experimental data on hydrodynamic coefficients for cylinders as a function of the Keulegan-Carpenter number (KC), the Reynolds number (Re) and the roughness parameters is available from laboratory and field tests. The real fluid effects, proximity of boundaries, fluid particle excursion lengths, surface roughness, vortex shedding, non-harmonic motions, etc. tend to modify the forces on the cylinder thus yielding non-constant values for the hydrodynamic coefficients. Theoretical studies of unsteady motions involving a sphere in a real fluid have so far been restricted to small Reynolds numbers (Wang 1965; Hjelmfelt *et al* 1967). The C_m for fixed spheres was found to vary between 1.43 and 1.73 within the range

of $0.2 \leq KC \leq 3.2$ (Harleman and Shapiro 1958). For a pilot study in the ocean on wave-induced forces on a fixed sphere with the inertia forces dominating the total force and Re ranging from 10^5 to 5×10^5, Grace and Zee (1977) found the average inertia coefficient to be 1.21 and the C_d to be 0.4. With the coefficients dependent on KC and Re, reasonable estimates of the hydrodynamic coefficients for a sphere are within the following bounds, $0.1 \leq C_d \leq 1.0$ and $1.0 \leq C_m \leq 1.5$ (Grace and Casino 1969; Grace and Zee 1978).

Using the measured wave excitation and response data together with the identified system parameters, a detailed study is conducted on the response behavior of both the MDOF and the SDOF systems. The study includes a sensitivity analysis on system parameters, and the effect of hydrodynamic coefficients on the response. Based on the individual response behavior and the R-MI/SO technique application, a comparative analysis between the two systems is performed.

1.2 Thesis Outline

An experiment was conducted at the O. H. Hinsdale Wave Laboratory at OSU on a multi-point moored submerged sphere (Yim *et al* 1993). A single-degree-of-freedom (SDOF) and a multi-degree-of-freedom (MDOF) configuration were tested and the measured input and output data are used for the parameter identification and analysis of the system. The thesis is organized in four parts.

Chapter 2 discusses three alternate multiple-input/single-output (MI/SO) models for the SDOF system and using the Reverse MI/SO (R-MI/SO) technique, the most suitable model is selected. The effects of hydrodynamic inertia and drag coefficients on the nonlinear response are evaluated with the aid of R-MI/SO technique.

Chapter 3 extends the nonlinear-structure nonlinearly-damped (NSND) model developed and validated for the SDOF system to MDOF system. The MDOF tests that yield subharmonic responses are used for the application of R-MI/SO technique. Using the identified parameters, a sensitivity analysis is performed to determine the effects of system parameters on the identified response. The effects of Keulegan-Carpenter number (KC) and Reynolds number (Re) on the hydrodynamic coefficients are evaluated. A similar analysis is conducted on the SDOF system using the identified system parameters. The subharmonic surge response of both systems is compared in the latter part of the chapter.

Additional tests on the MDOF system that yield superharmonic surge and heave responses are analyzed in Chapter 4. The procedures developed in Chapter 3 for the MDOF system are applied and the results are compared with the MDOF tests yielding subharmonic response.

Chapter 5 summarizes the observations from the parameter identification and analysis of SDOF and MDOF systems.

2. SDOF MODELING AND SYSTEM IDENTIFICATION

2.1 SDOF System Considered

The experimental model consists of a submerged moored neutrally buoyant sphere excited by regular and random waves. Springs are attached to the sphere to provide the restoring force with one series at an angle of 60° (four-point system) and another at 90° (two-point system). Although the mooring lines are linearly elastic, depending on the mooring angles, the restoring force may be nonlinear with stiffness nonlinearity varying from a strongly nonlinear two-point system to an almost linear four-point system (Gottlieb and Yim 1992). To examine the nonlinear effects, the tests with the strongest nonlinear geometric configuration subjected to periodic wave excitation with band-limited white noise are considered in this study (Yim *et al* 1993).

Two configurations of the system are tested. The first is that of a single-degree-of-freedom (SDOF) system with the sphere restricted to move only in the surge direction by passing a rigid steel rod through the center of the sphere. The second is a multi-degree-of-freedom (MDOF) system with both surge and heave (rod removed). The focus of this chapter is on the modeling and parameter identification of the SDOF system. Plan and profile views of this setup are given in Fig.2.1.

2.2 Governing Equations of Motion

The equations of motion for the SDOF moored structural system subject to periodic waves perturbed with white noise excitation are derived in this section.

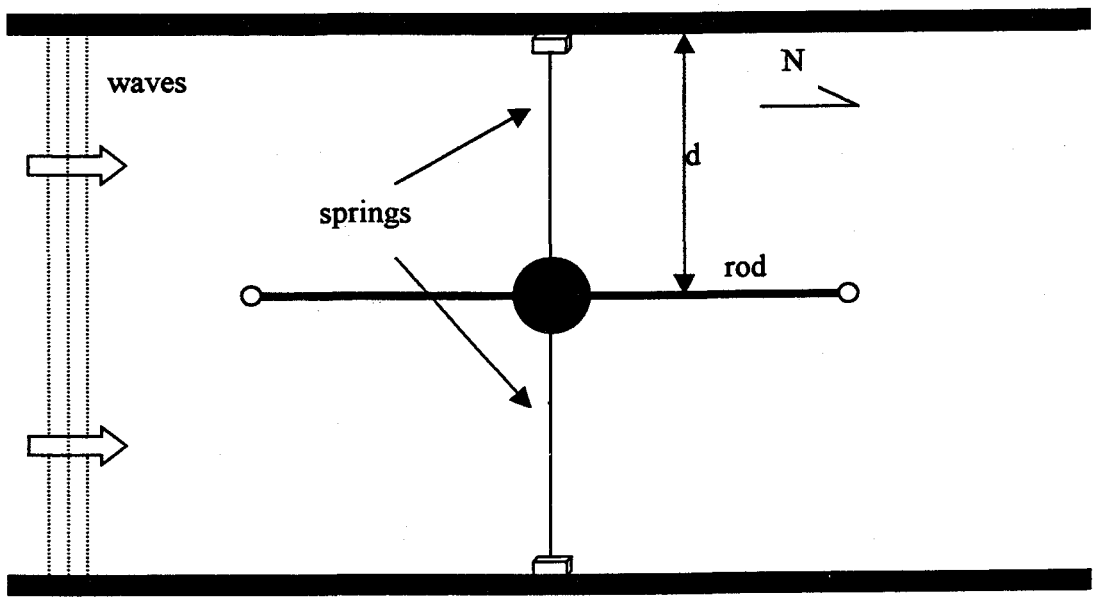

(a)

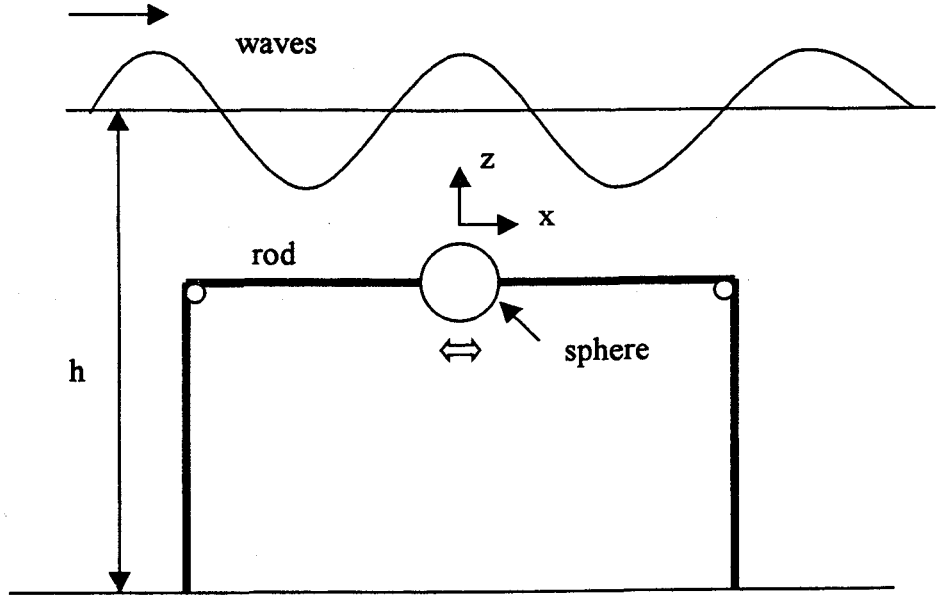

(b)

Fig.2.1 SDOF experimental set up: a) plan, b) profile view

The excitation force takes into account both nonlinear drag and inertia effects on a submerged symmetric small body using the Morison equation (Sarpkaya and Isaacson 1981). Through an appropriate transformation, the randomness in the wave field is incorporated into the hydrodynamic forcing terms. By considering surge as the generalized displacement coordinate, the governing equation of motion for the SDOF mooring system can be written as

$$m\ddot{x}(t) + C_s\dot{x}(t) + R(x(t)) = f(t) \tag{2.1}$$

where m = mass of the sphere, f(t) = hydrodynamic force acting on the sphere, C_s = linear structural damping coefficient, R(x(t)) = nonlinear restoring force, $x(t), \dot{x}(t), \ddot{x}(t)$ are the system response, velocity and acceleration respectively. In the SDOF model, due to the presence of a rod passing through the center (used to prevent vertical (heave) and side (sway) motions, Fig.2.1), the structural damping mechanism also include a time dependent Coulomb friction component originating from the (time varying) lift force and combined drag/lift moment. As a first approximation, it is assumed here that the structural damping can be lumped to an equivalent linear structural-damping coefficient C_s. The nonlinear restoring force and excitation force are described in the following subsections.

2.2.1 Restoring Force

The restoring force includes an elastic force due to the mooring lines and a vertical force due to hydrostatic buoyancy. Since the sphere used for the experiment was neutrally buoyant, the forcing caused by hydrostatic buoyancy is neglected (Yim *et al* 1993). The resulting inline force R(x(t)) may be derived from a potential function V(x(t)) which describes the pretensioned geometrical configuration of a symmetric small body (Gottlieb and Yim 1992).

$$V(x(t)) = K\left([l_1(x(t)) - l_c]^2 + [l_2(x(t) - l_c]^2\right) \tag{2.2a}$$

where K = spring constant, l_c = initial spring length, and l_1 and l_2 = spring lengths. With the mooring angles attached at 90°, the spring lengths l_1 and l_2 can be expressed as

$$l_{1,2} = l = \sqrt{d^2 + x(t)^2} \tag{2.2b}$$

where d = distance of the center of the sphere from the wall (Fig.2.1). Knowing that $R(x(t)) = \frac{d}{dx}(V(x(t))$, the restoring force R(x(t)) in the surge direction is derived as given below:

$$R(x(t)) = 4Kx(t)\left(1 - \frac{l_c}{l}\right) \tag{2.3a}$$

The restoring force can be approximated by a high order polynomial obtained through a least square approximation. Polynomials of various orders have been employed and an optimum fit within the experimental range is identified. The selected polynomial is expressed as

$$R'(x(t)) \cong a_1x(t) + a_2x(t)^2 + a_3x(t)^3 \tag{2.3b}$$

For the experimental model, a comparison of the approximate restoring force (R'(x(t)) in Eq.2.3a) with the geometric model restoring force (R(x(t)) in Eq.2.3b) is given in Fig.2.2a. It can be observed that R'(x(t)) matches very well with R(x(t)). A normalized (relative) error measure, $\frac{|R(x(t)) - R'(x(t))|}{|R(x(t))|}$, between the geometric model and approximate restoring force functions is given in Fig.2.2b. The error is found to be negligible (between 0.1 and 1%).

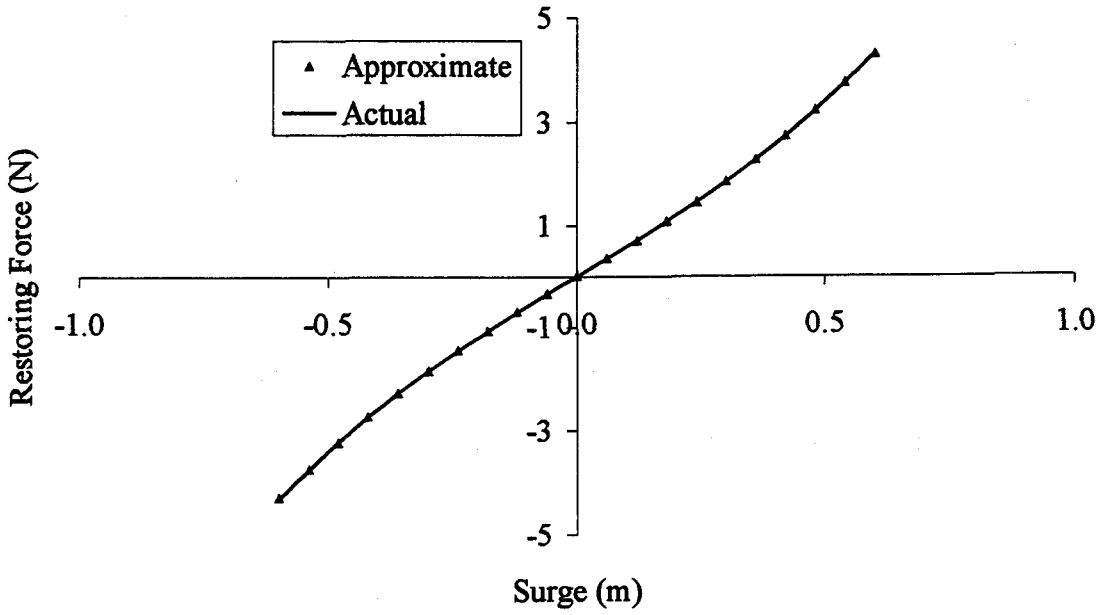

(a)

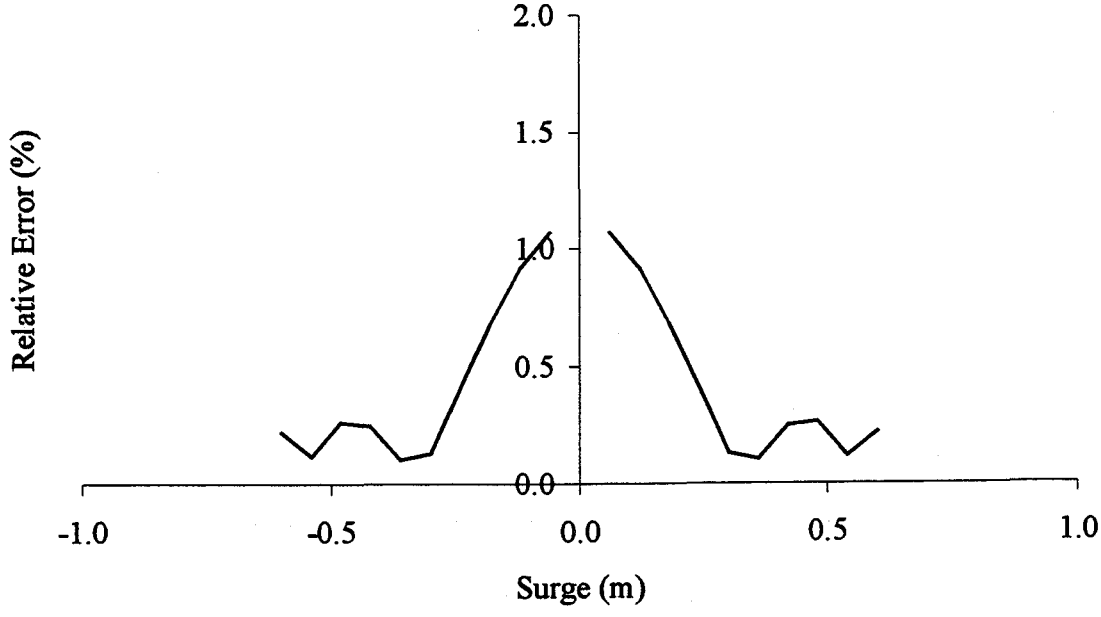

(b)

Fig.2.2 Comparison between the actual and approximate restoring force functions: a) force, b) relative error

2.2.2 Excitation Force

Using linear wave theory as described in Chakrabarti (1987), the horizontal water particle velocity is given by

$$u(t) = \omega a \frac{\cosh ks}{\sinh(kh)} \cos(kx(t) - \omega t) \tag{2.4a}$$

where u = water particle velocity in surge direction, a = dominant wave amplitude, ω = angular velocity, k = wave number, h = water depth and s = distance of the instantaneous center of the sphere from the bottom.

The excitation waves can be considered as a randomly perturbed regular wave field. With wave displacement, $\eta(t)$, measured, Eq.(2.4a) can be approximated by

$$u(t) = \omega \frac{\cosh ks}{\sinh(kh)} \eta(t) \tag{2.4b}$$

It is assumed that the random perturbations in the excitation are included in $\eta(t)$, given by

$$\eta(t) = a\cos(kx(t) - \omega t + \phi) + \xi(t) \tag{2.4c}$$

where $\xi(t)$ is a zero-mean delta-correlated white noise.

The horizontal water particle acceleration can also be approximated as

$$\dot{u}(t) = \omega \frac{\cosh ks}{\sinh(kh)} \dot{\eta}(t) \tag{2.5}$$

where $\dot{u}(t)$ is the water particle acceleration in surge direction.The system diagram for the calculation of water particle velocity and acceleration from the experimental wave input is given in Fig.2.3a.

When a rigid body is free to move in waves, an independent flow-fields (IFF) model is used as an alternating form for Morison equation (Chakrabarti 1987). A linear

superposition of two independent flow fields separating the wave motion and the structure motion is used and given by

$$f(t) = \rho \forall C_m \dot{u}(t) - \rho \forall C_a \ddot{x}(t) + \frac{\rho}{2} A_p C_d u(t)|u(t)| - \frac{\rho}{2} A_p C_d' \dot{x}(t)|\dot{x}(t)| \tag{2.6}$$

where

$$\forall = \frac{\pi}{6} D^3 \tag{2.7a}$$

$$A_p = \frac{\pi D^2}{4} \tag{2.7b}$$

ρ = mass density, D = diameter of sphere, C_a = added mass coefficient, C_d' = nonlinear structural damping coefficient, C_m = hydrodynamic inertia coefficient and C_d = hydrodynamic drag coefficient. The values of C_m and C_d may be obtained from wave experiments while the coefficients C_a and C_d' are derived from oscillating sphere in otherwise calm water. Also

$$C_m, C_d = f\left(Re_F = \frac{u_o D}{\upsilon}, KC_F = \frac{u_o T}{D} \right) \tag{2.8a}$$

$$C_a, C_d' = f\left(Re_N = \frac{\dot{x}_o D}{\upsilon}, KC_N = \frac{\dot{x}_o T_o}{D} \right) \tag{2.8b}$$

where u_o, $\dot{x}_o$ = amplitudes of the water particle and structure velocity, respectively, T and T_o = periods of oscillation of water particle and structure, respectively (they are often equal), υ = viscosity of the fluid, Re = Reynolds number, KC = Keulegan-Carpenter number. Note that suffix 'F' refers to far field and suffix 'N' to near field as defined in Chakrabarti (1987).

The schematic diagram of the SDOF system using the IFF model as a form of Morison force is given in Fig.2.3b, which delineates Eqs.(2.1 and 2.6).

A relative velocity (RV) model can also be used as an alternative form for Morison equation to express the forces on the sphere which are given by

$$f(t) = \rho \forall C_m \dot{u}(t) - m_a \ddot{x}(t) + \frac{\rho}{2} A_p C_d (u(t) - \dot{x}(t)) |u(t) - \dot{x}(t)| \tag{2.9}$$

In this case C_m and C_d are given by

$$C_m, C_d = f\left(Re_F = \frac{v_{ro} D}{\upsilon}, KC_F = \frac{v_{ro} T_r}{D} \right) \tag{2.10}$$

where v_{ro} = amplitude of v_r, the relative velocity and T_r = combined period of v_r. The schematic diagram of the SDOF system with the RV model representing Eqs.(2.1 and 2.9) is given in Fig.2.3c.

Laya *et al* (1984) discussed the region of applicability of the RV and IFF models in terms of reduced velocity, V_R, defined by

$$V_R = \frac{u_o T_o}{D} \tag{2.11}$$

It is observed that for low KC and high V_R, as in the case of the experimental system considered, the IFF model is more applicable. Due to the lack of a comprehensive experimental study on the determination of the appropriate forms of the Morison equation (which itself is empirical) for different combinations of parameters and experimental settings, it has been difficult to assess the appropriateness of the various forms of the Morison hydrodynamic force expression. However, the R-MI/SO technique can be used as a tool to find the appropriate form of the equation best suitable for the experimental system under consideration.

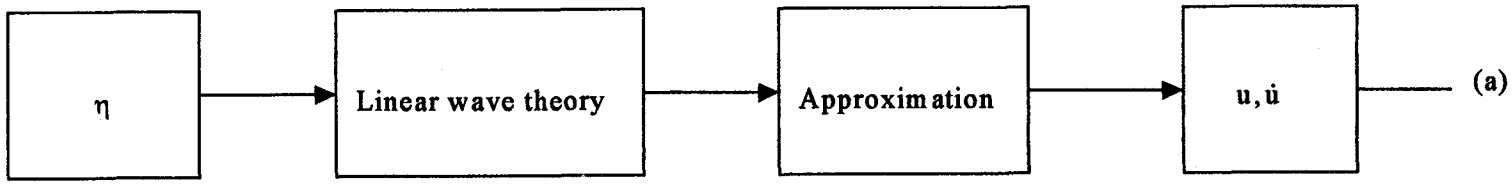

(a)

Fig.2.3 Schematic diagram of the SDOF system: a) system diagram for the calculation of wave velocity and acceleration, b) RV model, c) IFF model

Fig.2.3a ------- (A)

$$f_{ih}(t) = C_m \rho \forall \dot{u}$$

$$f_d(t) = \frac{1}{2}\rho C_d A_p (u-\dot{x})|u-\dot{x}|$$

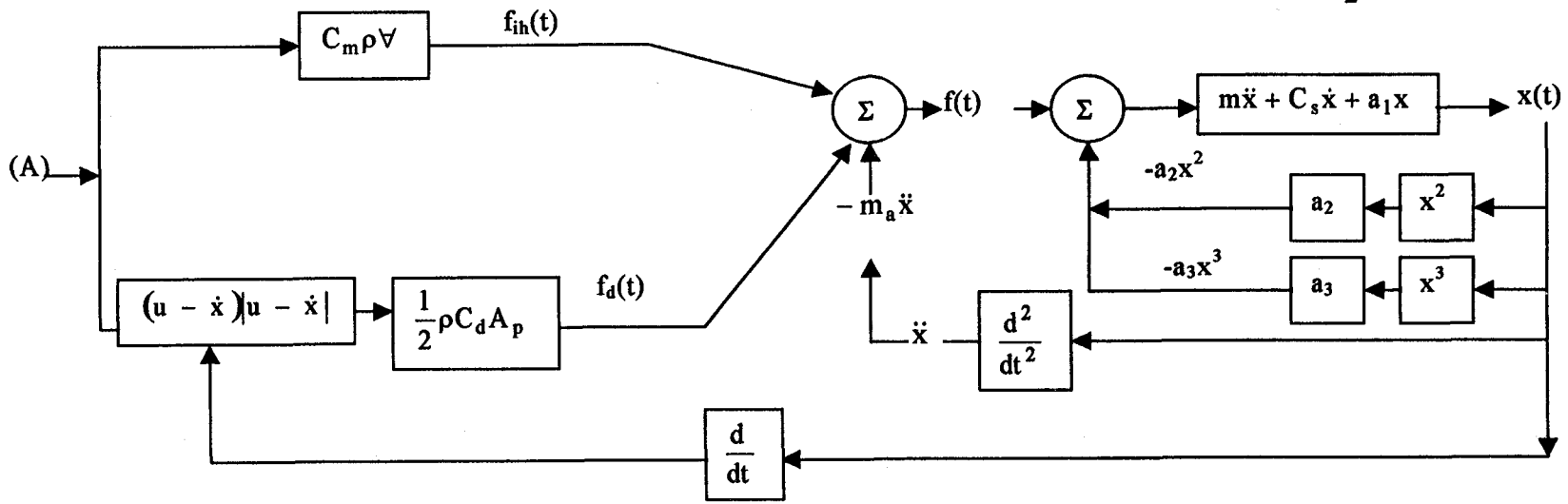

(b)

Fig.2.3 Continued

Fig.2.3a ------ (A)

$$f_d'(t) = \frac{1}{2}\rho C_d' A_p \dot{x}|\dot{x}|$$

$$f_{ih}(t) = C_m \rho \forall \dot{u}$$

$$f_d(t) = \frac{1}{2}\rho C_d A_p u|u|$$

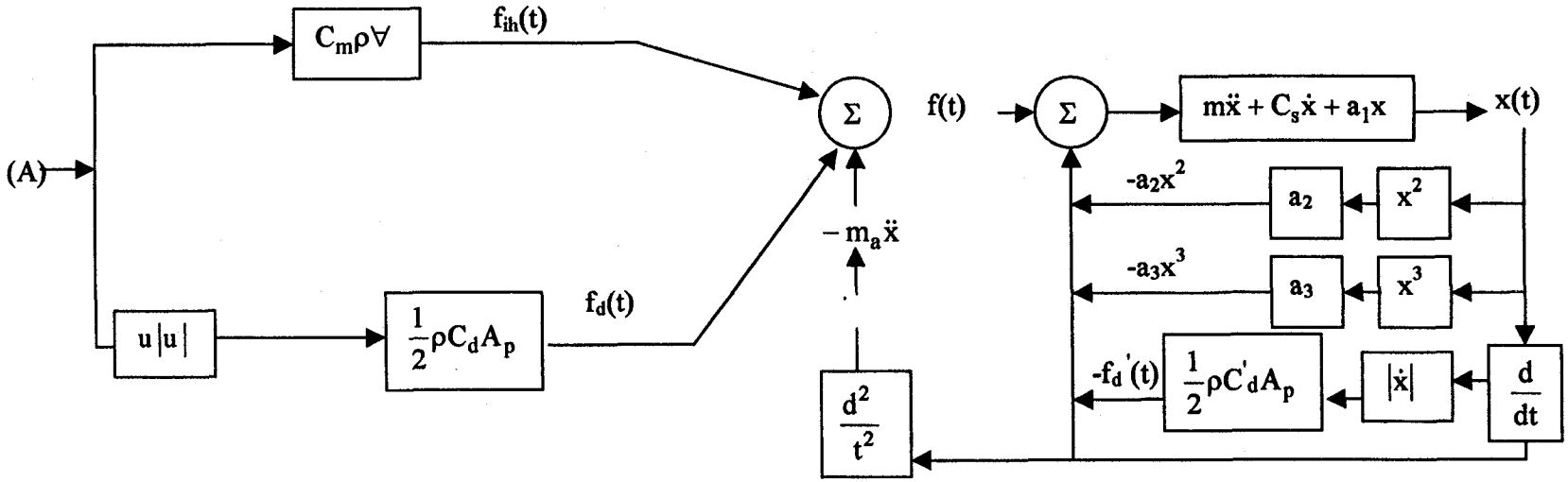

(c)

Fig.2.3 Continued

2.3 R-MI/SO Technique Modeling

The R-MI/SO technique can be applied to most nonlinear systems subjected to random excitation irrespective of the nature of the distribution, e.g., Gaussian or non-Gaussian (Bendat *et al* 1992). The relative contribution of linear and nonlinear system properties, whether or not the system properties are frequency dependent, and how the cumulative coherence functions are improved by adding nonlinear terms, can be determined using this technique. For the application of the R-MI/SO technique, three models that are distinguished by the different inputs and outputs used, are derived and discussed below.

2.3.1 Nonlinear-Structure Linearly-Damped Model

Rewriting the Eqs.(2.1,2.3 and 2.9) for the RV model, the nonlinear equation for the nonlinear-structure linearly-damped (NSLD) model is

$$(m+m_a)\ddot{x}(t)+C_s\dot{x}(t)+a_1x(t)+a_2x^2(t)+a_3x^3(t)=f_a(t) \tag{2.12a}$$

where

$$f_a(t)=\frac{1}{2}\rho C_d\frac{\pi D^2}{4}(u(t)-\dot{x}(t))|u(t)-\dot{x}(t)|+\rho\frac{\pi}{6}D^3C_m\dot{u}(t) \tag{2.12b}$$

The nonlinear relative motion coupled damping is treated implicitly in the excitation force. Values of the inertia and drag coefficients are assumed in order to evaluate the force f_a given by Eq.(2.12b), which is treated as the model input and the system response as the model output. Fourier transforming both sides of Eq.(2.12a) gives the frequency domain relation

$$\left(a_1+j(2\pi f)C_s-(2\pi f)^2(m+m_a)\right)X(f)+A_2(f)X_2(f)+A_3(f)X_3(f)=F_a(f) \tag{2.13}$$

where

$$F_a(f) = \Im[f_a(t)] \tag{2.14a}$$

$$X_2(f) = \Im[x^2(t)] \tag{2.14b}$$

$$X_3(f) = \Im[x^3(t)] \tag{2.14c}$$

$$A_2(f) = a_2 \tag{2.14d}$$

$$A_3(f) = a_3 \tag{2.14e}$$

In the absence of nonlinear terms $x^2(t)$ and $x^3(t)$, H(f) represents the frequency response function of an ideal constant parameter linear system that relates the displacement output x(t) to the force input $f_a(t)$ given by

$$H(f) = \frac{X(f)}{F_a(f)} = \left[a_1 + j(2\pi f)C_s - (2\pi f)^2(m + m_a)\right]^{-1} \tag{2.15}$$
$$= a_1[1 - (f/f_n)^2 + 2\zeta_s(f/f_n)]^{-1}$$

where the natural frequency f_n and damping ratio ζ_s are defined, respectively, by

$$f_n = \frac{1}{2\pi}\sqrt{\frac{a_1}{(m + m_a)}} \tag{2.16a}$$

$$\varsigma_s = \frac{C_s}{2\sqrt{a_1(m + m_a)}} \tag{2.16b}$$

When the nonlinear term is present, H(f) relates the displacement output x(t) to an effective force $f_e(t)$ given by

$$f_e(t) = f_a(t) - a_2x^2(t) - a_3x^3(t) \tag{2.17}$$

The single-input/single-output nonlinear forward model with feedback Eq.(2.13) is delineated in Fig.2.4a. Identification of this system requires a time-consuming iterative approach because of the presence of the feed back terms, a_2x^2 and a_3x^3. Because the forward way of analysis is difficult, an alternative reverse dynamic viewpoint is considered (Bendat

et al 1992). To apply the R-MI/SO technique, the input/output roles are mathematically interchanged. This reverse dynamic system can be viewed as a three-input/single-output nonlinear model without a feedback term as shown in Fig.2.4b.

The associated Fourier transform relation is given by

$$F_a(f) = A_1(f)X_1(f) + A_2(f)X_2(f) + A_3(f)X_3(f) \tag{2.18a}$$

where

$$X_1(f) = \Im[x_1(t)] \tag{2.19a}$$

$A_1(f)$, is defined as the linear impedance function which is given by

$$A_1(f) = [H(f)]^{-1} = a_1\left(1 - (f/f_n)^2 + 2j\zeta_s(f/f_n)\right) \tag{2.19b}$$

The system gain and phase factors of Eq.(2.19b) are given by

$$|A_1(f)| = a_1\left[\sqrt{\left(1-(f/f_n)^2\right)^2 + (2\zeta_s(f/f_n))^2}\right] \tag{2.20a}$$

$$\phi(f) = \tan^{-1}\left[\frac{2\zeta_s f/f_n}{1-(f/f_n)^2}\right] \tag{2.20b}$$

The minimum gain factor occurs at the resonance frequency, f_r, of the system. By maximizing Eq.(2.19b), it can be shown that for structures having damping ratio $\zeta_s \le 0.5$, (Clough and Penzien 1993), resonance frequency is given by

$$f_r = f_n\sqrt{1-2\zeta_s^2} \tag{2.20c}$$

Hence the minimum value of gain factor that occurs at resonance is given by

$$|A_1(f_r)| = a_1\left[2\zeta_s\sqrt{1-\zeta_s^2}\right] \tag{2.20d}$$

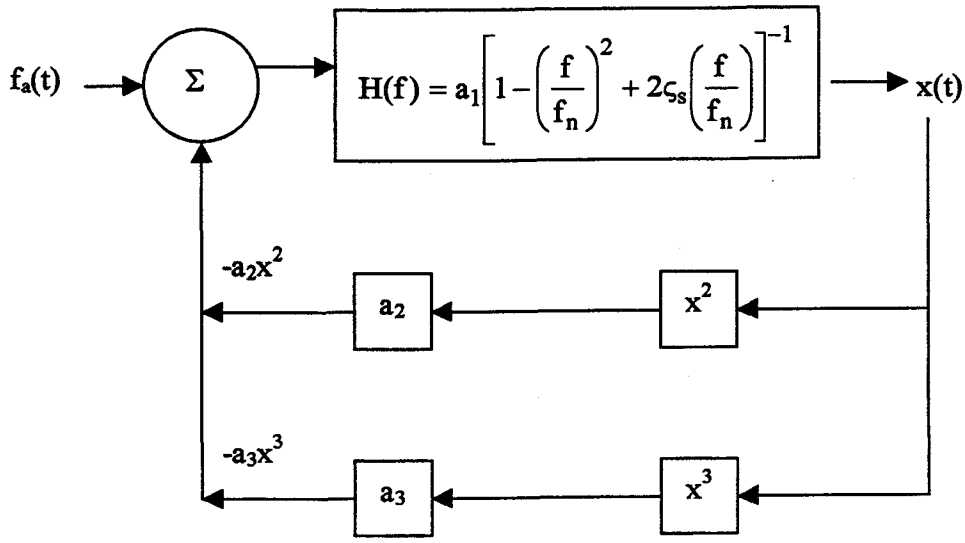

(a)

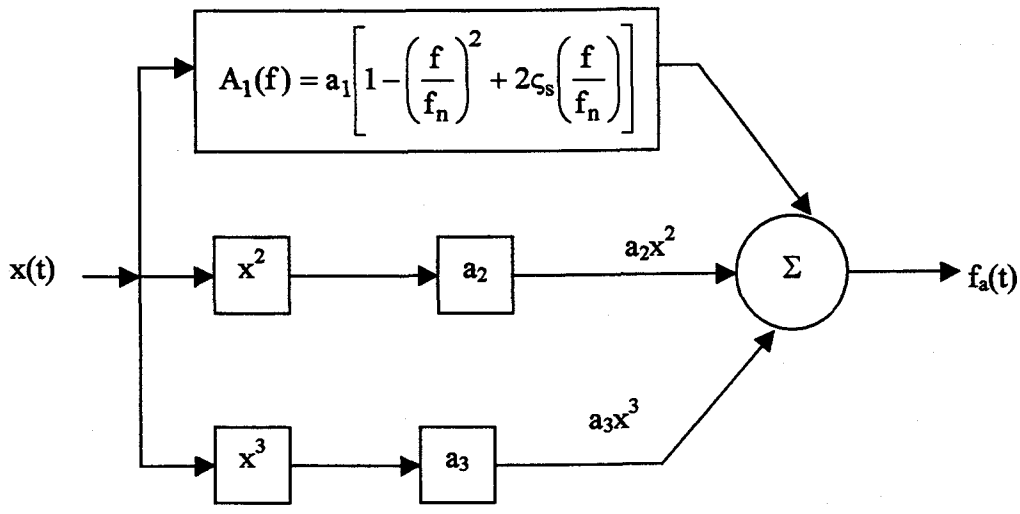

(b)

Fig.2.4 The nonlinear-structure linearly-damped (NSLD) model: a) with feedback, b) without feedback

For lightly damped systems, the resonance frequency, f_r and the minimum value of the gain factor can be approximated (Bendat *et al* 1992) by

$$f_r \approx f_n \qquad |A_1(f_r)| \approx 2a_1\zeta_s \tag{2.20d}$$

The physical parameters of the mooring system can therefore be estimated as follows

$$a_1 \approx A_1(0) \tag{2.21a}$$

$$C_a = \frac{m_a}{(\pi/6\rho D^3)} \tag{2.21b}$$

$$C_s = 2\zeta_s\sqrt{(a_1(m+m_a))} \approx \frac{|A_1(f_n)|}{2\pi f_n} \tag{2.21c}$$

$X_2(f)$, $X_3(f)$, $A_2(f)$ and $A_3(f)$ are given by Eq.(2.14). Reverse dynamic inputs $x(t)$, $x^2(t)$ and $x^3(t)$ are usually correlated. Procedures to replace the correlated inputs with a new set of uncorrelated inputs are applied to convert the nonlinear model to an equivalent three-input/single-output linear model (Bendat *et al* 1992). The resulting impedance functions $A_1(f)$, $A_2(f)$ and $A_3(f)$ yield all the system properties.

2.3.2 Nonlinear-Structure Coupled Hydrodynamic-Damped Model

In the nonlinear-structure coupled hydrodynamic-damped (NSCHD) model, the nonlinear relative motion coupled damping is treated explicitly and the R-MI/SO technique is applied to identify the damping coefficient C_d along with other linear and nonlinear coefficients. The nonlinear equation representing NSCHD model is given by

$$(m+m_a)\ddot{x}(t)+C_s\dot{x}(t)+a_1x(t)+a_1x^2(t)+a_3x^3(t)-C_m(u(t)-\dot{x}(t))|u(t)-\dot{x}(t)| = f_b(t) \tag{2.22a}$$

where

$$f_b(t) = \rho\frac{\pi}{6}D^3 C_m \dot{u}(t) \tag{2.22b}$$

The corresponding single-input/single-output nonlinear forward NSCHD model with feedback is shown in Fig.2.5a.

The nonlinear forward model is converted to a reverse dynamic model by applying the R-MI/SO procedures. The corresponding reverse dynamic NSCHD model without feedback is given in Fig.2.5b. The associated Fourier transform relation can be written as

$$A_1(f)X_1(f) + A_2(f)X_2(f) + A_3(f)X_3(f) + A_4(f)X_4(f) = F_b(f) \tag{2.23a}$$

where

$$X_4(f) = \Im\left[(u(t) - \dot{x}(t))|u(t) - \dot{x}(t)|\right] \tag{2.23b}$$

$$A_4(f) = \frac{1}{2}\rho C_d \frac{\pi D^2}{4} \tag{2.23c}$$

$$F_2(f) = \Im[f_2(t)] \tag{2.23d}$$

The frequency response functions $A_1(f)$ (described by Eqs.2.19-21), $A_2(f)$ (Eq.2.14d) and $A_3(f)$ (Eq.2.14c), identify all the system properties and $A_4(f)$ (Eq.2.23c) gives the hydrodynamic coefficient, C_d.

2.3.3 Nonlinear-Structure Nonlinearly-Damped Model

The nonlinear equation of motion for the nonlinear-structure nonlinearly-damped (NSND) model is given by

$$(m + m_a)\ddot{x}(t) + C_s\dot{x}(t) + a_1 x(t) + a_2 x^2(t) + a_3 x^3(t) + \rho C_d' \frac{\pi D^2}{4}\dot{x}(t)|\dot{x}(t)| = f_4(t) \tag{2.24a}$$

$$\text{where, } f_4(t) = \rho\frac{\pi}{6}D^3 C_m \dot{u}(t) + \rho C_d \frac{\pi D^2}{4}u(t)|u(t)| \tag{2.24b}$$

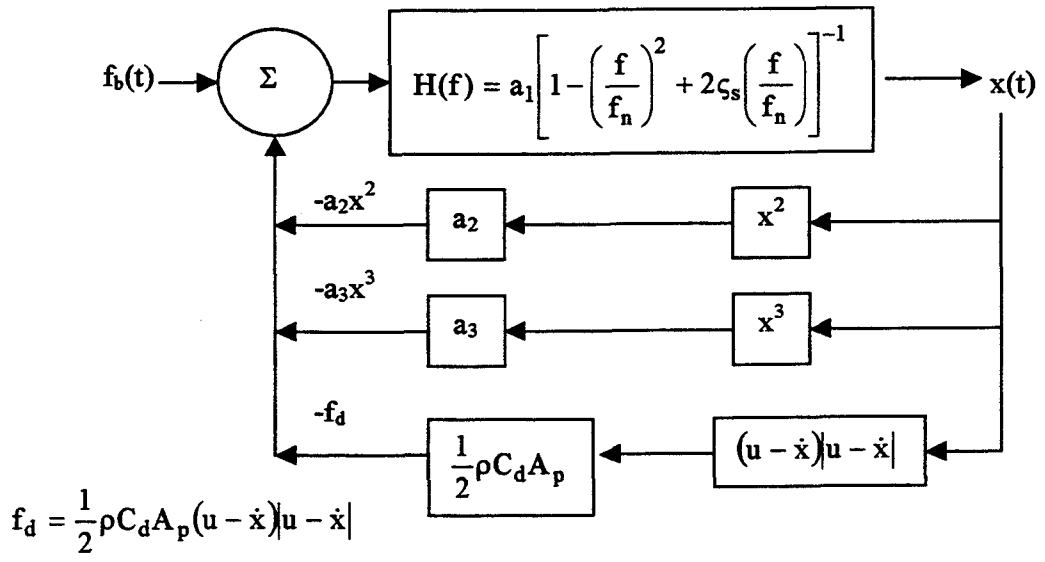

(a)

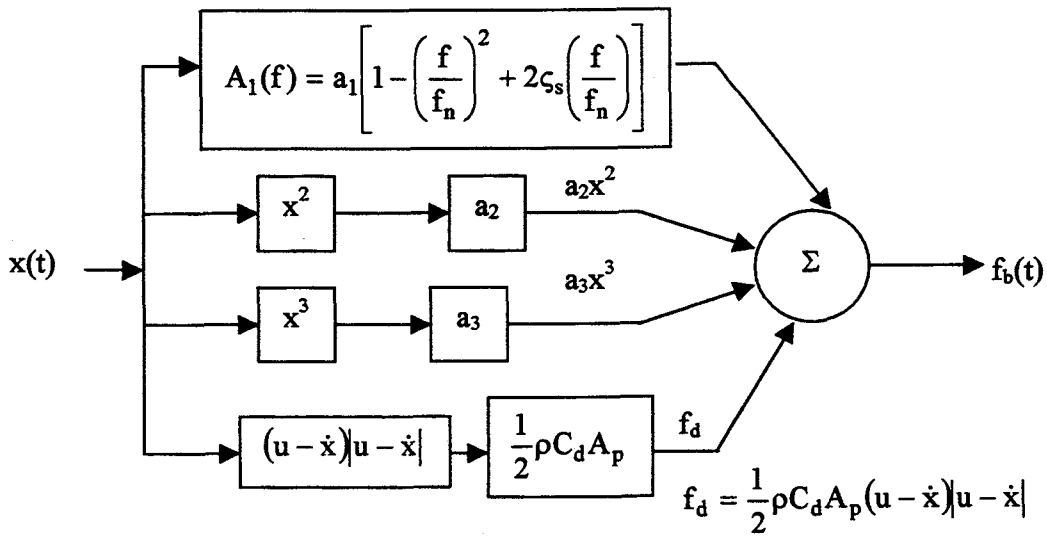

(b)

Fig.2.5 The nonlinear-structure coupled hydrodynamically-damped (NSCHD) model: a) with feedback, b) without feedback

The corresponding single-input/single-output nonlinear forward model with feedback is shown in Fig.2.6a. The nonlinear forward model is converted to reverse dynamic model by applying the R-MI/SO procedures. The corresponding reverse dynamic four-input/single-output nonlinear model without feedback is given in Fig.2.6b. The associated Fourier transform relation can be written as

$$A_1(f)X_1(f) + A_2(f)X_2(f) + A_3(f)X_3(f) + A_4'(f)X_4'(f) = F_4(f) \tag{2.25a}$$

where

$$X_4'(f) = \Im[\dot{x}(t)|\dot{x}(t)|] \tag{2.25b}$$

$$A_4'(f) = \frac{1}{2}\rho C_d' \frac{\pi D^2}{4} \tag{2.25c}$$

$$F_4(f) = \Im[f_4(t)] \tag{2.25d}$$

Using the frequency response functions $A_1(f)$ (Eqs.2.19-21), $A_2(f)$ (Eq.2.14d), $A_3(f)$ (Eq.2.14e) and $A_4'(f)$ (Eq.2.25c), the system properties are identified.

2.4 Comparisons of Alternative System Models

The reverse nonlinear system identification methods discussed in the above sections have been applied to the SDOF ocean mooring system. Eight tests were conducted on the sphere with periodic plus white noise excitations (Yim *et al* 1993). The wave velocity and acceleration are numerically evaluated using a central-difference method (Gerald and Wheatley 1989). The sampling interval used in the experiment was 0.0625 second (16 Hz), which yields a Nyquist frequency of 8 Hz. The total number of samples of the excitation and response time histories for spectral simulations is 8192 (512 seconds), with sub-record lengths of 1024 for the Fourier transforms (64 seconds).

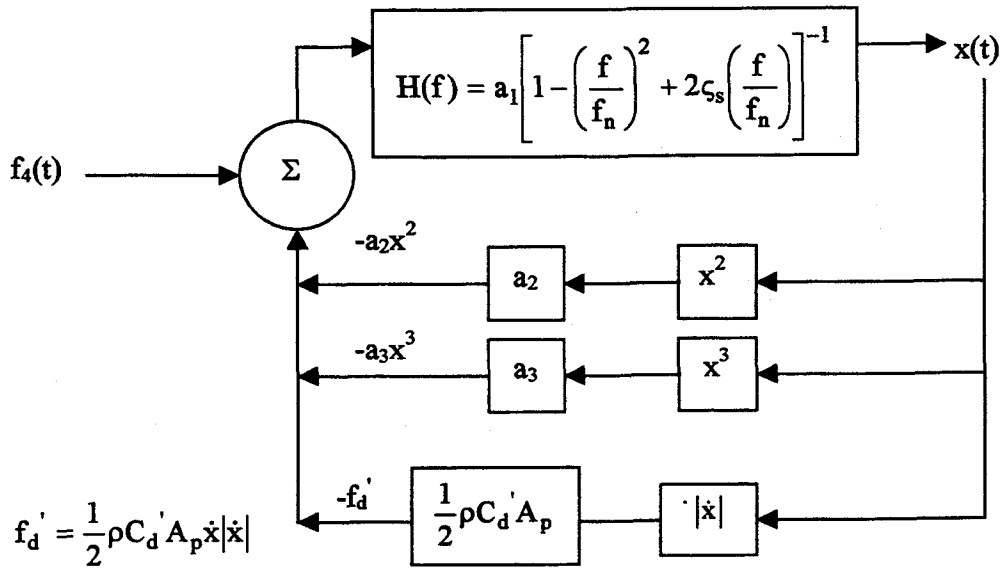

(a)

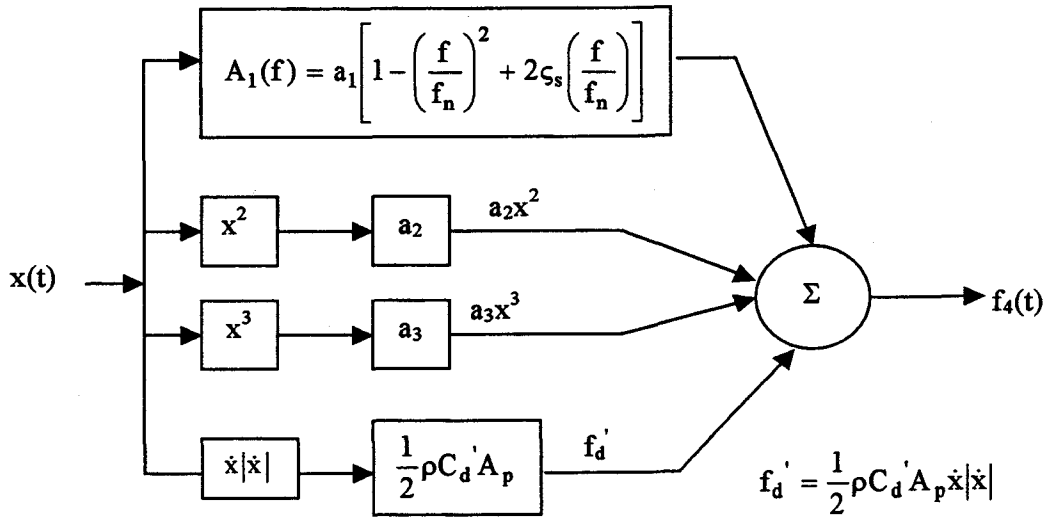

(b)

Fig.2.6 The nonlinear-structure nonlinearly-damped (NSND) model a) with feedback b) without feedback

A typical segment of the time series and the spectra (of the entire record) for an experimental data set of wave and response are given in Fig.2.7. The wave and response spectral densities, $S_{\eta\eta}$ and S_{xx} respectively, are plotted against frequency, f, in Fig.2.7 b and d. It can be observed from Fig.2.7d that the dominant response of the sphere is subharmonic.

Different formulations of the system model are applied for all the data sets and compared. A summary of the three mathematical models, NSLD, NSCHD and NSND models, are given below:

- NSLD MODEL

$$(m+m_a)\ddot{x}(t)+C_s\dot{x}(t)+a_1x(t)+a_2x^2(t)+a_3x^3(t)=f_a(t)$$

$$\text{where, } f_a(t)=\frac{1}{2}\rho C_d\frac{\pi D^2}{4}(u(t)-\dot{x}(t))|u(t)-\dot{x}(t)|+\rho\frac{\pi}{6}D^3C_m\dot{u}(t)$$

- NSCHD MODEL

$$(m+m_a)\ddot{x}(t)+C_s\dot{x}(t)+a_1x(t)+a_1x^2(t)+a_3x^3(t)-C_m(u(t)-\dot{x}(t))|u(t)-\dot{x}(t)|=f_b(t)$$

$$\text{Where, } f_b(t)=\rho\frac{\pi}{6}D^3C_m\dot{u}(t);\ C_{m=}\frac{1}{2}\rho C_d\frac{\pi D^2}{4}$$

- NSND MODEL

$$(m+m_a)\ddot{x}(t)+C_s\dot{x}(t)+a_1x(t)+a_2x^2(t)+a_3x^3(t)+\rho C_d'\frac{\pi D^2}{4}\dot{x}(t)|\dot{x}(t)|=f_c(t)$$

$$f_c(t)=\rho\frac{\pi}{6}D^3C_m\dot{u}(t)+\rho C_d\frac{\pi D^2}{4}u(t)|u(t)|$$

The comparative results presented for the data given in Fig.2.7 are discussed in detail below. It can be observed from the figure that the excitation and response spectral energy

bandwidths lie between 0.1-0.55 Hz and this interval is chosen as the frequency range for subsequent comparisons.

2.4.1 Coherence Function Analysis

The linear, nonlinear and cumulative coherence estimates with the uncorrelated inputs and the associated uncorrelated outputs of the three nonlinear (NSLD, NSCHD and NSND) models are plotted as a function of frequency in Fig.2.8. For all three models, the nonlinear contribution is significant between f = 0.1 and 0.3 Hz where the subharmonic response energy is observed (Fig.2.7d). The system behavior is almost linear beyond 0.3 Hz as shown in Fig.2.8. Among the nonlinear coherence estimates, contribution from square term (i.e., x^2) is the most significant especially near the natural frequency of the system (f_n=0.23 Hz). According to Gottlieb (1991), the restoring force function for an axis-symmetric body behaves in an anti-symmetric manner and can be represented by a polynomial with odd functions only. In contrary, the coherence diagram shows that the even (square) term (x^2) is present and its contribution is more than that of the odd (cubic) term (x^3). This is because the sphere response, especially the nonlinear subharmonic component, is not symmetrical with respect to the static equilibrium position. Comparing Figs.2.7c and 2.8, it can be observed that the contribution of the square term is predominant in the area of subharmonic region. The goodness-of-fit of the chosen model is thus always decided by the coherence functions that provide an absolute measure of how well each term of the model fits the data at specific frequencies of interest. The coherence of the relative damping term (Fig.2.8b) and the nonlinear structural damping term (Fig.2.8c), in the range of 5-10 % have improved the respective cumulative coherence estimates.

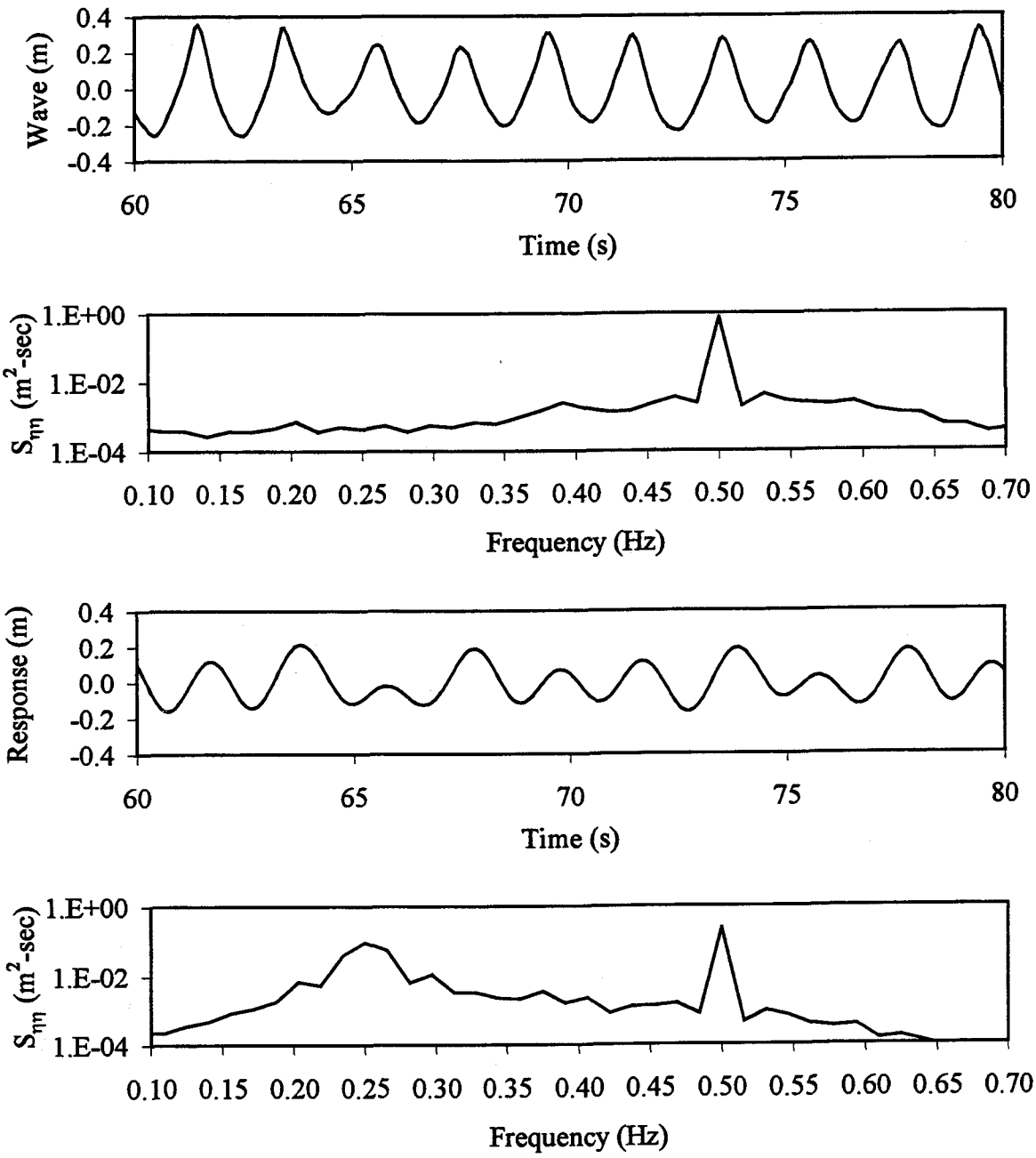

Fig.2.7 Experimental data: a) (first) wave time series, b) (second) wave spectra, c) (third) response time series, d) (fourth) response spectra

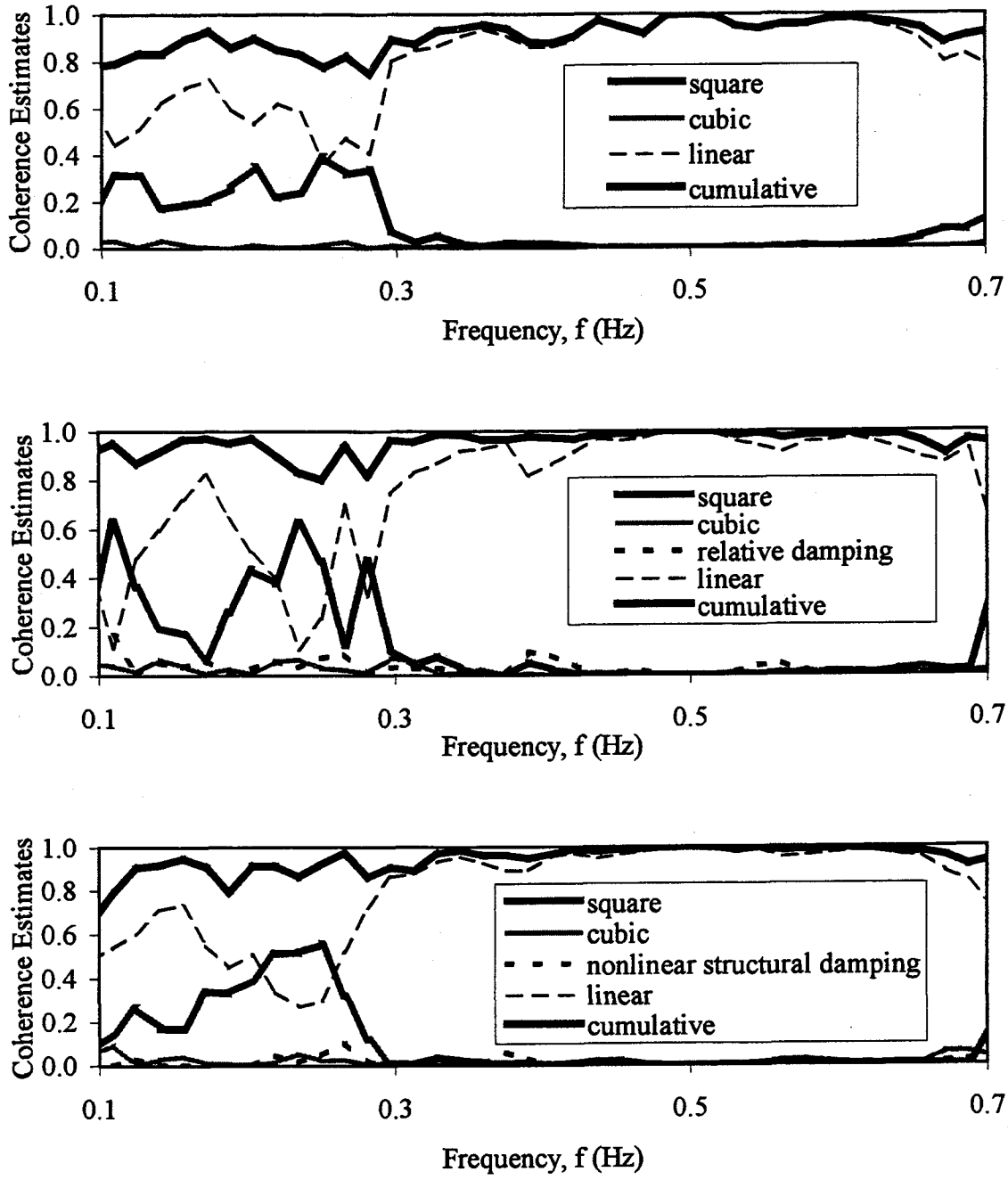

Fig.2.8 Coherence estimates: a) (top) NSLD model, b) (middle) NSCHD model, c) (bottom) NSND model

2.4.2 Spectral Density Analysis

It is difficult to assess and select the most suitable model for the experimental system based on the coherence estimates. Using the identified parameters, the response is evaluated for each model by solving the respective ordinary differential equations, (Eqs.2.12, 2.22 and 2.24) using a fourth-order Runge-Kutta method (Gerald and Wheatley 1989). The predicted responses from the various models are compared with the experimental response in the frequency domain as shown in Fig.2.9. The primary resonance region for the NSCHD model is close to that of the measured response, but the NSLD model has a higher primary energy level. The NSLD model does not generate a matching nonlinear response. Similarly, the subharmonic response simulated by the NSCHD model is not comparable with the actual measured response. Thus, the above mentioned models are not suitable for the experimental system considered. However, the response simulated by the NSND model matches well with the experimental response both in the primary as well as the subharmonic resonance regions. Hence, this model can represent the experimental system well and a comparison of time series and spectra between the identified response using NSND model and the experimental response is given in Fig.2.10.

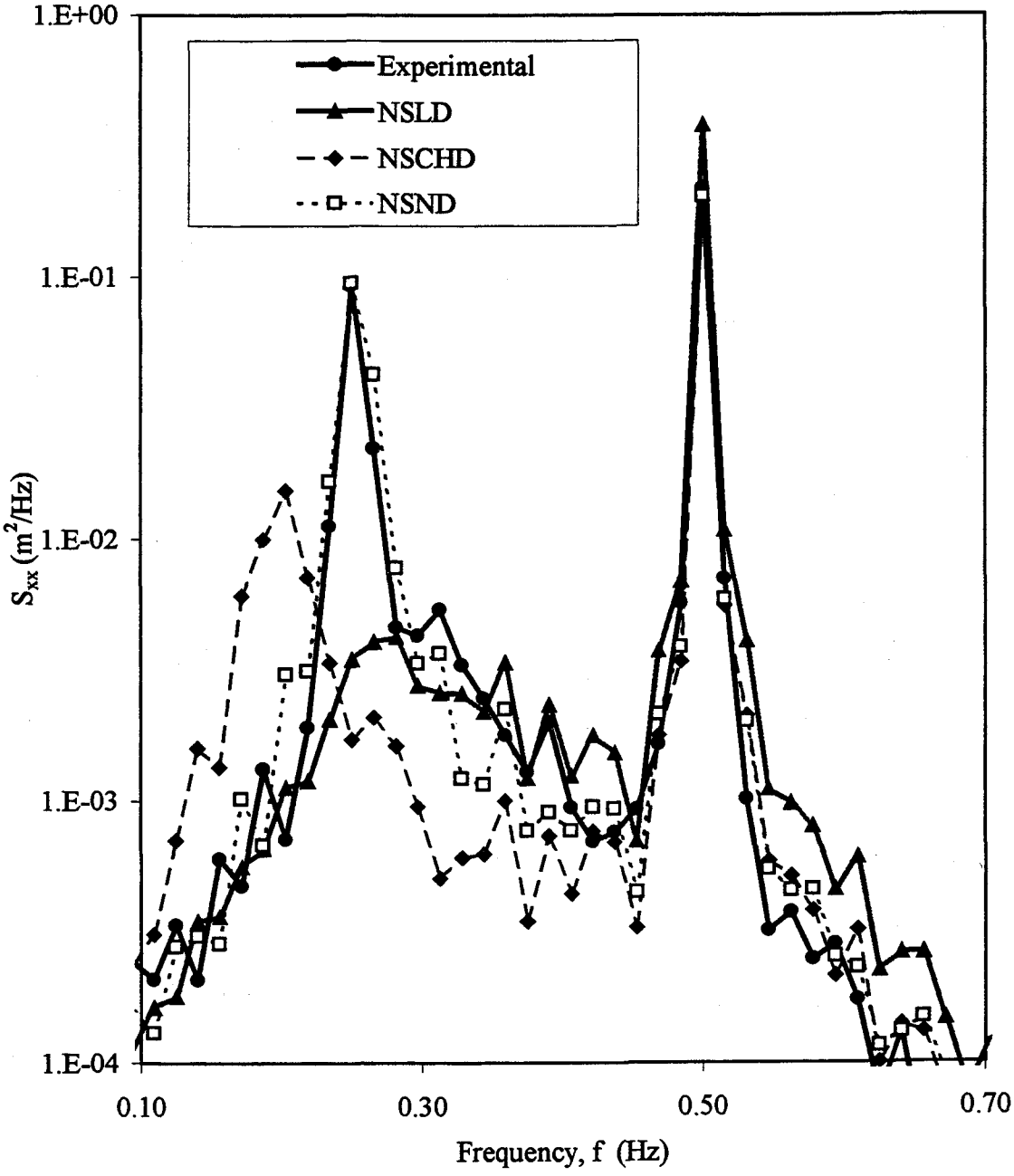

Fig.2.9 Comparison of identified responses using alternative models with the experimental response

2.5 System Parameter Identification

2.5.1 Impedance Function Analysis

The linear and nonlinear impedance functions, both magnitude and phase as a function of frequency are given in Fig.2.11a-f. The magnitude of the linear impedance function gives all the linear system parameters such as the stiffness coefficient (a_1), damping coefficient (C_s), mass (M), added mass coefficient (C_a) and natural frequency (f_n) by using Eqs.2.19-21. The phase for the linear impedance function changes from nearly 0° to 180° at the natural frequency as shown in Fig.2.11b. The nonlinear impedance functions $A_2(f)$ (Eq.23), $A_3(f)$ (Eq.24), $A_4'(f)$ (Eq.51) give the nonlinear stiffness coefficients, a_2 and a_3 and nonlinear structural damping coefficient C_d' respectively. Fig.2.11c and e give the magnitude of the nonlinear stiffness coefficients normalized with the average value plotted as a function of the frequency, f. It can be observed from Figs.2.11d and 11f that the phase angles for $A_2(f)$ and $A_3(f)$ shift between $^{-}180°$ and 180°, indicating a negative sign for the identified coefficients, a_2 and a_3. The magnitude and phase diagrams for C_d' are given in Fig2.11g and h. It can be observed from the phase angle diagram that the damping term, which is proportion to response velocity, is 90° out of phase with the measured displacement as expected.

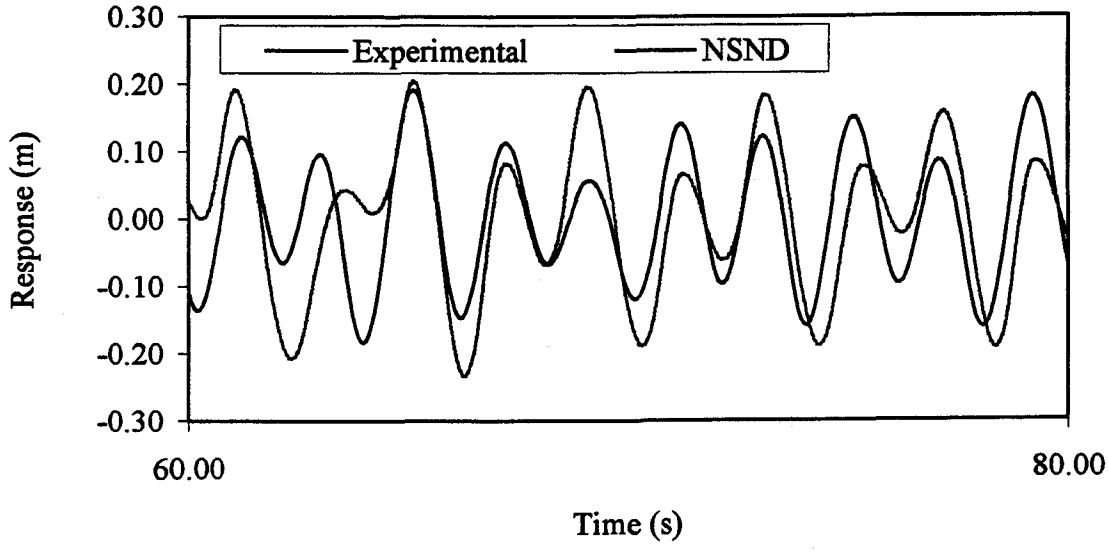

(a)

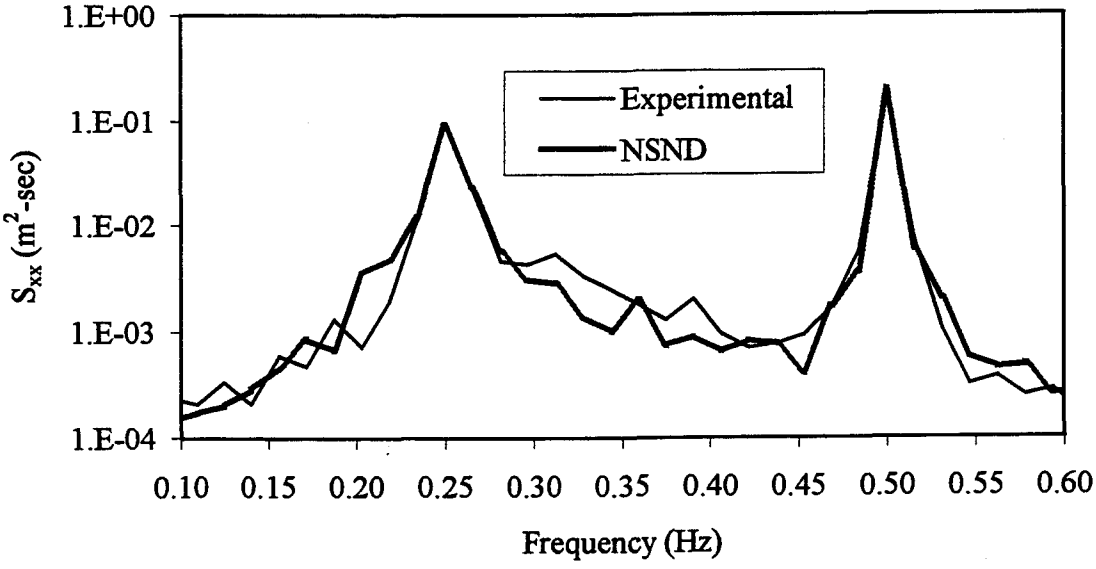

(b)

Fig.2.10 Comparison of simulated response using NSND model with the experimental response: a) time series, b) spectra

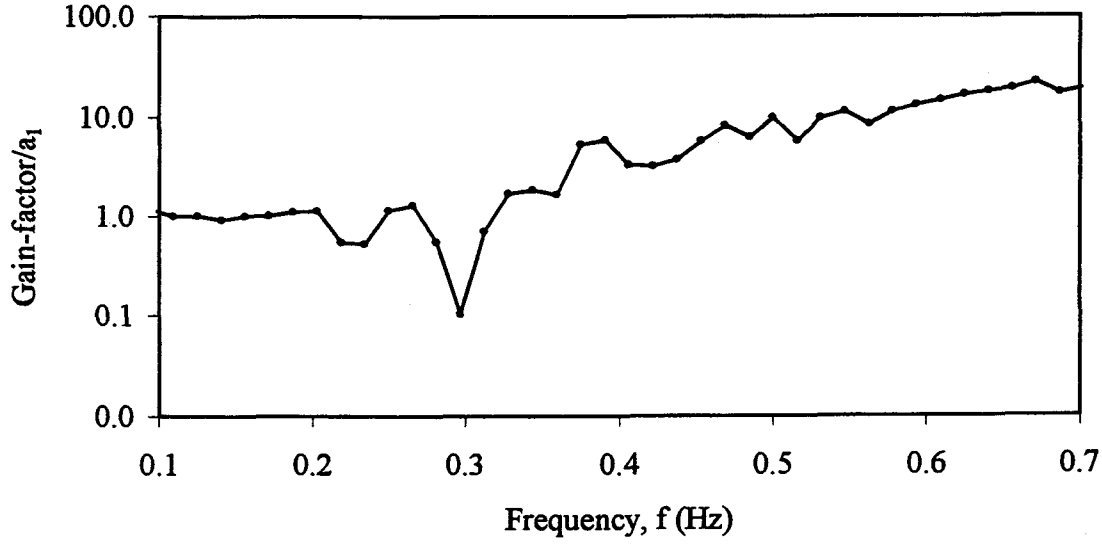

(a)

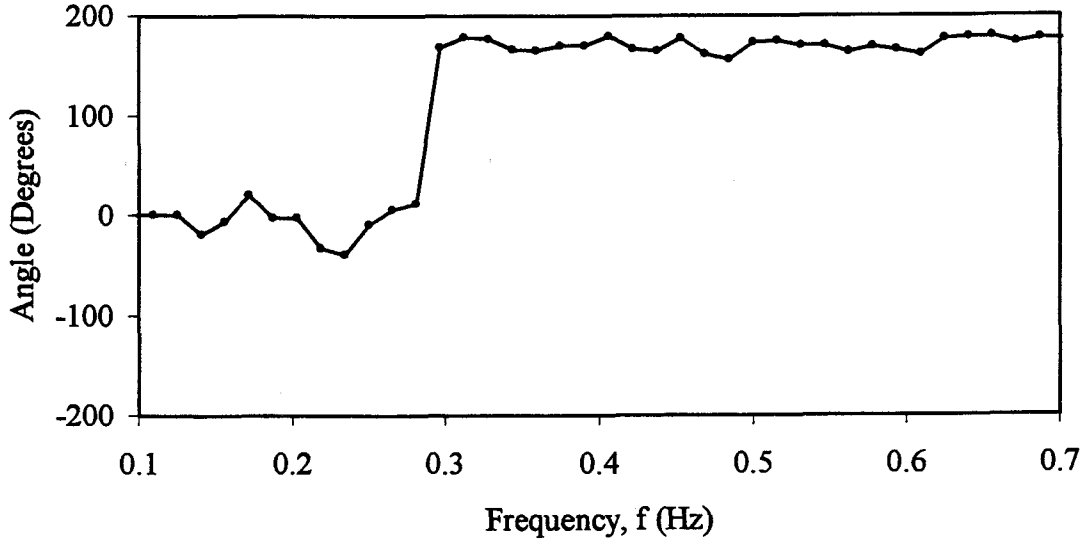

(b)

Fig.2.11 Normalized impedance functions: a) a_1 magnitude, b) a_1 phase, c) a_2 magnitude, d) a_2 phase, e) a_3 magnitude, f) a_3 phase, g) C_d' magnitude, h) C_d' phase

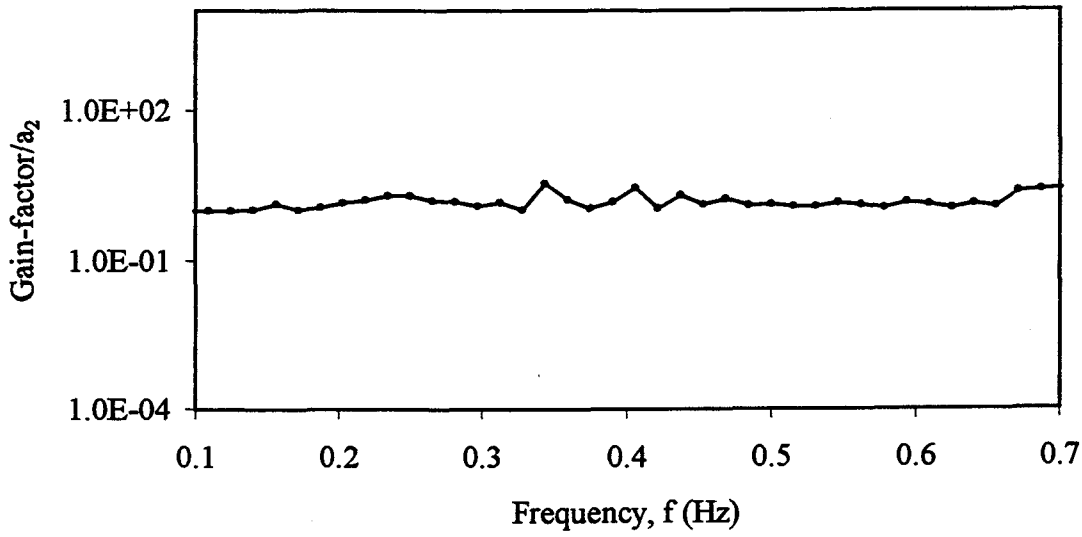

(c)

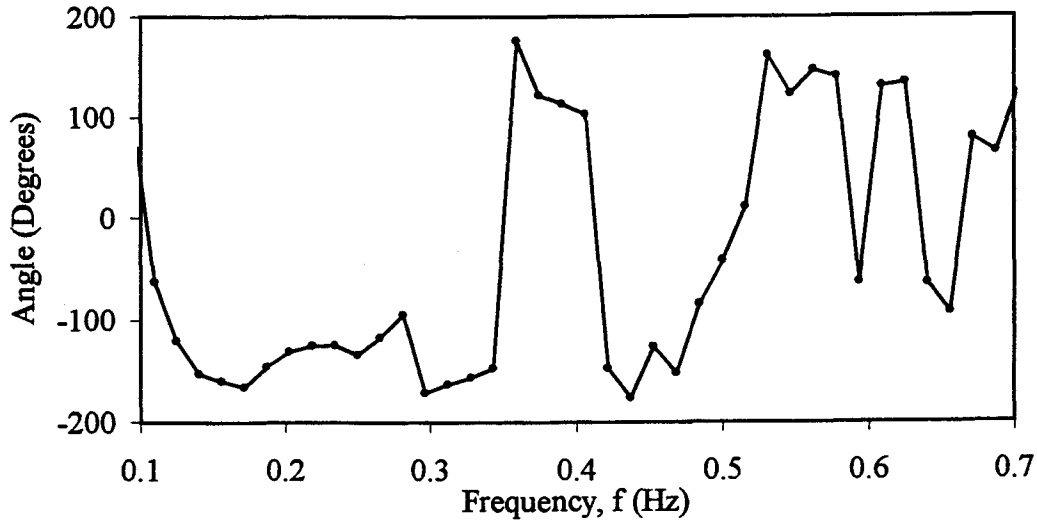

(d)

Fig.2.11 Continued

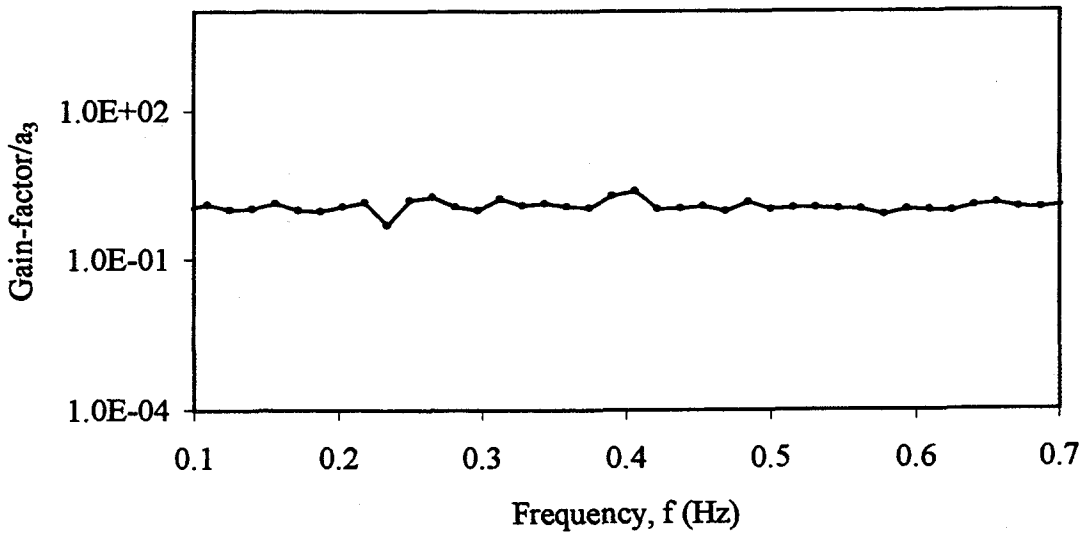

(e)

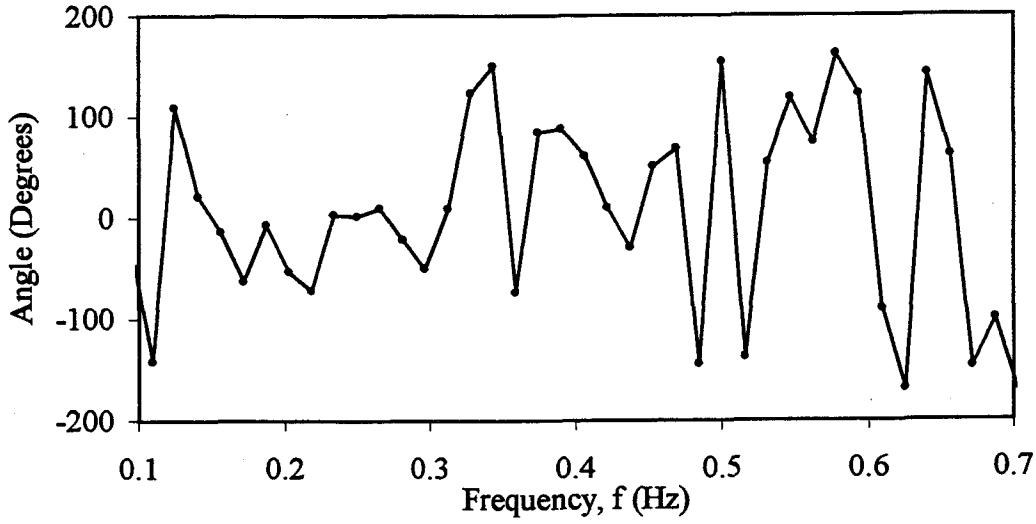

(f)

Fig.2.11 Continued

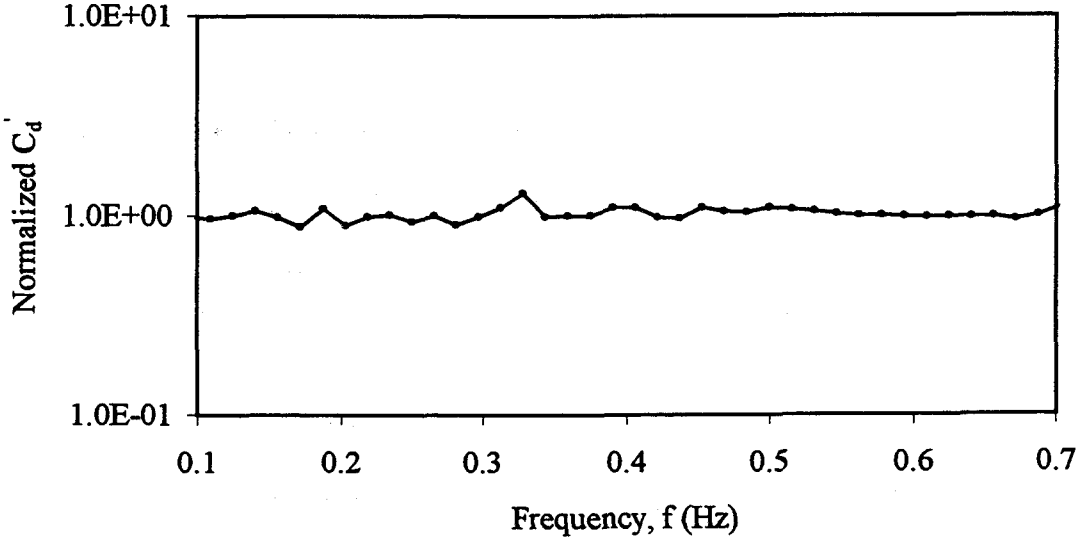

(g)

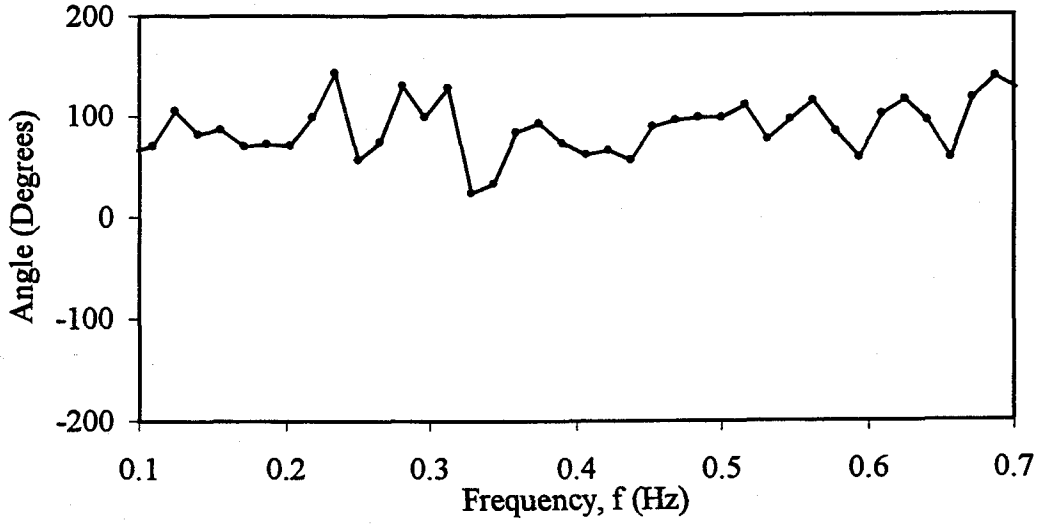

(h)

Fig.2.11 Continued

2.5.2 Effects of Hydrodynamic Coefficients on System Response

The NSND model requires the knowledge of C_d and C_m for the evaluation of hydrodynamic force on the sphere. As mentioned earlier, the effect of C_m and C_d on the nonlinear response has not been studied before according to the author's knowledge.

In order to understand the system's behavior, C_m is altered within the range of 1-1.5 and the R-MI/SO technique is then applied. The identified properties are tabulated for different C_m in Table 2.1a. From the table, magnitudes of C_a, a_1, a_2, a_3, C_d', ζ_s and C_s increase with increasing C_m. The natural frequency identified is constant for all the cases. The responses simulated using the parameters are compared with the measured response in Fig.2.12a. The primary resonance energy of all the predicted responses is practically constant and agrees favorably with that of the measured response. Note that the subharmonic energy of the predicted response decreases with increasing values of inertia coefficient and $C_m = 1.3$ matches well with the experimental response.

C_d is varied between 0.2-1.0 and the properties are identified as given in Table 2.1b. The parameters remain consistent for different C_d. The responses simulated using the parameters are compared with the measured response in Fig.2.12b and it can be observed that the response does not change significantly with the variation in C_d. Based on the water depth to wavelength (h/L) and diameter to wave height (D/H) ratios (Nath and Harleman 1970), the inertia effects dominate the total forces and the response is found to be insensitive to changes in C_d.

a)

C_m	C_a	C_d	a_1 lb/ft	a_2 lb/ft^2	a_3 lb/ft^3	C_d'	ζ_s	f_n
1.10	0.11	1.00	8.11	3.51	5.82	0.18	0.021	0.237
1.20	0.21	1.00	8.51	3.82	5.91	0.18	0.033	0.237
1.30	0.32	1.00	8.91	4.53	6.55	0.18	0.032	0.237
1.40	0.42	1.00	10.31	4.91	7.55	0.19	0.033	0.237
1.50	0.51	1.00	11.14	5.16	8.26	0.19	0.035	0.237

b)

C_d	C_m	C_d	a_1 lb/ft	a_2 lb/ft^2	a_3 lb/ft^3	C_d'	ζ_s	f_n
0.20	1.30	0.30	8.90	4.50	6.20	0.18	0.021	0.237
0.50	1.30	0.30	9.01	4.69	6.41	0.18	0.033	0.237
0.80	1.30	0.30	8.91	4.68	6.41	0.19	0.032	0.237
1.00	1.30	0.30	8.91	4.69	6.50	0.19	0.035	0.237

Table 2.1: Identified system parameters using NSND model by varying hydrodynamic coefficients: a) C_m, b) C_d (English units)

a)

C_m	C_a	C_d	a_1 N/m	a_2 N/m^2	a_3 N/m^3	C_d'	ζ_s	f_n
1.10	0.11	1.0	119.1	167.4	911.3	0.18	0.021	0.237
1.20	0.21	1.0	122.4	180.3	924.1	0.18	0.033	0.237
1.30	0.32	1.0	132.0	215.7	1020.7	0.18	0.032	0.237
1.40	0.42	1.0	151.3	235.1	1175.3	0.19	0.033	0.237
1.50	0.51	1.0	161.0	244.7	1284.8	0.19	0.035	0.237

b)

C_d	C_m	C_d	a_1 N/m	a_2 N/m^2	a_3 N/m^3	C_d'	ζ_s	f_n
0.20	1.30	0.30	128.8	215.7	972.4	0.18	0.021	0.237
0.50	1.30	0.30	128.8	219.0	988.6	0.18	0.033	0.237
0.80	1.30	0.30	132.0	219.0	1004.7	0.19	0.032	0.237
1.00	1.30	0.30	132.0	219.0	1004.7	0.19	0.035	0.237
1.0	1.3	0.3	132.0	222.2	1020.7	0.19	0.035	0.237

Table 2.1: Identified system parameters using NSND model by varying hydrodynamic coefficients: a) C_m, b) C_d (SI units)

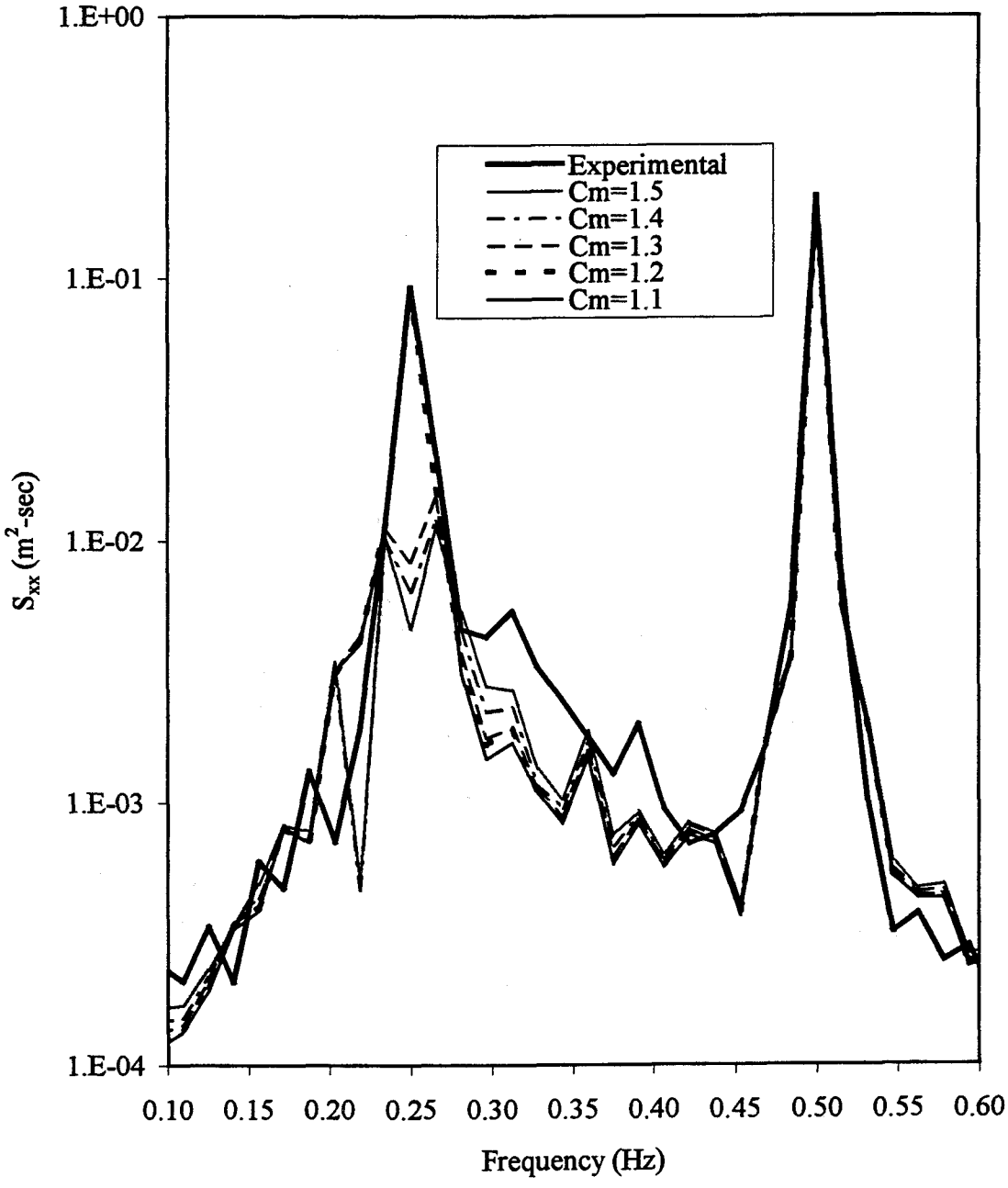

(a)

Fig.2.12 Comparison of identified response using NSND model with the measured response by varying hydrodynamic coefficients: a) C_m, b) C_d

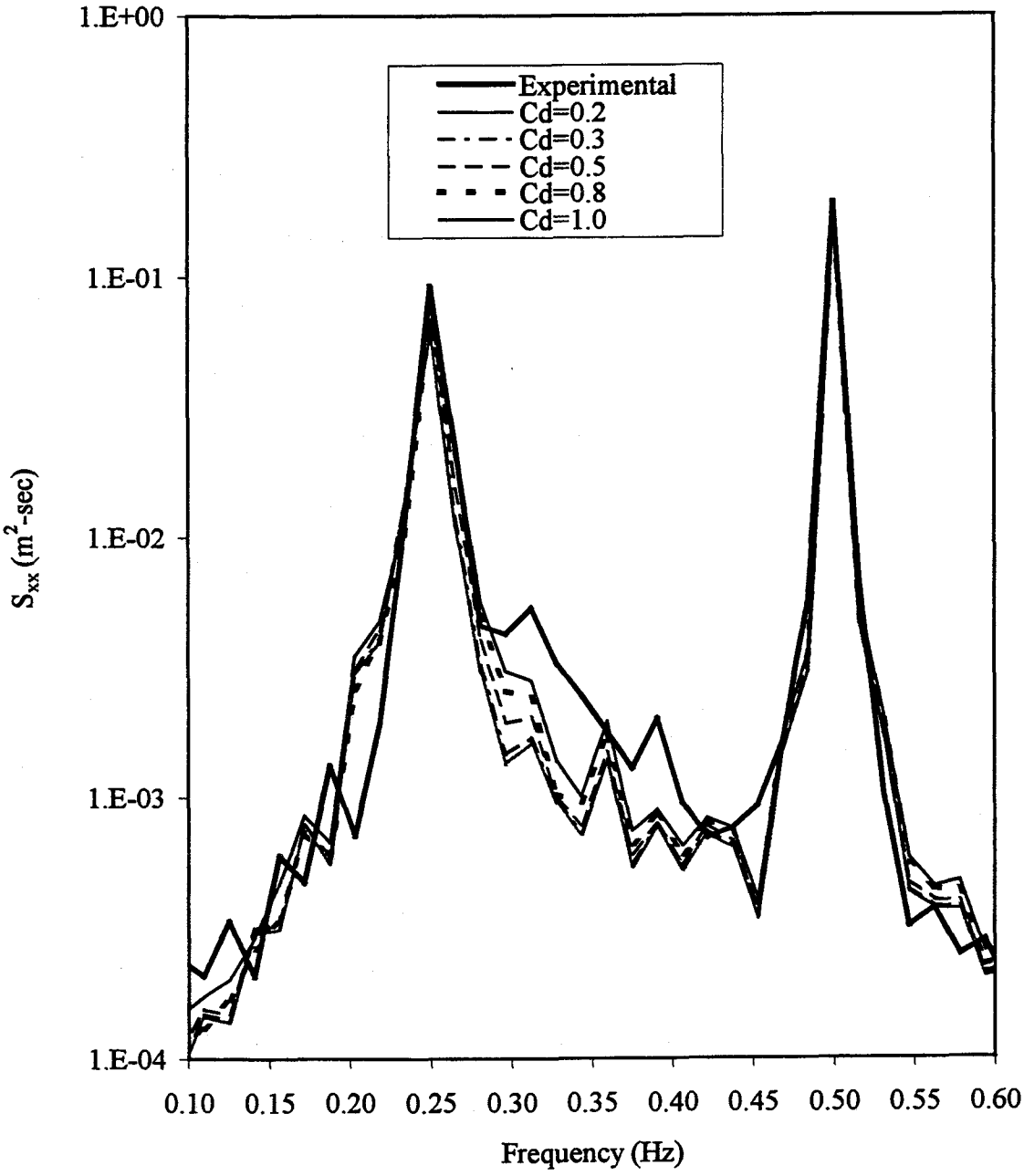

(b)

Fig.2.12 Continued

3. MDOF EXTENSION AND COMPARISONS

3.1 MDOF System Considered

The MDOF experimental model consists of a submerged moored neutrally buoyant sphere excited by periodic waves with white noise perturbations. Springs were used to support the sphere and provide a restoring force. The string pots were attached to measure the sphere movement. The restoring force is geometrically nonlinear with the springs attached at an angle of 90°. The configuration of the model is given in Fig.3.1. Pitch motion is observed to be negligible compared to surge and heave motions (Yim *et al* 1993). With the knowledge of string pot measurements and the distances between the sphere and the respective string pots, the readings are converted to surge and heave by two-dimensional geometrical transformations (Lin 1994).

3.2 Governing Equations of Motions

The equations of motion for the SDOF moored structural systems (Chapter 2) subject to periodic wave excitation with white noise perturbations are extended to the MDOF surge-heave model. By considering surge (x_1) and heave (x_3) as the generalized displacement coordinates, assuming that structural damping can be lumped into an equivalent linear structural damping coefficient C_{s1} and C_{s3}, and the nonlinear restoring force represented by $R_1(x_1,x_3,t)$ and $R_3(x_1,x_3,t)$, the governing equation of motion for the above mooring system can be written as

$$m\ddot{x}_1(t) + C_{s1}\dot{x}_1(t) + R_1(x_1(t), x_3(t)) = f_1(t) \qquad (3.1a)$$

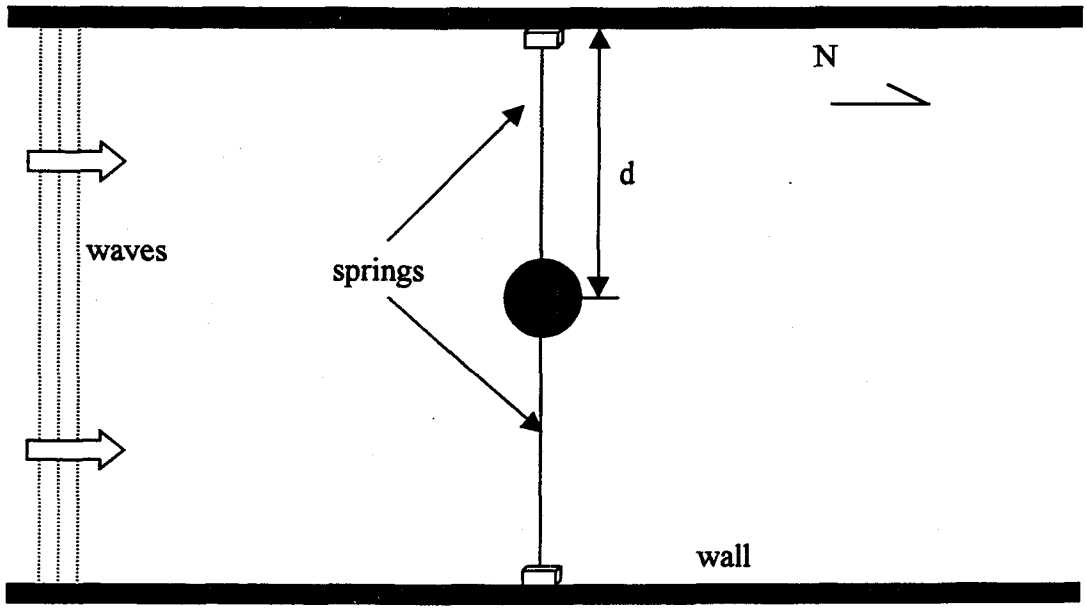

(a)

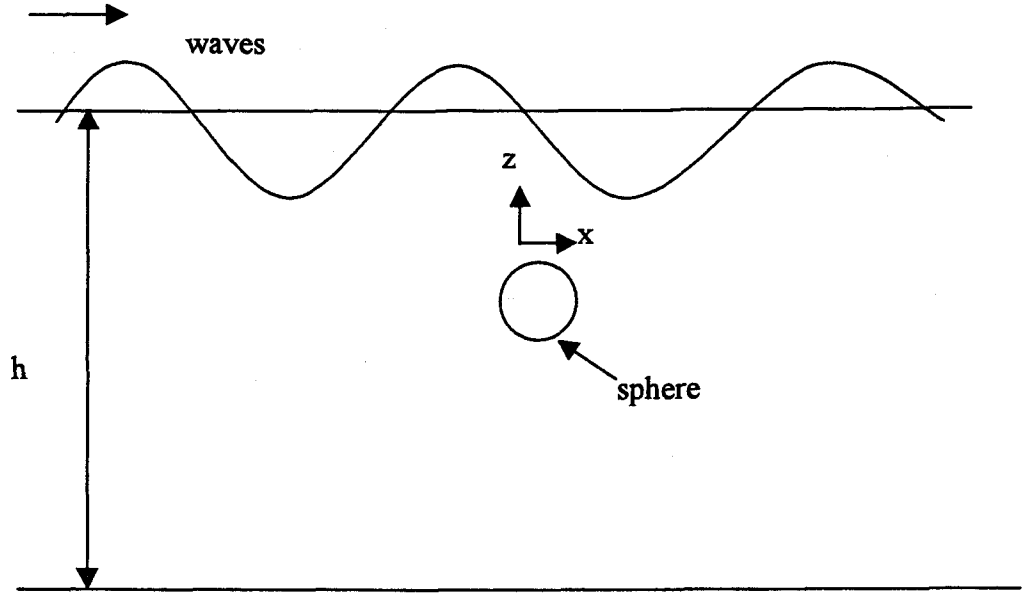

(b)

Fig.3.1 MDOF experimental set up: a) plan, b) profile view

$$m\ddot{x}_3(t) + C_{s3}\dot{x}_3(t) + R_3(x_1(t), x_3(t)) = f_3(t) \tag{3.1b}$$

where m = mass of the sphere, $f_1(t)$, $f_3(t)$ = excitation force in surge and heave directions respectively and $\dot{x}_1(t)$, $\dot{x}_3(t)$, $\ddot{x}_1(t)$, $\ddot{x}_3(t)$ = sphere velocity and acceleration in surge and heave directions, respectively. Because of symmetry, there is no coupling between the inertia forces. Hence the off-diagonal mass terms (m_{13} and m_{31}) are zero.

The MDOF mooring restoring forces are derived from the potential function which describes the pretensioned geometrical configuration of a symmetric small body (Gottlieb and Yim 1992) and the resulting coupled expressions in surge and heave are given below:

$$R_1(x_1(t), x_3(t)) = 4Kx_1(t)\left(1 - \frac{l_c}{l}\right) \tag{3.2a}$$

$$R_3(x_1(t), x_3(t)) = 4Kx_3(t)\left(1 - \frac{l_c}{l}\right) \tag{3.2b}$$

where $l = \sqrt{d^2 + x_1(t)^2 + x_3(t)^2}$ = instantaneous spring length, l_c = initial spring length, K = spring constant, and d = distance of the center of the sphere from the wall.

The restoring forces in surge and heave direction are approximated by selected third order polynomials obtained using a least-square approximation given by

$$R_1(x_1(t), x_3(t)) = a_1x_1(t) + a_2{x_1}^2(t) + a_3{x_1}^3(t) + c_{12}x_1(t){x_3}^2(t) \tag{3.3a}$$

$$R_3(x_1(t), x_3(t)) = b_1x_3(t) + b_3{x_3}^3(t) + c_{21}{x_1}^2(t)x_3(t) \tag{3.3b}$$

Note that a square term in the surge direction is included due to its biased (mean offset) response. The comparisons of the polynomials (Eq.3.3) with the geometric model restoring forces (Eq.3.2) are given in Figs.3.2a and b.

a)

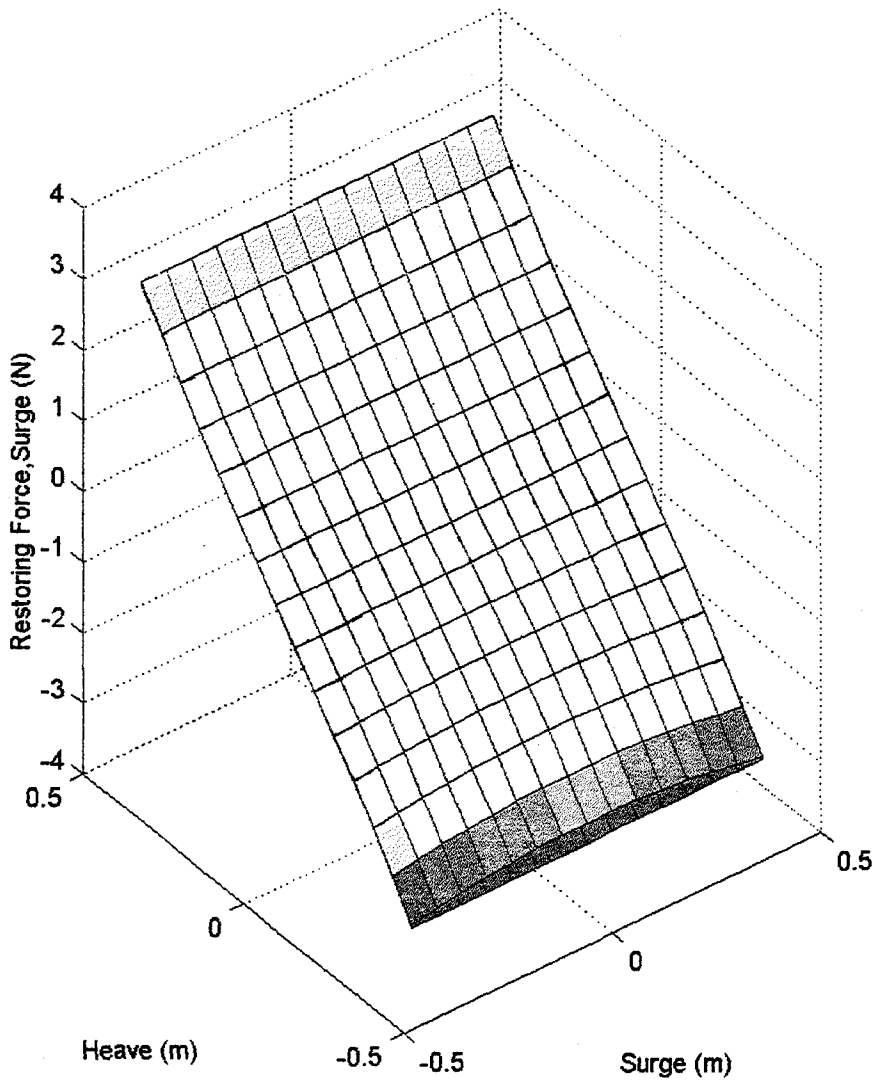

Fig.3.2 Comparison between the actual and approximate restoring force functions: a) surge, b) heave

b)

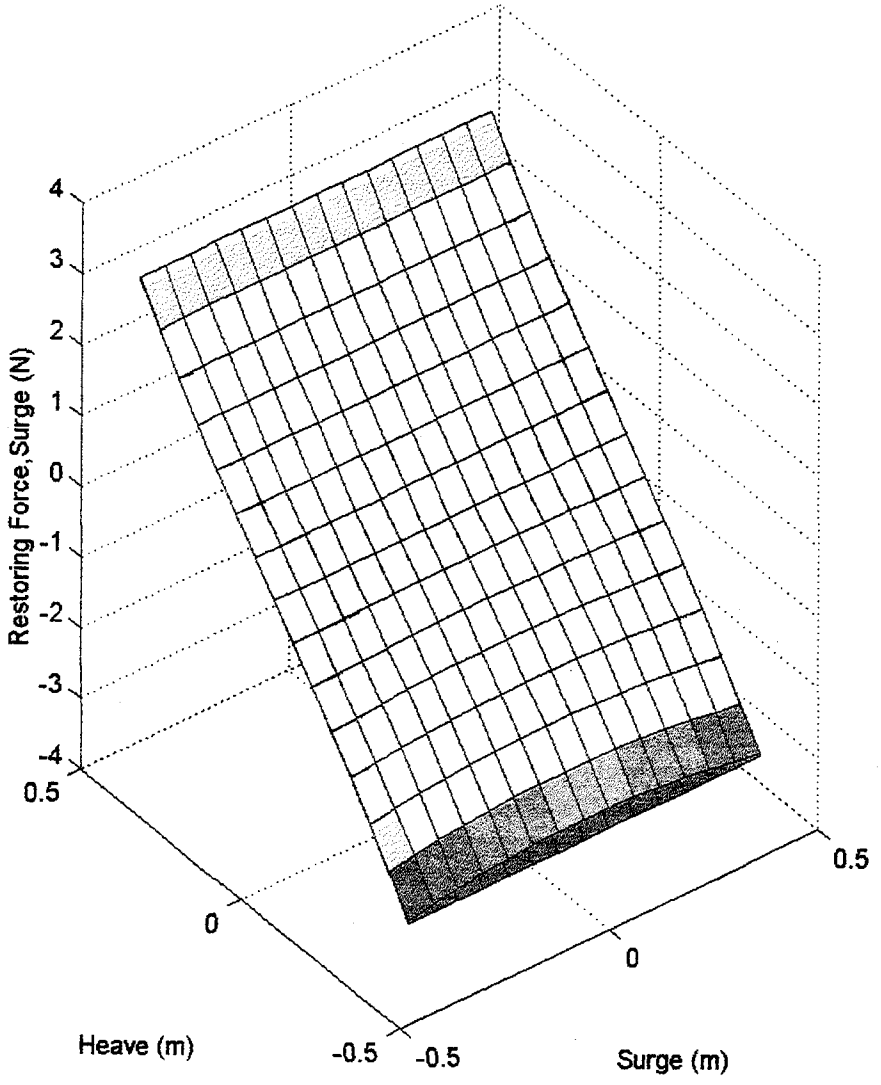

Fig.3.2 Continued

a)

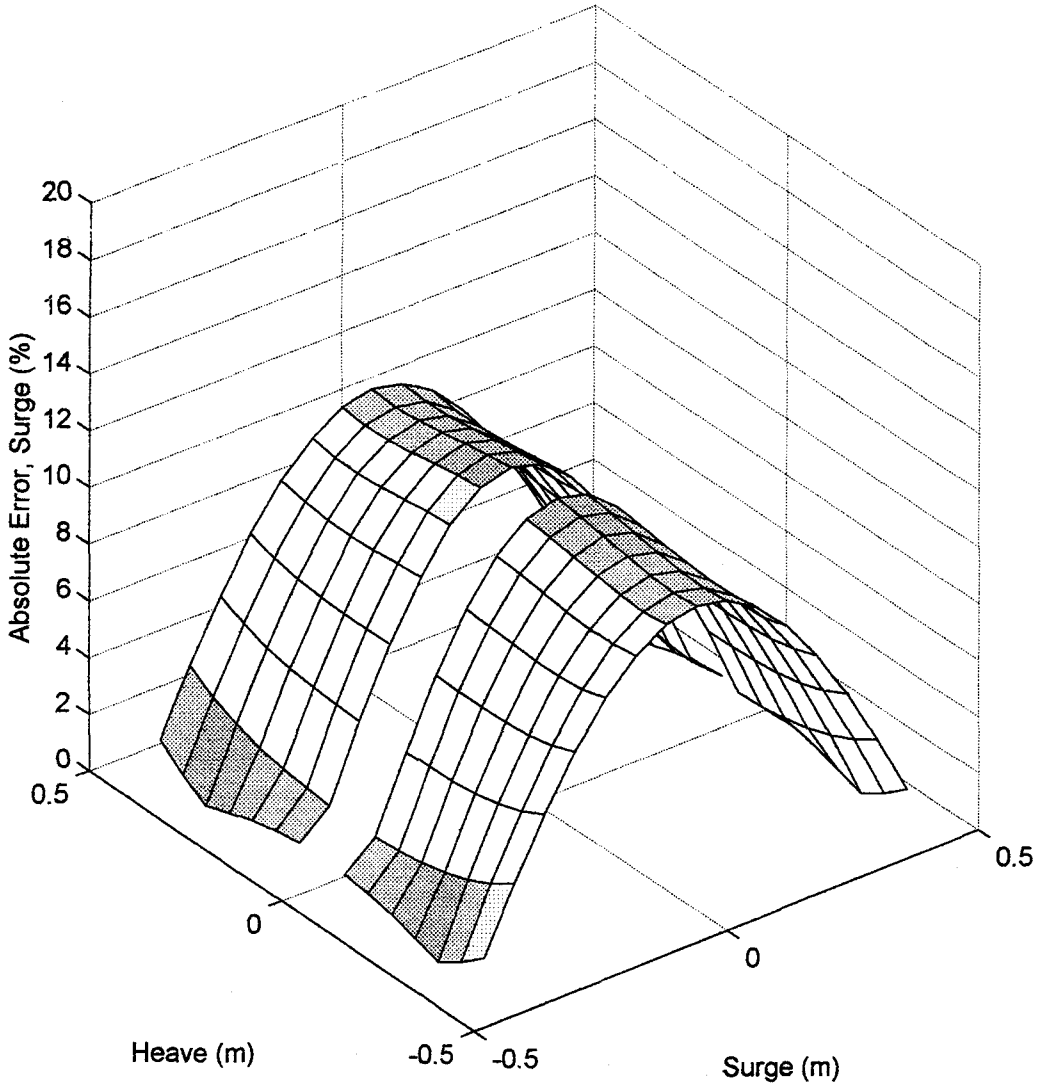

Fig.3.3 Relative error between the actual and approximate restoring force functions: a) surge, b) heave

b)

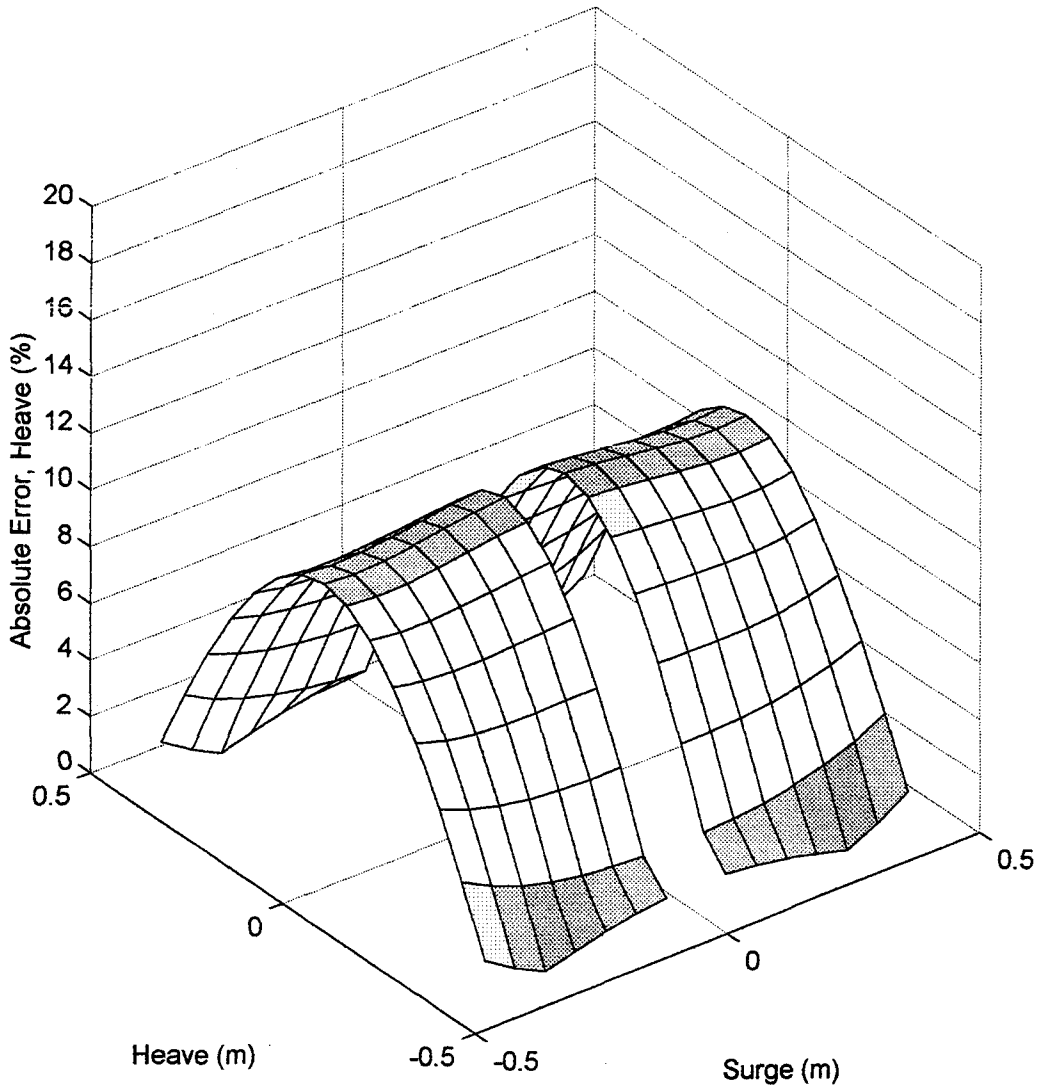

Fig.3.3 Continued

The relative error ($\frac{|R_{1,3}x - R'_{1,3}x|}{|R_{1,3}x|}$) between the geometric model and approximate errors are given in Figs.3.3a and b. The normalized errors in both surge and heave directions behave in a similar manner and varies between 0 to 10 %. However, the error in absolute magnitude of the restoring forces at low displacement is mostly insignificant compared to the other terms (i.e., inertia, damping and wave excitation forces) in the dynamic equation of motion (Eq.3.1).

Following the results of R-MI/SO technique application on SDOF system (Chapter 2), an Independent Flow Fields (IFF) model is used to represent the hydrodynamic excitation force on the MDOF model.

They are given by

$$f_1(t) = \rho \forall C_m \dot{u}_1(t) - m_a \ddot{x}_1(t) + \frac{\rho}{2} A_p C_d u_1(t)|u_1(t)| - \frac{\rho}{2} A_p C_{d1}' \dot{x}_1(t)|\dot{x}_1(t)| \quad (3.4a)$$

$$f_3(t) = \rho \forall C_m \dot{u}_3(t) - m_a \ddot{x}_3(t) + \frac{\rho}{2} A_p C_d u_3(t)|u_3(t)| - \frac{\rho}{2} A_p C_{d3}' \dot{x}_3(t)|\dot{x}_3(t)| \quad (3.4b)$$

where

$$\forall = \frac{\pi}{6} D^3 \quad (3.5a)$$

$$A_p = \frac{\pi D^2}{4} \quad (3.5b)$$

$$m_a = \frac{\pi}{6} D^3 C_a \quad (3.5c)$$

ρ = mass density, D = diameter of sphere, C_a = added mass coefficient, C_d' = nonlinear structural damping coefficient, C_m = hydrodynamic inertia coefficient and C_d = hydrodynamic drag coefficient. For the sphere (which has a constant projected area) used in

this experimental study, the coefficients are taken as the same in both the surge and heave directions and they are given by

$$C_m, C_d = f\left(Re_F = \frac{u_o D}{\upsilon}, KC_F = \frac{u_o T}{D}\right) \tag{3.6a}$$

$$C_a, C_{d1,3}' = f\left(Re_N = \frac{\dot{x}_o D}{\upsilon}, KC_N = \frac{\dot{x}_o T_o}{D}\right) \tag{3.6b}$$

where u_o, $\dot{x}_o$ = amplitudes of the water particle and structure velocity, respectively, T and T_o = periods of oscillation of water particle and structure (often equal), υ = viscosity of the fluid, Re = Reynolds number, KC = Keulegan-Carpenter number, suffix 'F' refers to far field and suffix 'N' to near field.

Using linear wave theory (Chakrabarti 1987), the deterministic water particle velocities can be written as

$$u_1(t) = \omega a \frac{\cosh k(x_3(t)+s)}{\sinh(kh)} \cos(kx_1(t) - \omega t) \tag{3.7a}$$

$$u_3(t) = \omega a \frac{\sinh k(x_3(t)+s)}{\sinh(kh)} \sin(kx_1(t) - \omega t) \tag{3.7b}$$

where $u_1(t)$, $u_3(t)$ are water particle velocity in surge and heave directions respectively, ω = angular velocity, a = wave amplitude, k = wave number, h = water depth and s = distance of the instantaneous center of the sphere from the bottom.

The wave excitation containing a periodic component with white noise perturbations may be considered as a randomly perturbed regular wave field. With wave displacement given by $\eta(t)$, measured for the experiment considered, Eqs.(3.7a,b) can be approximated by

$$u_1(t) = \omega \frac{\cosh k(x_3(t)+s)}{\sinh(kh)} \eta(t) \tag{3.8a}$$

$$u_3(t) = \frac{\sinh k(x_3(t)+s)}{\sinh(kh)}\dot{\eta}(t) \tag{3.8b}$$

It is assumed that the random perturbations in the excitation are included in $\eta(t)$, given by

$$\eta(t) = a\cos(kx_1(t) - \omega t + \phi) + \xi(t) \tag{3.9a}$$

Where $\xi(t)$ is a zero-mean delta-correlated white noise.

The horizontal and vertical, water particle acceleration can also be approximated as

$$\dot{u}_1(t) = \omega_o \frac{\cosh k_o(x_3(t)+s)}{\sinh(k_o h)}\dot{\eta}(t) \tag{3.9c}$$

$$\dot{u}_3(t) = \frac{\sinh k_o(x_3(t)+s)}{\sinh(k_o h)}\ddot{\eta}(t) \tag{3.9d}$$

where $\dot{u}_1(t)$ and $\dot{u}_3(t)$ are the water particle acceleration in surge and heave directions, respectively. The schematic diagram for the MDOF system using IFF model as the alternative form of Morison Equation for representing force is dilineated in Figs.3.4a-c.

3.3 Nonlinear-Structure Nonlinearly-Damped Model

Based on R-MI/SO results of the SDOF system, the nonlinear-structure nonlinearly-damped (NSND) surge-heave model is selected and extended to the MDOF experimental system. The mathematical formulation of the NSND model and the application of R-MI/SO technique (Bendat *et al* 1992) to change the dynamic roles of inputs and outputs has been described in detail for the SDOF system (Chapter 2). In this study, the methodology is extended to MDOF system and the detailed formulation of the model is given in Appendix A. The schematic diagram for the NSND model before and after application of R-MI/SO technique is given in Fig3.5a-b.

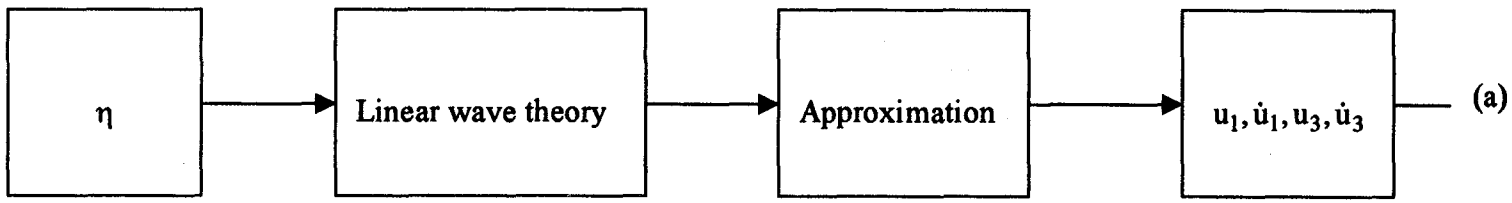

(a)

Fig.3.4 Schematic diagram OF the MDOF system: a) system diagram for the calculation of wave velocity and acceleration, b) surge c) heave

$$f_{d1}(t) = \frac{1}{2}\rho C_d A_p u_1 |u_1| \qquad f_{d1}'(t) = \frac{1}{2}\rho C_{d1}' A_p \dot{x}_1 |\dot{x}_1|$$

$$f_{ih1}(t) = C_m \rho \forall \dot{u}_1$$

Fig.3.4a ----- (A)

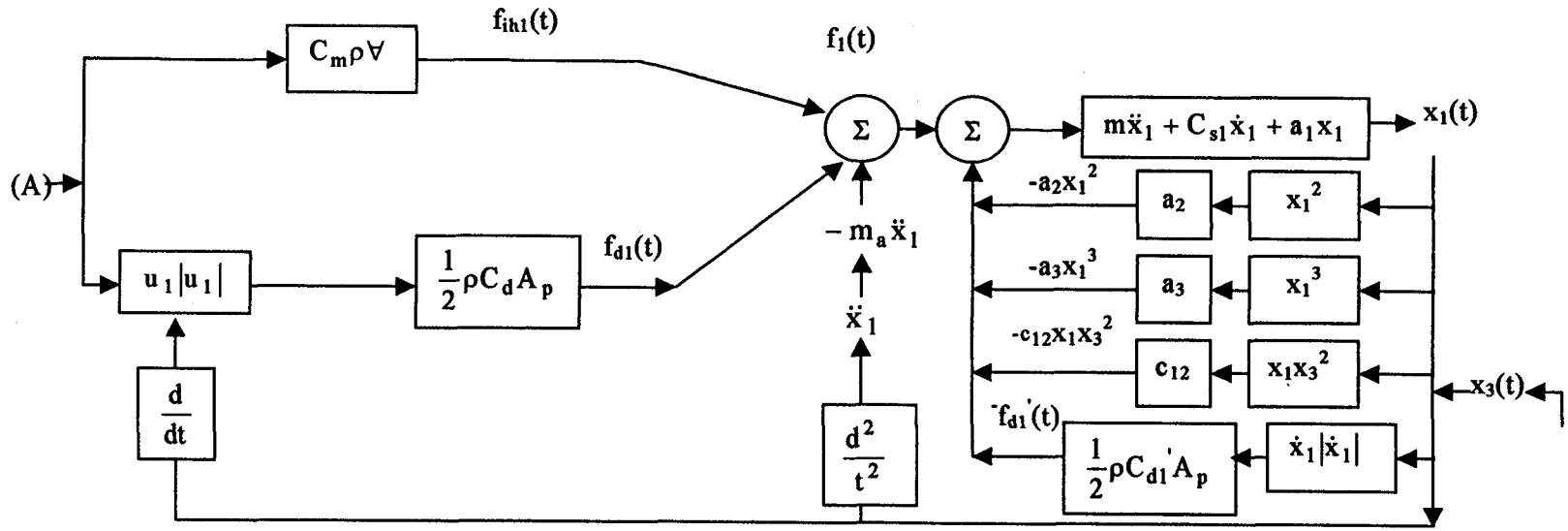

(b)

Fig.3.4 Continued

$$f_{d3}'(t) = \frac{1}{2}\rho C_{d3}' A_p \dot{x}_3 |\dot{x}_3| \qquad f_{d3}(t) = \frac{1}{2}\rho C_d A_p u_3 |u_3|$$

$$f_{ih3}(t) = C_m \rho \forall \dot{u}_3$$

Fig.3.4a -------- (A)

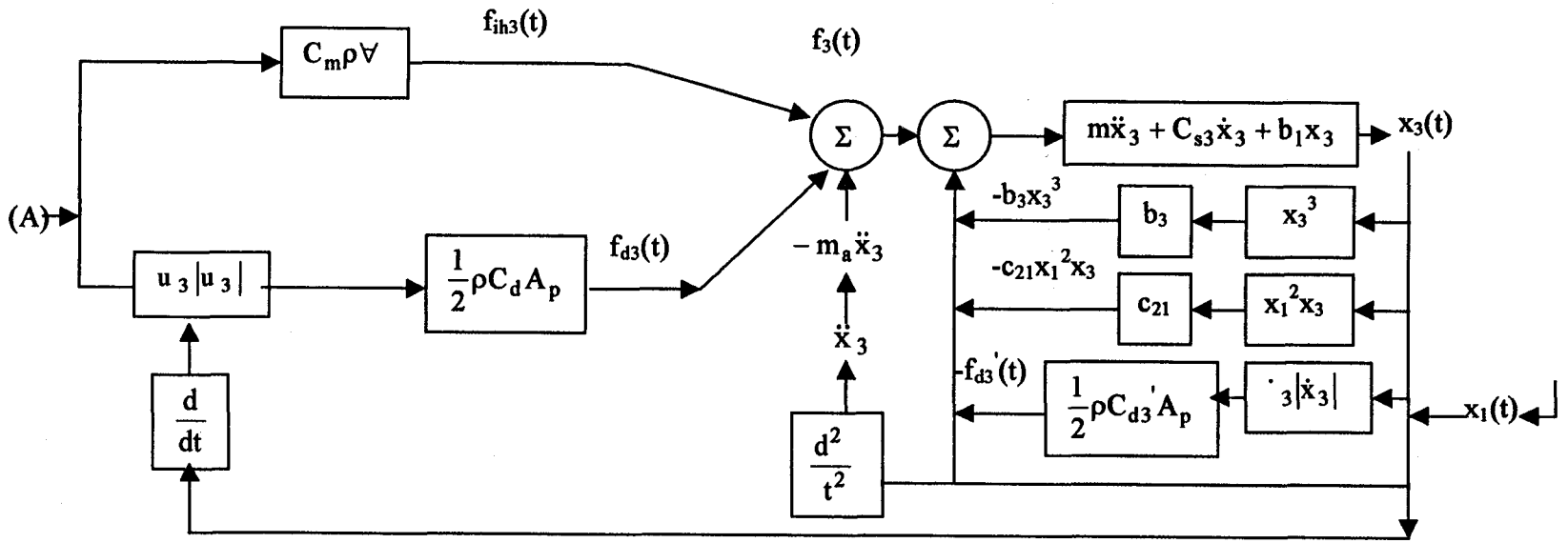

(c)

Fig.3.4 Continued

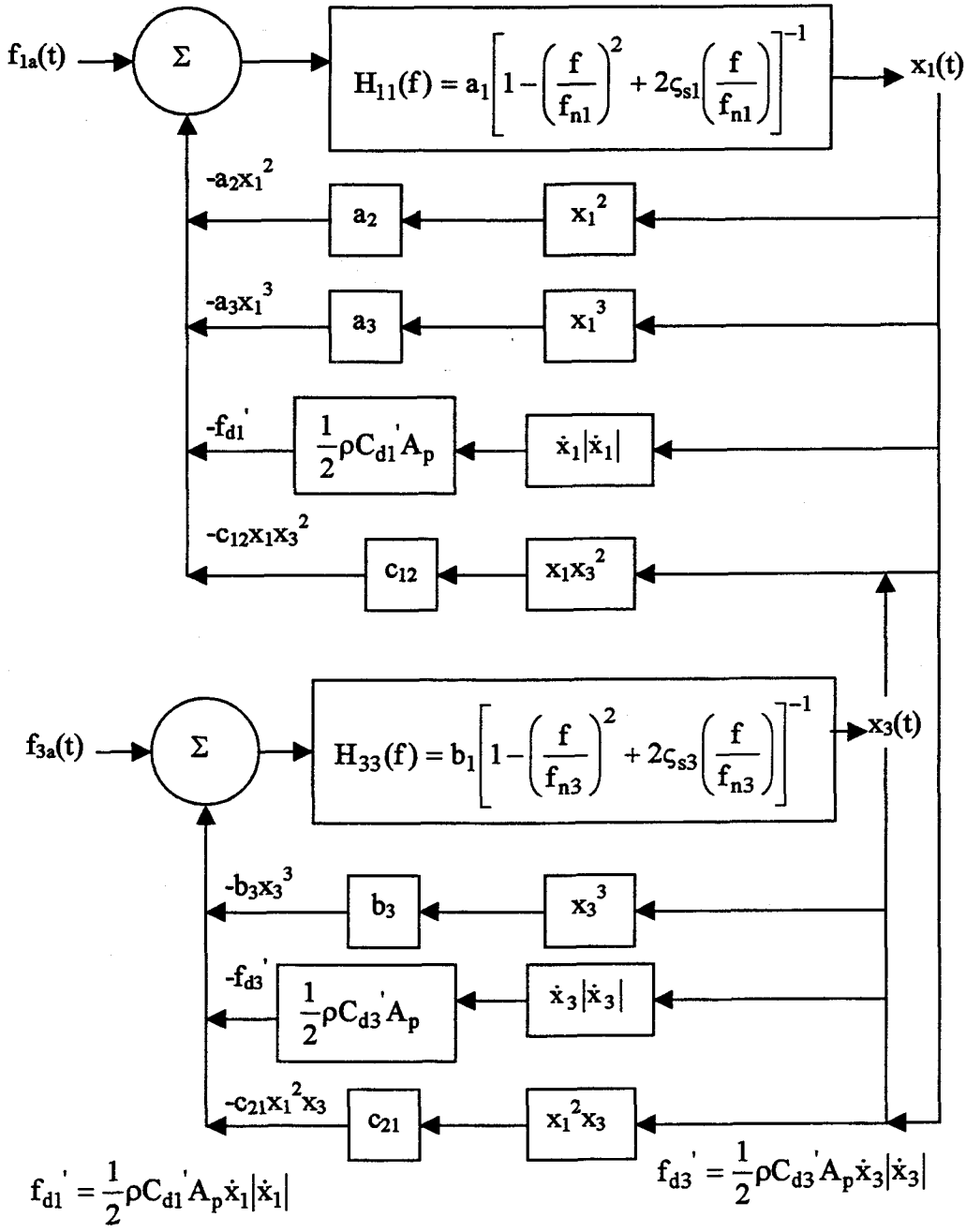

(a)

Fig.3.5 The nonlinear-structure nonlinearly-damped (NSND) model: a) with feedback, b) without feedback

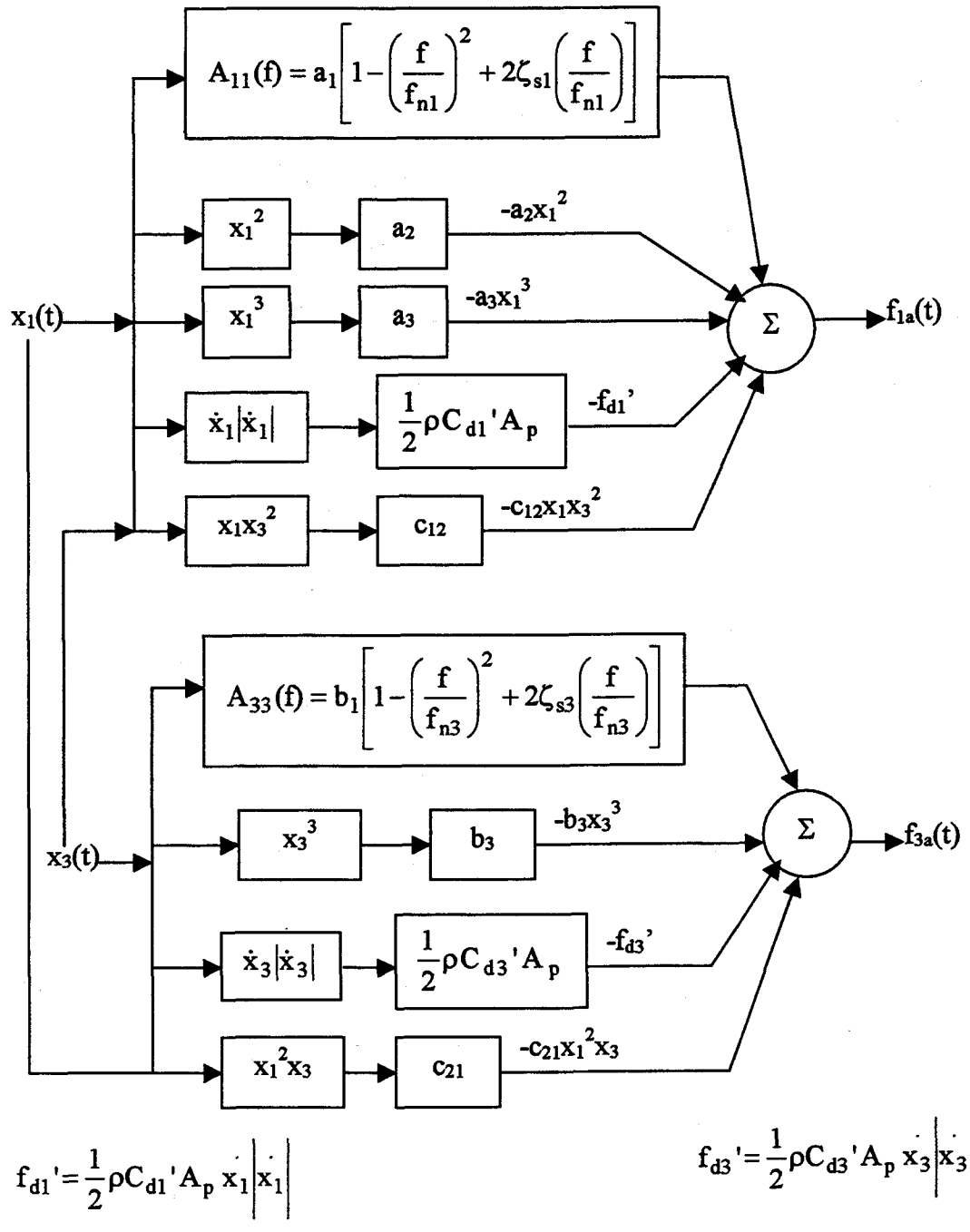

(b)

Fig.3.5 Continued

3.4 MDOF System Parameter Identification

By assuming C_m and C_d based on the results on SDOF system (Chapter 2), the hydrodynamic force is evaluated using Eq.3.4. The R-MI/SO technique is applied on the NSND model and the system parameters are identified for the experimental data. Using the identified parameters, surge and heave responses are simulated using Eqs.3.1, 3 and 4. A typical example of comparison between the identified and experimental data in the time and frequency domain is given in Fig.3.6. The heave and surge response spectral densities, normalized with the variance of corresponding wave data, given by S_{xxn} are plotted against frequency, f in Fig.3.6b and d. It can be observed that the simulated responses are comparable to the corresponding experimental responses in both surge and heave directions.

3.5 MDOF System Response Behavior

3.5.1 Time Series and Spectra

Three tests, ML1, ML2 and MH conducted on the sphere with the same wave period and varying wave heights with white noise as the wave excitation yield subharmonic response (Yim *et al* 1993). All the tests have the same wave period (T = 2.21 seconds), but they vary in wave heights. The data sets are labeled and grouped according to the variation in wave amplitude. The symbol 'M' stands for multi-degree-of-freedom, 'L' and 'H' represent low and high wave amplitude excitation, respectively. The wave velocity and acceleration are evaluated using the central difference method (Gerald and Wheatley 1989). The sampling interval used in the experiment is 0.0625 second, which yields a Nyquist frequency of 8 Hz.

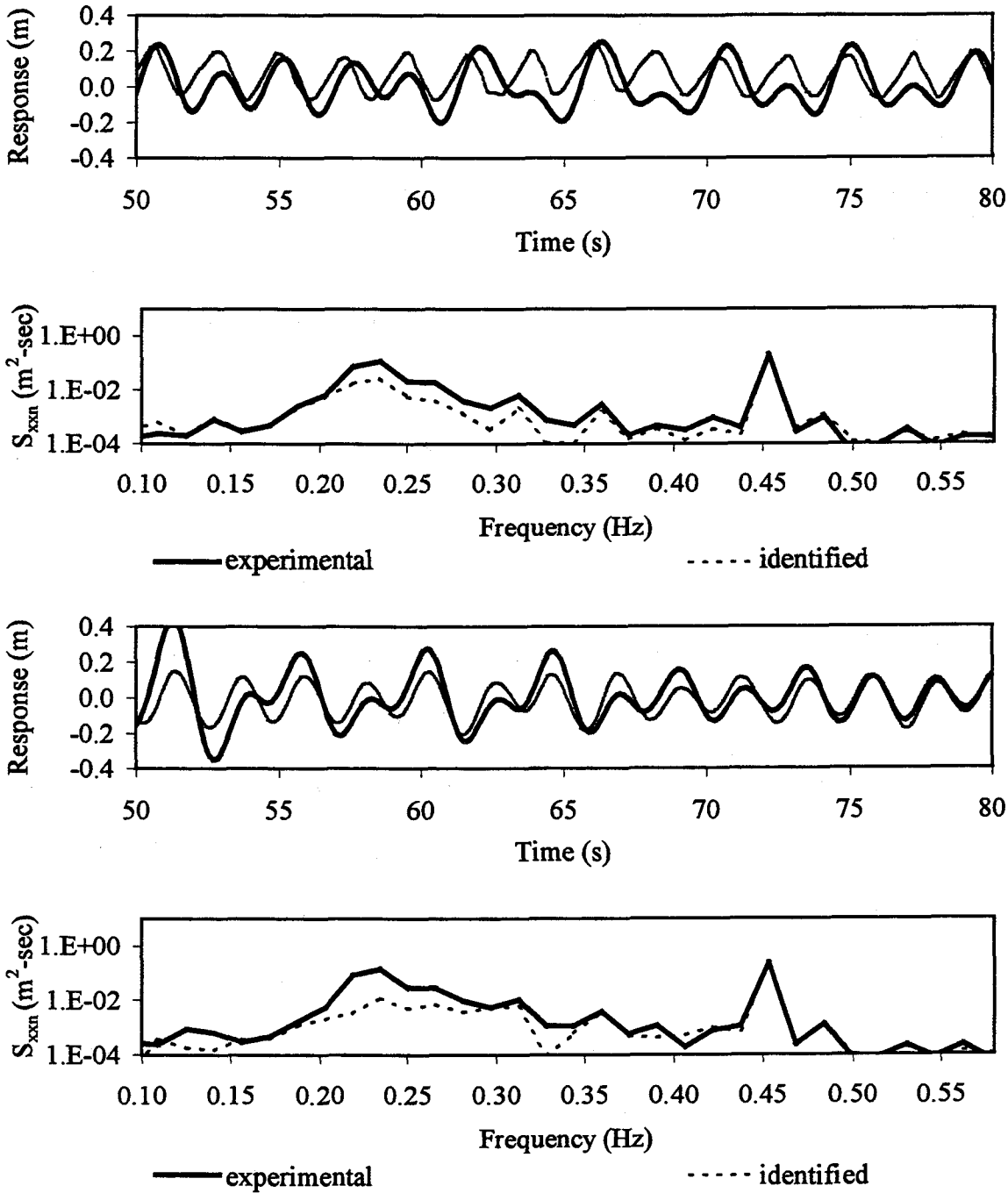

Fig.3.6 Comparison between identified and experimental response: a) (first) heave time series, b) (second) heave spectra, c) (third) surge time series, d) (fourth) surge spectra

The total number of samples of the excitation and response time histories for spectral simulations is 8192 (512 seconds), with sub-record lengths of 1024 and 50 % overlapping for the Fourier transforms.

A typical segment of the time series and the spectra of the entire record of wave and responses (surge and heave) for the data sets are given in Figs.3.7-8. The mean spectra, ML for ML1 and ML2 are also shown in Figs.3.7b, d and f. The input wave characteristics including wave height (H), Keulegan-Carpenter number (KC_F), Reynolds number (Re_F), C_m and C_d are given in Table 3.1a. The identified system parameters, a_1, a_2, a_3, b_1, b_3, c_{12}, c_{21}, ζ_1, ζ_3, $C_{d1,3}$ and $f_{n1,3}$ using the R-MI/SO technique are shown in Table 3.1b.

3.5.2 Sensitivity Analysis

As observed in Section 3.4, the parameters identified by R-MI/SO technique generate a response comparable with the experimental daa. In order to obtain an optimal range of system parameters, a sensitivity analysis is conducted. Each system parameter identified using the technique is varied for a range in specific increments while keeping all the other identified parameters constant (Table 3.1b) and the surge and heave responses are simulated for each variation by solving Eqs.3.1, 3 and 4. The results are compared against each other in both time and frequency domains. The optimal range and most suitable value of system parameters are tabulated in Table 3.2. The table shows that the best value for the system parameters remain the same for all the data, but MH has a restricted range compared to ML1 and ML2. For large values of system parameters, numerical instability is observed for MH using the experimental sampling time interval of 0.0625seconds, while solving the ordinary differential equations, Eqs.3.1, 3 and 4.

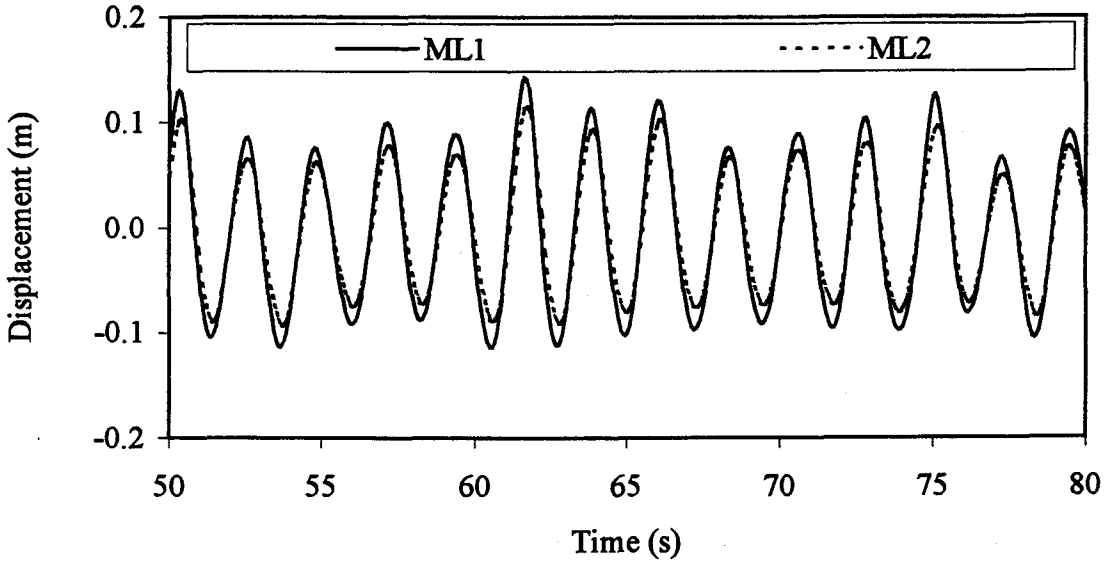

(a)

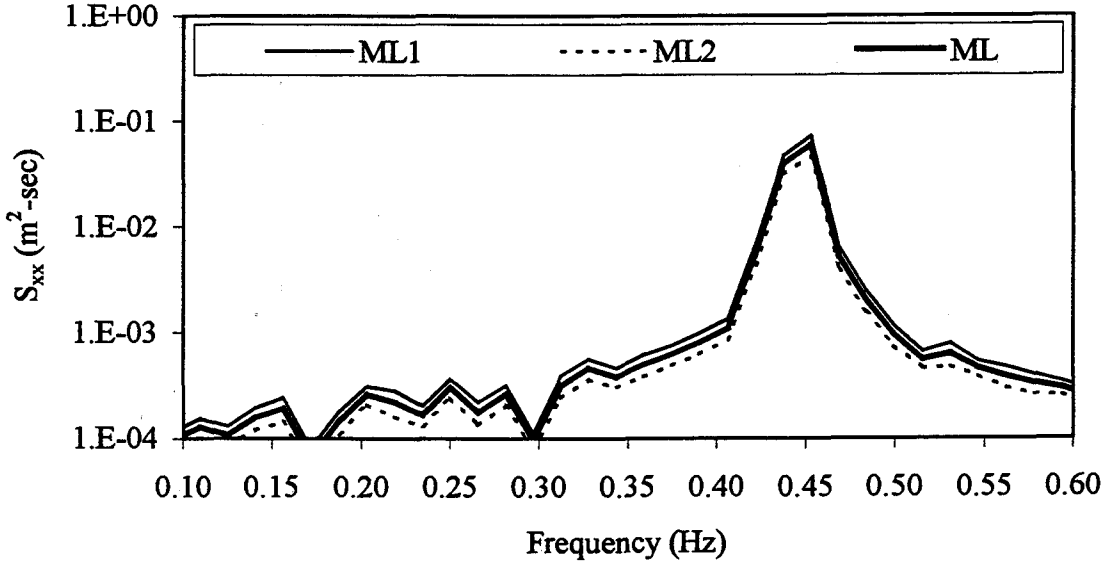

(b)

Fig.3.7 MDOF experimental data, ML1 and ML2: a) wave time series, b) wave spectra, c) heave time series, d) heave spectra, e) surge time series, f) surge spectra

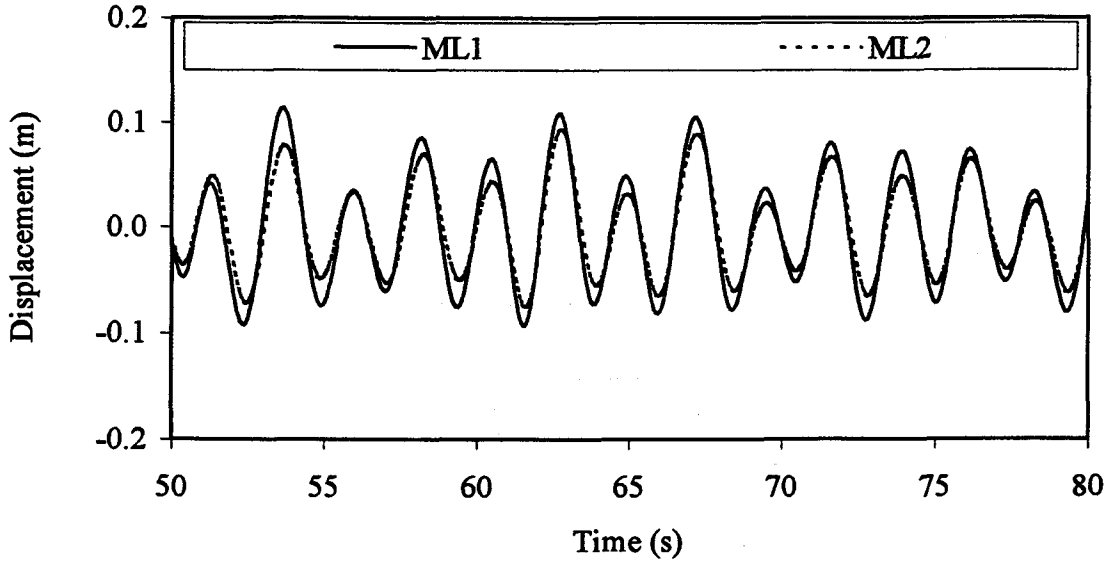

(c)

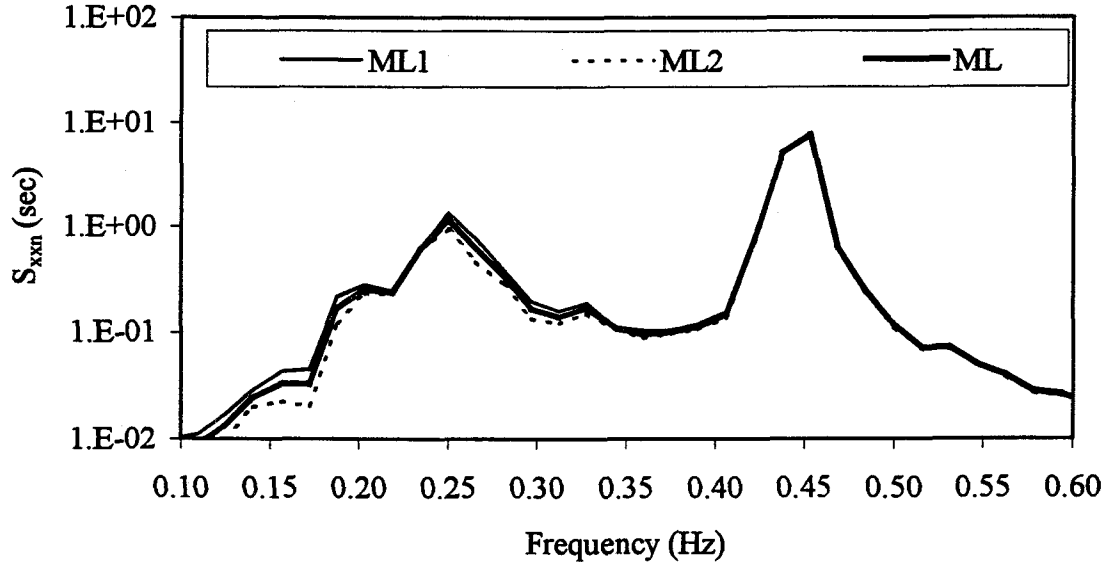

(d)

Fig.3.7 Continued

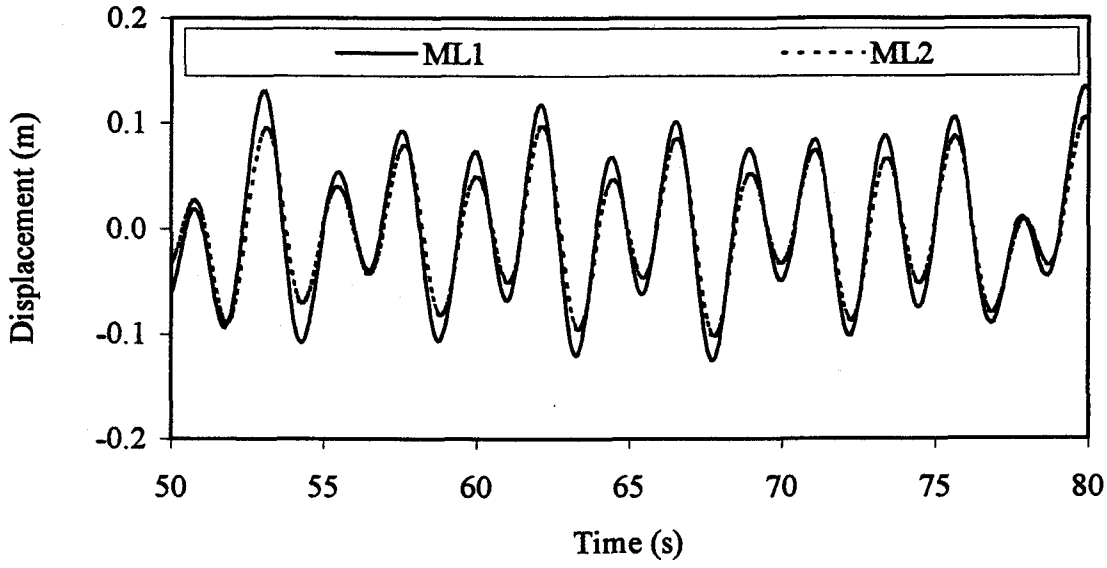

(e)

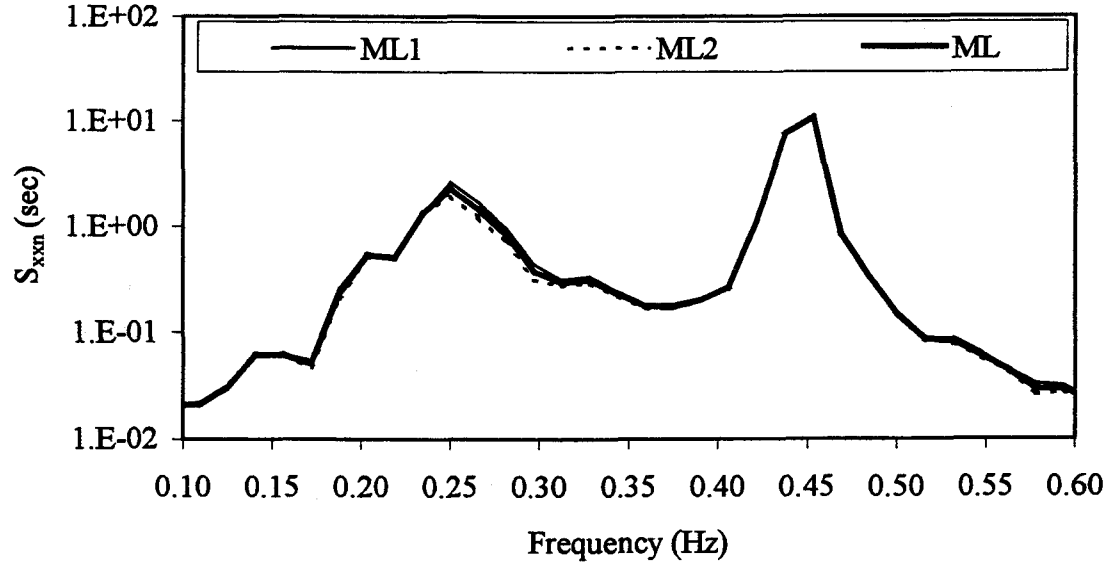

(f)

Fig.3.7 Continued

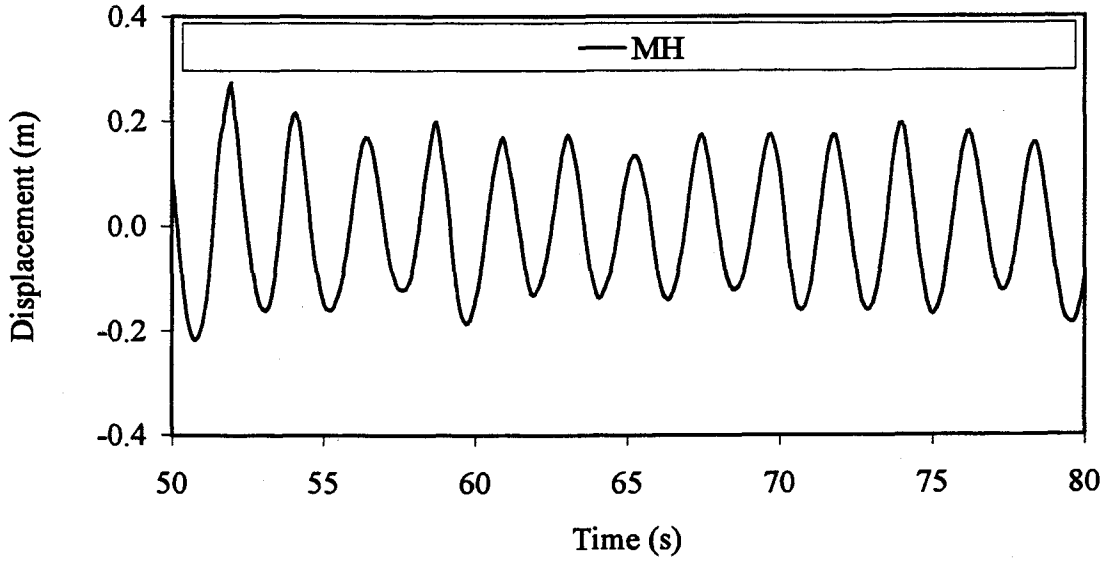

(a)

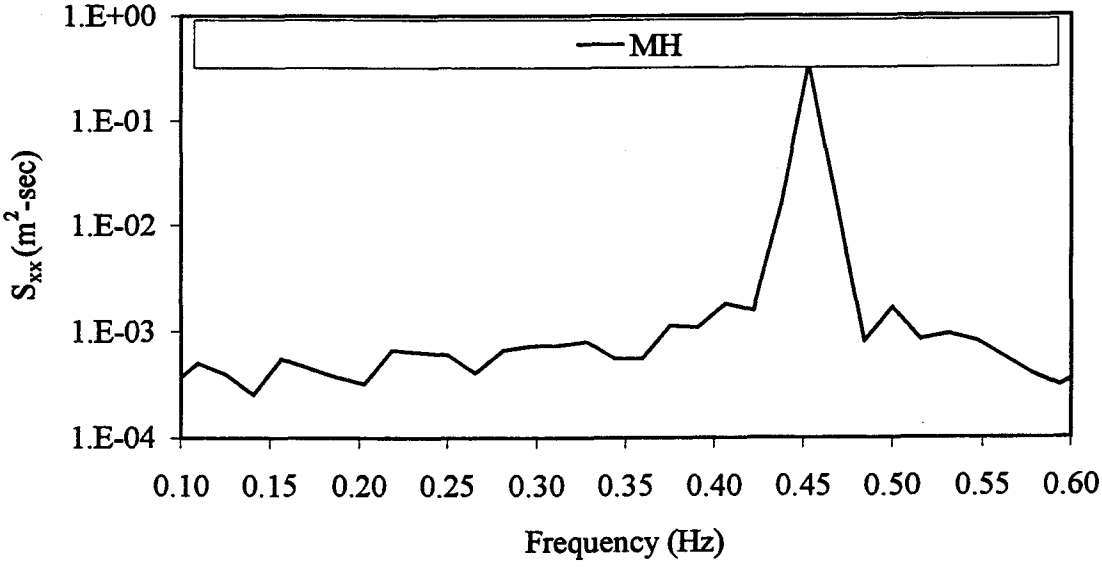

(b)

Fig.3.8 MDOF experimental data, MH: a) wave time series, b) wave spectra, c) heave time series, d) heave spectra, e) surge time series, f) surge spectra

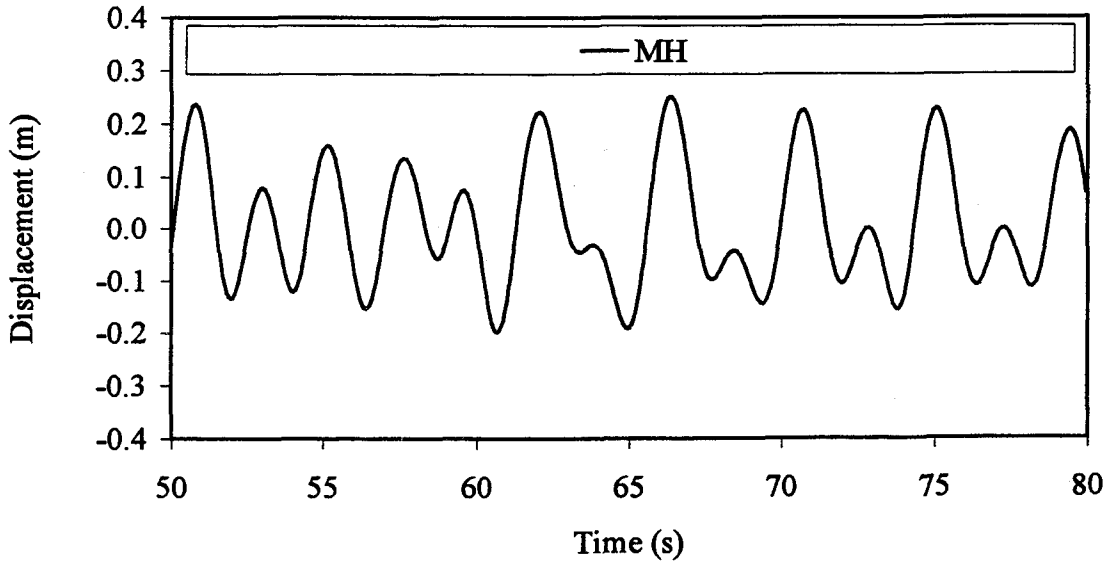

(c)

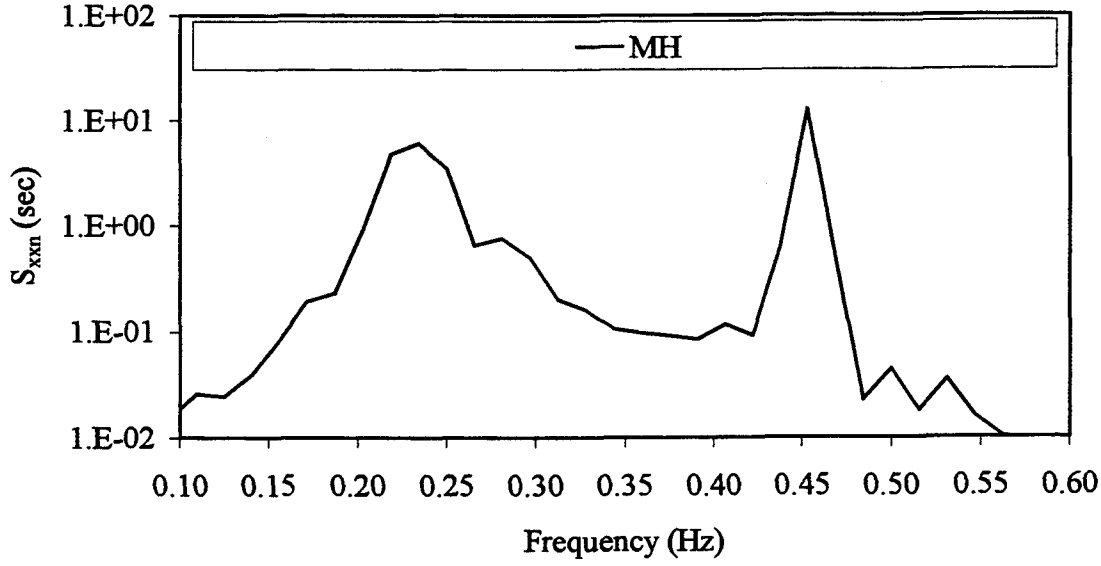

(d)

Fig.3.8 Continued

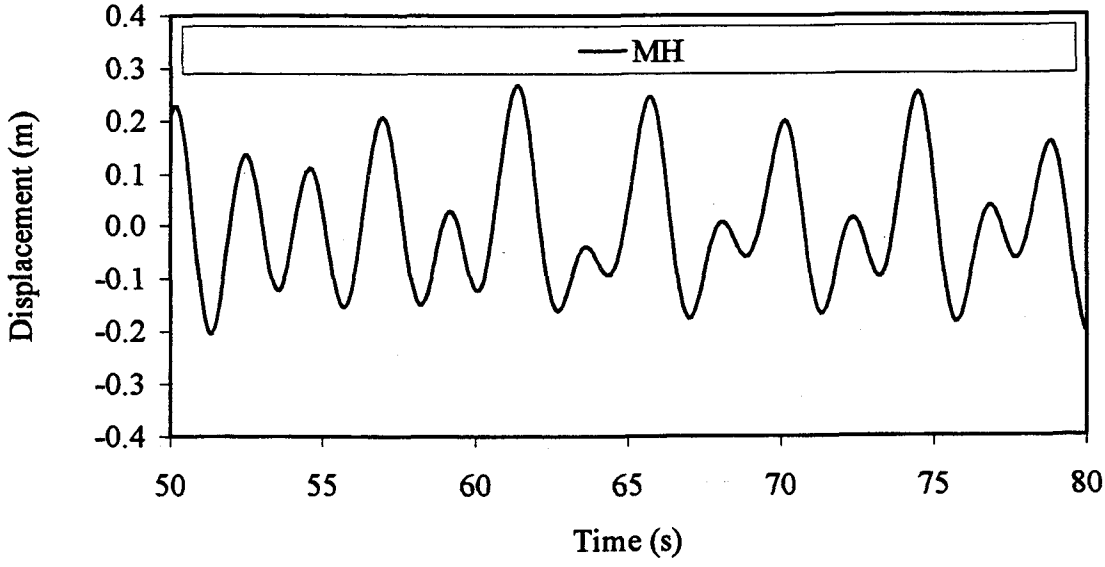

(e)

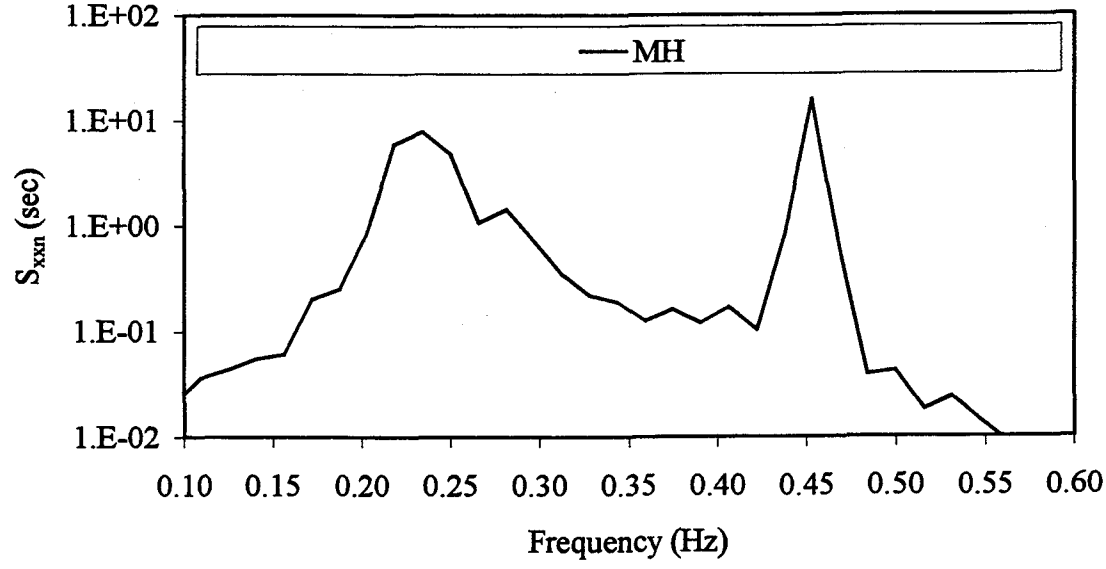

(f)

Fig.3.8 Continued

a)

Data	H (ft)	KC_F	Re_F	C_m	C_d
ML1	0.97	0.95	9.57e4	1.3	0.1- 0.9 (0.5)
ML2	0.77	0.76	7.70e4	1.3	0.1-0.9 (0.5)
ML3	1.57	1.54	1.57e5	1.2	0.1-0.9 (0.5)

b)

Data	a_1 lb/ft	a_2 lb/ft^2	a_3 lb/ft^3	b_1 lb/ft	b_3 lb/ft^3	c_{12} lb/ft^3	c_{21} lb/ft^3	$C_{d1,3}$	$\zeta_{1,3}$ %	$f_{n1,3}$ (Hz)
ML1	12.0	8.5	6.2	12.4	8.1	10.0	11.5	1.2	2.5	0.28
ML2	12.0	8.2	6.5	12.2	7.5	14.5	18.0	0.9	3.1	0.28
MH	12.5	7.2	6.1	12.0	5.1	12.2	12.5	0.5	3.2	0.29

Table 3.1 Characteristics of the MDOF subharmonic data: wave, b) identified system parameters (English units)

a)

Data	H (m)	KC_F	Re_F	C_m	C_d
ML1	0.29	0.95	9.57e4	1.3	0.1- 0.9 (0.5)
ML2	0.23	0.76	7.70e4	1.3	0.1-0.9 (0.5)
ML3	0.47	1.54	1.57e5	1.2	0.1-0.9 (0.5)

b)

Data	a_1 N/m	a_2 N/m^2	a_3 N/m^3	b_1 N/m	b_3 N/m^3	c_{12} N/m^3	c_{21} N/m^3	$C_{d1,3}$	$\zeta_{1,3}$ %	$f_{n1,3}$ (Hz)
ML1	173.9	405.7	972.4	180.3	1271.9	1568.1	1806.4	1.2	2.5	0.28
ML2	173.9	405.7	1020.7	177.1	1178.5	2273.3	2823.9	0.9	3.1	0.28
MH	180.3	344.5	956.3	173.9	801.8	1912.7	1961.0	0.5	3.2	0.29

Table 3.1 Characteristics of the MDOF subharmonic data: wave, b) identified system parameters (SI units)

Data	ML1	ML2	MH
a_1 (lb/ft)	10.8-13.2 (12.0)	10.7-13.5 (12.1)	10.8-13.2 (12.0)
a_2 (lb/ft^2)	5.5-8.5 (7.0)	5.4-8.7 (7.1)	6.8-7.0 (6.9)
a_3 (lb/ft^3)	1.1-11.1 (6.1)	1.0-11.0 (6.0)	5.5-6.5 (6.0)
b_1 (lb/ft)	10.8-13.2 (12.0)	10.8-14.2 (12.0)	11.5-12.5 (12.0)
b_3 (lb/ft^3)	1.0-8.0 (4.5)	1.0-8.0 (4.5)	4.4-5.0 (4.6)
c_{12} (lb/ft^3)	1.0-23.0 (12.0)	1.0-23.0 (12.0)	12.0-12.8 (12.4)
c_{21} (lb/ft^3)	1.0-23.0 (12.0)	1.0-23.0 (12.0)	12.0-12.7 (12.4)
$C_{d1,3}$	0.30-0.65 (0.43)	0.30-0.65 (0.43)	0.43-0.47 (0.45)
$\zeta_{1,3}$ (%)	1.0-4.0 (3.0)	1.0-4.0 (3.0)	2.8-3.2 (3.0)
$f_{n1,3}$ (Hz)	0.28	0.28	0.29

Table 3.2 Identified system parameters from the sensitivity analysis of the MDOF subharmonic data (English units)

Data	ML1	ML2	MH
a_1 (N/m)	157.8-193.2 (173.9)	154.6-196.4 (177.1)	157.8-189.9 (173.9)
a_2 (N/m^2)	264.0-405.7 (334.9)	8-12.8 (10.5)	328.4-334.9 (328.4)
a_3 (N/m^3)	157.8-1725.9 (940.2)	4.9-53.6 (29.2)	1806.4-1961.0 (1883.7)
b_1 (N/m)	157.8-189.0 (173.9)	4.9-6.4 (5.4)	167.4-183.5 (173.9)
b_3 (N/m^3)	157.8-1255.8 (705.2)	4.9-39 (21.8)	689.1-785.7 (721.3)
c_{12} (N/m^3)	157.8-3606.4 (1883.7)	4.9-112 (58.5)	1883.7-2009.3 (1944.9)
c_{21} (N/m^3)	157.8-3606.4 (1883.7)	4.9-112 (58.5)	1883.7-1993.2 (1944.9)
$C_{d1,3}$	0.30-0.65 (0.43)	0.30-0.65 (0.43)	0.43-0.47 (0.45)
$\zeta_{1,3}$ (%)	1.0-4.0 (3.0)	1.0-4.0 (3.0)	2.8-3.2 (3.0)
$f_{n1,3}$ (Hz)	0.28	0.28	0.29

Table 3.2 Identified system parameters from the sensitivity analysis of the MDOF subharmonic data (SI units)

By reducing the time step by one-fourth and interpolating the experimental wave data at the intermediate points, the numerical solution is found to be sufficiently accurate. The corresponding computer programs are attached in Appendix C.

The observations from the sensitivity analysis are summarized through spectral diagrams in the following paragraphs. Since the data sets ML1 and ML2 exhibit similar behavior, the mean of the resulting spectra for each variation is obtained and used for the comparison. Individual variations for ML1 and ML2 are given in Appendix B.

The effects of varying a_1 on heave and surge responses for ML and MH are presented in Fig.3.9. The spectral density normalized with the variance of the corresponding wave data (S_{xxn}) is plotted against frequency for a_1 from 4 to 15 lb/ft (58.0 to 217.4 N/m)or a1n (the ratio of instantaneous value of a_1 to the best value of a_1 as given in Table 3.2) from 0.33 to 1.25. The heave response does not change significantly for ML, whereas in the secondary resonance region, response increases with the increase in a_1 for MH. From the surge response behavior, it can be observed from Fig.3.9b and d that there is a slight increase in the primary resonance energy as a_1 increases. The subharmonic resonance region shifts towards the right as a_1 increases.

When a_2 is increased from 0 to 10 lb/ft^2 (0 to 476.6 N/m^2) or a2n from 0 to 1.25, the response in the secondary resonance region for heave and surge increases slightly for ML as given in Fig.3.10a and b. The effects are more pronounced for MH (Fig.3.10b and d). The primary resonance region is not affected by changing a_2. Fig.3.11 shows that increasing a_3 increases from 0 to 10 lb/ft^3 (0 to 1568.1 N/m^3) or a3n from 0 to 2.5, decreases the subharmonic response and the variation is more prominent for MH.

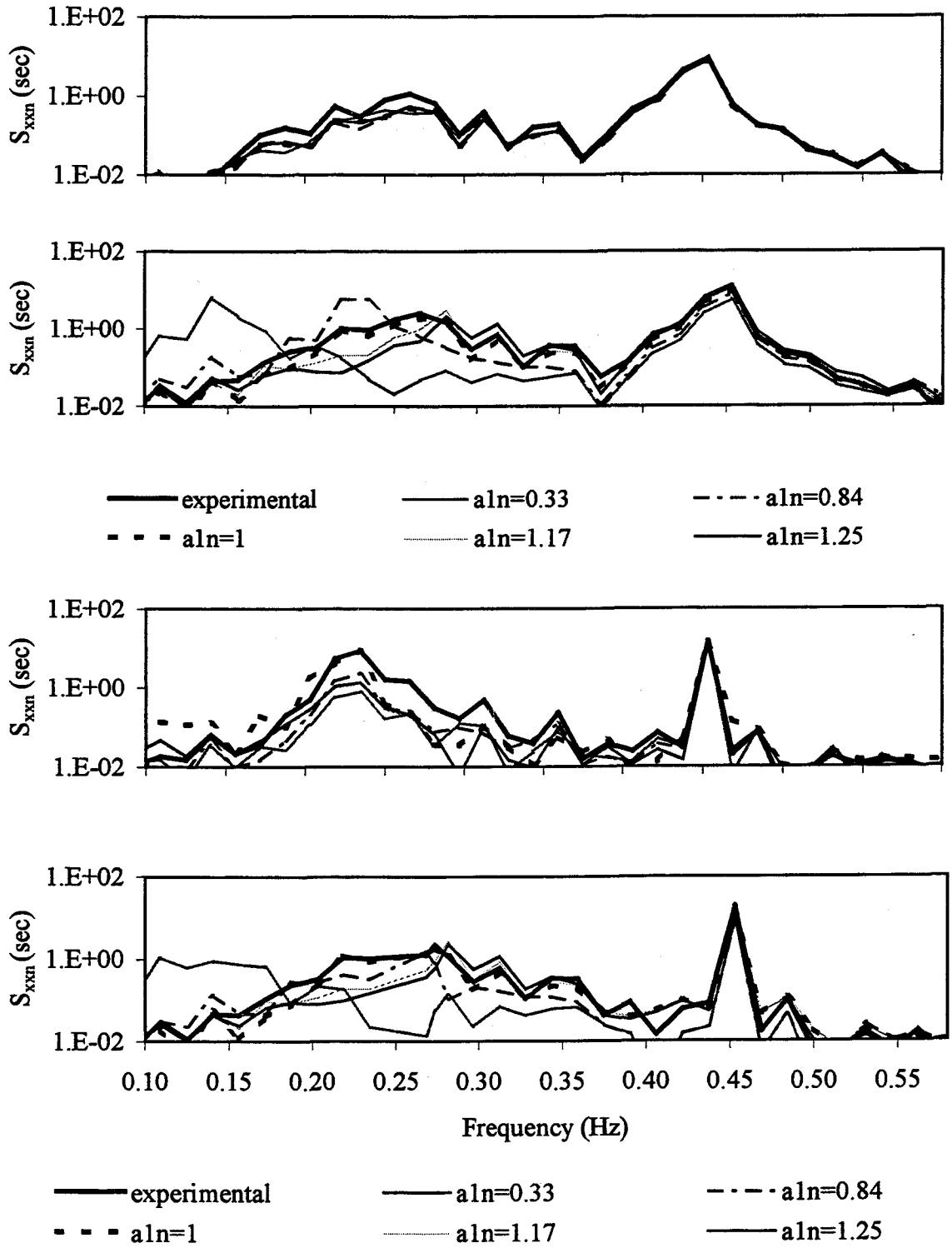

Fig.3.9 Effect of a_1 on MDOF system behavior: a) (first) MLH, b) (second) MLS, c) (third) MHH, d) (fourth) MHS

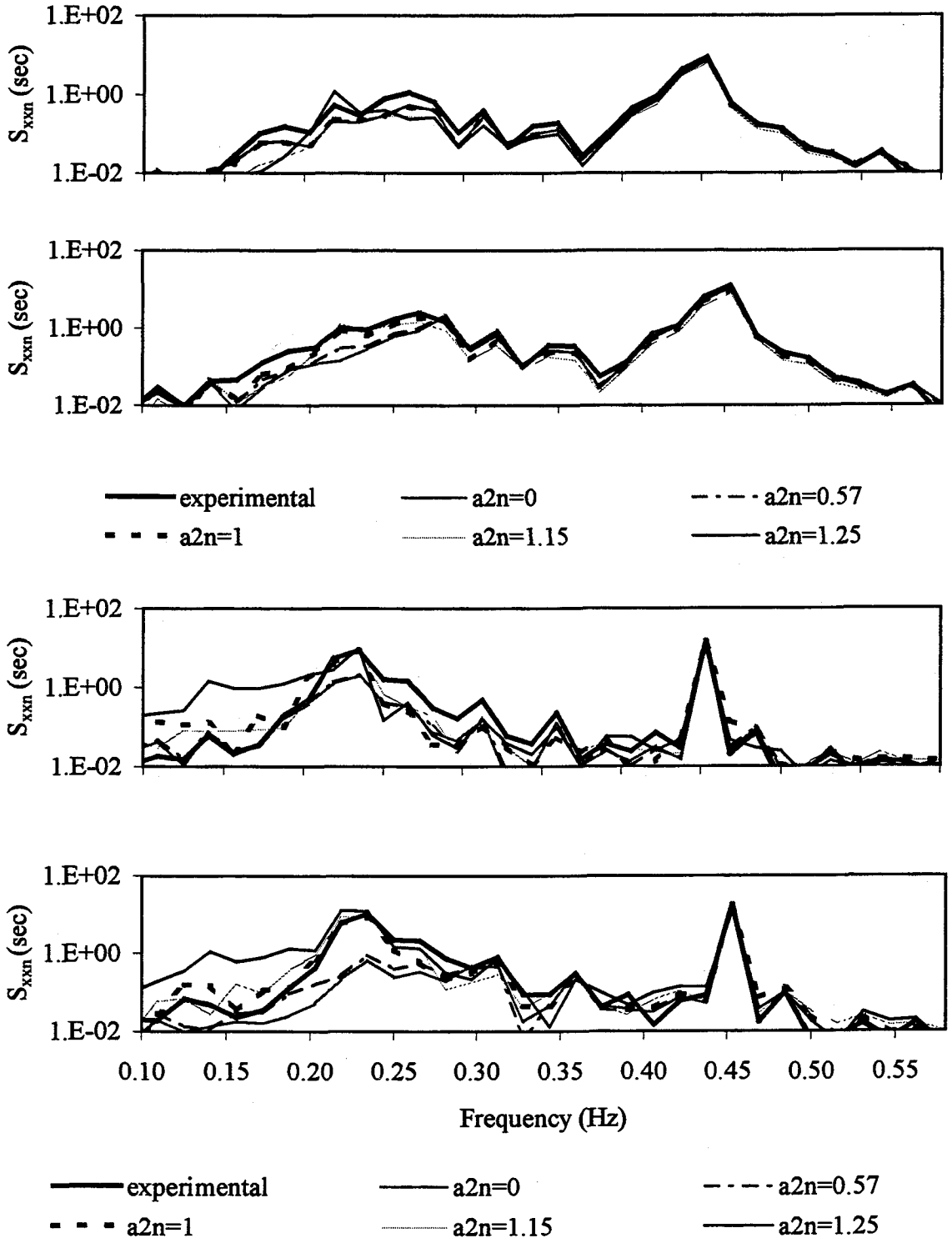

Fig.3.10 Effect of a_2 on MDOF system behavior: a) (first) MLH, b) (second) MLS, c) (third) MHH, d) (fourth) MHS

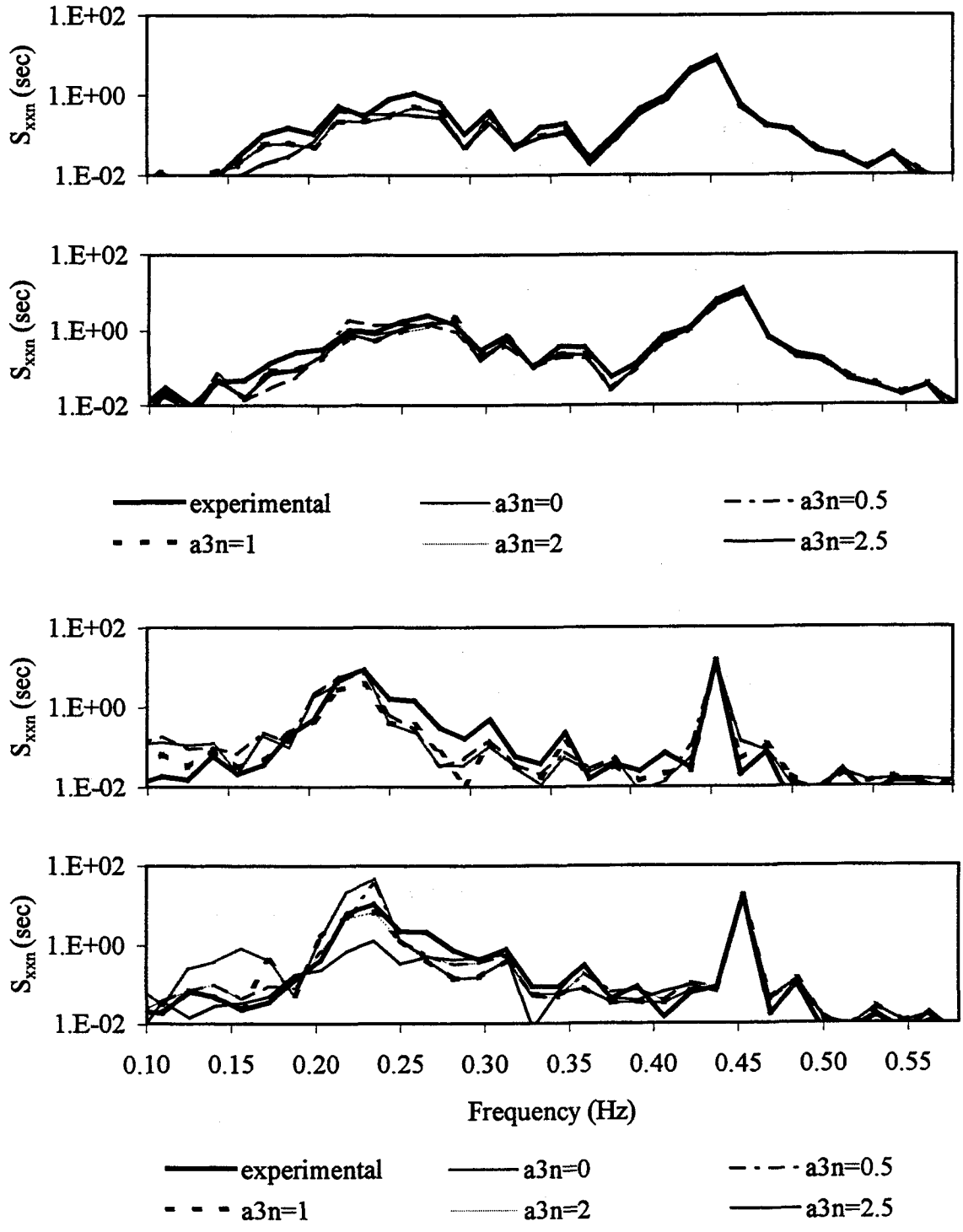

Fig.3.11 Effect of a_3 on MDOF system behavior: a) (first) MLH, b) (second) MLS, c) (third) MHH, d) (fourth) MHS

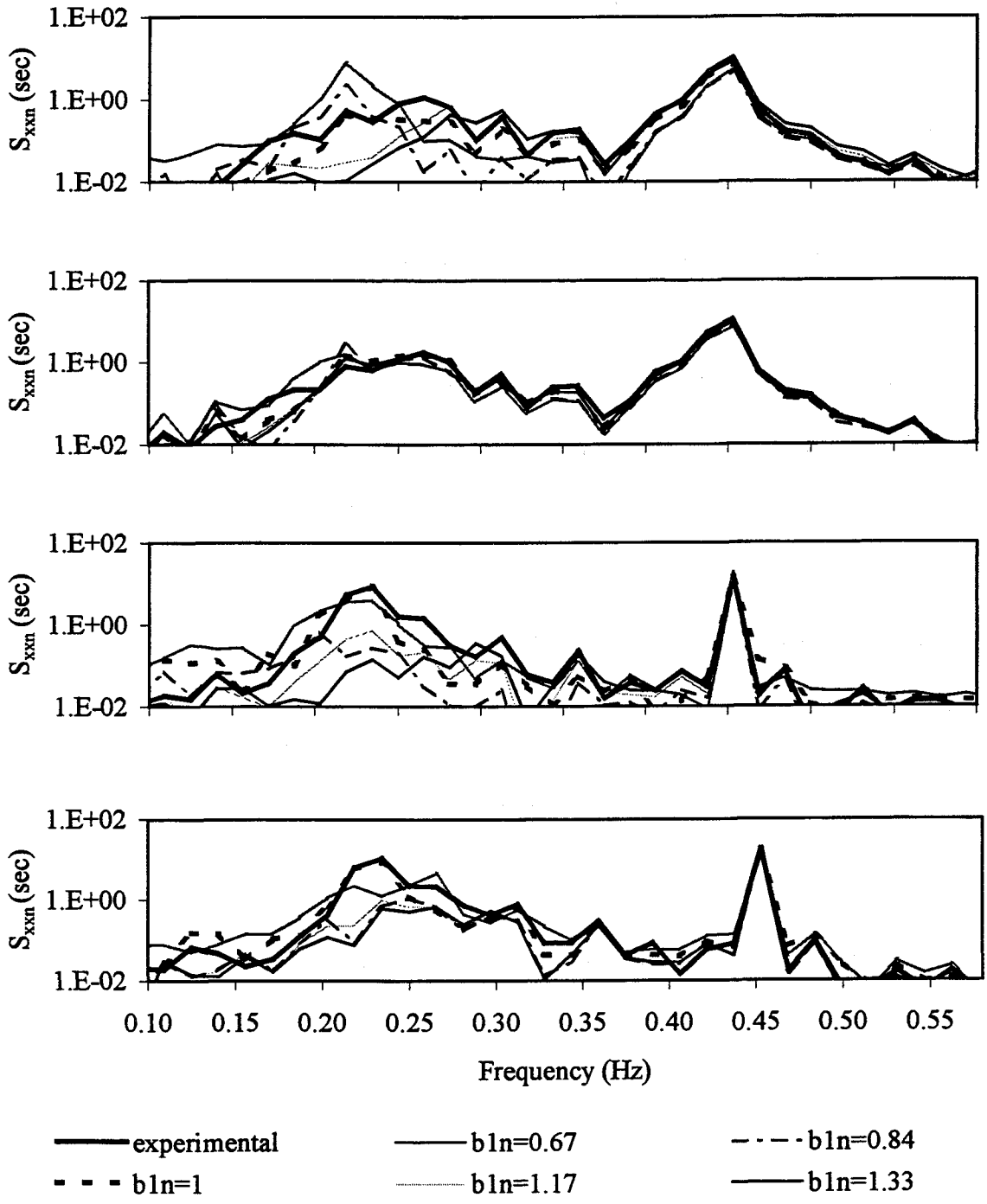

Fig.3.12 Effect of b_1 on MDOF system behavior: a) (first) MLH, b) (second) MLS, c) (third) MHH, d) (fourth) MHS

The effects of varying b_1 from 8 to 16 lb/ft (116.0 to 231.8 N/m) on the heave and surge responses for ML and MH are demonstrated in Fig.3.12. The surge response appears unaffected for ML, whereas the response in the secondary resonance region decreases with increasing a_1 for MH.

For the heave response, it can be observed from Fig.3.12b and d that the response in the primary resonance region increases and the subharmonic resonance region shift towards the right with increases in a_1. When b_3 is increased from 0 to 1.4 lb/ft^3 (0 to 219.6 N/m^3), the response in the secondary resonance region in heave and surge increases for ML and MH as given in Fig.3.13, where the effects are more pronounced for MH.

From Figs.3.14 and 15, it can be observed that by varying the coupled restoring force coefficient c_{12} and c_{21}, there is no significant effect on ML. For MH as shown in Figs.3.14-15 c and d, the response in the primary resonance region is not affected, but the secondary subharmonic response increases with increase in the coefficients.

By varying the linear structural damping coefficients ζ_1 and ζ_3 from 0 to 0.1, the subharmonic response decreases with increasing damping and the primary resonance region is not affected as demonstrated in Fig.3.17 and the effects are more noticeable for MH. A similar trend of decreasing subharmonic response with the increase in coefficients can be observed for C_{d1}' and C_{d3}' as shown in Fig.3.18 and 19.

3.5.3 Effects of KC and Re on Hydrodynamic Coefficients

From the optimal range and the most suitable value of KC_F, Re_F, C_m and C_d tabulated in Table 3.1a, it can be observed that the inertia coefficient C_m decreases with increasing KC_F and Re_F, but varying C_d has no effect on the response.

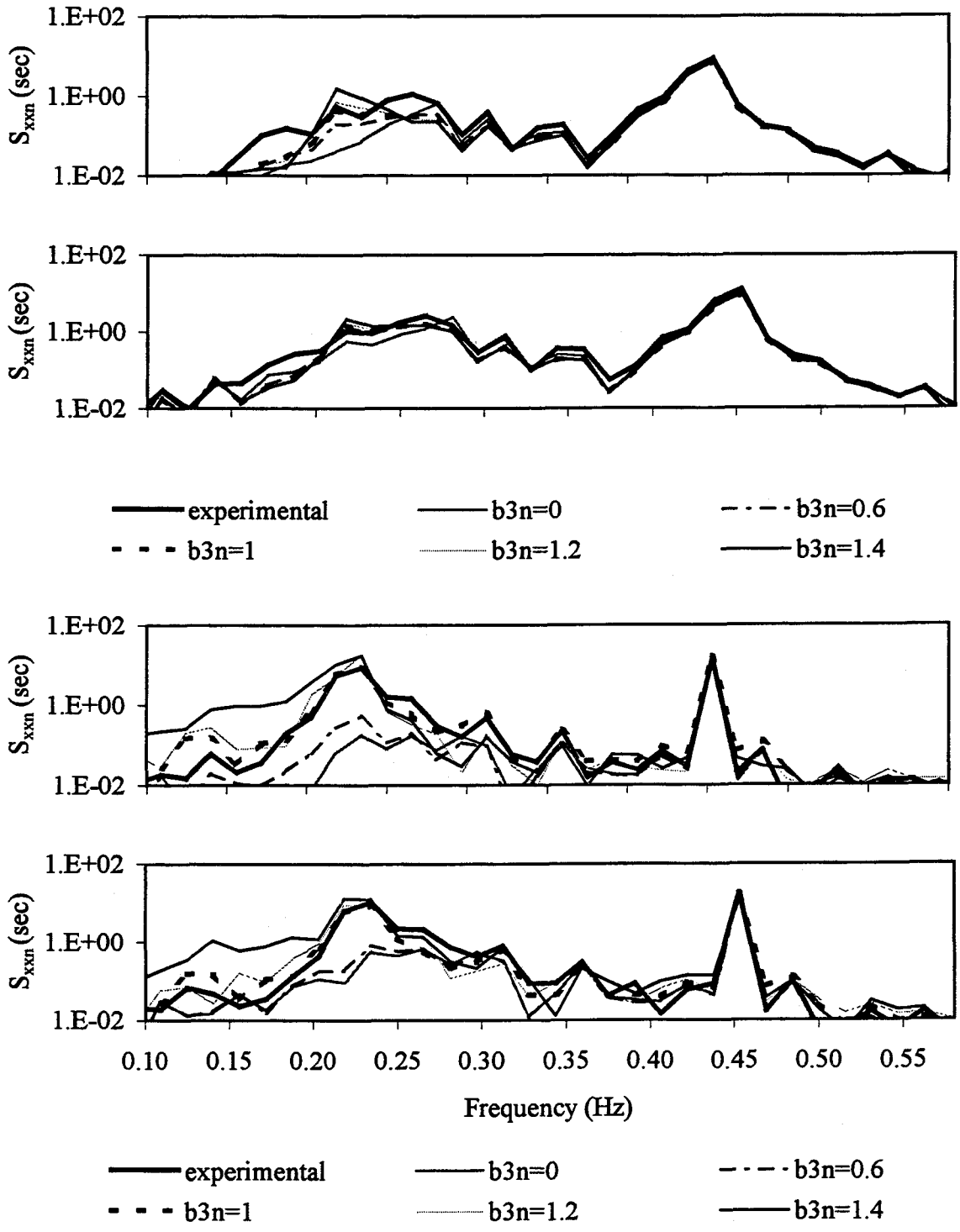

Fig.3.13 Effect of b_3 on MDOF system behavior: a) (first) MLH, b) (second) MLS, c) (third) MHH, d) (fourth) MHS

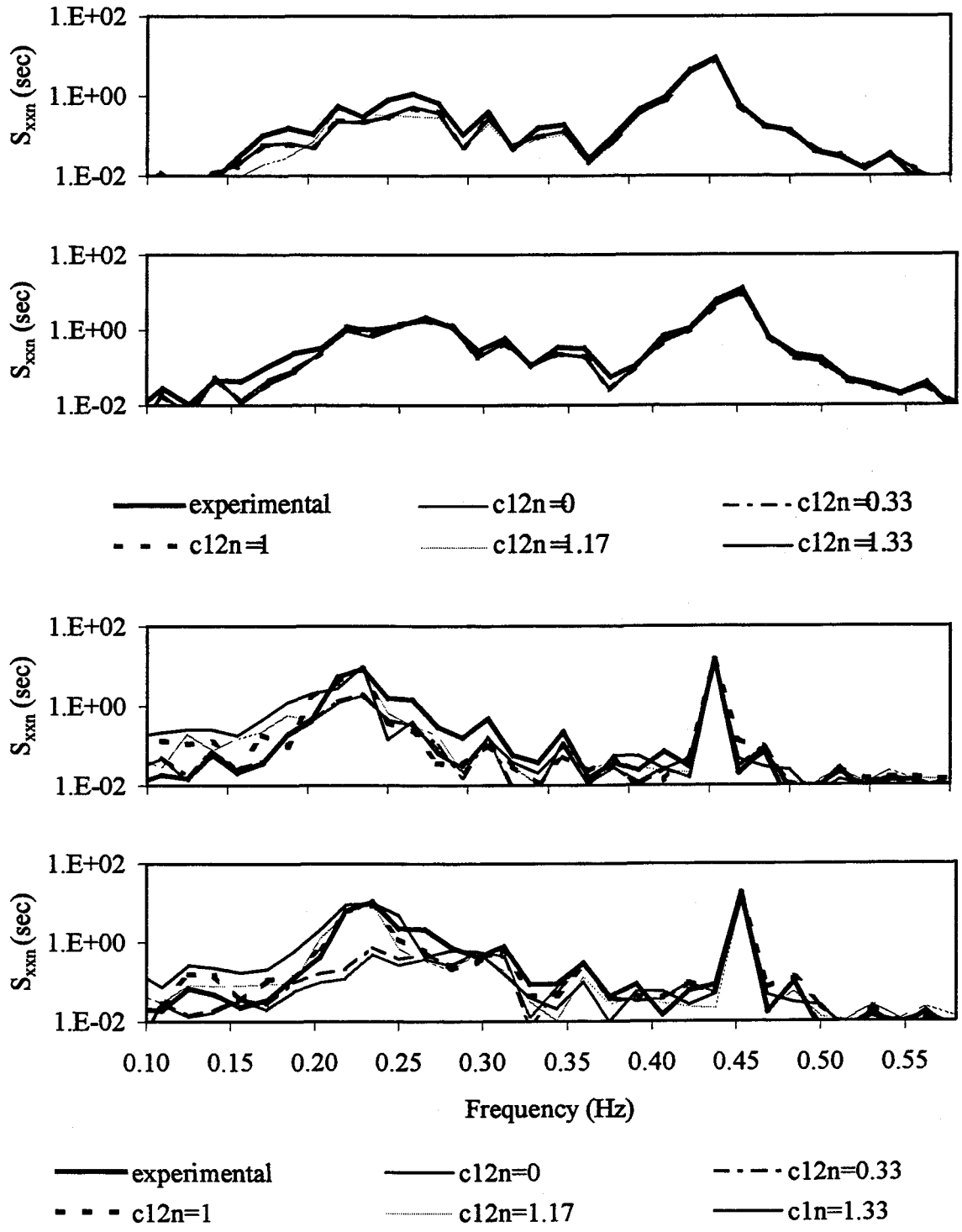

Fig.3.14 Effect of c_{12} on MDOF system behavior: a) (first) MLH, b) (second) MLS, c) (third) MHH, d) (fourth) MHS

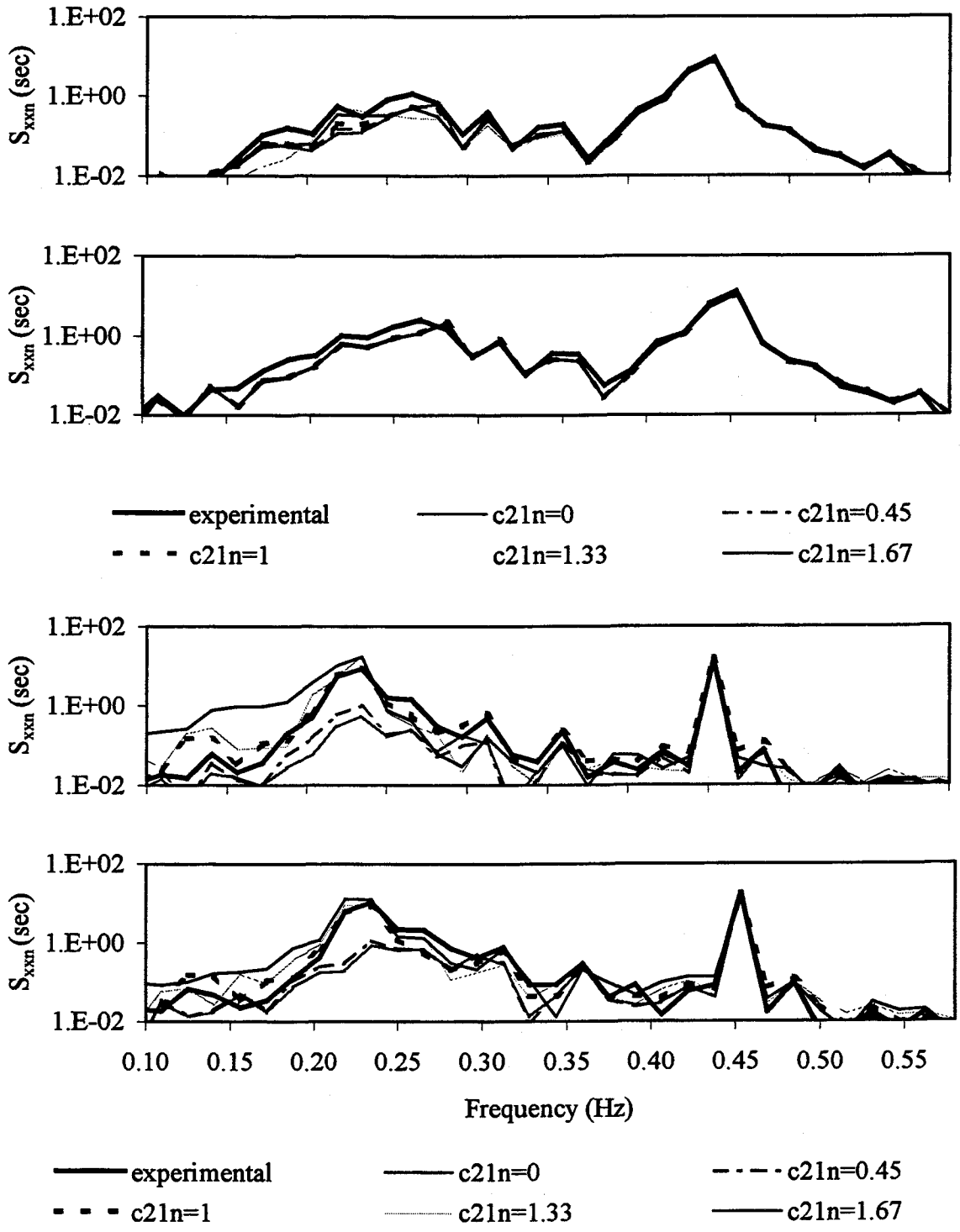

Fig.3.15 Effect of c_{21} on MDOF system behavior: a) (first) MLH, b) (second) MLS, c) (third) MHH, d) (fourth) MHS

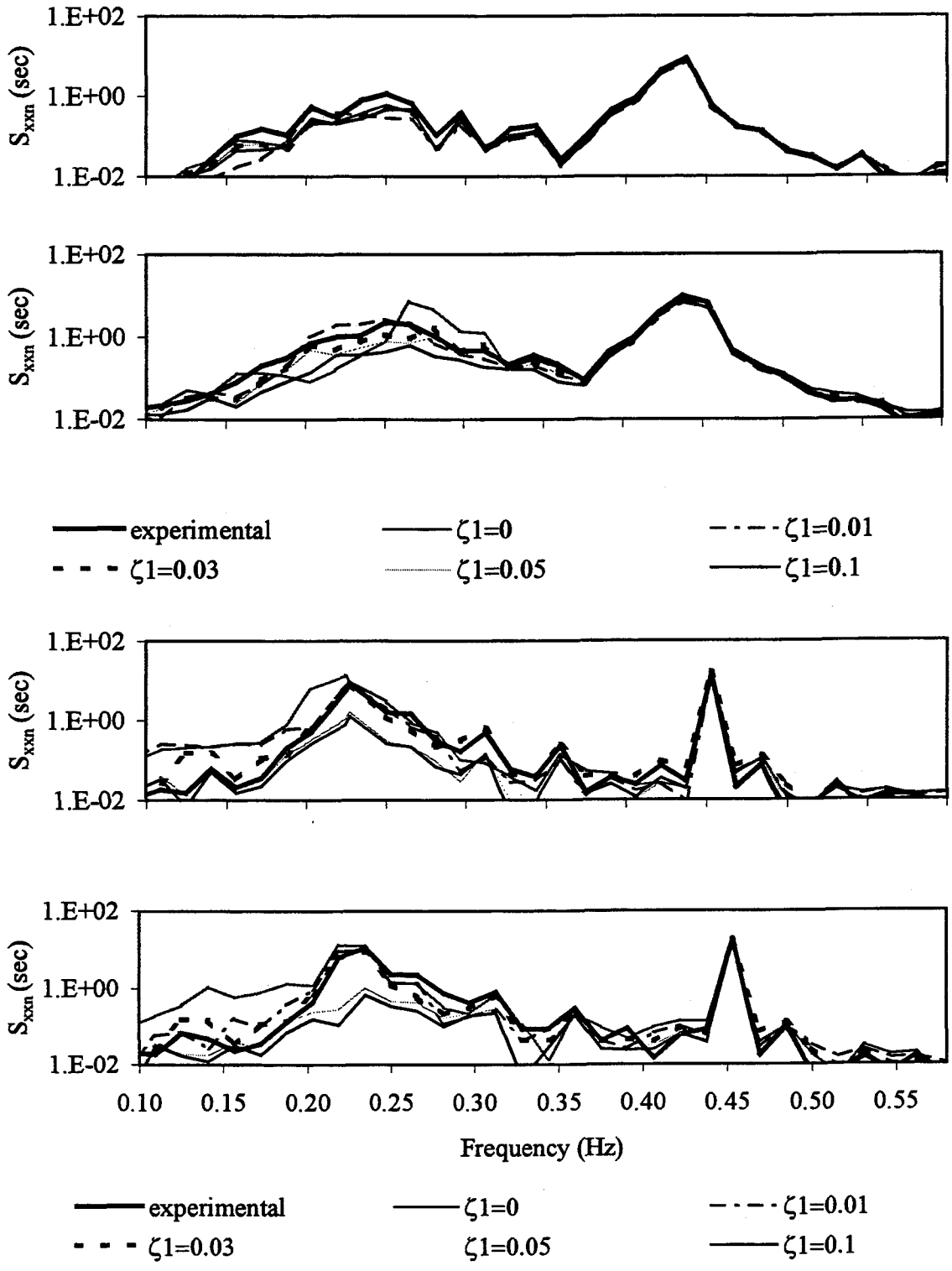

Fig.3.16 Effect of ζ_1 on MDOF system behavior: a) (first) MLH, b) (second) MHH, c) (third) MLS, d) (fourth) MHS

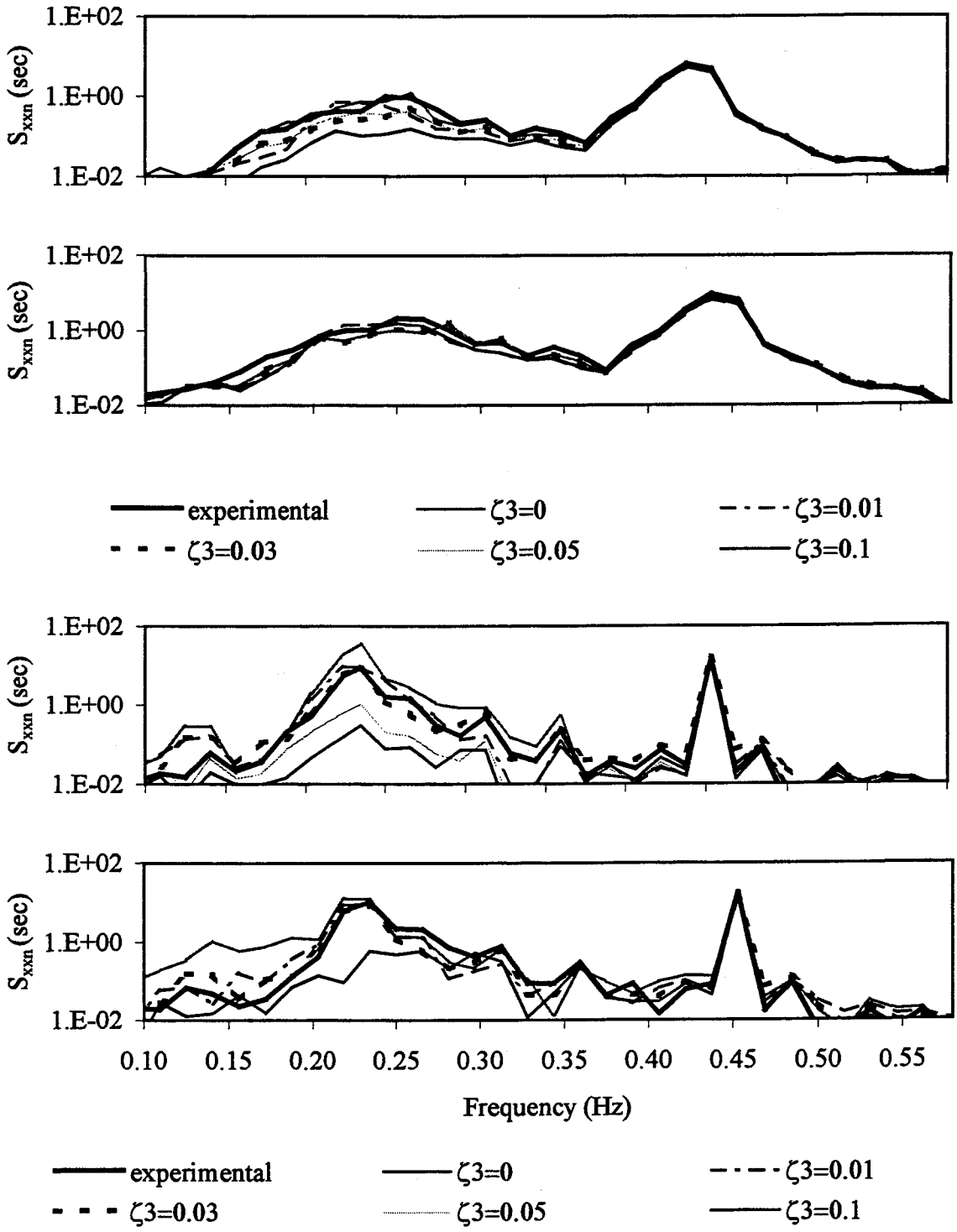

Fig.3.17 Effect of ζ_3 on MDOF system behavior: a) (first) MLH, b) (second) MHH, c) (third) MLS, d) (fourth) MHS

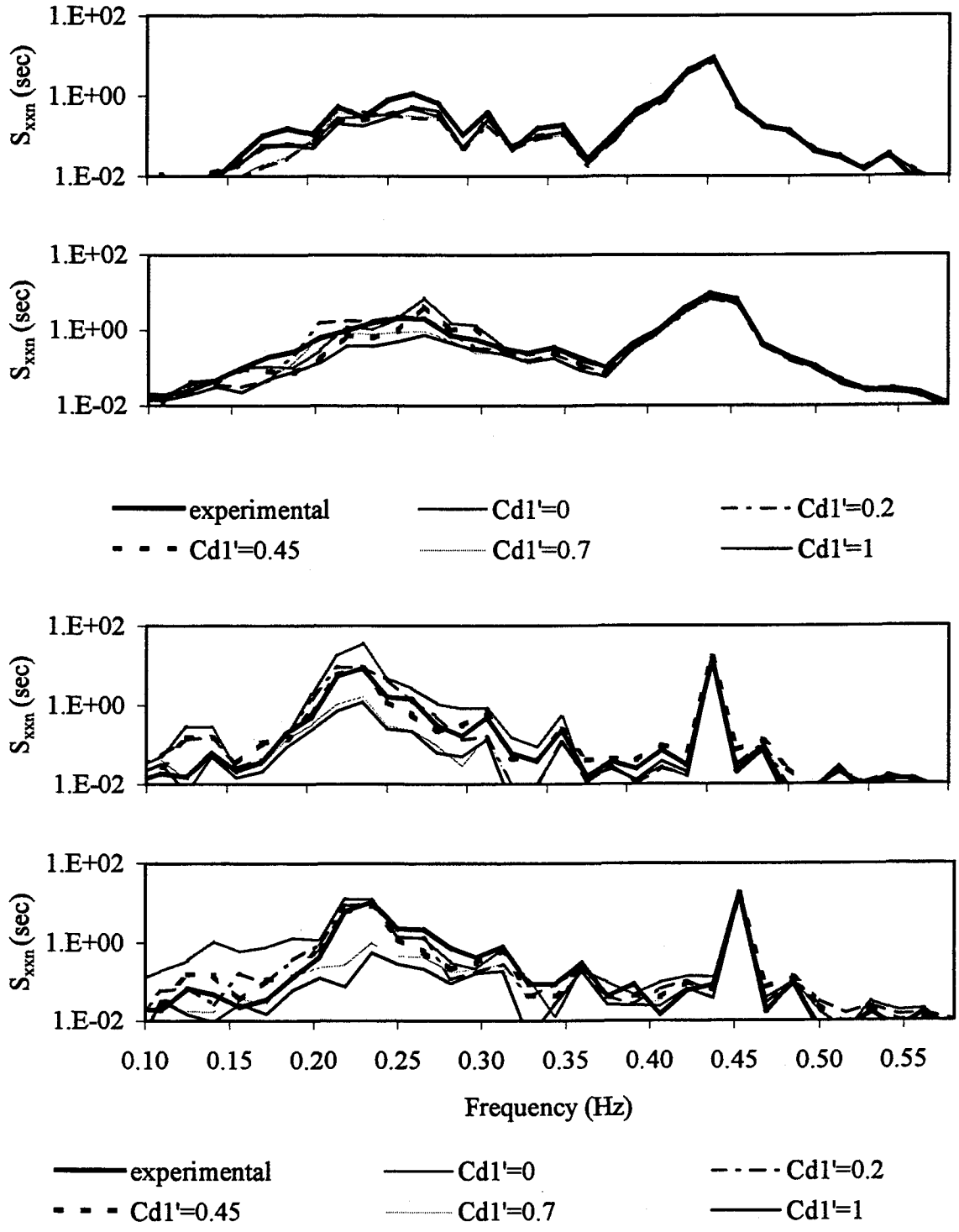

Fig.3.18 Effect of C_{d1}' on MDOF system behavior: a) (first) MLH, b) (second) MHH, c) (third) MLS ,d) (fourth) MHS

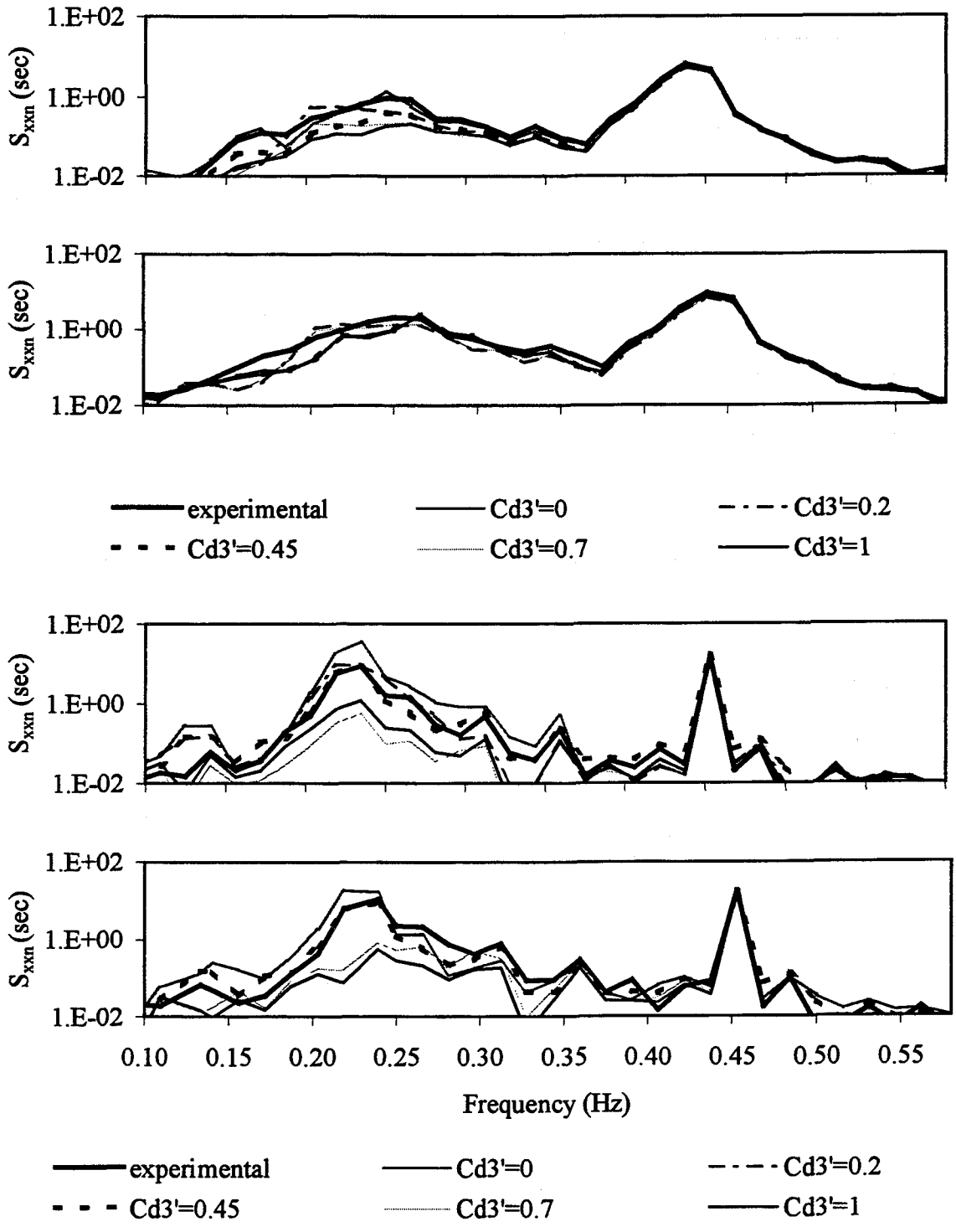

Fig.3.19 Effect of C_{d3}' on MDOF system behavior: a) (first) MLH, b) (second) MHH, c) (third) MLS, d) (fourth) MHS

3.6 SDOF System Response Behavior

3.6.1 Time Series and Spectra

Eight tests were performed on the SDOF configuration using periodic excitation with white noise perturbations (Yim *et al* 1993). Each of the tests displayed a certain degree of subharmonics in the sphere movement. The data sets SL1, SL2, SM1, SM2, SM3, SH1, SH2 and SH3 are grouped according to wave excitation amplitudes, where 'S' stands for single-degree-freedom, and 'L', 'M' and 'H' represents low, medium and high wave amplitudes, respectively. The wave time series (a typical segment) and spectra, response time series (a typical segment) and spectra for all the data sets grouped are given in Figs.3.20-22. The mean spectra for the three groups, SL, SM and SH are also shown in the figures and are considered to be representative of each group.

All the experimental data have wave period, T = 2 seconds and they vary in their wave heights and noise/signal ratio. The input wave characteristics such as wave height (H), C_m, C_d, Keulegan Carpenter number (KC_F) and Reynolds number (Re_F) are shown in the Table 3.3a. The system parameters, a_1, a_2, a_3, ζ_1 and C_{d1}' identified using the R-MI/SO technique are given in Table 3.3b.

3.6.2 Sensitivity Analysis

A sensitivity analysis is performed to determine the optimal range of the system parameters. Each parameter is varied in specific increments while keeping all the other identified parameters constant (Table 3.3b) and the surge and heave responses are simulated for each variation by solving Eqs.3.1, 3 and 4. The simulated responses using the identified parameters are compared against each other in both the time and frequency domains.

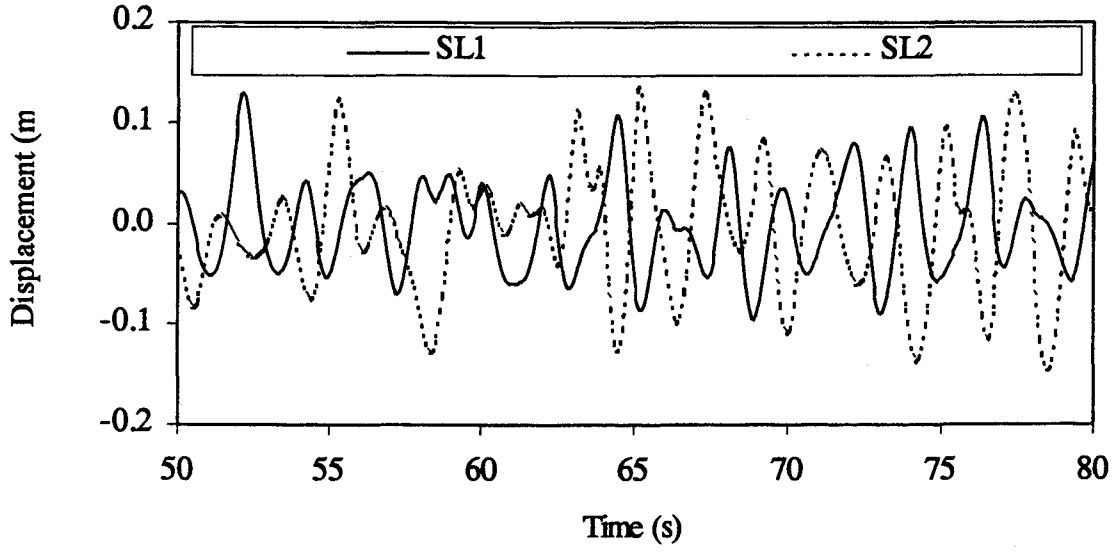

(a)

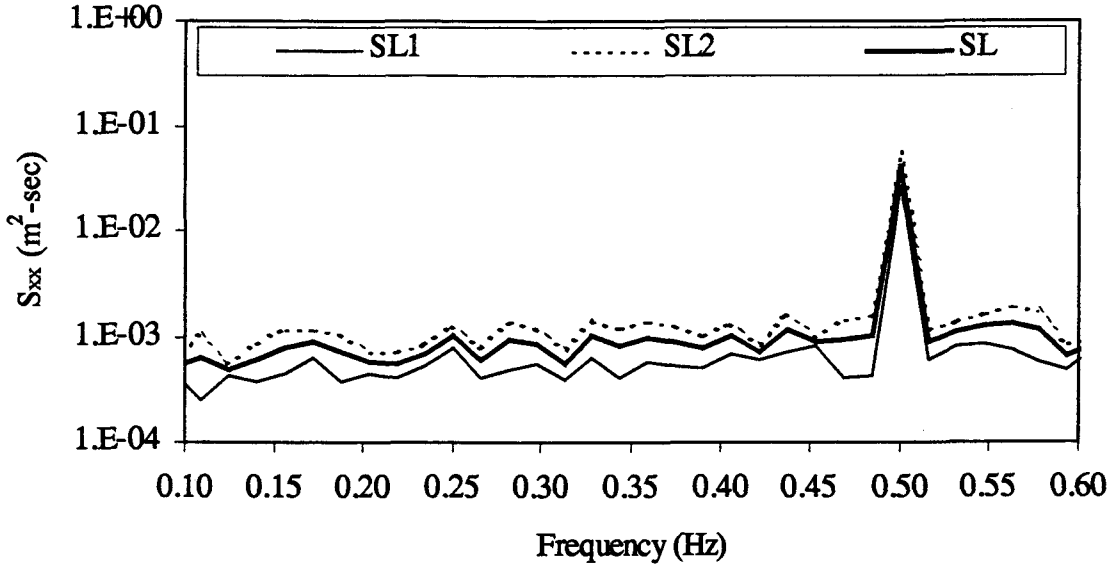

(b)

Fig.3.20 SDOF experimental low wave amplitude data: a) wave time series, b) wave spectra, c) response time series, d) response spectra

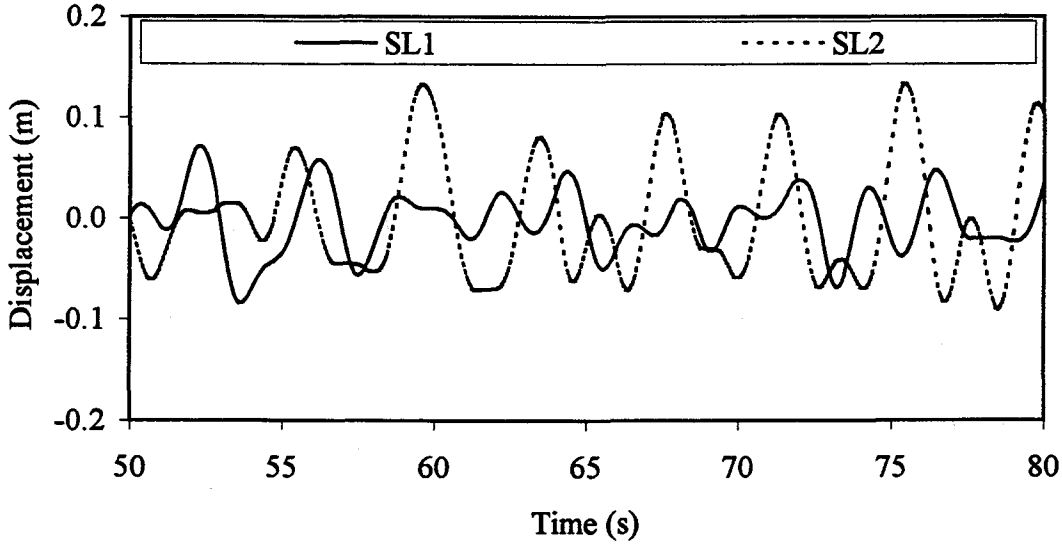

(c)

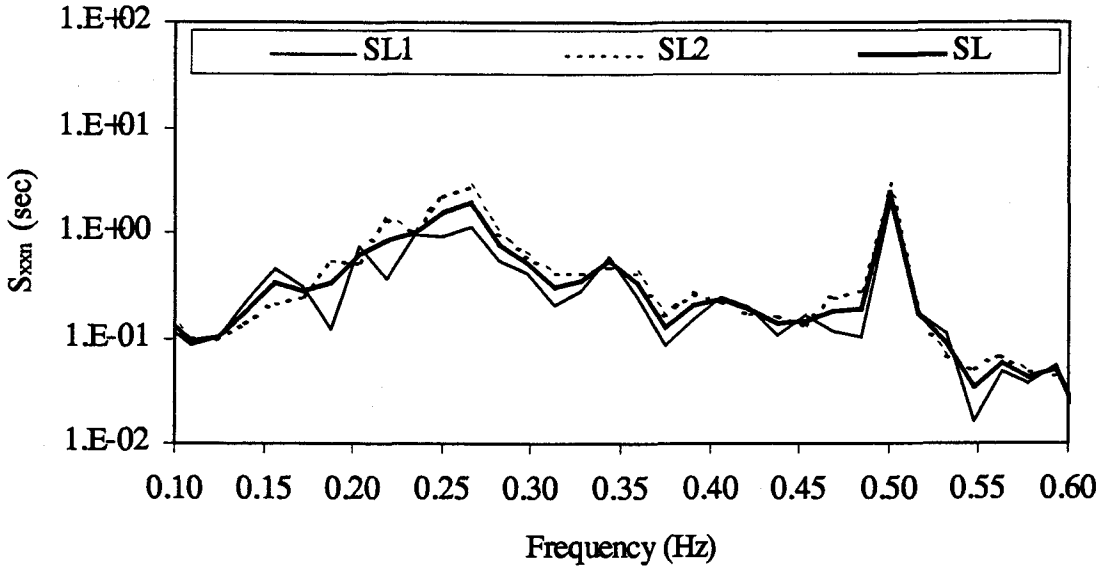

(d)

Fig.3.20 Continued

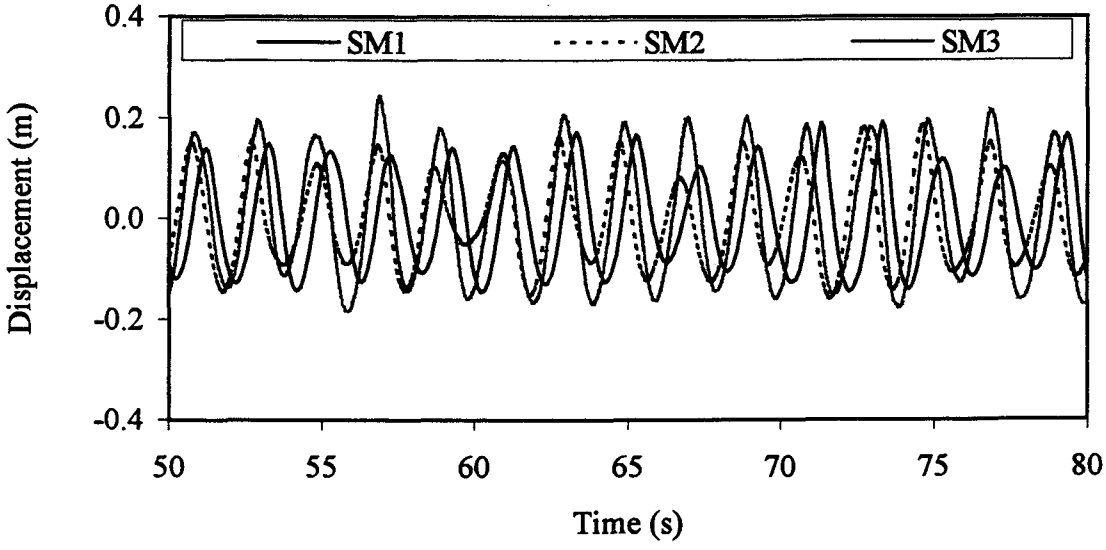

(a)

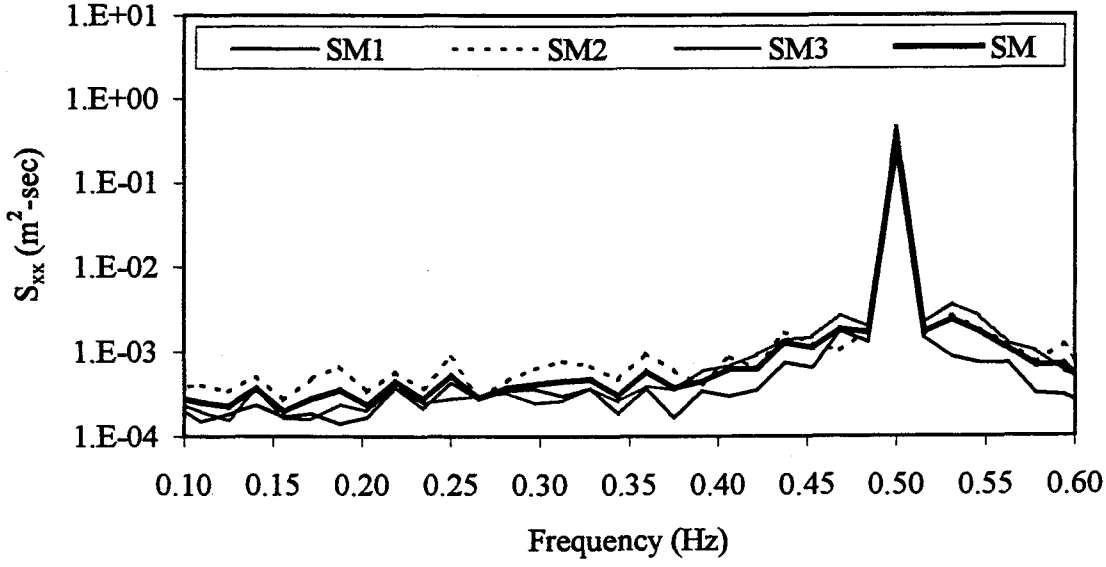

(b)

Fig.3.21 SDOF experimental medium wave amplitude data: a) wave time series, b) wave spectra, c) response time series, d) response spectra

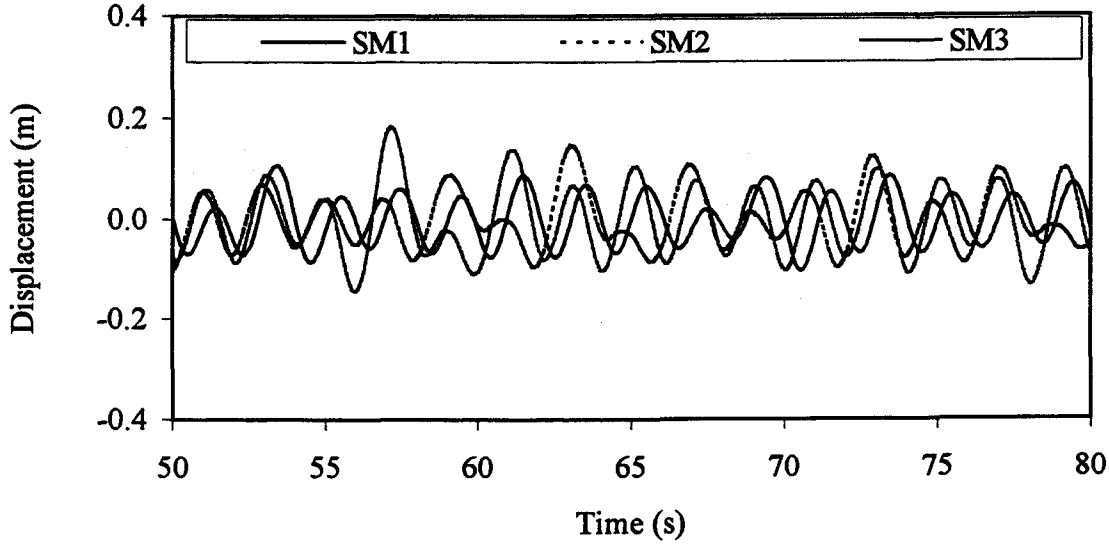

(c)

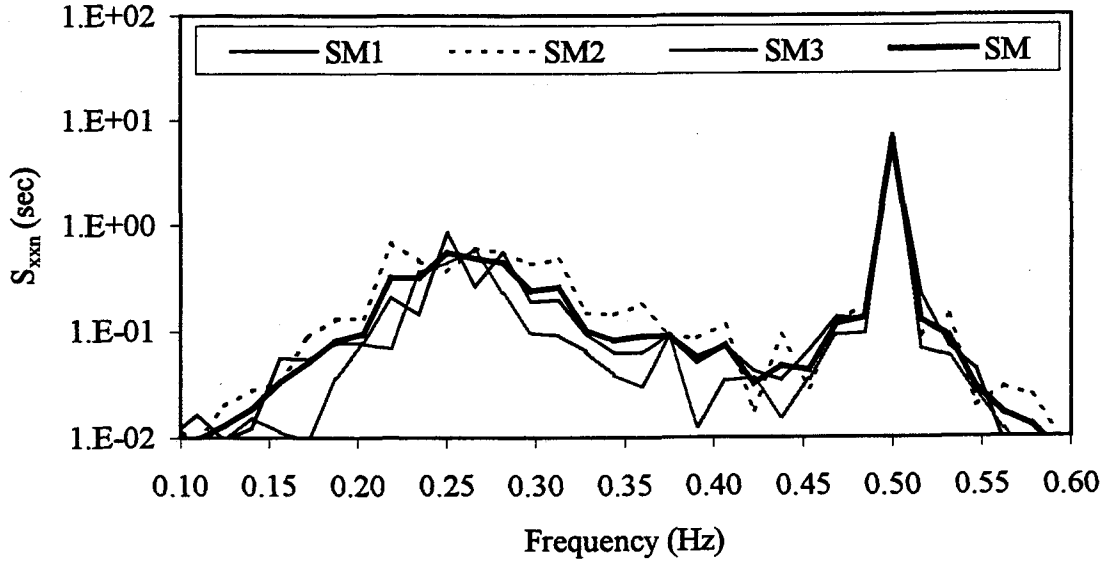

(d)

Fig.3.21 Continued

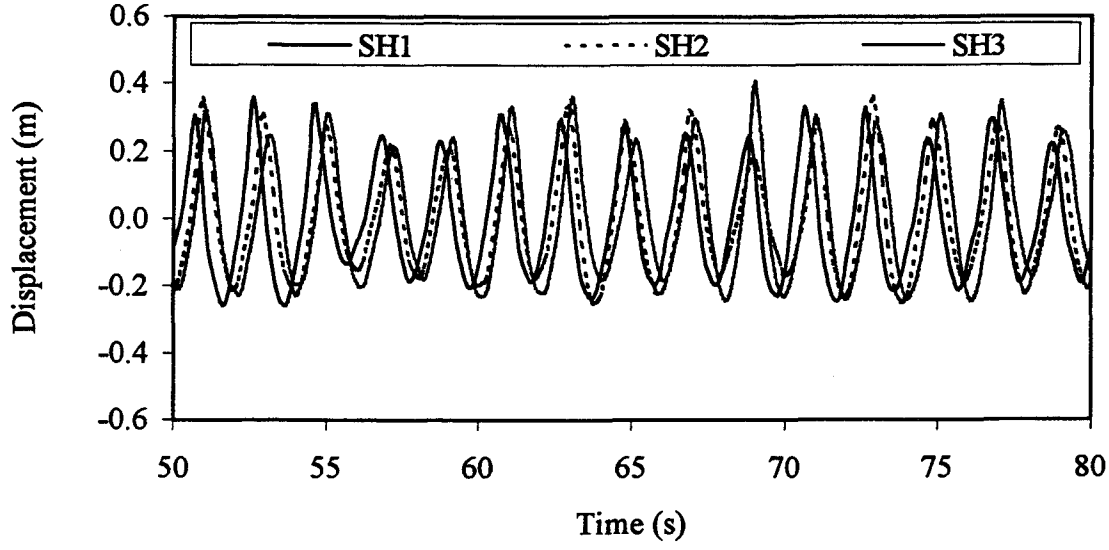

(a)

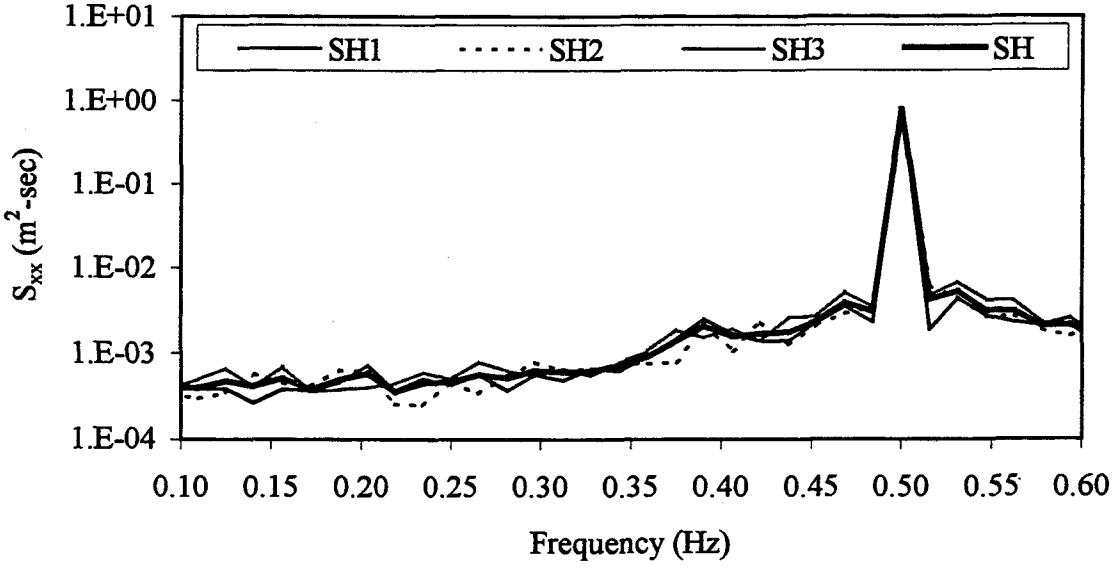

(b)

Fig.3.22 SDOF experimental high wave amplitude data: a) wave time series, b) wave spectra, c) response time series, d) response spectra

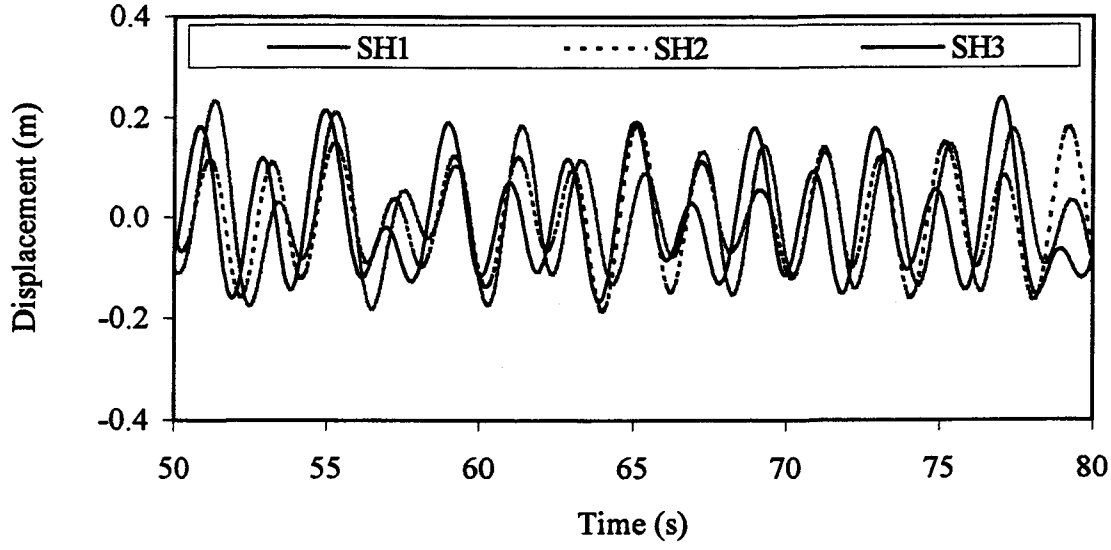

(c)

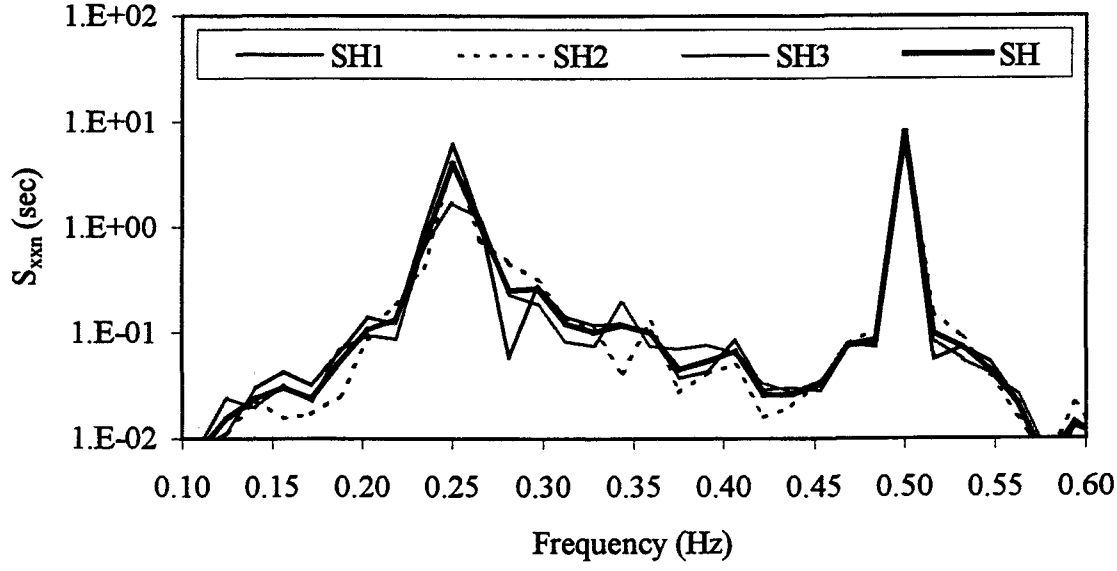

(d)

Fig.3.22 Continued

Data	H (ft)	C_m	C_d	KC_F	Re_F
SL1	0.57	1.4	0.1- 0.9 (0.5)	0.56	5.7045
SL2	0.8	1.4	0.1-0.9 (0.5)	0.79	7.80E4
SM1	1.2	1.3	0.1-0.9 (0.5)	1.18	1.20E5
SM2	1.2	1.3	0.1- 0.9 (0.5)	1.18	1.20E5
SM3	1.6	1.3	0.1-0.9 (0.5)	1.57	1.60E5
SH1	2.2	1.1	0.1-0.9 (0.5)	2.16	2.20E5
SH2	2.2	1.1	0.1-0.9 (0.5)	2.18	2.22E5
SH3	2.2	1.1	0.1-0.9 (0.5)	2.20	2.30E5

Data	a_1 (lb/ft)	a_2 (lb/ft^2)	a_3 (lb/ft^3)	C_{d1}	ζ_1 (%)	f_{n1} (Hz)
SL1	8.8	6.6	4.6	2.5	3.5	0.22
SL2	8.7	5.9	5.2	3.5	3.4	0.23
SM1	8.8	5.5	5.5	3.0	3.0	0.23
SM2	9.0	5.4	4.9	1.5	2.9	0.24
SM3	8.7	4.3	4.5	1.0	2.8	0.23
SH1	8.8	4.5	4.4	0.8	3.0	0.23
SH2	8.9	4.4	4.4	0.2	3.2	0.23
SH3	8.6	4.0	4.0	0.3	3.1	0.22

Table 3.3 Characteristics of the SDOF subharmonic data: wave, b) identified system parameters (English units)

Data	H (m)	C_m	C_d	KC_F	Re_F
SL1	0.17	1.4	0.1- 0.9 (0.5)	0.56	5.7045
SL2	0.24	1.4	0.1-0.9 (0.5)	0.79	7.80E4
SM1	0.35	1.3	0.1-0.9 (0.5)	1.18	1.20E5
SM2	0.36	1.3	0.1- 0.9 (0.5)	1.18	1.20E5
SM3	0.49	1.3	0.1-0.9 (0.5)	1.57	1.60E5
SH1	0.66	1.1	0.1-0.9 (0.5)	2.16	2.20E5
SH2	0.66	1.1	0.1-0.9 (0.5)	2.18	2.22E5
SH3	0.67	1.1	0.1-0.9 (0.5)	2.20	2.30E5

Data	a_1 (N/m)	a_2 (N/m^2)	a_3 (N/m^3)	C_{d1}	ζ_1 (%)	f_{n1} (Hz)
SL1	128.8	315.6	721.3	2.5	3.5	0.22
SL2	125.6	280.1	814.7	3.5	3.4	0.23
SM1	128.8	260.8	863.0	3.0	3.0	0.23
SM2	132.0	257.6	769.6	1.5	2.9	0.24
SM3	125.6	206.1	689.1	1.0	2.8	0.23
SH1	128.8	209.3	689.1	0.8	3.0	0.23
SH2	128.8	209.3	689.1	0.2	3.2	0.23
SH3	125.6	190.0	627.9	0.3	3.1	0.22

Table 3.3 Characteristics of the SDOF subharmonic data: wave, b) identified system parameters (SI units)

From the sensitivity analysis, the optimal range and the most suitable value of the system parameters are obtained and tabulated in Table 3.4. Since the data sets belong to L, M and H groups exhibit similar behavior, the mean of the resulting spectra for each variation is discussed in the following paragraphs. Individual variations of the spectral diagrams for the tests are given in Appendix B.

The effect of varying linear stiffness coefficient, a_1 on SL, SM and SH are demonstrated in Fig.3.23. The spectral density normalized with the variance of experimental wave data (S_{xxn}) is plotted against frequency for a_1 from 4 to 14 lb/ft (58.0 to 202.9 N/m) or a1n (the ratio of instantaneous value of a_1 to the best value of a_1 as given in Table 3.4) from 0.5 to 1.6. It can be observed that there is a slight increase in the primary resonance response as a_1 increases. The subharmonic resonance region shifts towards the right with increasing a_1. The trend can be observed more clearly (from SL to SH) as the wave amplitude increases. When a_2 is increased from 0 to 10 lb/ft^2 (0 to 476.6 N/m^2), there is no significant change on the data group SL as shown in Fig.3.24a. But the response in the secondary resonance region increases from a2n = 0 to 2.5 for SM and SH, and the effects are more pronounced for the latter. Response in the primary resonance region is affected with changing a_2. Fig.3.25 shows that varying a_3 from 0 to 10 lb/ft^3 (0 to 1568.1 N/m^3) or a3n from 0 to 2.5, affects only the response in the secondary resonance region, which decreases as a_3 increases and the variation is most noticeable for MH. With regards to varying the linear structural damping coefficient ζ_1 = 0 to 0.1, the response in the subharmonic region decreases with increasing damping and the primary resonance region remains unaffected as demonstrated in Fig.3.26.

Data	a_1 (lb/ft)	a_2 (lb/ft^2)	a_3 (lb/ft^3)	C_{d1}	ζ_1 (%)	f_{n1} (Hz)
SL1	8.4-9.2 (8.8)	1.0-8.0 (4.5)	1.0-9.0 (5.0)	1.5-2.5 (2.0)	1.0-4.0 (3.0)	0.23
SL2	8.3-9.0 (8.7)	1.0-8.0 (4.5)	1.0-9.0 (5.0)	1.5-2.5 (2.0)	1.0-4.0 (3.0)	0.23
SM1	8.4-9.2 (8.8)	1.0-8.0 (4.5)	1.0-8.0 (4.5)	1.5-2.5 (2.0)	1.5-4.0 (3.3)	0.23
SM2	8.4-9.3 (8.9)	3.0-6.0 (4.5)	3.0-6.0 (4.5)	0.3-0.7 (0.5)	2.0-4.0 (3.0)	0.24
SM3	8.5-9.3 (8.8)	3.0-6.0 (4.5)	3.0-6.0 (4.5)	0.3-0.7 (0.5)	2.0-4.0 (3.0)	0.23
SH1	8.4-9.6 (9.0)	3.5-6.0 (4.7)	3.5-6.0 (4.7)	0.1-0.2 (0.15)	2.5-4.0 (3.3)	0.23
SH2	8.4-9.3 (8.9)	4.0-5.0 (4.5)	4.0-5.0 (4.5)	0.1-0.2 (0.15)	2.0-4.0 (3.0)	0.23
SH3	8.4-9.4 (9.0)	4.2-5.0 (4.6)	4.2-5.0 (4.6)	0.1-0.2 (0.15)	2.0-4.0 (3.0)	0.22

Table 3.4 Identified system parameters from the sensitivity analysis of the SDOF subharmonic data (English units)

Data	a_1 (N/m)	a_2 (N/m^2)	a_3 (N/m^3)	C_{d1}	ζ_1 (%)	f_{n1} (Hz)
SL1	122.4-32.0 (128.8)	48.3-378.0 (215.7)	157.8-1410.4 (772.8)	1.5-2.5 (2.0)	1.0-4.0 (3.0)	0.23
SL2	119.1-132.0 (125.6)	48.3-380.0 (215.7)	157.8-1410.4 (772.8)	1.5-2.5 (2.0)	1.0-4.0 (3.0)	0.23
SM1	122.4-132.0 (128.8)	48.3-380.0 (215.7)	157.8-1255.8 (708.4)	1.5-2.5 (2.0)	1.5-4.0 (3.3)	0.23
SM2	122.4-135.2 (128.8)	141.7-286.6 (215.7)	470.1-933.8 (708.4)	0.3-0.7 (0.5)	2.0-4.0 (3.0)	0.24
SM3	122.4-135.2 (125.6)	141.7-286.6 (215.7)	470.1-933.8 (708.4)	0.3-0.7 (0.5)	2.0-4.0 (3.0)	0.23
SH1	122.4-138.5 (132.0)	167.4-286.6 (225.4)	550.6-933.8 (740.6)	0.1-0.2 (0.15)	2.5-4.0 (3.3)	0.23
SH2	122.4-135.2 (128.8)	190.0-238.3 (215.7)	627.9-772.8 (708.4)	0.1-0.2 (0.15)	2.0-4.0 (3.0)	0.23
SH3	122.4-135.2 (132.0)	199.6-238.3 (219.0)	660.1-772.8 (708.4)	0.1-0.2 (0.15)	2.0-4.0 (3.0)	0.22

Table 3.4 Identified system parameters from the sensitivity analysis of the SDOF subharmonic data (SI units)

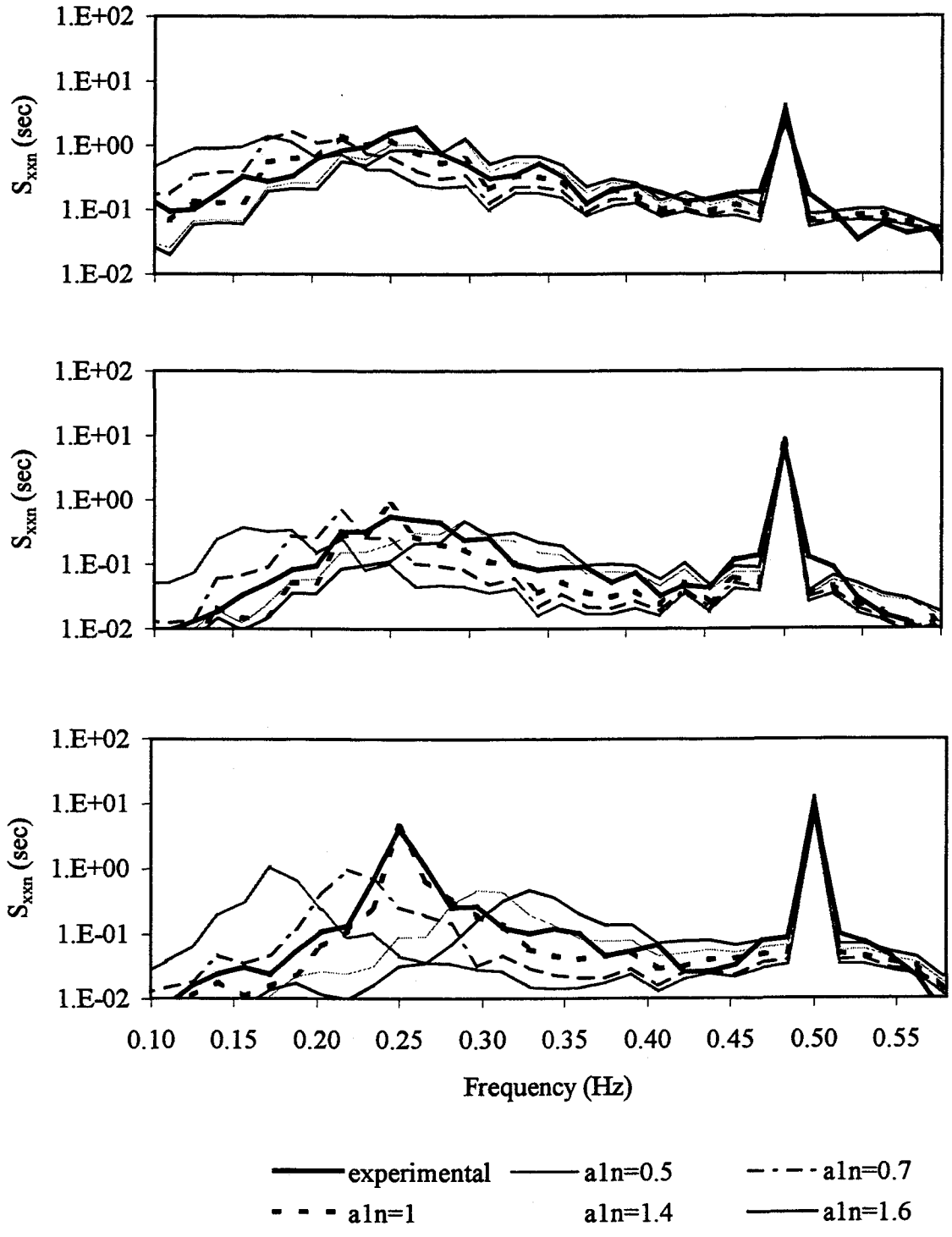

Fig.3.23 Effect of a_1 on SDOF system behavior: a) (top) SL, b) (middle) SM, c) (bottom) SH

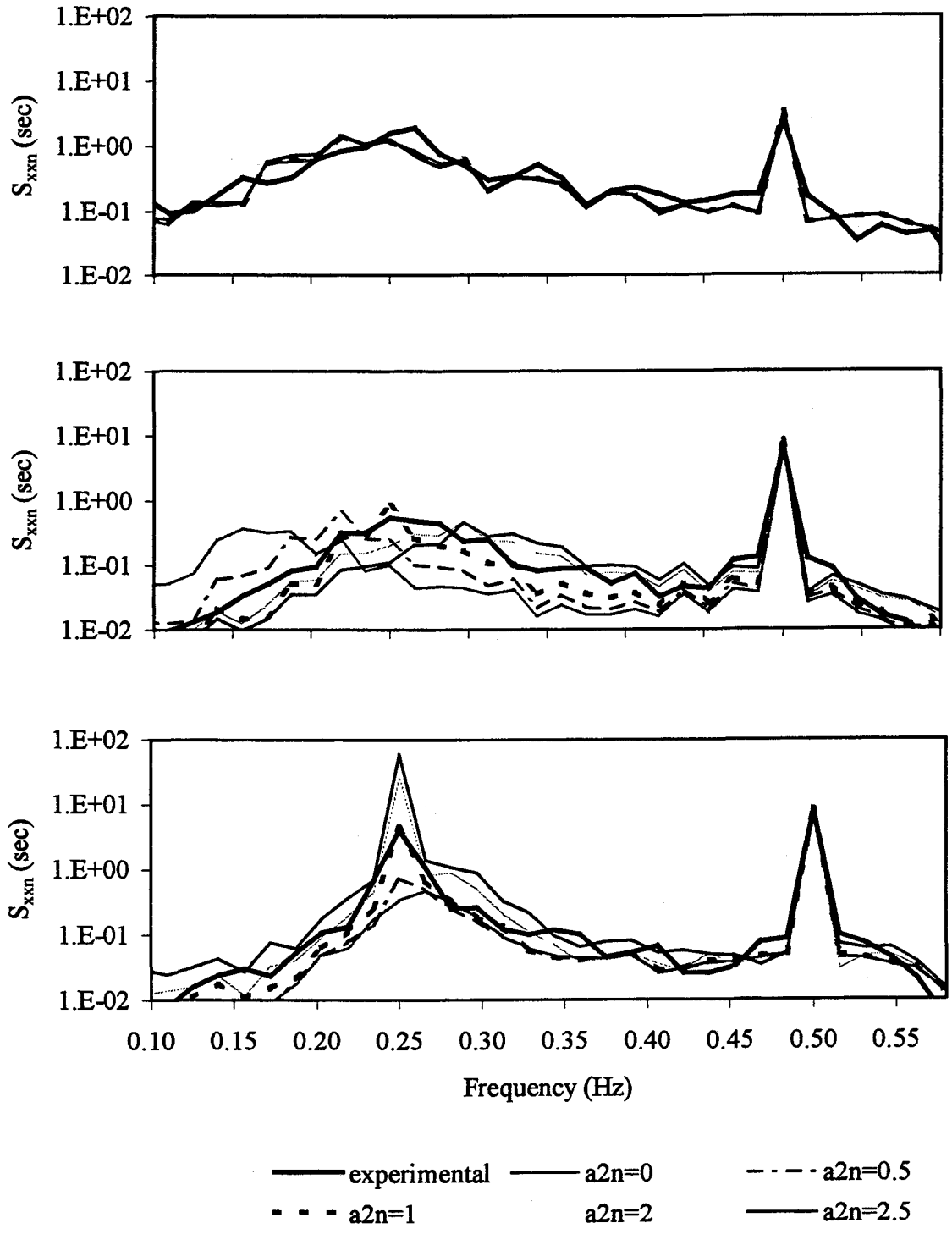

Fig.3.24 Effect of a_2 on SDOF system behavior: a) (top) SL, b) (middle) SM, c) (bottom) SH

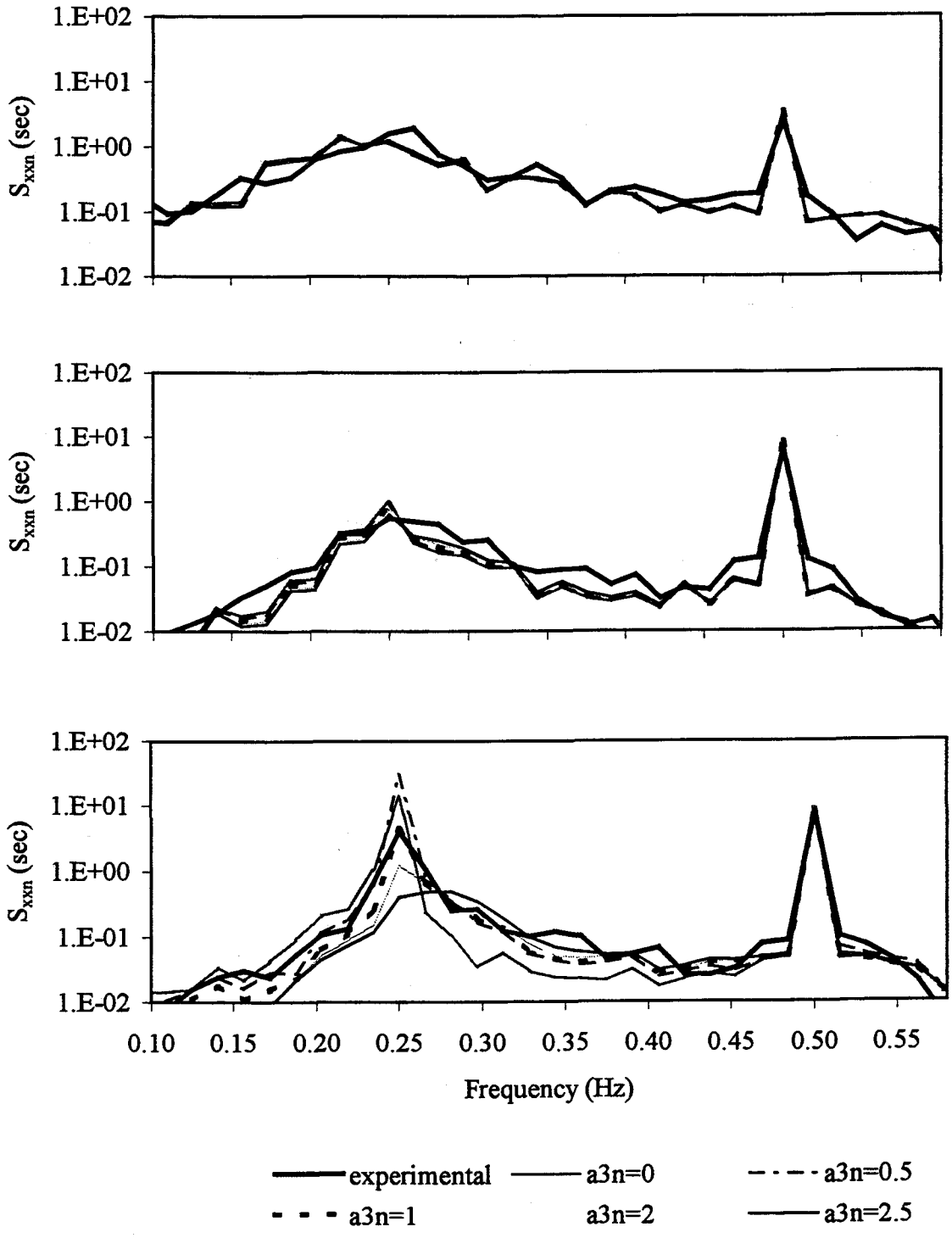

Fig.3.25 Effect of a_3 on SDOF system behavior: a) (top) SL, b) (middle) SM, c) (bottom) SH

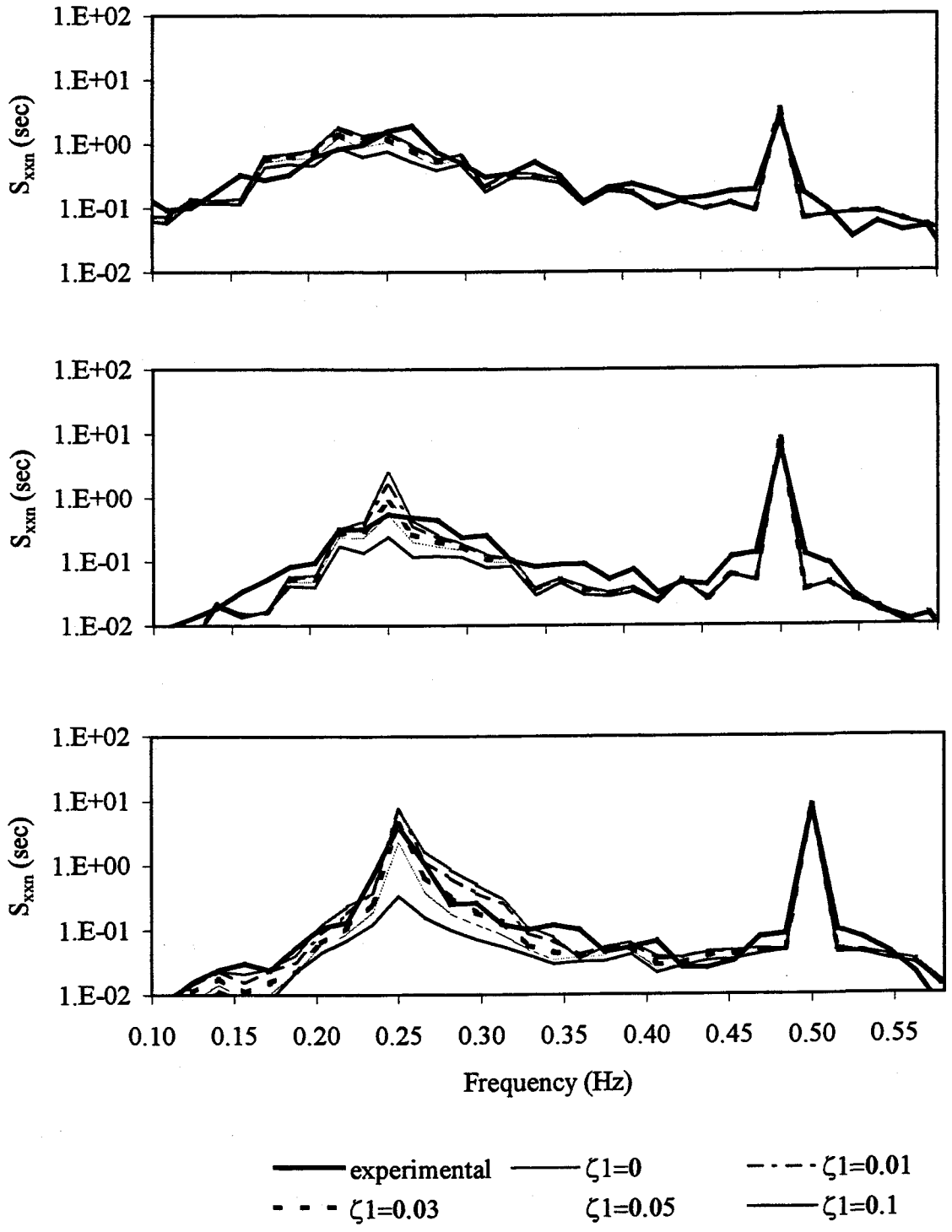

Fig.3.26 Effect of ζ_1 on SDOF system behavior: a) (top) SL, b) (middle) SM, c) (bottom) SH

The effects of varying C_{d1}' on the identified response from Fig.3.27 shows that the secondary resonance region generally decreases with increasing C_{d1}'. However the optimum range that identify response comparable to the experimental response differs for the data groups SL, SM and SH. The most suitable value goes as high as 2 for ML and it decreases to 0.5 for SM and 0.15 for SH. This apparent behavior is probably caused by the inability of the model to approximate accurately the actual nonlinear behavior of the complex damping mechanism of the SDOF configuration. In the physical system, with the rod passing through the center of the sphere, the Coulomb frictional component, which is proportional to the magnitude of the normal reaction force between the sphere and the supporting rod. Because the sphere is neutrally buoyant, this normal force is proportional to the magnitude of the oscillatory vertical force. The nonlinear effects become more prominent for responses at lower wave amplitudes because of the stop-and-go (sticky motion) behavior due to static friction of the sphere become relatively more significant, thus affecting the prediction capability.

3.6.3 Effects of KC and Re on Hydrodynamic Coefficients

It can be observed from the optimal range and the most suitable value of KC_F, Re_F, C_m and C_d for the SDOF experimental data tabulated in Table 3.3a that the inertia coefficient C_m decreases with the increase in KC_F and Re_F. C_m varies between 1.4-1.1 for $1.34 \times 10^5 \leq Re_F \leq 5.21 \times 10^5$ and $1.19 \leq KC_F \leq 4$. The response is insensitive to C_d and it has a wide range as shown in Table 3.3a.

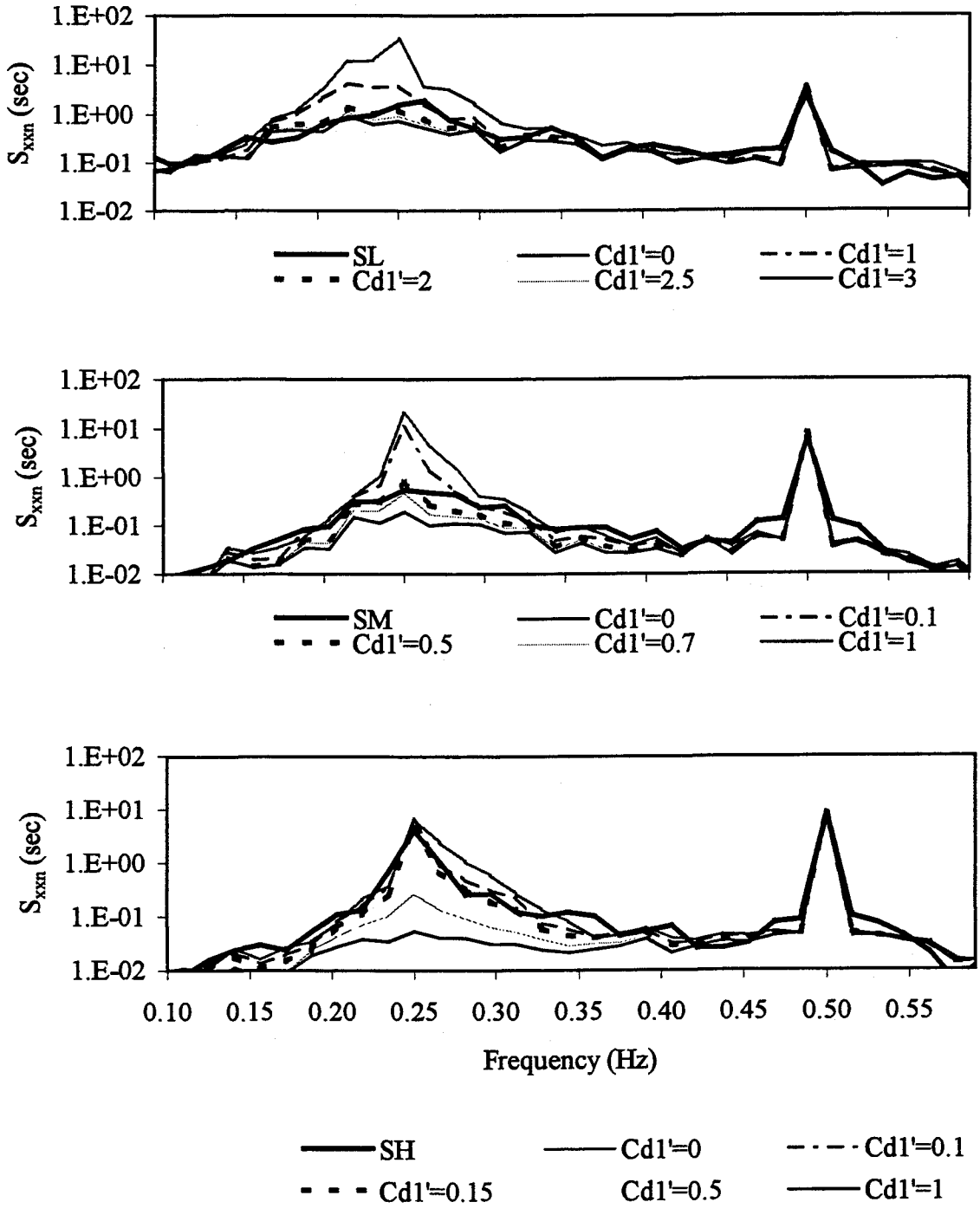

Fig.3.27 Effect of C_{d1}' on SDOF system behavior: a) (top) SL, b) (middle) SM, c) (bottom) SH

3.7 Comparison of MDOF and SDOF System Behaviors

The surge response behavior of MDOF and SDOF systems described in Sections 3.5 and 6 are compared in this section. Specifically, comparisons of the wave excitation and surge response time series, R-MI/SO technique application, identified parameters, results for the sensitivity analysis on surge system parameters, and the effect of hydrodynamic coefficients between SDOF and MDOF are presented and discussed in this section.

3.7.1 Time Series, Phase Diagrams and Wave Spectra

From the Table 3.1a and 3a, it can be found that the wave excitation characteristics of MH and SM3 closely matches each other, and hence suitable for comparisons. The time series and spectra of the input and output of these two tests are presented in Fig.3.28 and the phase diagrams in Fig.3.29. It can be observed from the wave spectra in Fig.3.28 that the wave amplitude matches closely, however, there is a slight difference in the wave period. Comparing surge response time series and spectra from Fig.3.28c and d, the SM3 response amplitude is smaller in magnitude than MH. This can be attributed to the friction between the rod and the sphere that might have reduced the sphere movement for the SDOF system. The phase diagrams given in Fig.3.29 exhibit a similar behavior between SDOF and MDOF surge data with stable equilibrium point at (0,0).

3.7.2 Reverse Multiple-Input/Single-Output (R-MI/SO) Technique Application

The R-MI/SO technique is applied to identify the linear and nonlinear parameters of both the SDOF and MDOF systems.

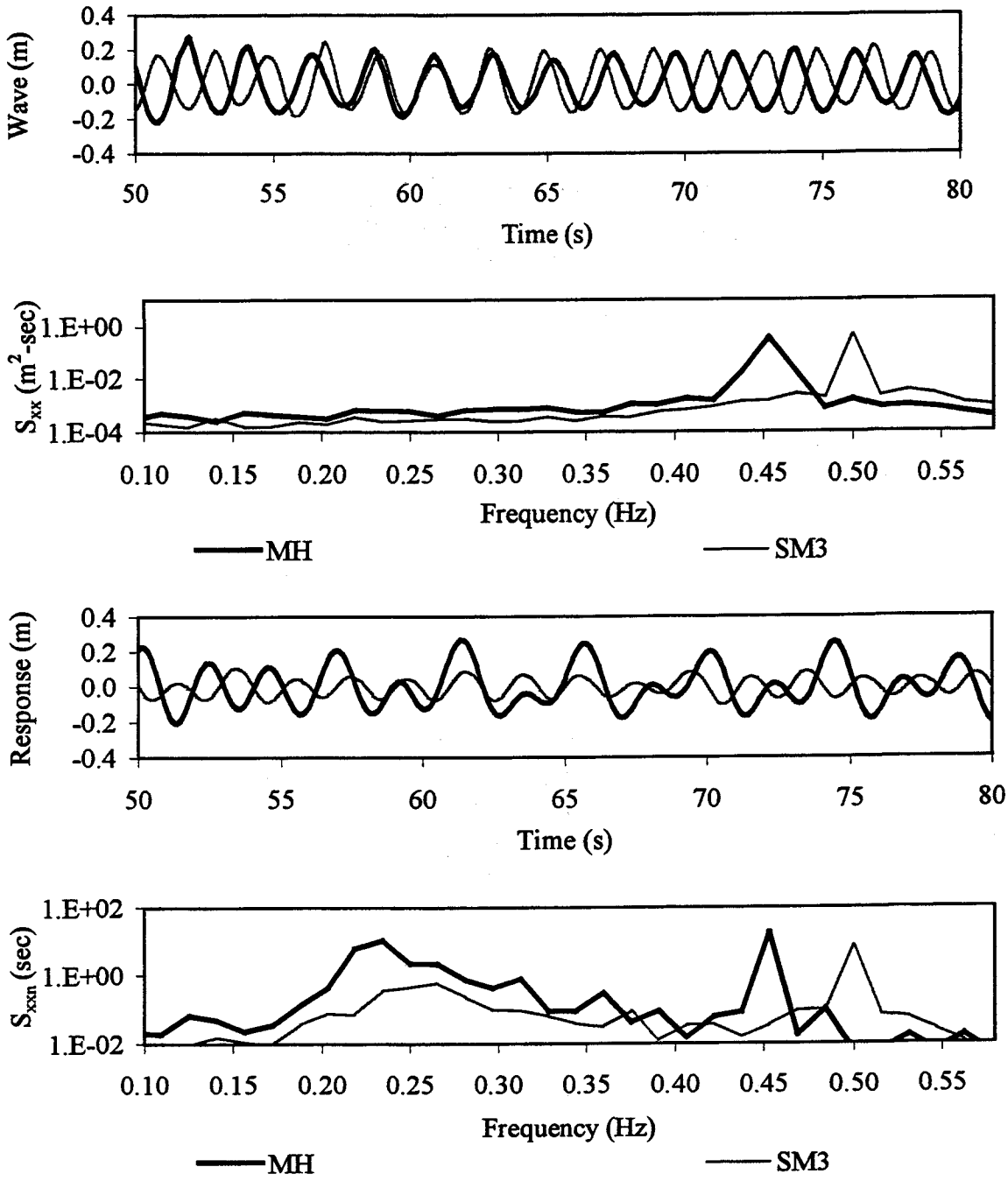

Fig.3.28 Comparison of MDOF and SDOF data: a)(first) wave time series, b) (second) wave spectra, c) (third) surge time series, d) (fourth) surge spectra

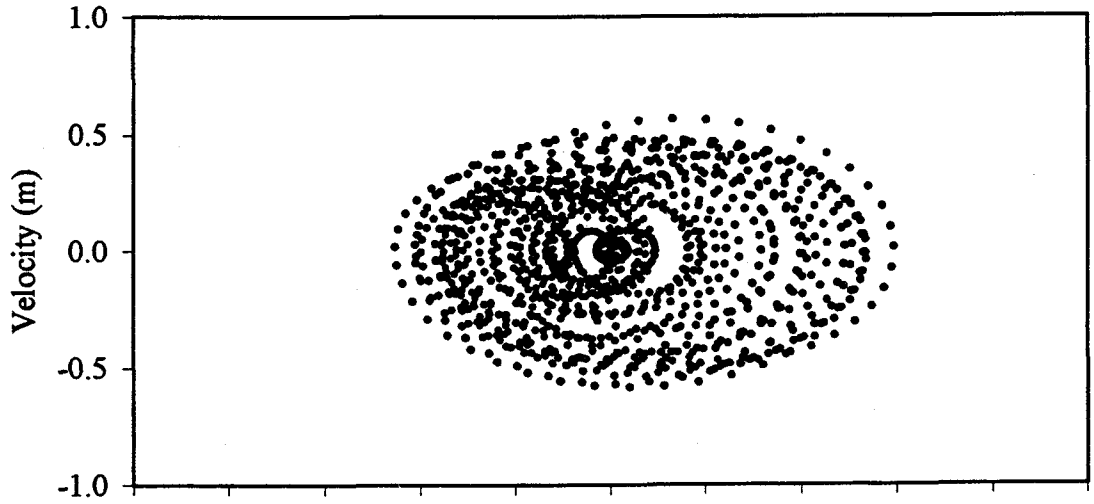

(a)

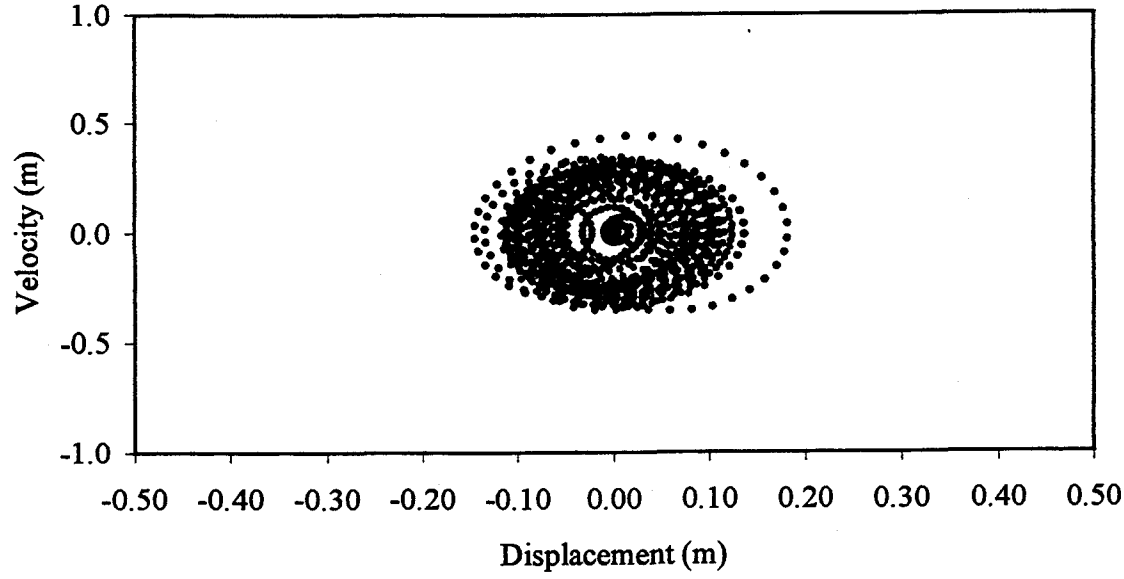

(b)

Fig.3.29 Comparison of MDOF and SDOF phase diagrams: a) MH, b) SM3

Several alternative MI/SO models have been derived for the SDOF system based on the how each term in the equation is treated either as a mathematical input or output and also depending upon the equation used to represent the hydrodynamic force (Chapter 2). The NSND model has been found to be the most appropriate representation of the SDOF experimental system and has been extended to MDOF system in this chapter. Both models identify system parameters that generate a matching response with that of the experimental data. The formulation of the computational technique is straightforward, simple and efficient. The standard multiple-input/single-output procedures are incorporated in MATLAB 5.2 (MathWorks, Inc.) and once the program developed for SDOF model, it can easily be extended to systems with arbitrary degrees of freedom.

3.7.3 Identified System Parameters

By equating the heave response, $x_3 = 0$, the governing equations (Eqs.3.1-9) given for the surge-heave model is reduced to surge motion only and the identified parameters in surge for SDOF and MDOF system tabulated in Table 3.1b and 2b are compared. In general, it can be observed that the parameters of the MDOF system are larger in magnitude compared to those of the SDOF system. The average natural frequency of the system, f_{n1} identified using the MDOF data is 0.28 Hz and that of the SDOF system is 0.23 Hz. The nonlinear structural damping coefficient, Cd_1', varies among the three groups of SDOF data, SL, SM and SH and as mentioned in Section 3.7.2, this could be due to the presence of rod in the SDOF system, which affects the "Coulomb" type damping not included in the modeling.

3.7.4 Sensitivity Analysis

Based on the sensitivity analysis presented in Section 3.6.2 and 3.7.2, it can be observed that varying the surge system parameters (a_1, a_2, a_3, ζ_1 and C_{d1}) have similar effects on the SDOF and MDOF systems. Similar to the MDOF tests where there are two categories of data (depending on low or high wave excitation amplitude) which exhibit similar behaviors within each category, the SDOF tests are grouped into three categories. However, there are more experimental tests for the SDOF system available to confirm the surge response behavior.

3.7.5 Effects of KC and Re on Hydrodynamic Coefficients

Application of the R-MI/SO technique on SDOF and MDOF, NSND models require the knowledge of C_d and C_m for the evaluation of hydrodynamic force on the sphere. Dependence of the inertia coefficient, C_m on Reynolds number (Re_F) and Keulegan-Carpenter number (KC_F) for the MDOF and SDOF systems are demonstrated in Fig.3.30. Both systems display a similar trend with C_m decreasing with the increase in Re_F and KC_F and vary between 1.4-1.1 for $1.34 \times 10^5 \leq Re_F \leq 5.21 \times 10^5$ and $1.19 \leq KC_F \leq 4$. Wave tank tests on a vertical cylinder (Chakrabarti 1987) shows that C_m decreases from 2.4 to 2 with the increase of KC_F from 1 to 6 and also decreases with increase in Re_F and the above results for sphere also show the same pattern with the lower range of magnitude. From numerical simulations, it is found that the predicted response is insensitive to variations in C_d within the range of 0.1 to 1.1.

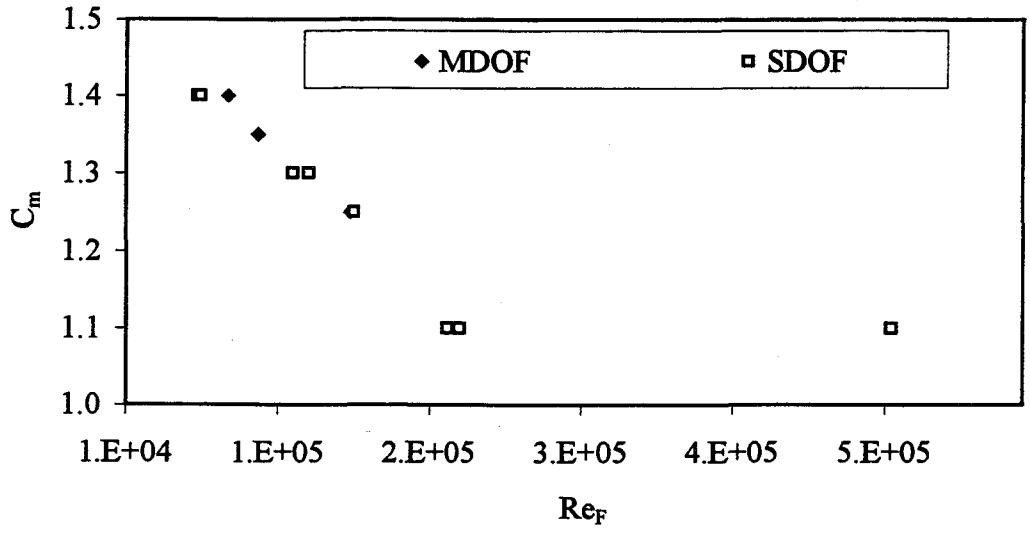

(a)

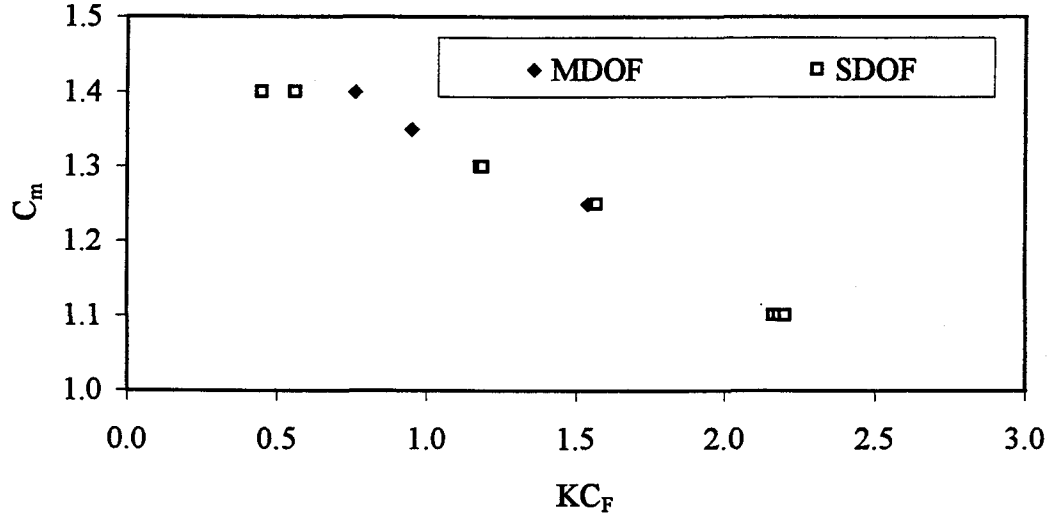

(b)

Fig.3.30 Effect of Reynolds and Keulegan Carpenter numbers on C_m and C_d: a) Re_F, b) KC_F

Based on the water depth to wavelength (h/L) and diameter to wave height (D/H) ratios (Nath and Harleman 1970), the inertia effects dominate the total forces for both MDOF and SDOF systems. Hence it is not possible to accurately determine the exact value of C_d.

4. MDOF SUPERHARMONIC RESPONSE BEHAVIOR

4.1 Introduction

In addition to the tests that yield subharmonic responses, superharmonic responses are also observed for the MDOF system (Yim *et al* 1993). The system formulation, parameter identification and response analysis and sensitivity studies are identical as described in Chapter 3. The results are demonstrated and discussed in this Chapter. Comparisons of the response with those corresponding to the MDOF subharmonic responses are presented.

4.2 MDOF System Superharmonic Response Behavior

4.2.1 Time Series and Spectra

Two tests, MSP1 and MSP2 conducted on the sphere using periodic wave excitation with white noise perturbations yield superharmonic response. The wave period for both tests is T = 8.4 seconds. The data sets are labeled and grouped according to wave amplitude. The wave velocity and acceleration are evaluated using the central difference method (Gerald and Wheatley 1989). The sampling interval used in the experiment is 0.0625 second, which yields a Nyquist frequency of 8 Hz. The total number of samples of the excitation and response time histories for spectral simulations is 8192 (512 seconds), with sub record lengths of 1024 for the Fourier transforms (64 seconds).

A typical segment of the time series and the spectra of the entire record of wave and responses (surge and heave) for the data sets are given in Figs.4.1-2.

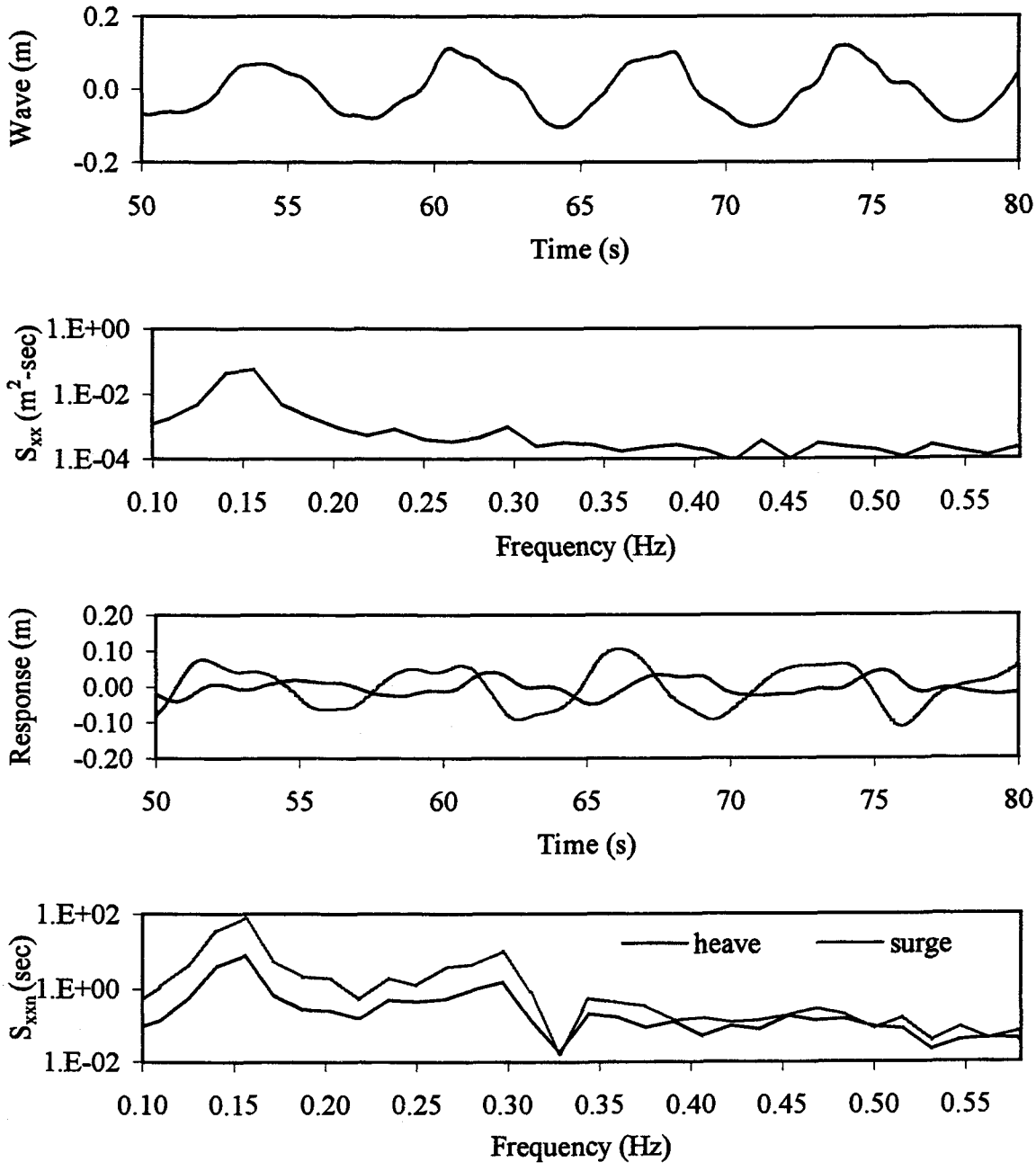

Fig.4.1 MDOF experimental data, MSP1: a) (first) wave time series, b) (second) wave spectra, c) (third) response time series, d) (fourth) response spectra

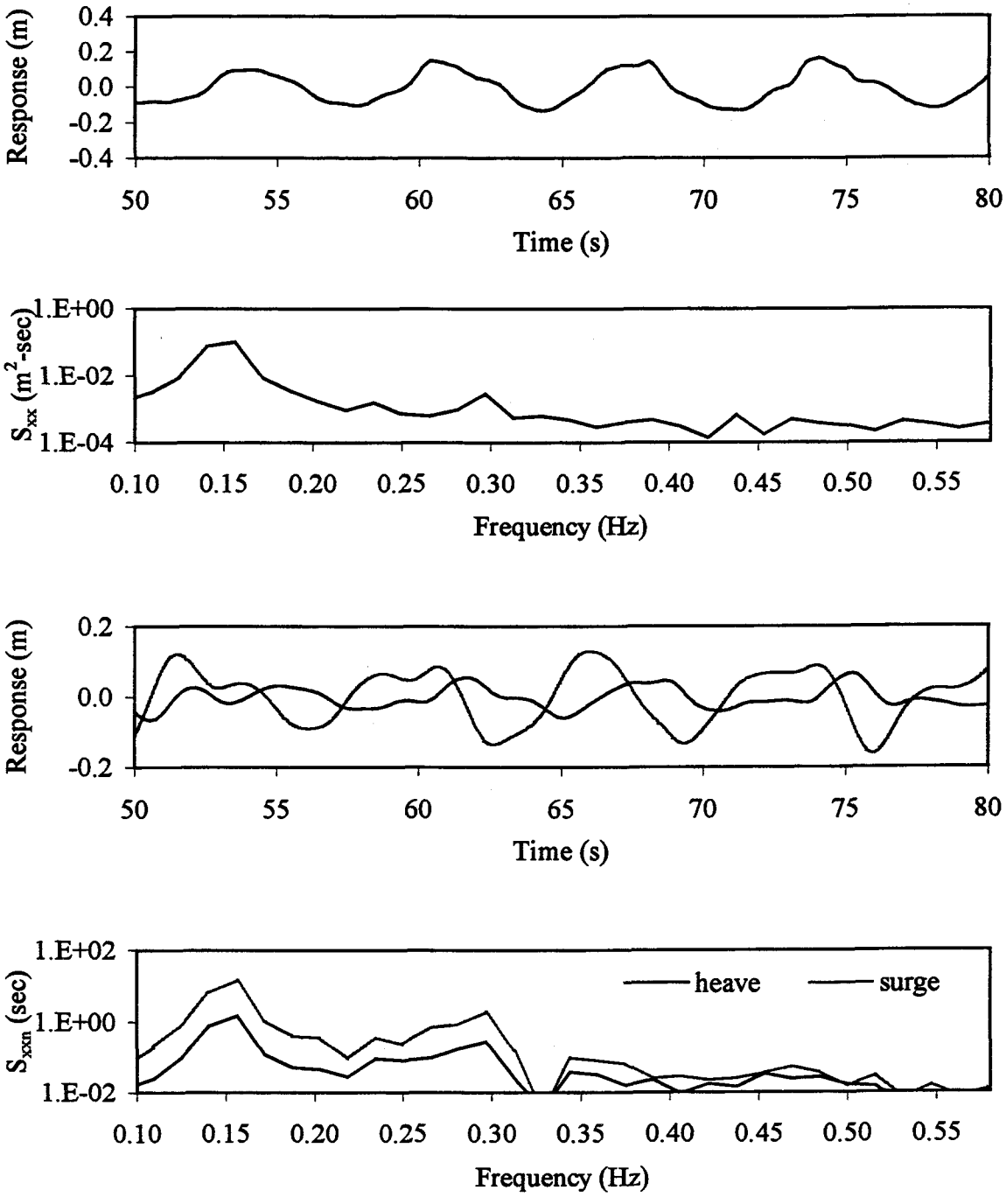

Fig.4.2 MDOF experimental data, MSP2: a) (first) wave time series, b) (second) wave spectra, c) (third) response time series, d) (fourth) response spectra

The input wave characteristics such as wave height (H), Keulegan-Carpenter number (KC_F) and Reynolds number (Re_F) and the identified system parameters, a_1, a_2, a_3, b_1, b_3, c_{12}, c_{21}, ζ_1, ζ_3, C_{d1}' and C_{d3}' using the R-MI/SO technique are shown in Table 4.1.

4.2.2 Sensitivity Analysis

A sensitivity analysis is conducted to determine an optimal range of system parameters. Each parameter is varied in specific increments while keeping all the other identified properties constant (Table 4.1) and the surge and heave responses are simulated for each variation. The results are compared against each other in both time and frequency domains. The optimal range and most suitable value of system parameters are tabulated in Table 4.2 and they remain consistent for both tests. The observations are summarized through spectral diagrams in the following paragraphs.

The effects of varying a_1 on heave and surge responses for MSP1 and MSP2 are presented in Fig.4.3. The spectral density normalized with the variance of measured wave data (S_{xxn}) is plotted against frequency for a_1 from 4 to 15 lb/ft (58.0 to 217.4 N/m) or a1n (the ratio of instantaneous value of a_1 to the best value of a_1 as given in Table 4.1) from 0.33 to 1.25. The heave response appears unaffected for both tests. For the surge response behavior (Fig.4.3b and d), the primary response decreases with increasing a_1. The energy of the superharmonic response increases slightly with increasing a_1.

When a_2 is increased from 0 to 10 lb/ft^2 (0 to 476.6 N/m^2) or a2n=0 to 1.25, the response in the secondary resonance (superharmonic) region for heave decreases slightly for MSP1 and MSP2 as given in Fig.4.4a and c. The primary resonance region does not appear to be affected by variations in a_2.

Data	H (ft)	KC_F	Re_F	C_m	C_d
MSP1	0.26	0.81	2.75e4	0.4	0.1- 0.9 (0.5)
MSP2	0.27	0.90	3.1e4	0.4	0.1-0.9 (0.5)

Data	a_1 lb/ft	a_2 lb/ft^2	a_3 lb/ft^3	b_1 lb/ft	b_3 lb/ft^3	c_{12} lb/ft^3	c_{21} lb/ft^3	$C_{d1,3}$	$\zeta_{1,3}$ %	$f_{n1,3}$ (Hz)
MSP1	12.0	8.5	6.2	12.4	8.1	10.0	11.5	1.2	2.5	0.28
MSP2	12.0	8.2	6.5	12.2	7.5	14.5	18.0	0.9	3.1	0.28

Table 4.1 Characteristics of the MDOF superharmonic data: wave, b) identified system parameters (English units)

Data	H (m)	KC_F	Re_F	C_m	C_d
MSP1	0.87	0.81	2.75e4	0.4	0.1- 0.9 (0.5)
MSP2	0.9	0.90	3.1e4	0.4	0.1-0.9 (0.5)

Data	a_1 N/m	a_2 N/m^2	a_3 N/m^3	b_1 N/m	b_3 N/m^3	c_{12} N/m^3	c_{21} N/m^3	$C_{d1,3}$	$\zeta_{1,3}$ %	$f_{n1,3}$ (Hz)
MSP1	173.9	405.7	972.4	180.3	1271.9	1568.1	1806.4	1.2	2.5	0.28
MSP2	173.9	405.7	1020.7	177.1	1178.5	2273.3	2823.9	0.9	3.1	0.28

Table 4.1 Characteristics of the MDOF superharmonic data: wave, b) identified system parameters (SI units)

Data	MSP1	MSP2
a_1 (lb/ft)	10.8-13.2 (12.0)	10.7-13.5 (12.1)
a_2 (lb/ft^2)	5.5-8.5 (7.0)	5.5-8.5 (7.0)
a_3 (lb/ft^3)	1.0-11.0 (6.0)	1.0-11.0 (6.0)
b_1 (lb/ft)	10.8-13.2 (12.0)	10.8-14.2 (12.0)
b_3 (lb/ft^3)	1.0-8.0 (4.5)	1.0-8.0 (4.5)
c_{12} (lb/ft^3)	1.0-23.0 (12.0)	1.0-23.0 (12.0)
c_{21} (lb/ft^3)	1.0-23.0 (12.0)	1.0-23.0 (12.0)
$C_{d1,3}$	0.3-0.7 (0.4)	0.3-0.7 (0.4)
$\zeta_{1,3}$ (%	1.0-4.0 (3.0)	1.0-4.0 (3.0)

Table 4.2 Identified system parameters from the sensitivity analysis of the MDOF superharmonic data (English units)

Data	MSP1	MSP2
a_1 (N/m)	157.8-193.2 (173.9)	154.6-196.4 (177.1)
a_2 (N/m^2)	264.0-405.7 (334.9)	257.6-412.2 (338.1)
a_3 (N/m^3)	157.8-1725.9 (940.2)	157.8-1725.9 (940.2)
b_1 (N/m)	157.8-190.0 (173.9)	157.8-206.1 (173.9)
b_3 (N/m^3)	157.8-1255.8 (705.2)	157.8-1255.8 (705.2)
c_{12} (N/m^3)	157.8-3606.4 (1883.7)	157.8-3606.4 (1883.7)
c_{21} (N/m^3)	157.8-3606.4 (1883.7)	157.8-3606.4 (1883.7)

Table 4.2 Identified system parameters from the sensitivity analysis of the MDOF superharmonic data (SI units)

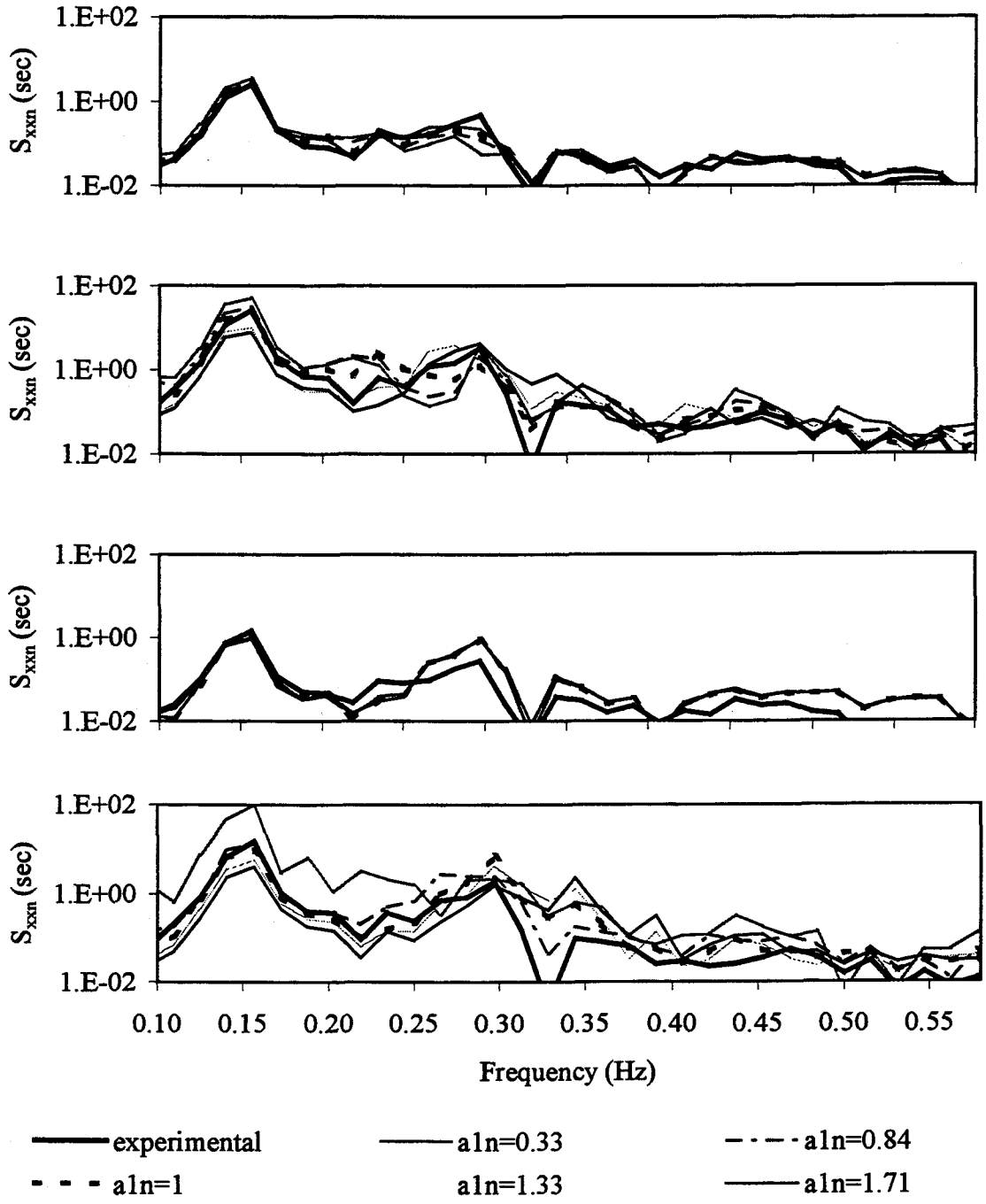

Fig 4.3: Effect of a_1 on MDOF system behavior a) (first) MSP1H, b) (second) MSP1S, c) (third) MSP2H, d) (fourth) MSP2S

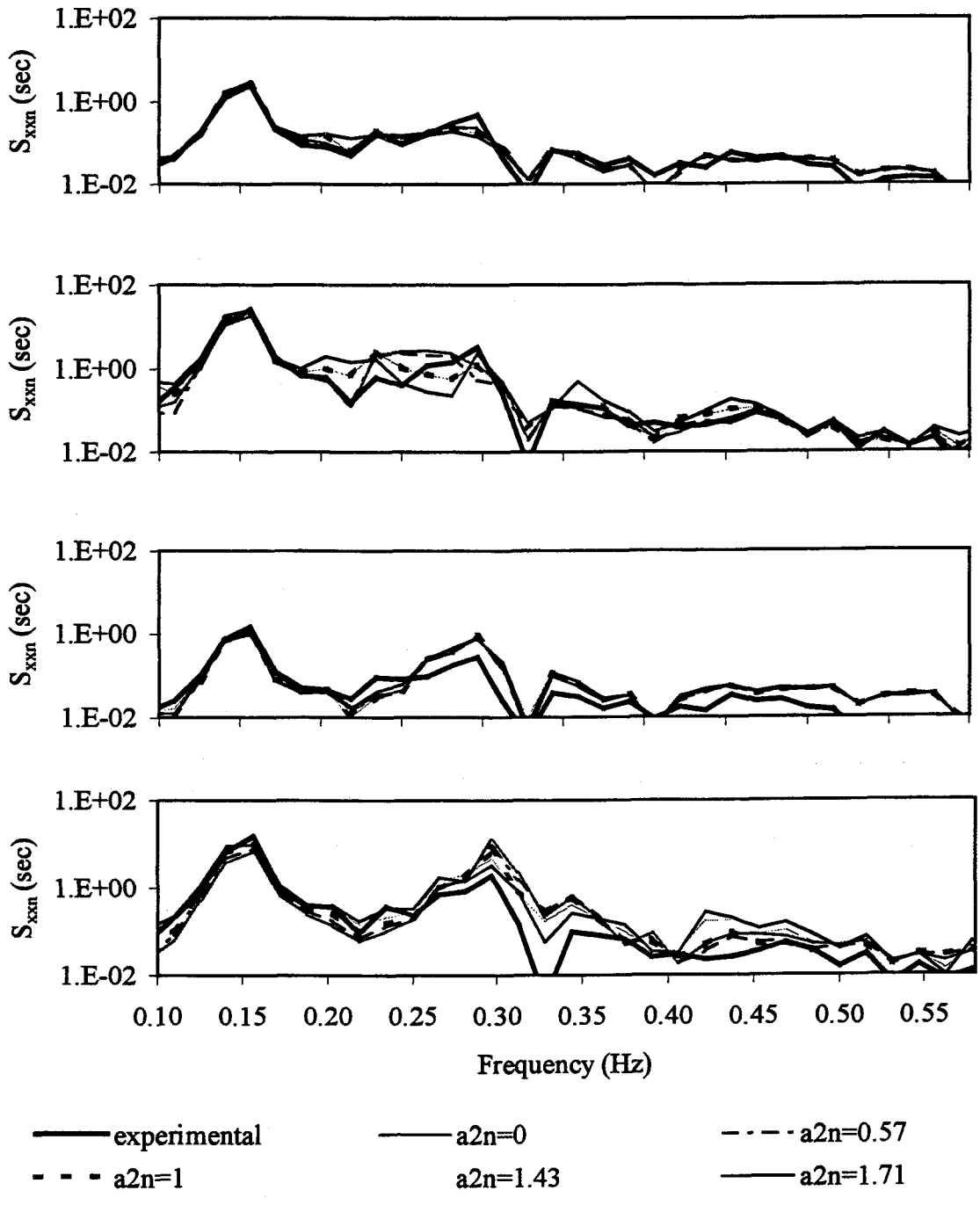

Fig.4.4 Effect of a_2 on MDOF system behavior: a) (first) MSP1H, b) (second) MSP1S, c) (third) MSP2H, d) (fourth) MSP2S

The effects of varying a_3 on the identified responses as given in Fig.4.5 show that only the response in the secondary resonance region is influenced, which increases with a_3 (from 0 to 10 lb/ft^3 (0 to 1568.1 N/m^3)or a3n from 0 to 2.5).

The effect of varying b_1 from 8 to 16 lb/ft (115.9 to 231.9 N/m) on the heave and surge responses for MSP1 and MSP2 are demonstrated in Fig.4.6. The surge response does not change significantly for either test. For the heave response, it can be observed from Fig.4.6b and d that the primary and the superharmonic resonance energy decreases with increasing b_1. When b_3 is varied from 0 to 1.4 lb/ft^3 (0 to 219.6 N/m^3), the heave and surge responses for either test are not affected as shown in Fig.4.7.

From Figs.4.8 and 9, it can be observed that by varying the coupled restoring force coefficients, c_{12} and c_{21}, there is no significant influence on the identified responses of MSP1 and MSP2. By varying the linear structural damping coefficients, ζ_1 and ζ_3, from 0 to 0.1, the superharmonic response decreases with increasing damping values and the primary resonance region does not appear to be affected as demonstrated in Fig.4.10 and 11. A similar trend of decreasing superharmonic response with increasing nonlinear damping coefficients can be observed for C_{d1}' and C_{d3}' as shown in Fig.4.12 and 13.

4.2.3 Comparison with MDOF Subharmonic Response

Comparing the sensitivity analysis results between tests that yield subharmonic and superharmonic response, it can be observed that varying system parameters have opposite effect. For ML1, ML2 and MH (tests that yield subharmonic responses), increasing a_1 has an effect of increasing the primary and decreasing the subharmonic surge response. But the primary response decreases and subharmonic response increases for MSP1 and MSP2.

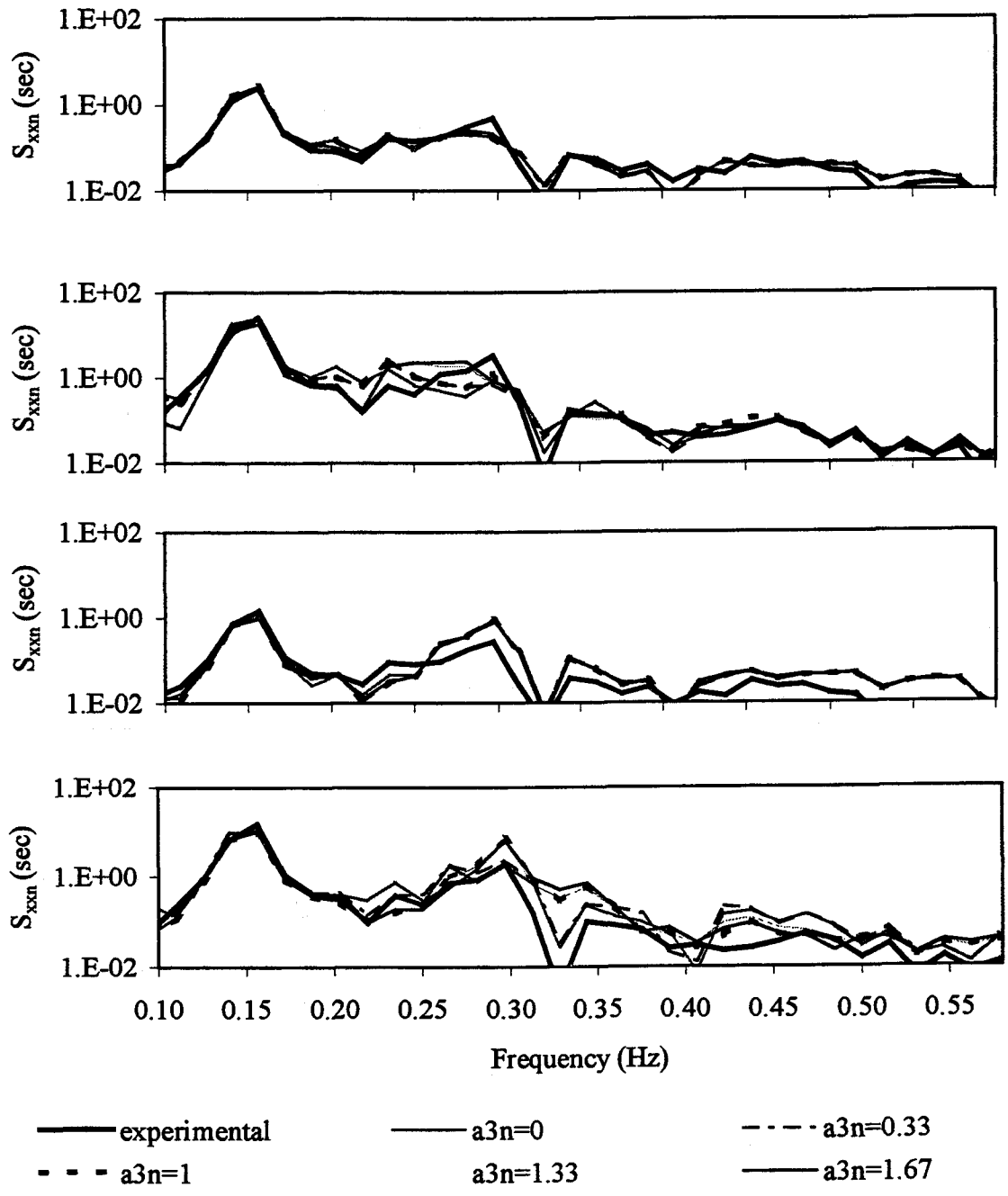

Fig.4.5 Effect of a_3 on MDOF system behavior: a) (first) MSP1H, b) (second) MSP1S, c) (third) MSP2H, d) (fourth) MSP2S

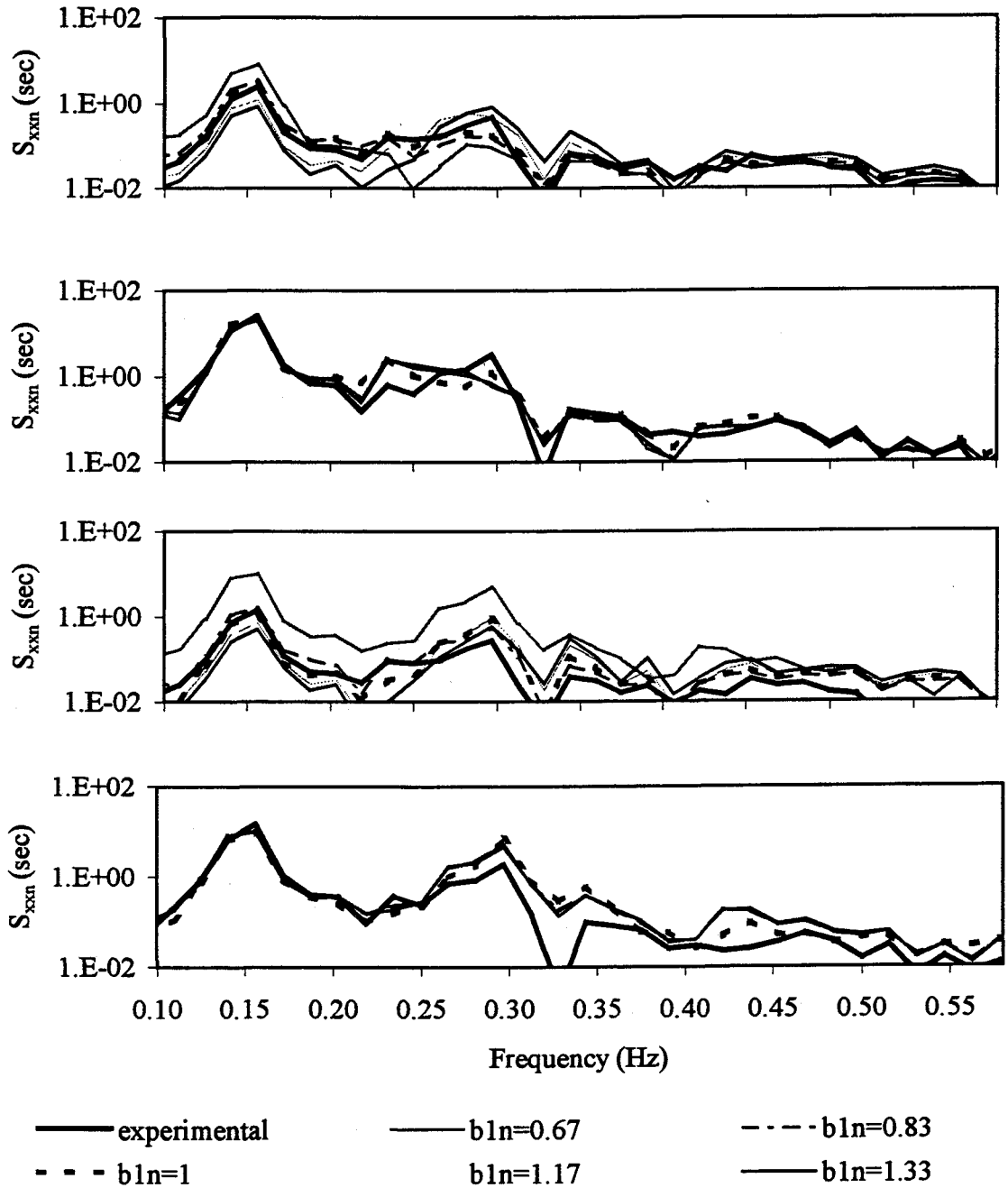

Fig.4.6 Effect of b_1 on MDOF system behavior: a) (first) MSP1H, b) (second) MSP1S, c) (third) MSP2H, d) (fourth) MSP2S

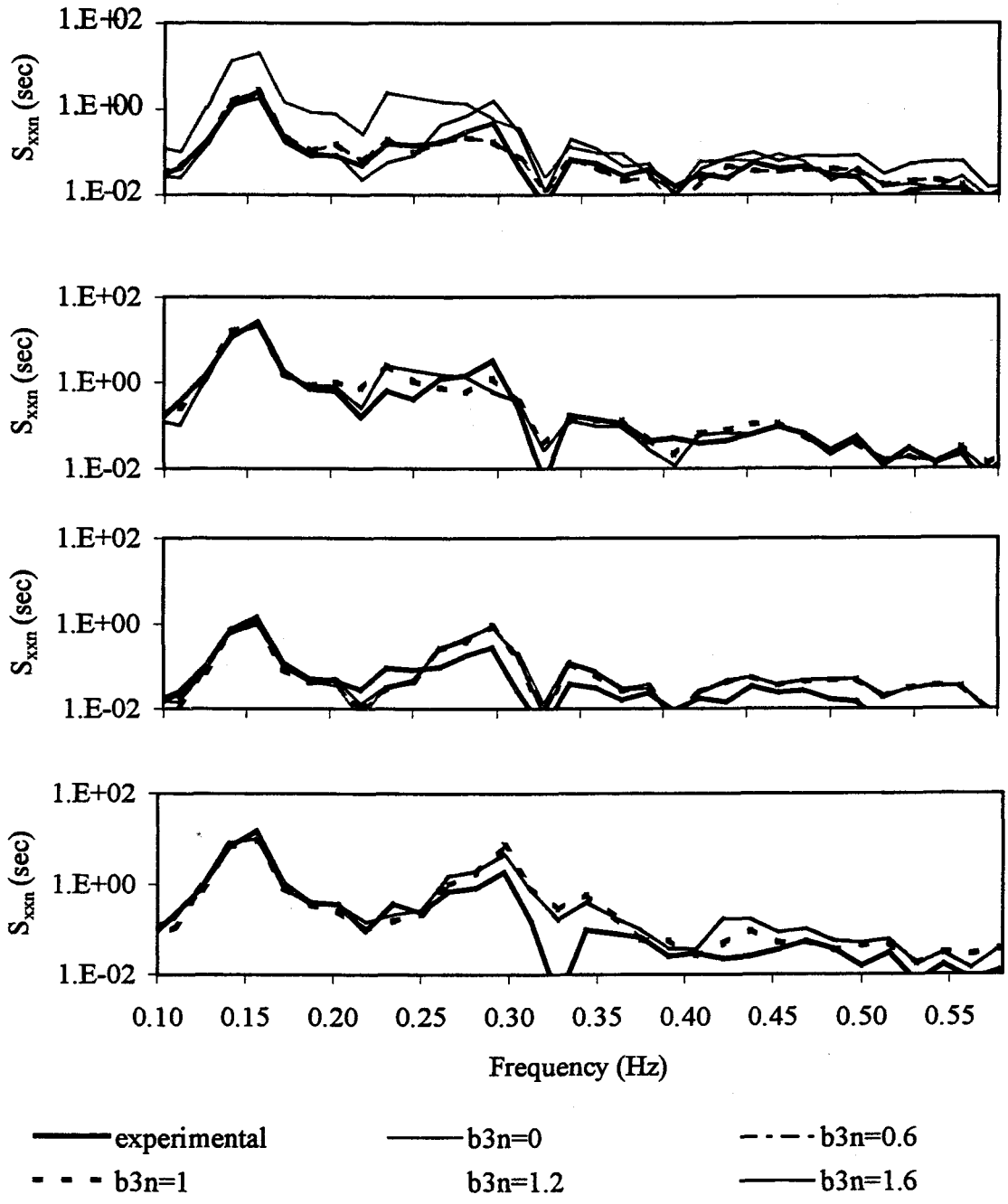

Fig.4.7 Effect of b_3 on MDOF system behavior: a) (first) MSP1H, b) (second) MSP1S, c) (third) MSP2H, d) (fourth) MSP2S

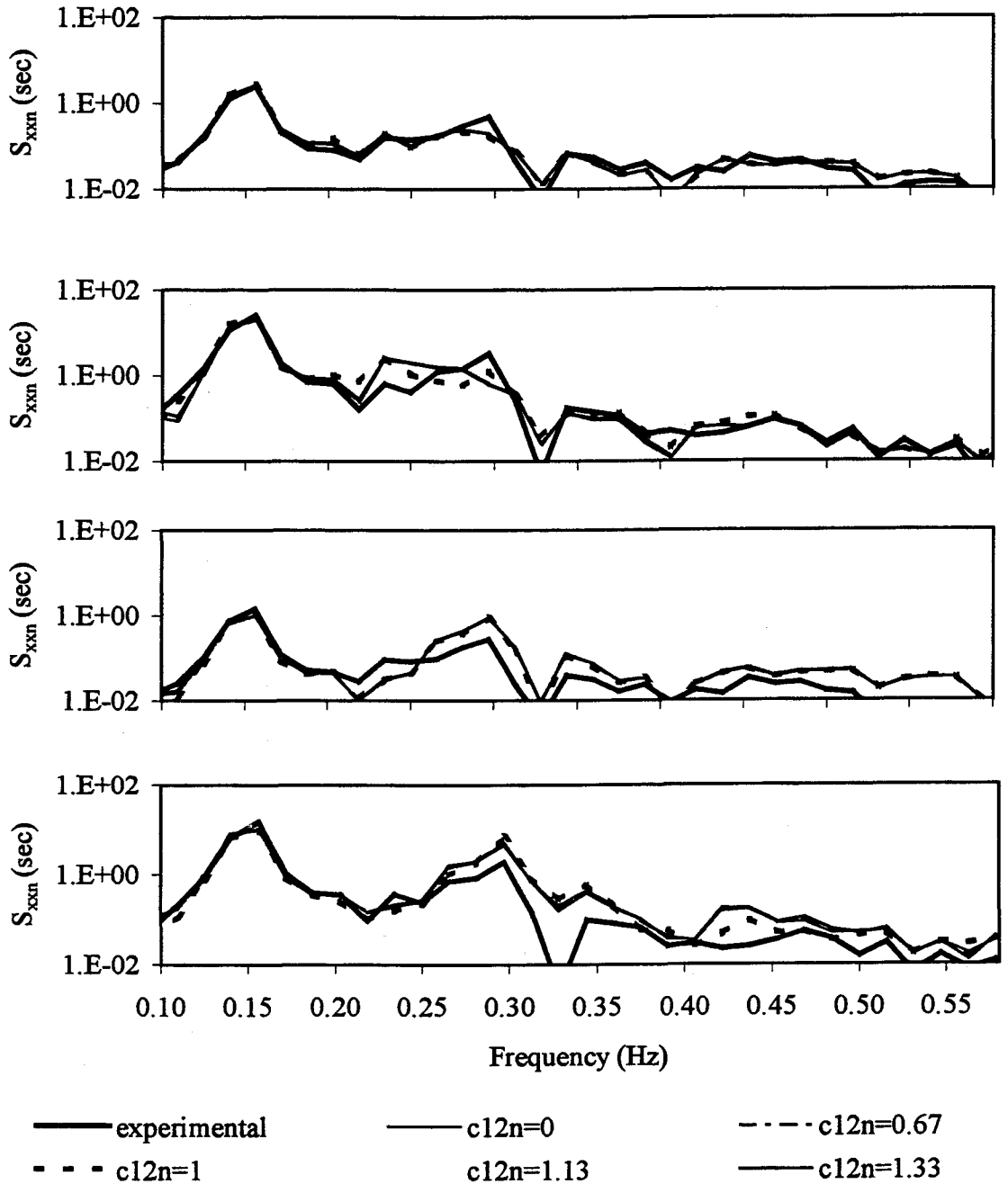

Fig.4.8 Effect of c_{12} on MDOF system behavior: a) (first) MSP1H, b) (second) MSP1S, c) (third) MSP2H, d) (fourth) MSP2S

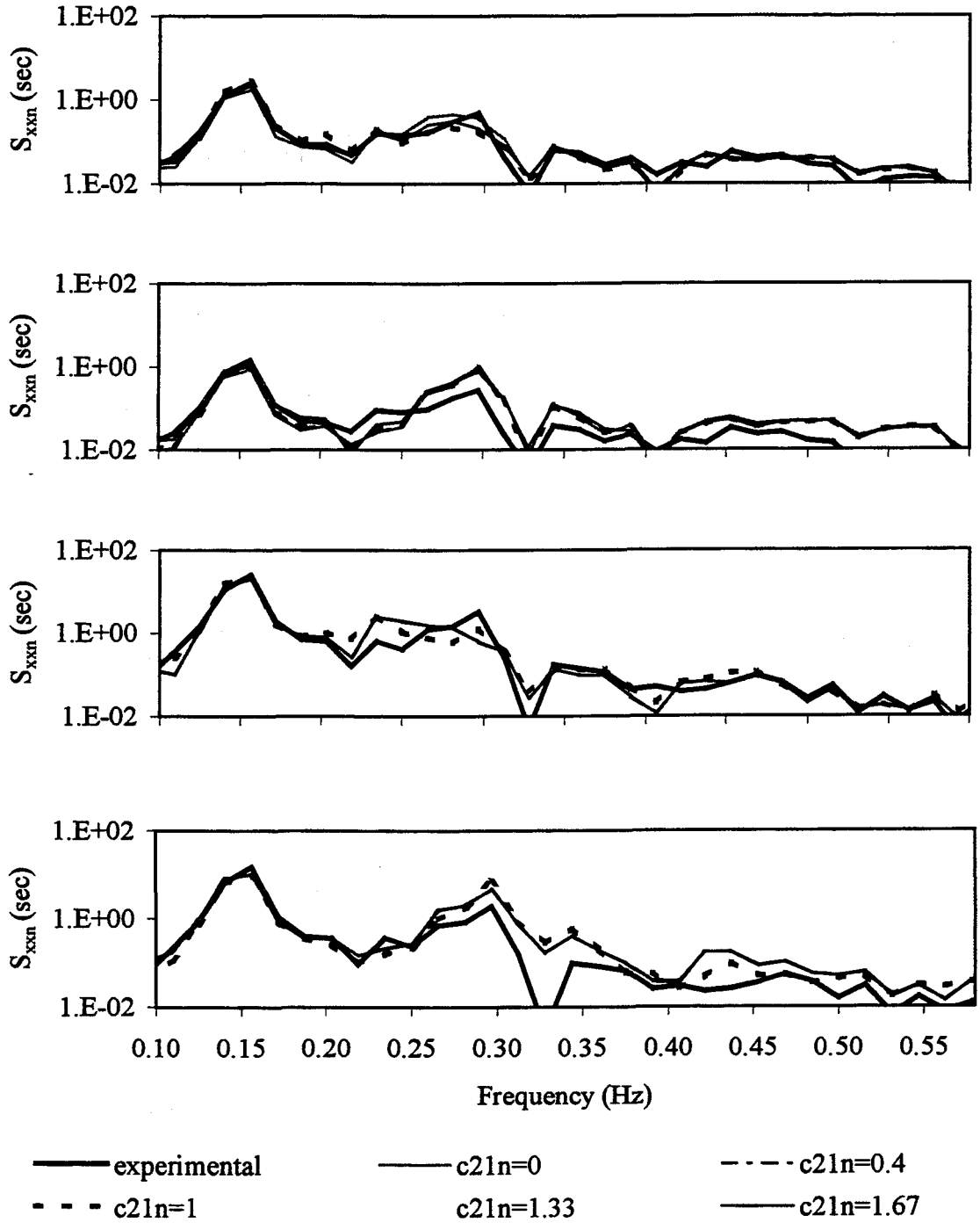

Fig.4.9 Effect of c_{21} on MDOF system behavior: a) (first) MSP1H, b) (second) MSP1S, c) (third) MSP2H, d) (fourth) MSP2S

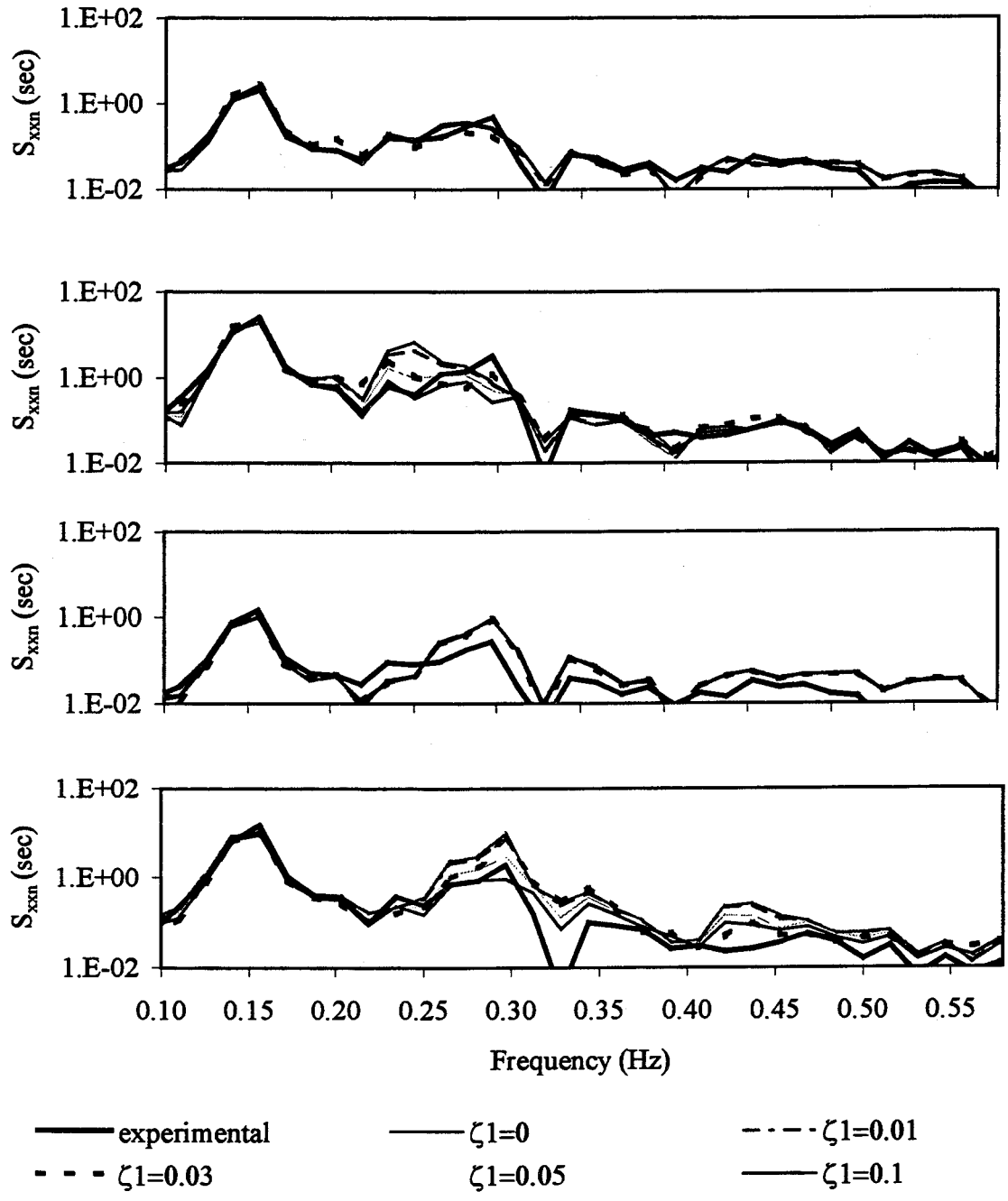

Fig.4.10 Effect of ζ_1 on MDOF system behavior: a) (first) MSP1H, b) (second) MSP1S, c) (third) MSP2H, d) (fourth) MSP2S

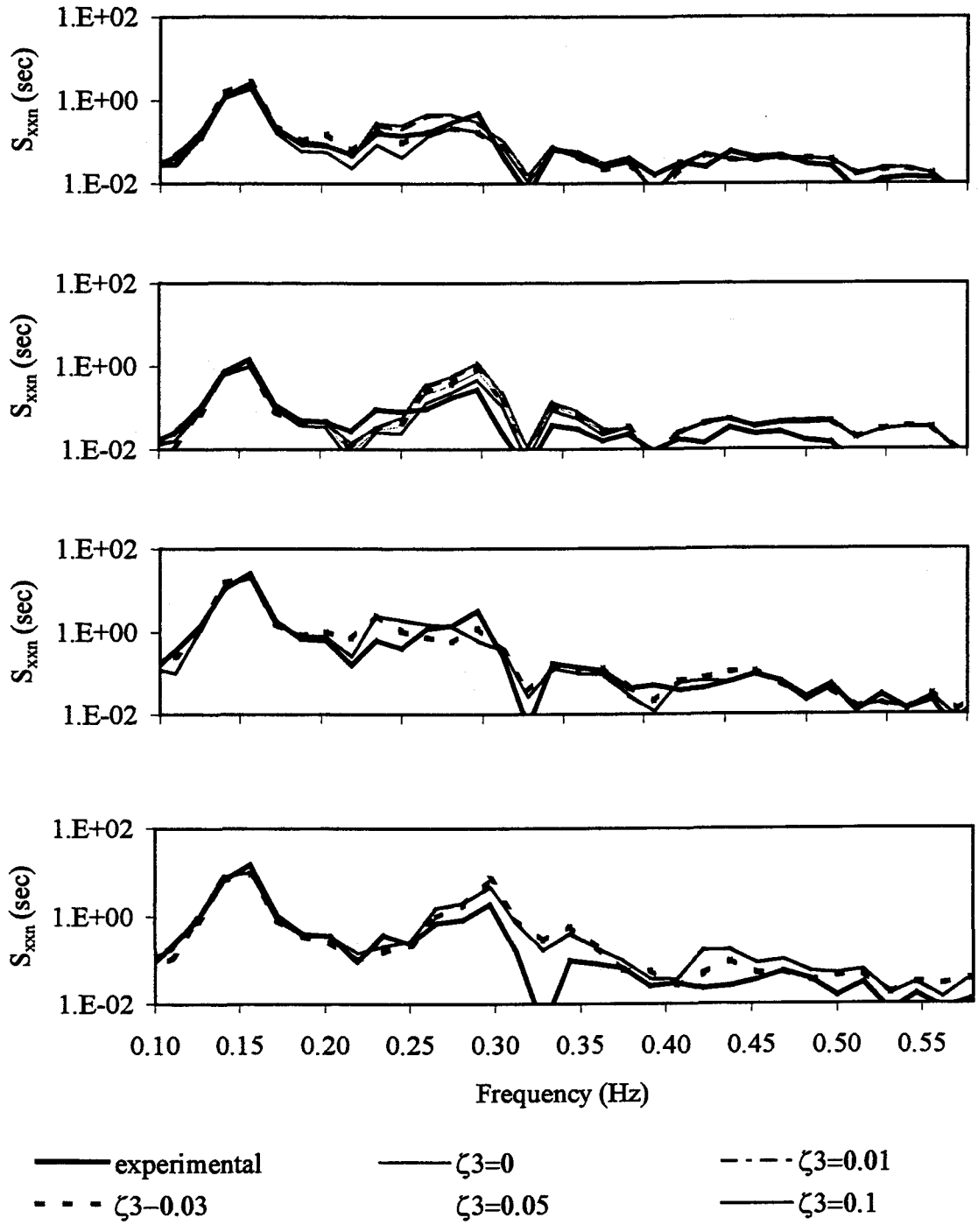

Fig.4.11 Effect of ζ_3 on MDOF system behavior: a) (first) MSP1H, b) (second) MSP1S, c) (third) MSP2H, d) (fourth) MSP2S

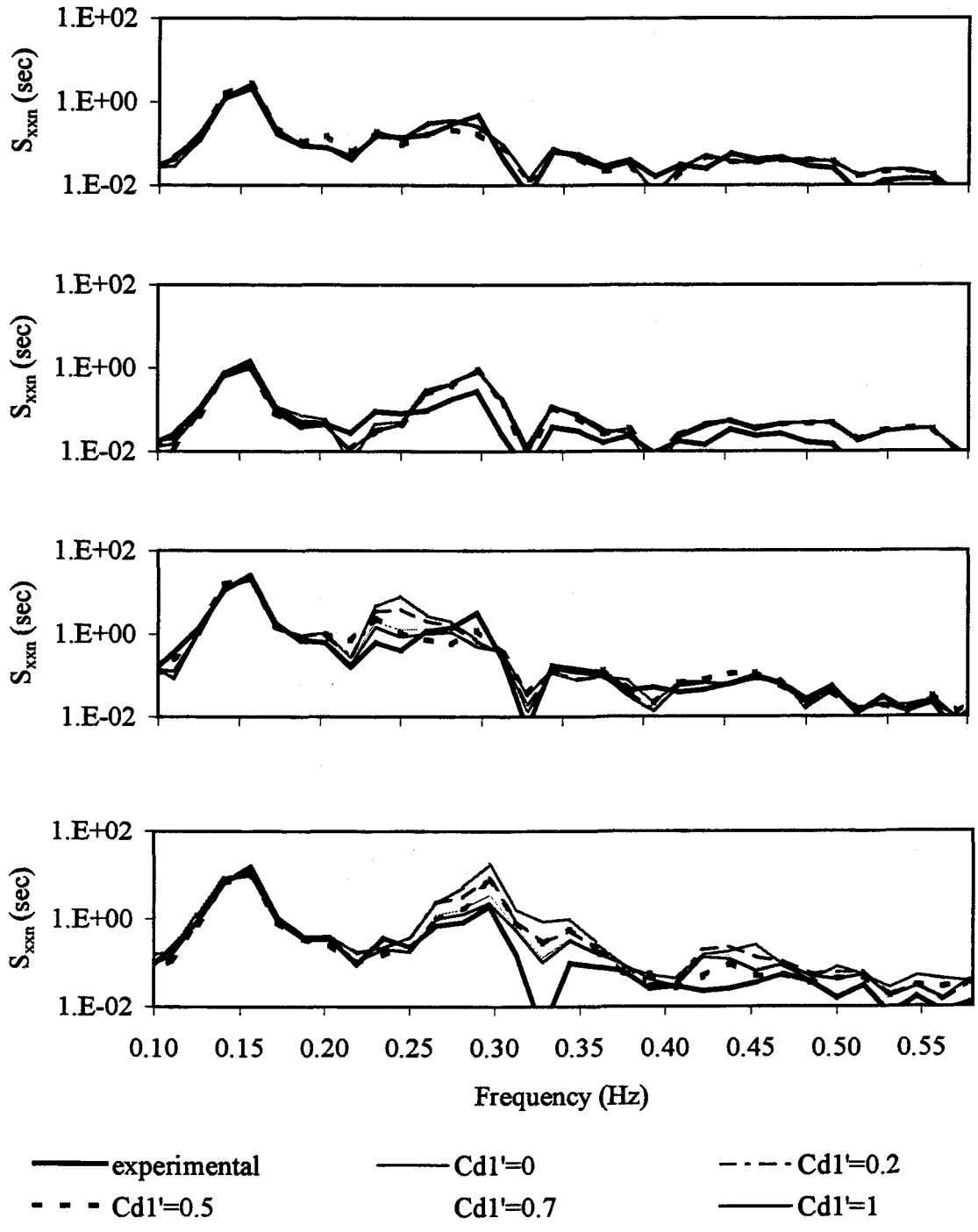

Fig.4.12 Effect of Cd_1' on MDOF system behavior: a) (first) MSP1H, b) (second) MSP1S, c) (third) MSP2H, d) (fourth) MSP2S

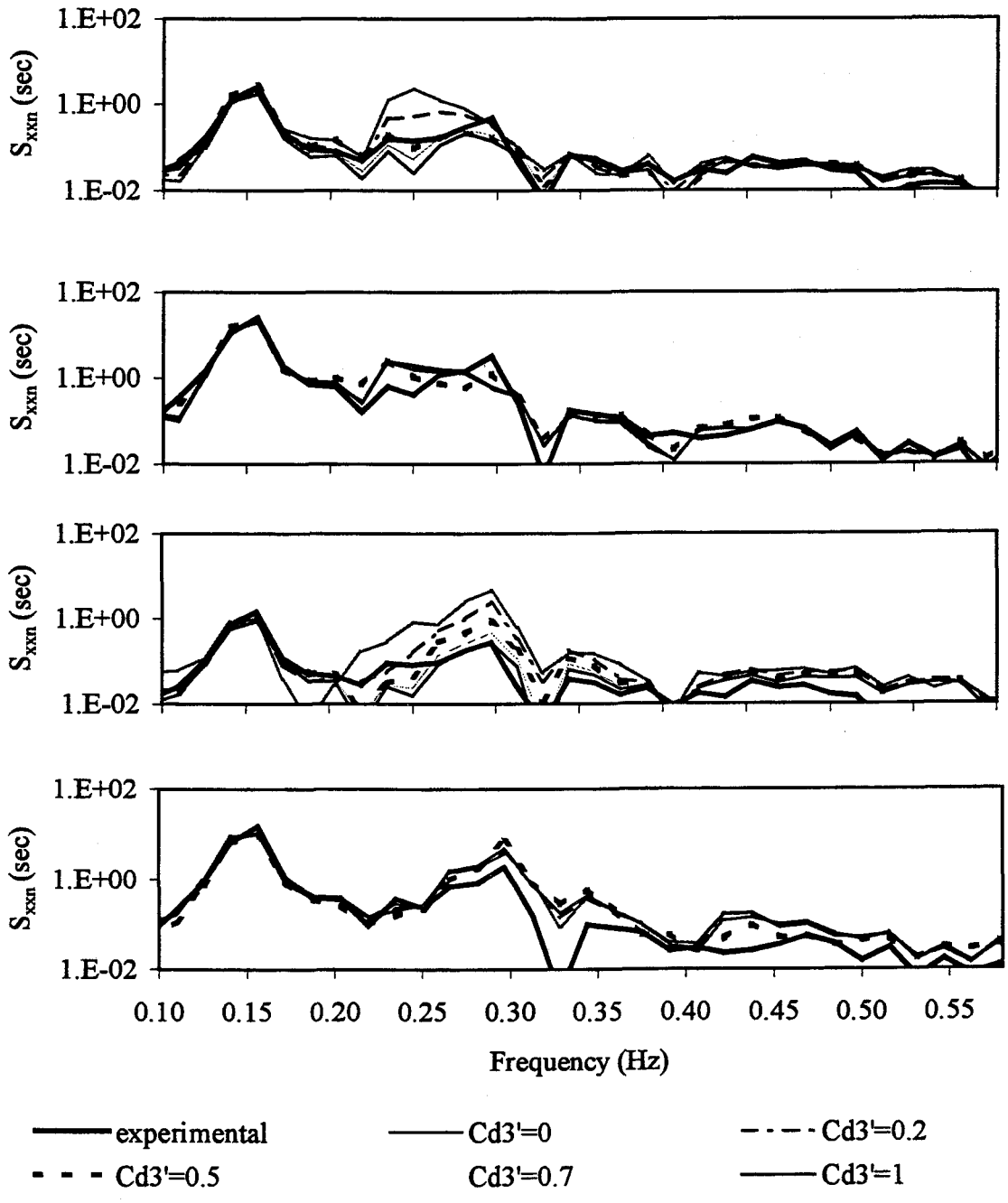

Fig.4.13 Effect of Cd_3' on MDOF system behavior: a) (first) MSP1H, b) (second) MSP1S, c) (third) MSP2H, d) (fourth) MSP2S

When the stiffness parameter in heave, b_1 is increased, the effects are similar for heave as observed for the surge response when a_1 is increased.

Since MSP1 and MSP2 are subjected to low wave excitation amplitude similar to ML1 and ML2, the effects of varying nonlinear parameters on the response are not significant. When the linear (ζ_1 and ζ_3) and nonlinear (C_{d1}' and C_{d3}') damping parameters are increased, the nonlinear response in the secondary resonance region decreases for all the five tests.

5. CONCLUSIONS

5.1 Summary

The multi-point moored experimental structure considered is formulated as a single-degree-of-freedom (SDOF) surge and a multi-degree-of-freedom (MDOF) surge-heave, submerged, hydrodynamically damped and excited nonlinear oscillator. The elastic mooring cables are taut and the resulting restoring force is geometrically nonlinear and is approximated by high order polynomials using least square method.

Three alternate multiple-input/single-output models are examined to determine the most appropriate representation for the SDOF configuration. The Reverse Multiple-Input/Single-Output (R-MI/SO) technique is adapted to identify the linear and nonlinear system parameters and thereby the surge response. The identified responses are compared with the corresponding measured data in time and frequency domain to select model that predict the most comparable response.

The nonlinear-structure nonlinearly damped (NSND) model developed and validated for the SDOF configuration is then extended to the MDOF system. Using the identified parameters, a sensitivity analysis is performed on both SDOF and MDOF systems and the effect of system parameters on the response is evaluated. The dependency of the hydrodynamic coefficients on Keulegan-Carpenter (KC) and Reynolds (Re) numbers are also demonstrated. The surge response behavior of both systems are then analyzed and compared.

A similar study of parameter identification and analysis is accomplished using MDOF tests that yield superharmonic response. Using the sensitivity analysis results, the subharmonic and superharmonic response behaviors of the MDOF system are compared.

5.2 Concluding Remarks

Parameter identification and the analysis of SDOF and MDOF systems are performed and the salient features are summarized below:

- Among the three models developed in this study -- nonlinear-structure linearly-damped (NSLD) model, nonlinear-structure coupled hydrodynamically-damped (NSCHD) model, and nonlinear-structure nonlinearly-damped (NSND) model -- subject to the application of the reverse multi-input/single-output (R-MI/SO) technique, the NSND model is determined to be the most suitable analytical model for the experimental system. The NSLD and NSCHD models incorporate relative motion hydrodynamic damping and the system properties identified do not simulate a comparable response with the measured response. With the low Keulegen-Carpenter number and high reduced velocity, the NSND model based on independent flow fields force, is found to be more appropriate for the experimental system.
- Even though the NSCHD model has the capability of identifying drag coefficient, all the predicted parameters are lower in magnitude than that of the actual system parameters identified by NSND model. By treating the drag force as mathematical output along with the system response, the input total force becomes smaller in magnitude and that causes error in identifying the parameters and thereby the system response.

- With the aid of individual coherence functions, it is observed that the quadratic restoring-force polynomial term contributes the most among the nonlinear coherence estimates of the NSND model.
- The NSND model requires the knowledge of the hydrodynamic coefficients, C_d and C_m, for the evaluation of hydrodynamic force on the sphere. The R-MI/SO technique is employed to evaluate the effect of coefficients on the SDOF system response. The results of the R-MI/SO application on the NSND model with C_m varying within a wide range show that the identified natural frequency remains constant, but the linear and nonlinear parameters tend to increase with the increase in C_m. When compared in the frequency domain, the subharmonic energy of the simulated response decreases with increasing values of inertia coefficient and the primary resonance region practically remains constant. For the range of wave heights, wave length, and the structural dimension considered, the inertia force dominates, and variations in the drag coefficient, C_d, does not appear to have significant effect on the identified response.
- NSND models developed for both SDOF and MDOF systems, when subjected to R-MI/SO technique, identify system parameters that simulate a response that matches with the experimental data. The formulation of the computational technique is straightforward, simple and efficient. The standard multiple-input/single-output procedures once developed for SDOF model can easily be extended to systems with higher degrees of freedom.
- A comparison between the MDOF and SDOF surge response time series and spectra show that the response amplitude is comparatively smaller for the SDOF system. This could be due to the restricted movement of SDOF system by the rod passing through the

center of the sphere. The identified surge parameters for the MDOF system in general are larger in magnitude compared to the SDOF parameters.

- The sensitivity analysis of the MDOF system reveals that the effects on the responses become more significant with increasing wave excitation amplitude. The optimum value of system parameters is practically identical for the tests subject to low and high amplitude excitation, but the latter has a restricted range that identifies response matching the experimental response. Increasing linear surge stiffness parameter a_1 has an effect of increasing the primary response and shifting the subharmonic region towards the right for the surge whereas the heave response in the subharmonic resonance region also increases. When the stiffness parameter in heave, b_1 is increased, the heave response is more influenced as expected with the increase in primary response and a right shift of the secondary resonance region. A slight decrease in the surge response is also observed. It is observed that the primary response is not significantly influenced by variations of nonlinear parameters within the range considered. Increasing nonlinear stiffness parameters a_2 and b_3 increases surge and heave subharmonic responses whereas when a_3 has an opposite effect. The subharmonic responses increase with the increase in coupled parameters, c_{12} and c_{21} and decrease with the linear (ζ_1 and ζ_3) and nonlinear (C_{d1}' and C_{d3}') damping parameters.
- SDOF surge response also demonstrates a similar trend as observed for the MDOF system when the surge parameters including a_1, a_2, a_3, ζ_1 and C_{d1}' are varied. Three groups are established among the tests depending on low, medium or high wave excitation amplitude based on the response behavior. The response variation gets more significant with the increase in wave amplitude.

- For the SDOF system, the optimal value and range of nonlinear structural damping coefficient varies among the tests. This apparent behavior is probably caused by the inability of the model to approximate accurately the actual nonlinear behavior of the complex damping mechanism of the SDOF configuration as the Coulomb frictional component is not included in the mathematical model. The nonlinear effects seem to become more prominent at the lower wave amplitudes, resulting in high values with the errors lumped in the coefficient, C_{d1}'. With the rod removed for the MDOF configuration, such behavior is not observed.
- For the experimental data considered for both configurations, C_m varies between 1.1-1.3 for $5.3 \times 10^5 \leq Re_F \leq 7 \times 10^5$ and $4.7 \leq KC_F \leq 6.2$ and 1.3-1.5 for $1.3 \times 10^5 \leq Re_F \leq 3.7 \times 10^5$ and $1.2 \leq KC_F \leq 3.3$. In general, C_m increases with the decrease in Reynolds number and Keulegen-Carpenter number. This behavior is consistent with that of cylinders observed in the literature. Since the experimental wave characteristics fall within the inertia regime, it is not possible to accurately evaluate the drag coefficients. Indeed, the response is observed to be insensitive to variations in C_d.
- Comparing the sensitivity analysis results between tests that yield subharmonic and superharmonic response, it is observed that increasing the linear stiffness coefficient, a_1 has an effect of increasing the primary and decreasing the subharmonic surge response, however it has an opposite outcome on the superharmonic response. When the stiffness parameter in heave, b_1 is increased, the effects are similar for heave as observed for the surge response when a_1 is increased. When the linear (ζ_1 and ζ_3) and nonlinear (C_{d1}' and C_{d3}') damping parameters are increased, the nonlinear response in the secondary resonance region decreases for all the MDOF tests.

5.3 Future Research

Parameter identification and the response behavior of SDOF and MDOF systems are presented in this study. Using the R-MI/SO technique, it is found that NSND model, which incorporates independent flow fields force is the most appropriate model for the mooring system. This model requires the knowledge of hydrodynamic inertia and drag coefficients and an iterative procedure is used to determine the coefficients. With the wave characteristics lie in the inertia dominated region, it has been observed that varying the inertia coefficients within a small range changes the output response. For the future experiments, the hydrodynamic force acting on the sphere needs to be measured thus avoiding the iterative steps to evaluate the coefficients. Then, based on the wave, sphere response and the force measured, the hydrodynamic coefficients can be determined using R-MI/SO technique. Also more experiments need to be conducted in the drag dominated region to examine the influence of drag coefficient on the nonlinear response.

More experiments on SDOF and MDOF systems with similar input characteristics need to be conducted for better comparisons. During the experiment, the MDOF system configuration failed when subjected to large amplitude waves. An alternative setup needs to be designed that permits larger excursion. More experimental studies with a wider range of wave excitation amplitude are needed to better understand the MDOF system behavior and compare with that of SDOF system. For the SDOF constrained system, the nonlinear structural damping coefficient, C_{d1}', varies among the tests. This apparent behavior is probably caused by the inability of the model to replicate the actual nonlinear behavior of the complex damping mechanism of the SDOF configuration as the Coulomb frictional

component is not included in the mathematical model. For the future studies, the model should be refined to incorporate the Coulomb damping component.

BIBLIOGRAPHY

Bendat, J.S Nonlinear 1998. *SystemTechniques and Application.* New York: John Wiley & Sons, Inc.

Bendat, J.S., Palo, P.A., and Coppolino, R.N. 1992. A General Identification Technique for Nonlinear Differential Equations of Motion. *Probabilistic Engineering Mechanics* 7:43-61.

Bendat, J.S., and Piersol, A.G. 1993. *Engineering Applications of Correlation and Spectral Analysis.* New York: John Wiley Publishing.

Bernitsas, M.M., and J.S. Chung. 1990. Nonlinear Stability and Simulation of Two-Line Step Lowering and Mooring. *Applied Ocean Research* 11:153-166.

Bishop, S.R., and Virgin, L.N. 1988. The Onset of Chaotic Motions of a Moored Semi-Submersible. *Journal of Offshore Mechanics and Arctic Engineering* 110: 205-209.

Chakrabarti, S.K. 1987. *Hydrodynamics of Offshore Structures.* London: Computational Mechanics Publications

Clough, R.W., and Penzien, J. 1993. *Dynamics of Structures.* McGraw-Hill, Inc.

Edwins, P.J 1984. *Model Testing: Theory and Practice.* Letchworth, Hertordshire, England:Research Studies

Esmonde, H., Fitzpatrick, J.A., Rice, H.J., and Axisa, F 1990. Analysis of Non-Linear Squeeze Film Dynamics: Part I-Physical theory and modeling. *Flow Induced Vibration, ASME PVP* 189:171-177.

Esmonde, H., Axisa, F., Fitzpatrick, J.A., and Rice, A.J 1990. Analysis of Non-Linear Squeeze Film Dynamics: Part II-Experimental Measurement and Model Verification. *Flow Induced Vibration, ASME PVP* 189: 179-184.

Gottileb, O., and Yim, S.C.S.1992. Nonlinear Oscillations, Bifurcations and Chaos in a Multi-Point Mooring System with a Geometric Nonlinearity. *Applied Ocean Research* 14:6: 241-257.

Gottlieb, O., Yim, S.C.S., and Hudspeth, R.T. 1992. Analysis of Nonlinear Response of Articulated Tower. *International Journal of Offshore and Polar Engineering ASCE* 2:1:61-66.

Gottlieb, O., and Yim, S.C.S. 1993. Drag Induced Instabilities and Chaos in Mooring Systems. *International Journal of Ocean Engineering* 29:6:569-599.

Grace, R.A., and Casiano, F.M. 1969. Ocean Wave Forces on a Sub Surface Sphere. *Journal of Waterways and Harbour Division.* 95:291-312.

Grace, R.A., and Zee, G.T.Y.1978. Further Tests on Ocean Wave Forces on Sphere. *Journal of Waterway Port Coastal and Ocean Division.* 104:83-88.

Hjelmfelt, A.T, et al 1967. Dynamic Repsonse of a Restrained sphere in a Fluid. *Journal of the Engineering Mechanics Division, ASCE* 93:EM1:41-56.

Isaacson, M., and Phadke, A. 1994. Chaotic Motion of a Nonlinearly Moored Structure. *Proceedings. 4th International Offshore and Polar Engineering Conference* 111:338-345.

Laya, E.J., Connor, J.J., and Shyam Sundar, S. Hydrodynamic Forces on Flexible Offshore Structures. *Journal of Engineering Mechanics, ASCE* 199:3:433-488.

Lin, H. 1994. *Stochastic Analysis of a Nonlinear Ocean Structural System.* Ph.D. Dissertation. Oregon State University.

Lin, H., and Yim, S.C.S. 1996. Analysis of a Nonlinear System Exhibiting Chaotic, Noisy Chaotic and Random Behaviors. *Journal of Applied Mechanics ASME* 63:2:509-516.

Lin, H., and Yim, S.C.S. 1996. Deterministic and Stochastic Analyses of Chaotic and Overturning Responses of a Slender Rocking Object. *International Journal of Nonlinear Dynamics* 11:83-106.

Lin, H., and Yim, S.C.S. 1997. Noisy Nonlinear Motions of a Moored System, Part I: Analysis and Simulations. *Journal of Waterway, Port, Coastal and Ocean Engineering ASCE* 123:5:287-295.

Lin, H., Yim, S.C.S., and O. Gottlieb. 1998. Experimental investigation of response stability and transection behavior of a non-linear ocean structural system. *Ocean Engineering* 25:4-5:323-343.

Lin, H., and Yim, S.C.S. 1998. Experimental Calibration of Bifurcation Superstructure of Nonlinear System. *Journal of Engineering Mechanics ASCE* 124:4:471-475.

Rice, H.J., and Fitzpatrick, J.A 1988. A Generalized Technique for Spatial Analysis of Non-Linearization. *Mecahnical Systems and signal processing* 2 (2): 195-207.

Rice, H.J., and Fitzpatrick, J.A 1991. The Measurement of Nonlinear Damping on Single Degree-of-Freedom System. Transaction of the American Society of Mechanical Engineers. *Journal of Vibration and Acoustics* 113:132-140.

Sarpkaya, T., and M. Isaacson.1981. *Mechanics of Wave Forces on Offshore Structures.* Van Nostrand Reinhold.

Thompson, J.M.T.1983. *Complex Dynamics of Complaint Offshore Structures.* Proceedings of the Royal Society of London 387:1793:407-427.

Thompson, J.M.T., and Stewart, H.B. 1986. *Nonlinear Dynamics and Chaos.* John Wiley & Sons, Ltd.

Wang, C.Y 1965. The Flow Induced by an Oscillating sphere. *Journal of Sound and Vibration* 2:3:257-267.

Yim, S.C.S., Myrum, M.A., Gottileb, O., Lin, H., and Shih, I-M.1993. *Summary and Preliminary Analysis of Nonlinear Oscillations in a Submerged Mooring System Experiment.* Ocean Engineering Report No. OE-93-03. Office of Naval Research.

APPENDICES

APPENDIX A

A. FORMULATION OF THE NSND MODEL FOR THE MDOF SYSTEM

The R-MI/SO technique can be applied to most nonlinear systems subject to random excitation irrespective of the nature of the distribution (e.g., Gaussian or non-Gaussian (Bendat 1998)). The relative contribution of the linear and nonlinear system properties, whether or not the system properties are frequency dependent and how the cumulative coherence functions are improved by adding nonlinear terms can be determined using this technique.

The nonlinear equation for the MDOF NSLD model is

$$(m+m_a)\ddot{x}_1(t)+C_{s1}\dot{x}_1(t)+a_1x_1(t)+a_2{x_1}^2(t)+a_3{x_1}^3(t)+a_4{x_3}^2(t)x_1(t) \qquad \text{(A.1a)}$$
$$+\rho C'_{d1}\frac{\pi D^2}{4}\dot{x}_1(t)|\dot{x}_1(t)|=f_{1a}(t)$$

$$(m+m_a)\ddot{x}_3(t)+C_{s3}\dot{x}_3(t)+b_1x_3(t)+b_2{x_3}^3(t)+b_3{x_1}^2(t)x_3(t) \qquad \text{(A.1b)}$$
$$+\rho C'_{d3}\frac{\pi D^2}{4}\dot{x}_3(t)|\dot{x}_3(t)|=f_{3a}(t)$$

where

$$f_{1a}(t)=\frac{1}{2}\rho C_d\frac{\pi D^2}{4}u_1(t)|u_1(t)|+\rho\frac{\pi}{6}D^3C_m\dot{u}_1(t) \qquad \text{(A.2a)}$$

$$f_{3a}(t)=\frac{1}{2}\rho C_d\frac{\pi D^2}{4}u_3(t)|u_3(t)|+\rho\frac{\pi}{6}D^3C_m\dot{u}_3(t) \qquad \text{(A.2b)}$$

Values of the inertia and drag coefficients are assumed in order to evaluate the force $f_{1a}(t)$ and $f_{3a}(t)$ given by Eqs.(A.2a and b), which are treated as the model input and the system responses, x_1 and x_3, are treated as the model outputs.

Fourier transforming both sides of Eqs.(A.1a, b) gives the frequency domain relation

$$\left(a_1 + j(2\pi f)C_{s1} - (2\pi f)^2(m+m_a)\right)X_{11}(f) + A_{12}(f)X_{12}(f) + A_{13}(f)X_{13}(f) + A_{14}(f)X_{14}(f) + A_{15}(f)X_{15}(f) = F_{1a}(f) \quad \text{(A.3a)}$$

$$\left(b_1 + j(2\pi f)C_{s3} - (2\pi f)^2(m+m_a)\right)X_{31}(f) + A_{32}(f)X_{32}(f) + A_{33}(f)X_{33}(f) + A_{34}(f)X_{34}(f) = F_{3a}(f) \quad \text{(A.3b)}$$

where

$$F_{1a}(f) = \Im[f_{1a}(t)],\ F_{3a}(f) = \Im[f_{31a}(t)] \quad \text{(A.4)}$$

$$X_{11}(f) = \Im[x_1(t)],\ X_{31}(f) = \Im[x_3(t)] \quad \text{(A.5)}$$

$$X_{12}(f) = \Im\left[x_1^{\,2}(t)\right] \quad \text{(A.6)}$$

$$X_{13}(f) = \Im\left[x_1^{\,3}(t)\right],\ X_{32}(f) = \Im\left[x_3^{\,3}(t)\right] \quad \text{(A.7)}$$

$$X_{14}(f) = \Im\left[x_3^{\,2}(t)x_1(t)\right],\ X_{33}(f) = \Im\left[x_1^{\,2}(t)x_3(t)\right] \quad \text{(A.8)}$$

$$X_{15}(t) = \dot{x}_1(t)|\dot{x}_1(t)|,\ X_{35}(t) = \dot{x}_3(t)|\dot{x}_3(t)| \quad \text{(A.9)}$$

$$A_{12}(f) = a_2 \quad \text{(A.10)}$$

$$A_{13}(f) = a_3,\ A_{32}(f) = b_2 \quad \text{(A.11)}$$

$$A_{14}(f) = a_4,\ A_{33}(f) = b_3 \quad \text{(A.12)}$$

$$A_{15}(f) = \frac{1}{2}\rho C'_{d1}\frac{\pi D^2}{4},\ A_{34}(f) = \frac{1}{2}\rho C'_{d3}\frac{\pi D^2}{4} \quad \text{(A.13)}$$

In the absence of nonlinear terms, $H_{11}(f)$ and $H_{31}(f)$ represent the frequency response functions of an ideal constant parameter linear systems that relates the displacement outputs, $x_1(t)$ and $x_3(t)$, to the corresponding force inputs, $f_{1a}(t)$ and $f_{3a}(t)$, respectively. They are given by

$$H_{11}(f) = \frac{X_{11}(f)}{F_{1a}(f)} = \left[a_1 + j(2\pi f)C_{s1} - (2\pi f)^2(m + m_a)\right]^{-1} \quad \text{(A.14a)}$$

$$= a_1[1 - (f/f_{n1})^2 + 2\zeta_{s1}(f/f_{n1})]^{-1}$$

$$H_{31}(f) = \frac{X_{33}(f)}{F_{3a}(f)} = \left[b_1 + j(2\pi f)C_{s3} - (2\pi f)^2(m + m_a)\right]^{-1} \quad \text{(A.14b)}$$

$$= b_1[1 - (f/f_{n3})^2 + 2\zeta_{s3}(f/f_{n3})]^{-1}$$

where the natural frequencies, f_{n1}, f_{n3}, and the damping ratios, ζ_{s1}, ζ_{s3}, are defined by

$$f_{n1} = \frac{1}{2\pi}\sqrt{\frac{a_1}{(m + m_a)}}\ ,\ f_{n3} = \frac{1}{2\pi}\sqrt{\frac{b_1}{(m + m_a)}} \quad \text{(A.15)}$$

$$\varsigma_{s1} = \frac{C_{s1}}{2\sqrt{a_1(m + m_a)}}\ ,\ \varsigma_{s3} = \frac{C_{s3}}{2\sqrt{b_1(m + m_a)}} \quad \text{(A.16)}$$

When the nonlinear terms are present, $H_{11}(f)$ and $H_{31}(f)$ relates the displacement outputs to corresponding effective forces, $f_{1e}(t)$ and $f_{3e}(t)$, by

$$f_{1e}(t) = f_{1a}(t) - a_2x_1^2(t) - a_3x_1^3(t) - a_4x_3^2(t)x_1(t) - a_5\dot{x}_1(t)|\dot{x}_1(t)| \quad \text{(A.17)}$$

$$f_{31e}(t) = f_{31a}(t) - b_2x_1^3(t) - b_3x_1^2(t)x_3(t) - b_4\dot{x}_3(t)|\dot{x}_3(t)| \quad \text{(A.18)}$$

Identification of this system requires a time-consuming iterative approach because of the presence of the nonlinear feed back terms. Because the forward way of analysis is difficult, an alternative reverse dynamic viewpoint is considered (Bendat 1998). To apply the R-MI/SO technique, the input/output roles are mathematically interchanged.

The associated Fourier transform relation is given by

$$F_{1a}(f) = A_{11}(f)X_{11}(f) + A_{12}(f)X_{12}(f) + A_{13}(f)X_{13}(f) + A_{14}(f)X_{14}(f) + A_{15}(f)X_{15}(f) \quad \text{(A.19a)}$$

$$F_{3a}(f) = A_{31}(f)X_{31}(f) + A_{32}(f)X_{32}(f) + A_{33}(f)X_{33}(f) + A_{34}(f)X_{34}(f) \quad \text{(A.19b)}$$

$A_{11}(f)$ and $A_{31}(f)$ is defined as the linear impedance functions which is given by

$$A_{11}(f) = [H_{11}(f)]^{-1} = a_1\left(1 - (f/f_{n1})^2 + 2j\zeta_{s1}(f/f_{n1})\right) \tag{A.20a}$$

$$A_{31}(f) = [H_{31}(f)]^{-1} = b_1\left(1 - (f/f_{n3})^2 + 2j\zeta_{s3}(f/f_{n3})\right) \tag{A.20b}$$

The system gain and phase factors of Eqs.(A.20a,b) are given by

$$|A_{11}(f)| = a_1\left[\sqrt{\left(1 - (f/f_{n1})^2\right)^2 + (2\zeta_{s1}(f/f_{n1}))^2}\right] \tag{A.21a}$$

$$|A_{31}(f)| = b_1\left[\sqrt{\left(1 - (f/f_{n3})^2\right)^2 + (2\zeta_{s3}(f/f_{n3}))^2}\right] \tag{A.21b}$$

$$\phi_1(f) = \tan^{-1}\left[\frac{2\zeta_{s1}\, f/f_{n1}}{1-(f/f_{n1})^2}\right],\ \phi_3(f) = \tan^{-1}\left[\frac{2\zeta_{s3}\, f/f_{n3}}{1-(f/f_{n3})^2}\right] \tag{A.21c}$$

The minimum gain factor occurs at the resonance frequencies, f_{r1} and f_{r3}, of the system. By determining the maxima of Eqs.(A.21a,b), it can be shown that for structures having damping ratio $\zeta_s \leq 0.5$, (Clough and Penzien 1993), resonance frequencies are given by

$$f_{r1} = f_{n1}\sqrt{1-2\zeta_{s1}^2} \qquad f_{r3} = f_{n3}\sqrt{1-2\zeta_{s3}^2} \tag{A.22}$$

The minimum values of the gain factors that occur at resonance are given by

$$|A_{11}(f_{r1})| = a_1\left[2\zeta_{s1}\sqrt{1-\zeta_{s1}^2}\right] \tag{A.23}$$

$$|A_{13}(f_{r3})| = b_1\left[2\zeta_{s3}\sqrt{1-\zeta_{s3}^2}\right] \tag{A.24}$$

For lightly damped systems, the resonance frequencies and the minimum values of the gain factors can be approximated (Bendat 1998) by

$$f_{r1} \approx f_{n1},\ f_{r3} \approx f_{n3},\ |A_{11}(f_{r1})| \approx 2a_1\zeta_{s1},\ |A_{31}(f_{r3})| \approx 2b_1\zeta_{s3} \tag{A.25}$$

The physical parameters of the mooring system can therefore be estimated as follows

$$a_1 \approx A_{11}(0), \quad b_1 \approx A_{31}(0) \tag{A.26}$$

$$C_a = \frac{m_a}{(\pi/6\rho D^3)} \tag{A.27}$$

$$C_{s1} = 2\zeta_{s1}\sqrt{(a_1(m+m_a))} \approx \frac{|A_{11}(f_{n1})|}{2\pi f_{n1}} \tag{A.28a}$$

$$C_{s3} = 2\zeta_{s3}\sqrt{(b_1(m+m_a))} \approx \frac{|A_{31}(f_{n3})|}{2\pi f_{n3}} \tag{A.28b}$$

The reverse dynamic inputs may be correlated. Procedures to replace the correlated inputs with a new set of uncorrelated inputs are applied to convert the nonlinear model to an equivalent three-input/single-output linear model (Bendat 1998). The resulting impedance functions yield all the system properties given by Eqs.(A.10-A.13 and A.26-A.28).

APPENDIX B

B. SENSITIVITY ANALYSIS OF MDOF AND SDOF SYSTEMS

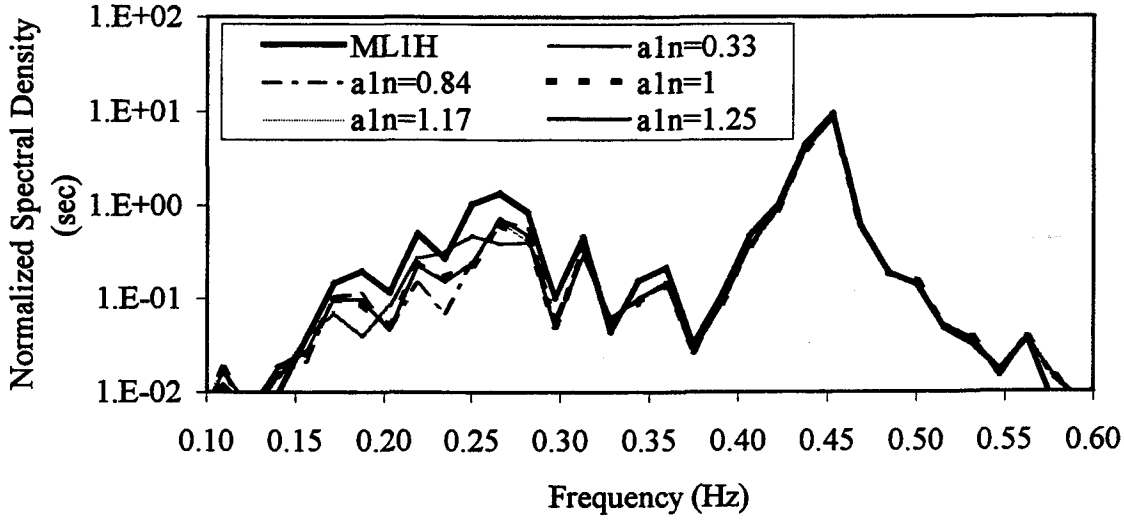

(a)

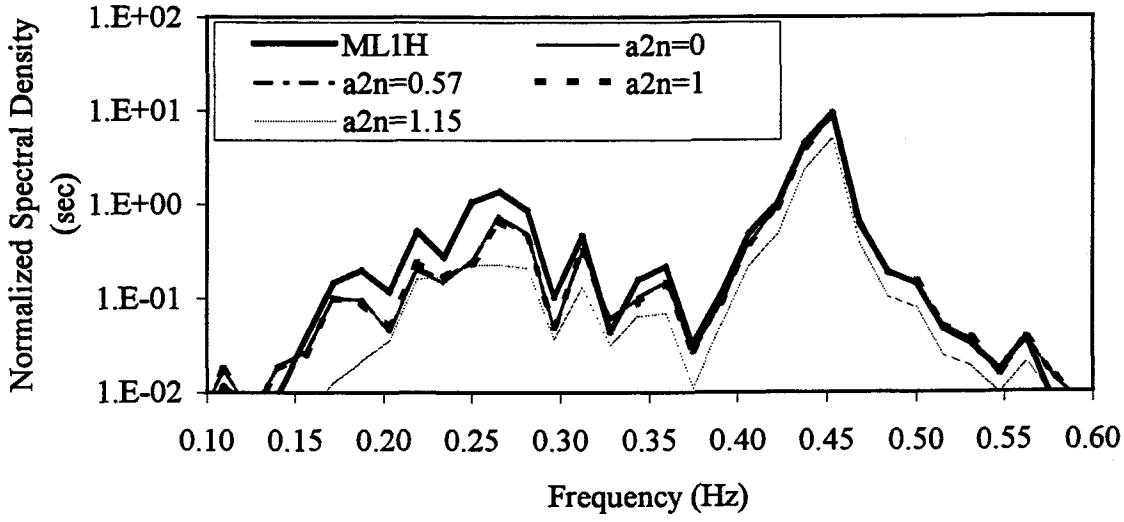

(b)

Fig.B.1 Effect of system parameters on heave response for ML1: a) a_1, b) a_2, c) a_3, d) b_1, e) b_3, f) c_{12}, g) c_{21}, h) ζ_1, i) ζ_3, j) C_{d1}', k) C_{d3}'

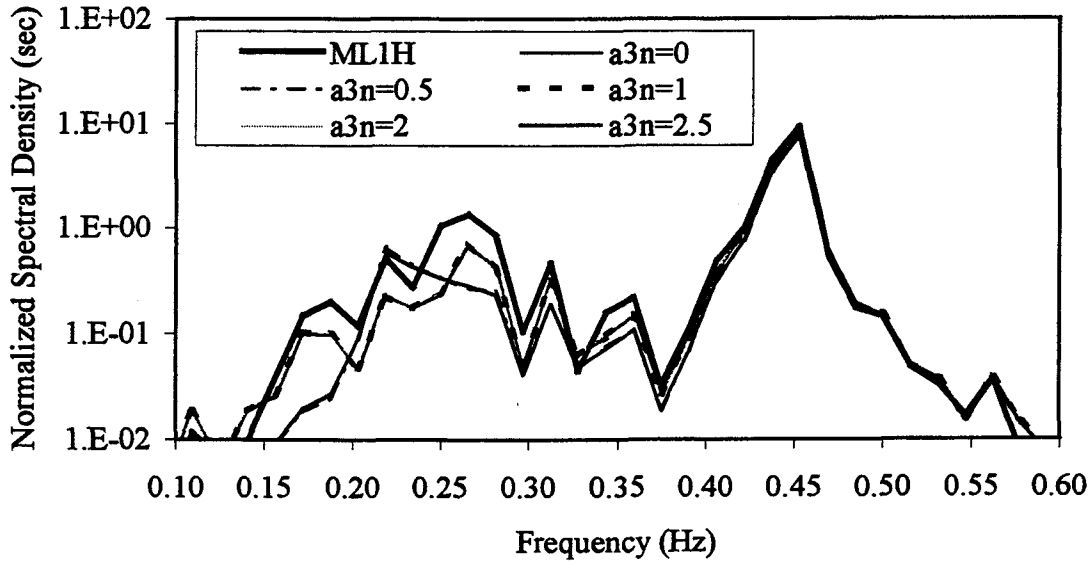

(c)

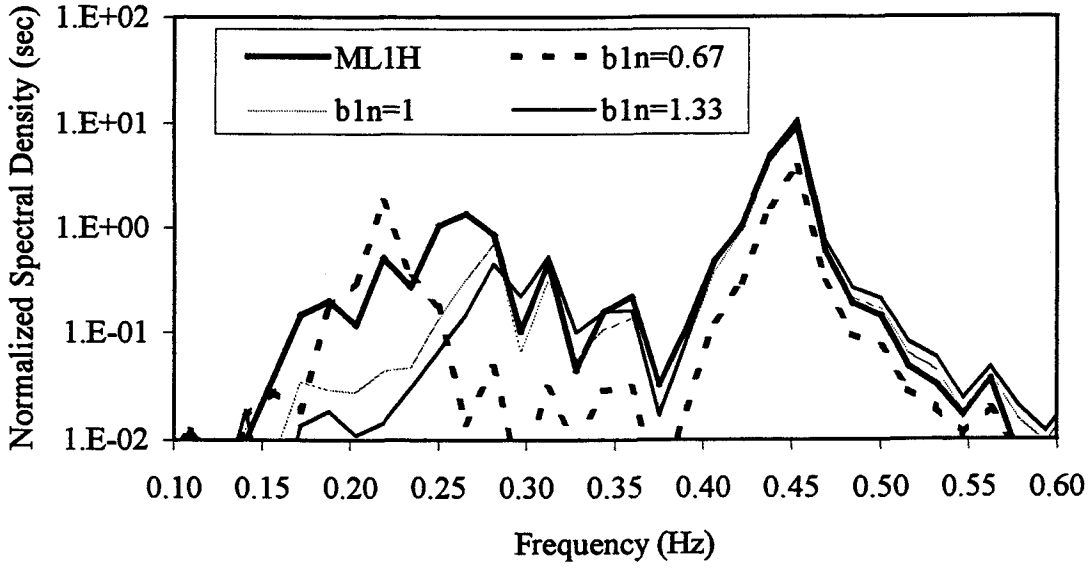

(d)

Fig.B.1 Continued

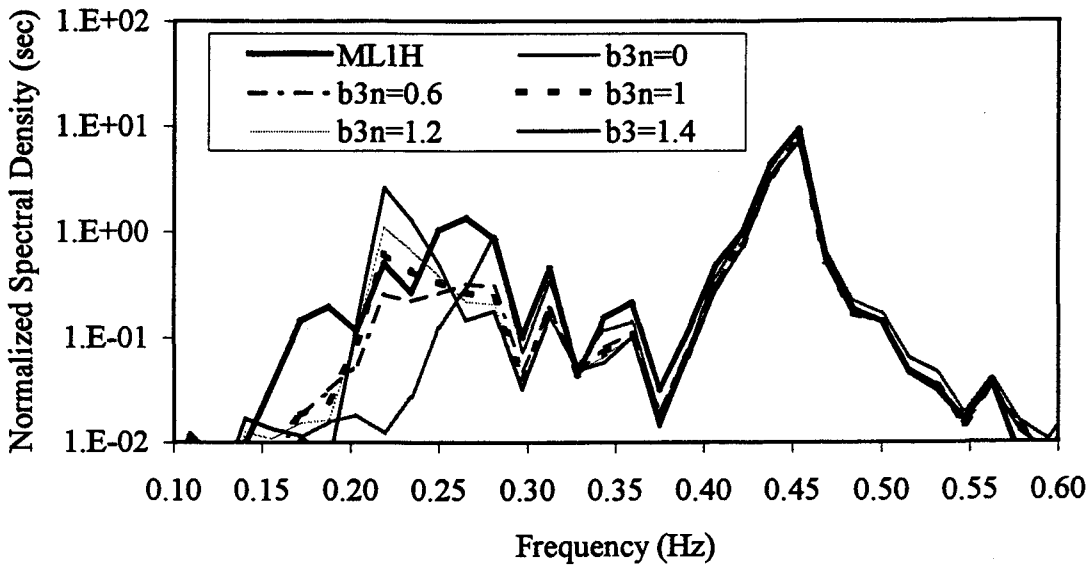

(e)

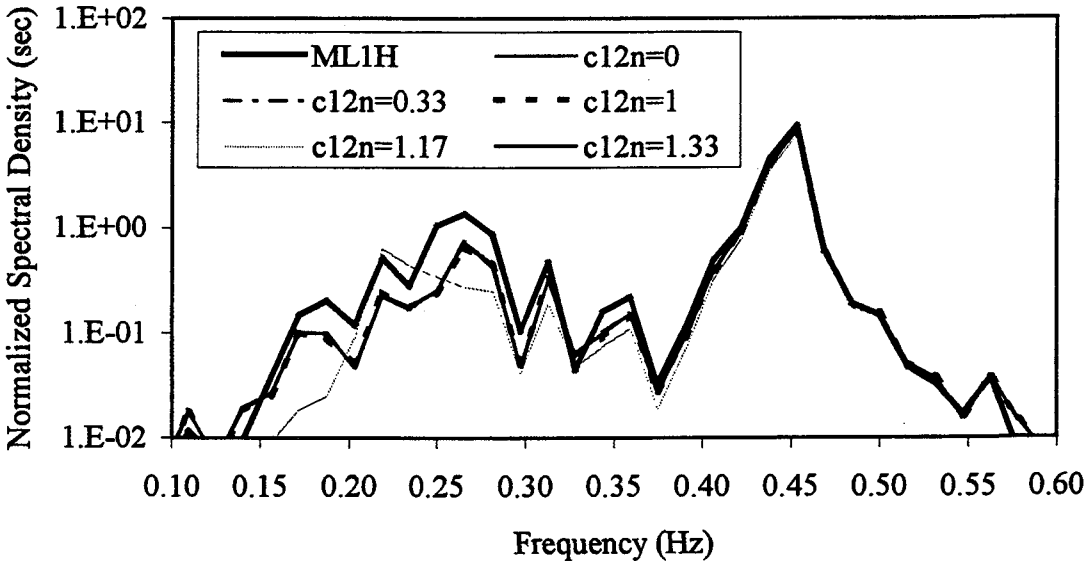

(f)

Fig.B.1 Continued

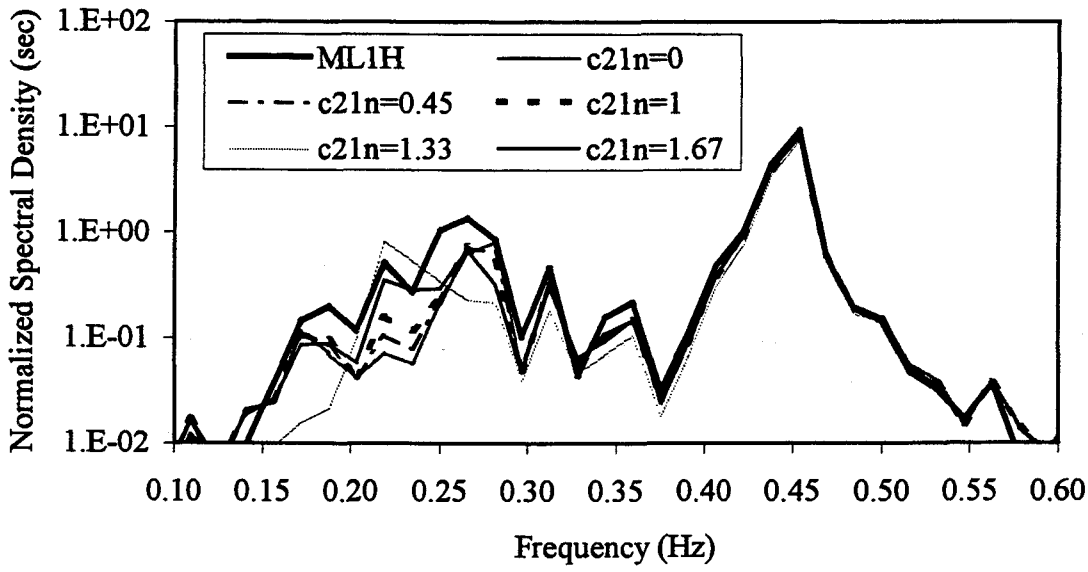

(g)

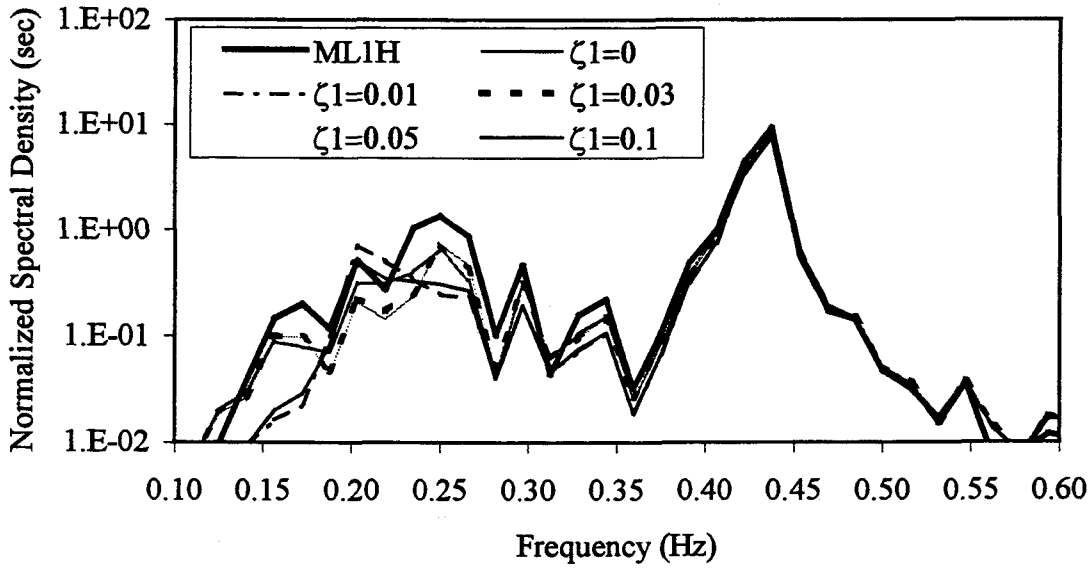

(h)

Fig.B.1 Continued

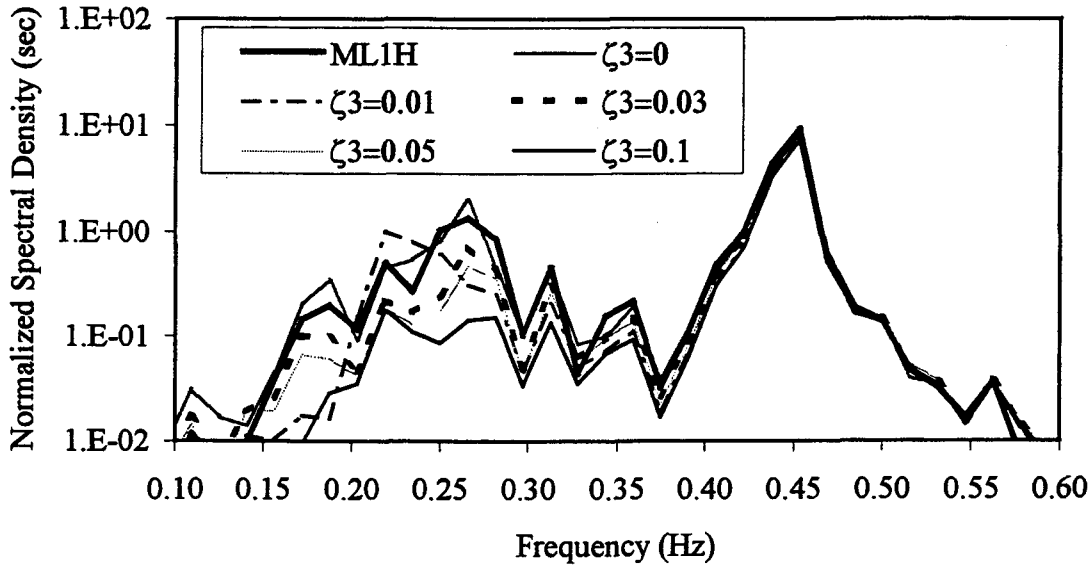

(i)

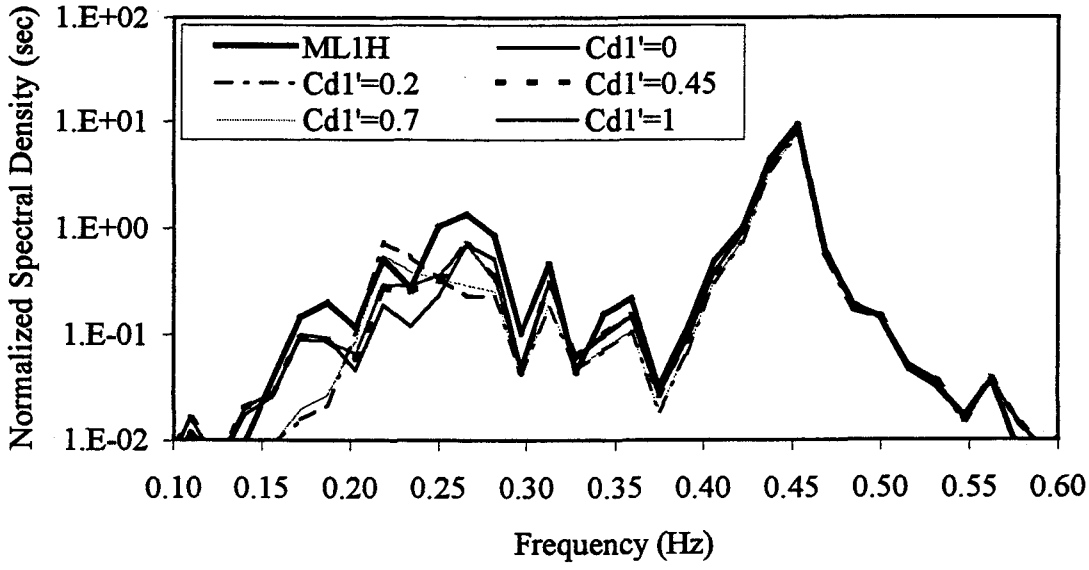

(j)

Fig.B.1 Continued

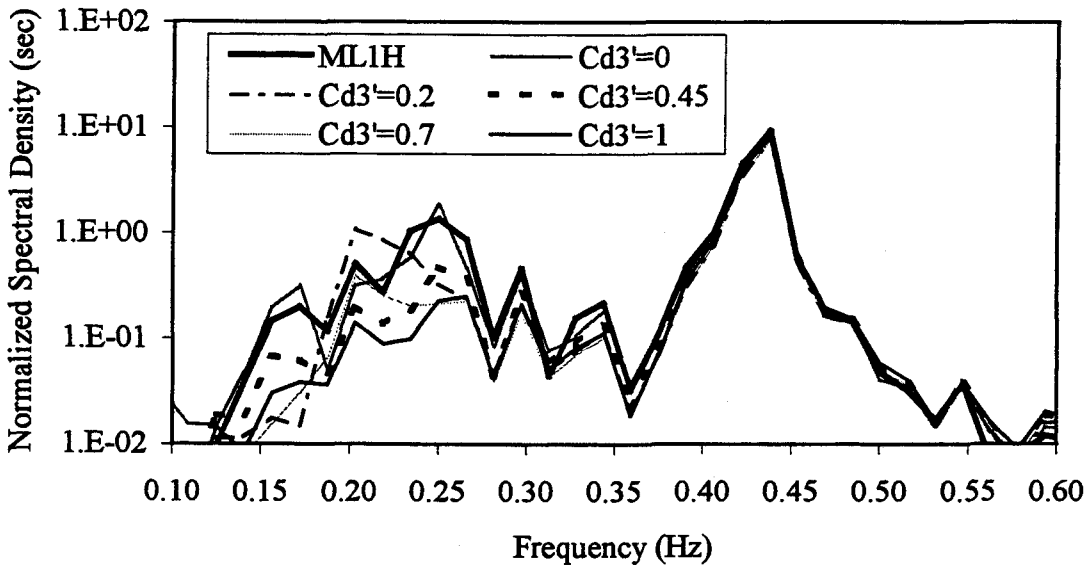

(k)

Fig.B.1 Continued

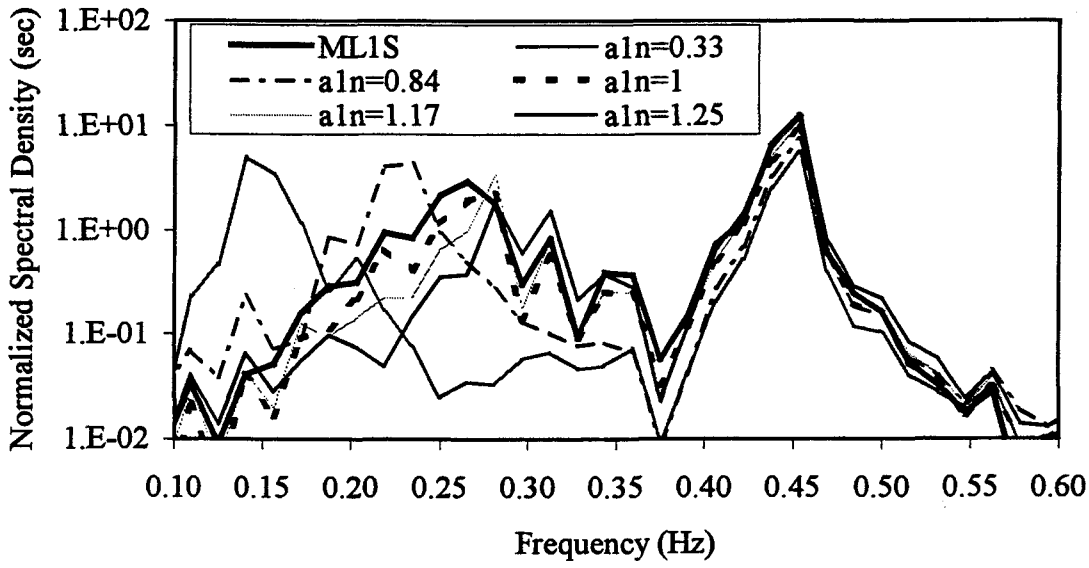

(a)

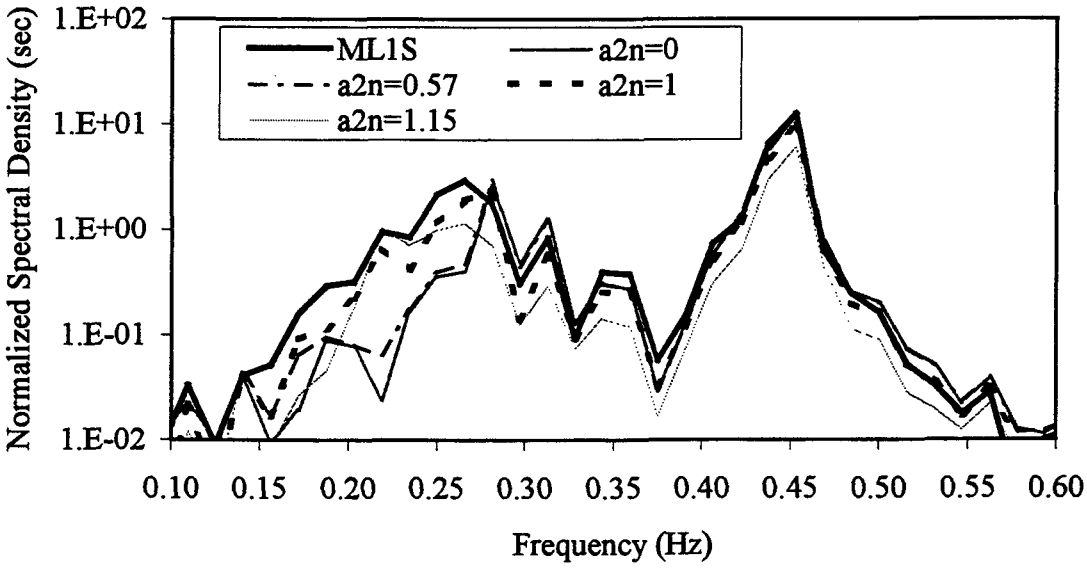

(b)

Fig.B.2 Effect of system parameters on surge response for ML1: a) a_1, b) a_2, c) a_3, d) b_1, e) b_3, f) c_{12}, g) c_{21}, h) ζ_1, i) ζ_3, j) C_{d1}', k) C_{d3}'

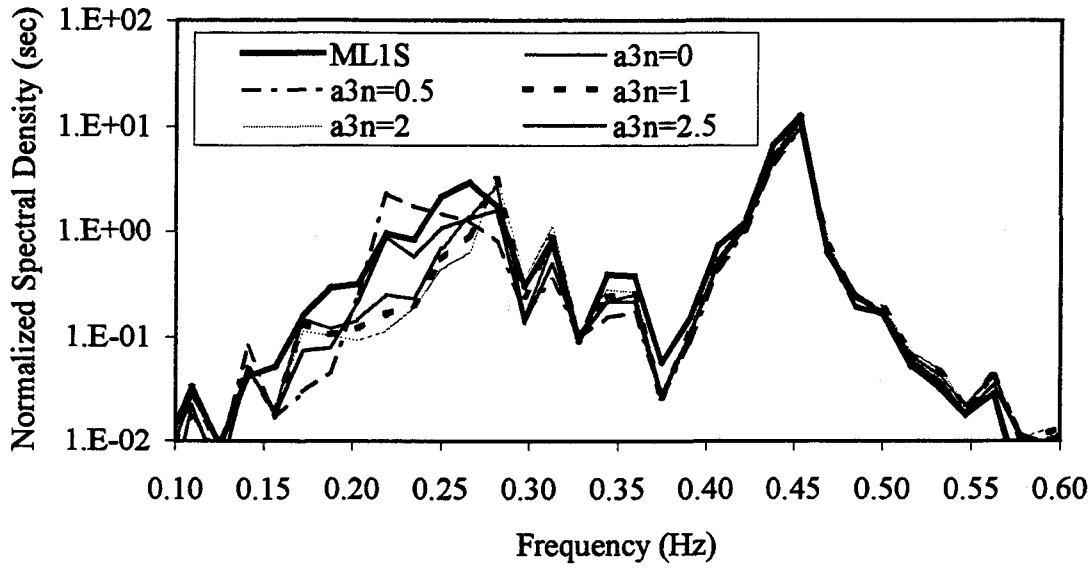

(c)

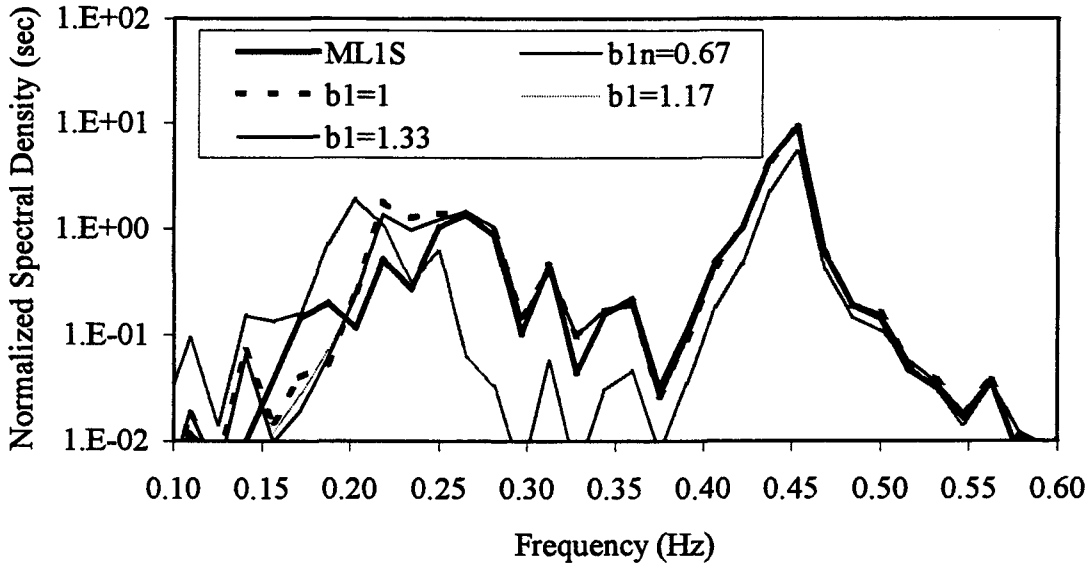

(d)

Fig.B.2 Continued

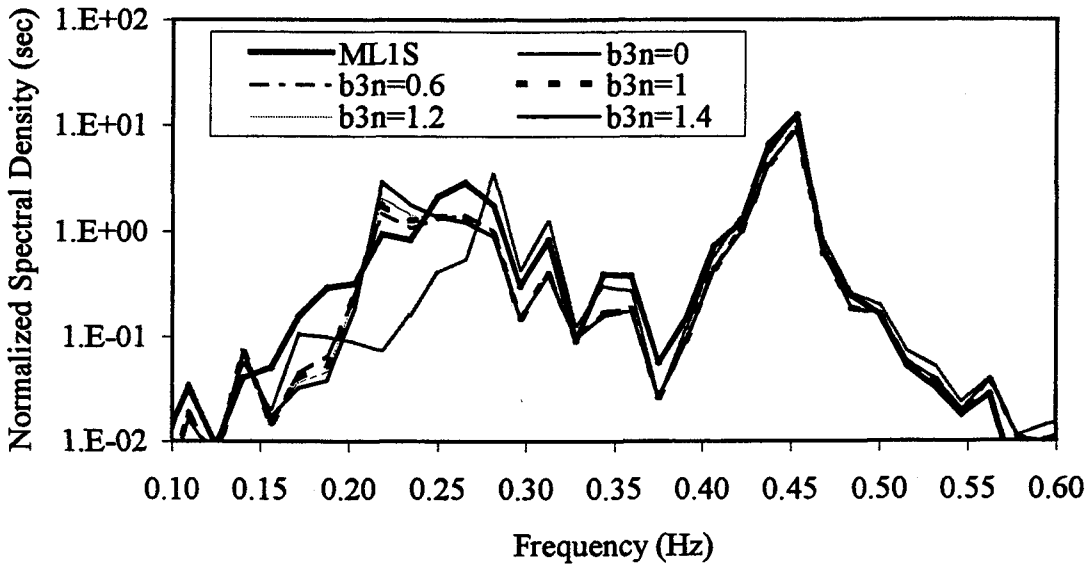

(e)

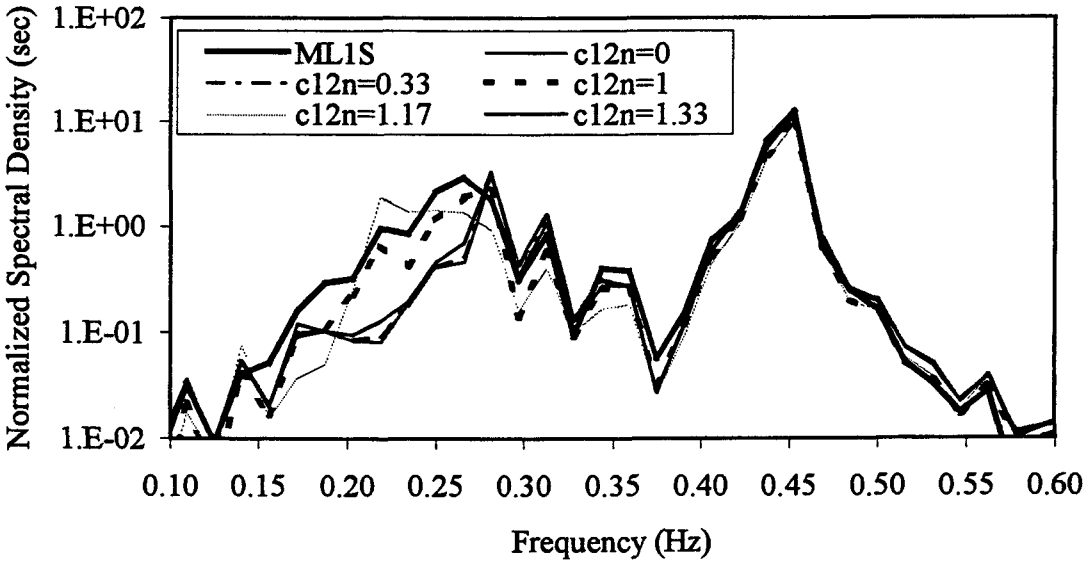

(f)

Fig.B.2 Continued

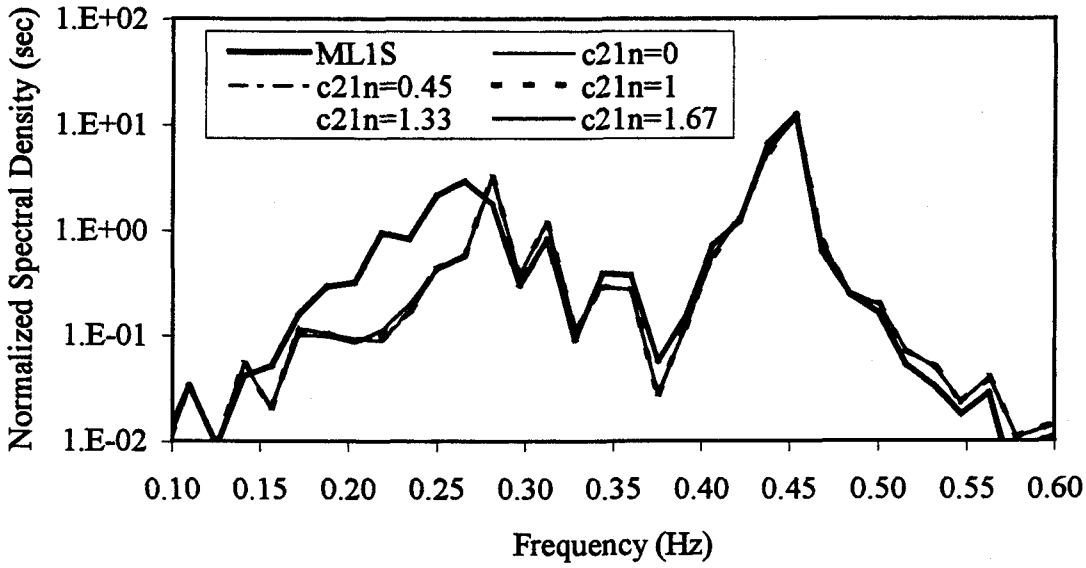

(g)

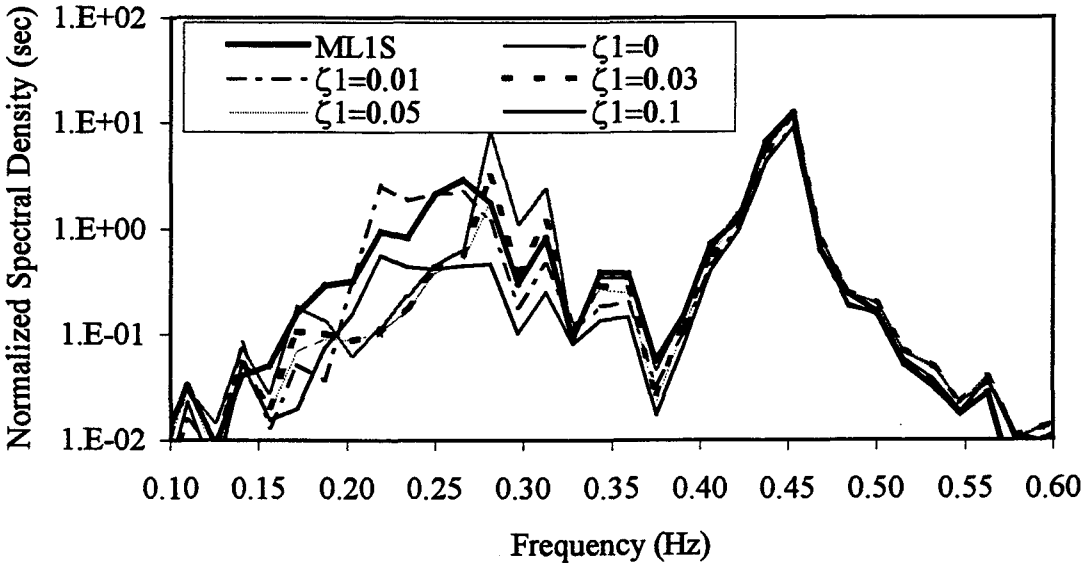

(h)

Fig.B.2 Continued

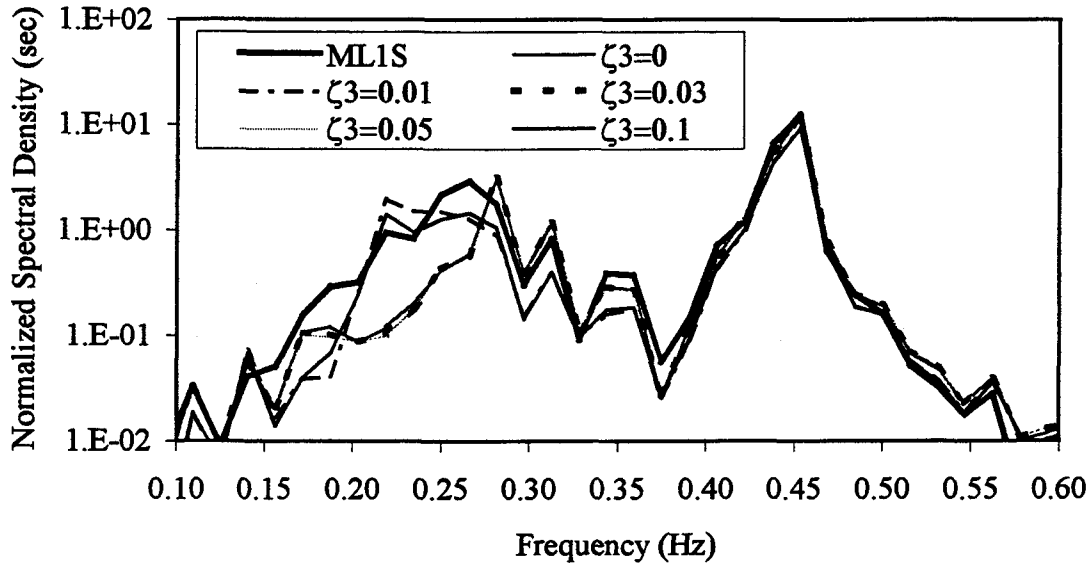

(i)

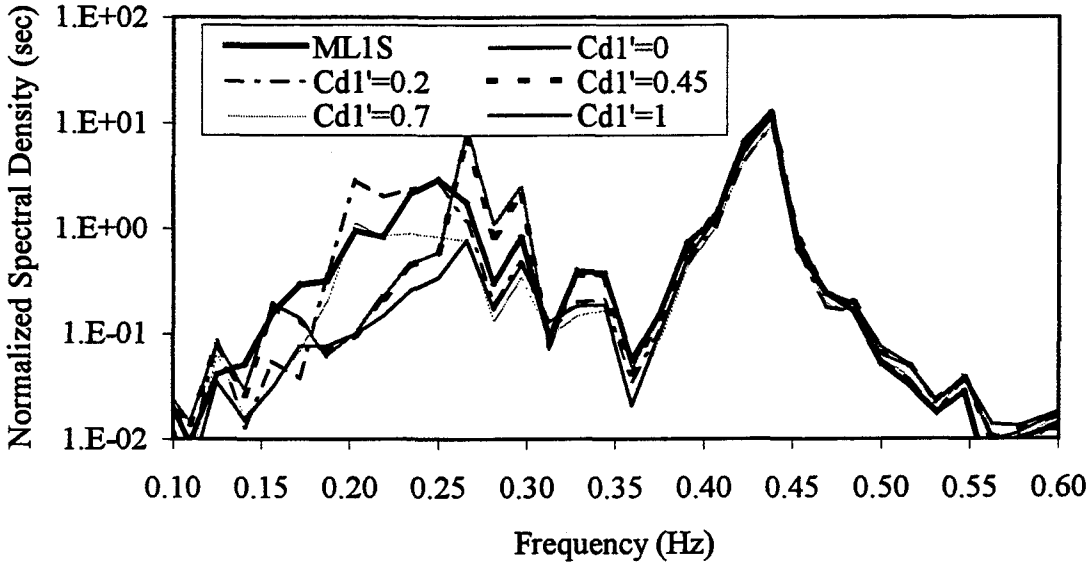

(j)

Fig.B.2 Continued

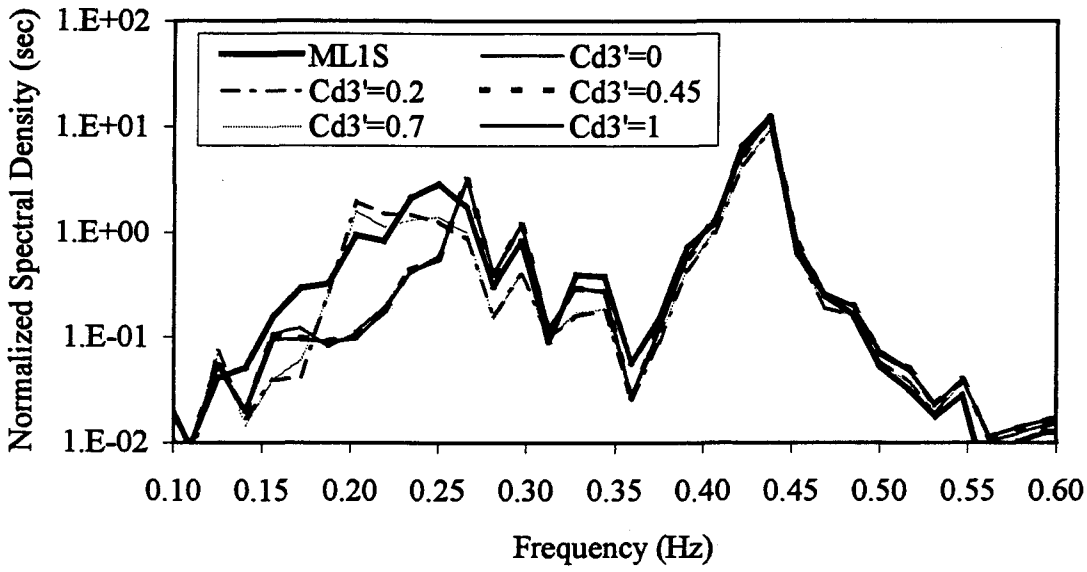

(k)

Fig.B.2 Continued

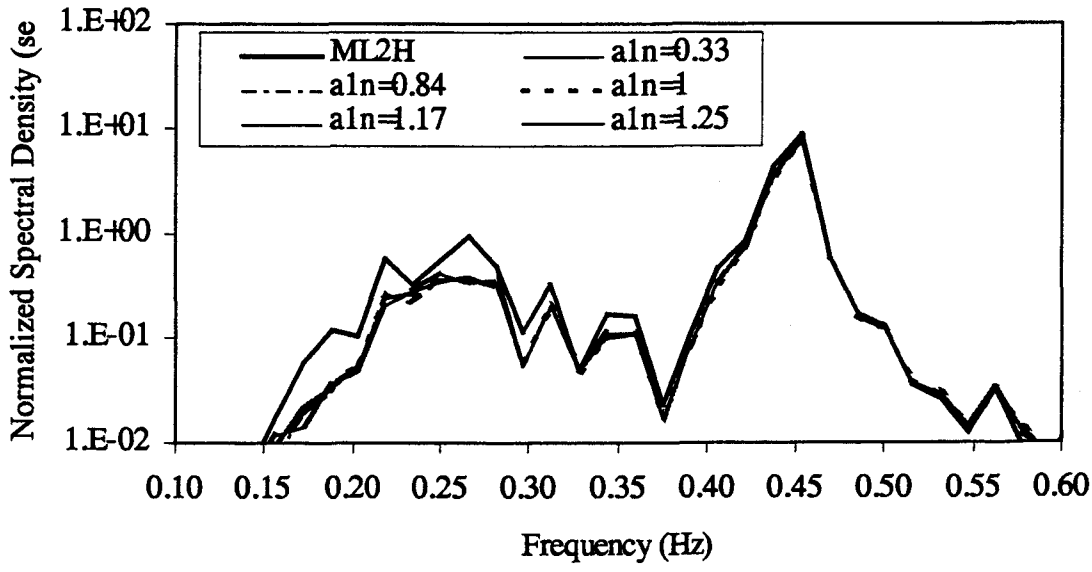

(a)

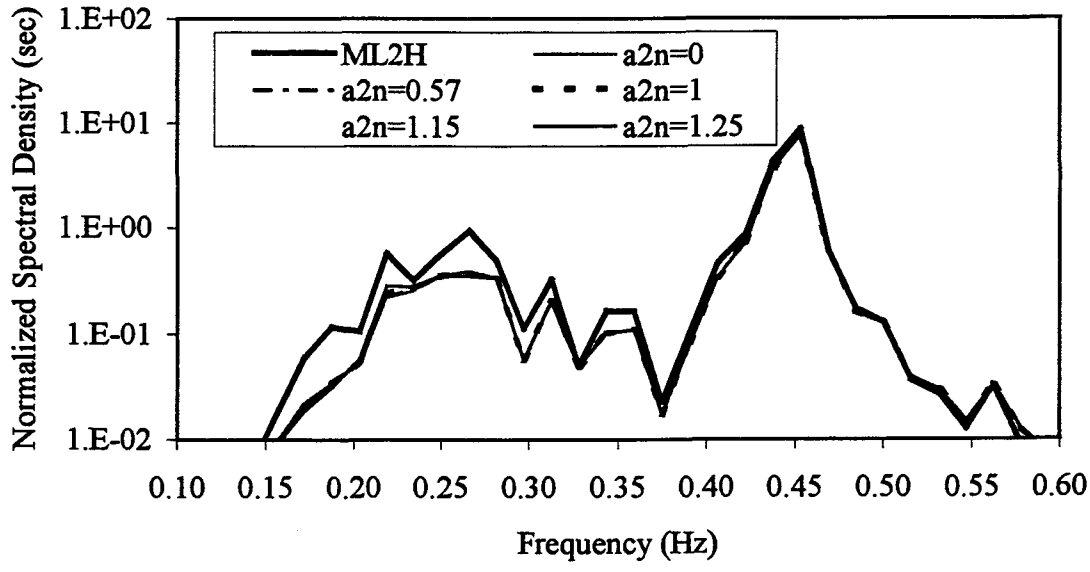

(b)

Fig.B.3 Effect of system parameters on heave response for ML2: a) a_1, b) a_2, c) a_3, d) b_1, e) b_3, f) c_{12}, g) c_{21}, h) ζ_1, i) ζ_3, j) C_{d1}', k) C_{d3}'

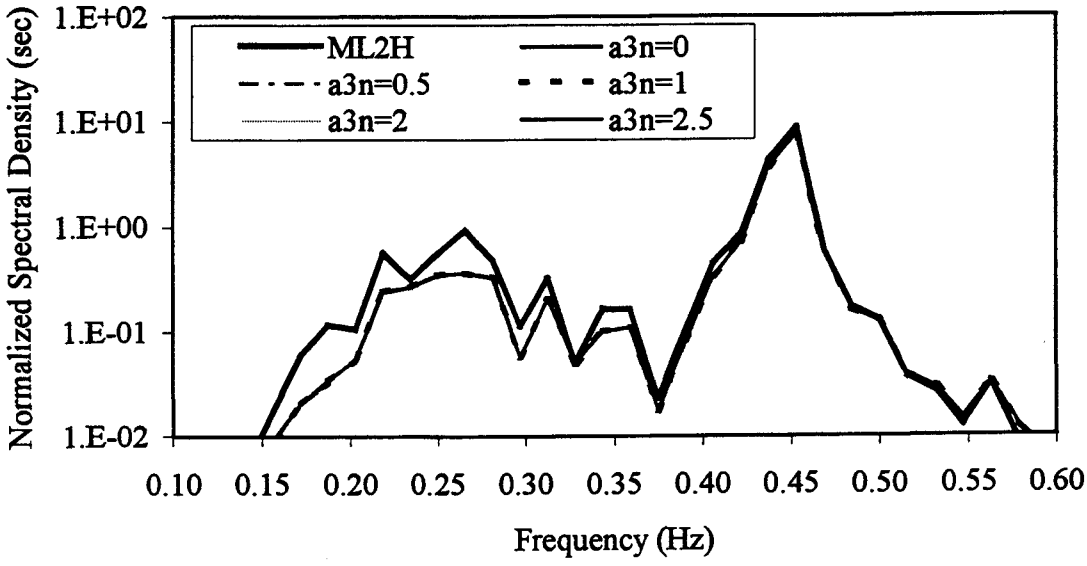

(c)

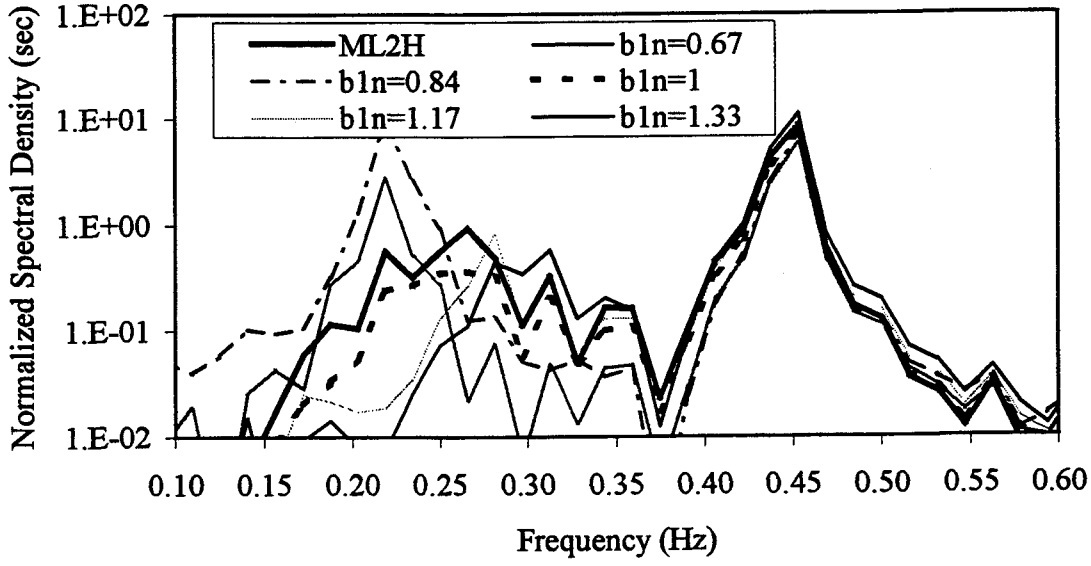

(d)

Fig.B.3 Continued

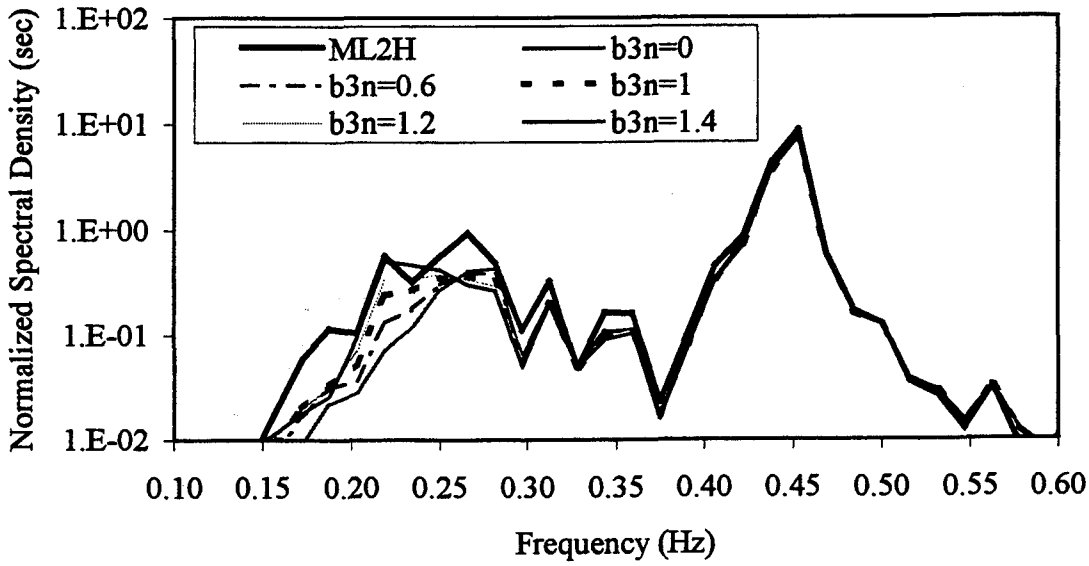

(e)

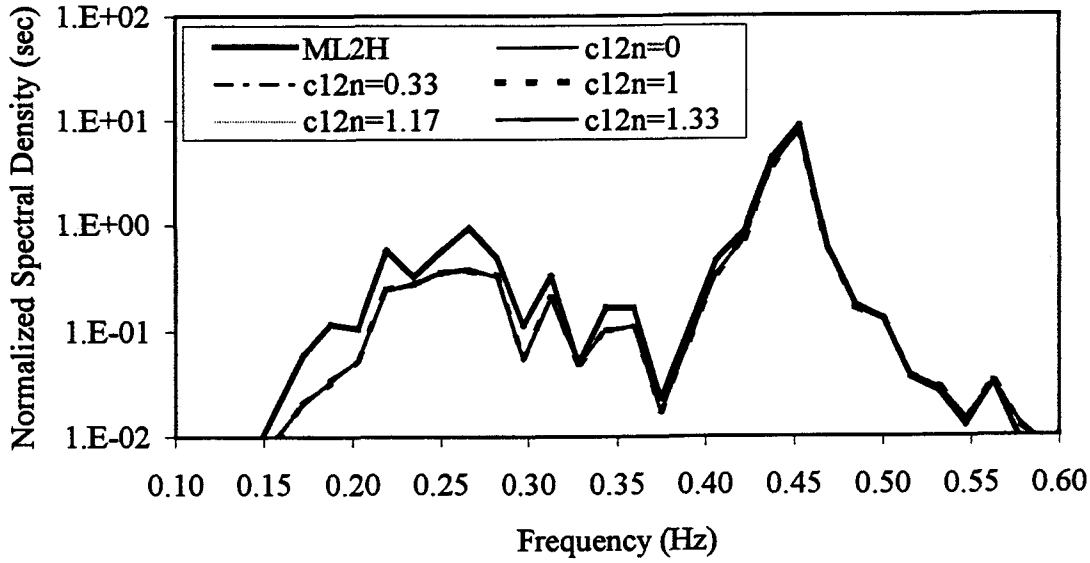

(f)

Fig.B.3 Continued

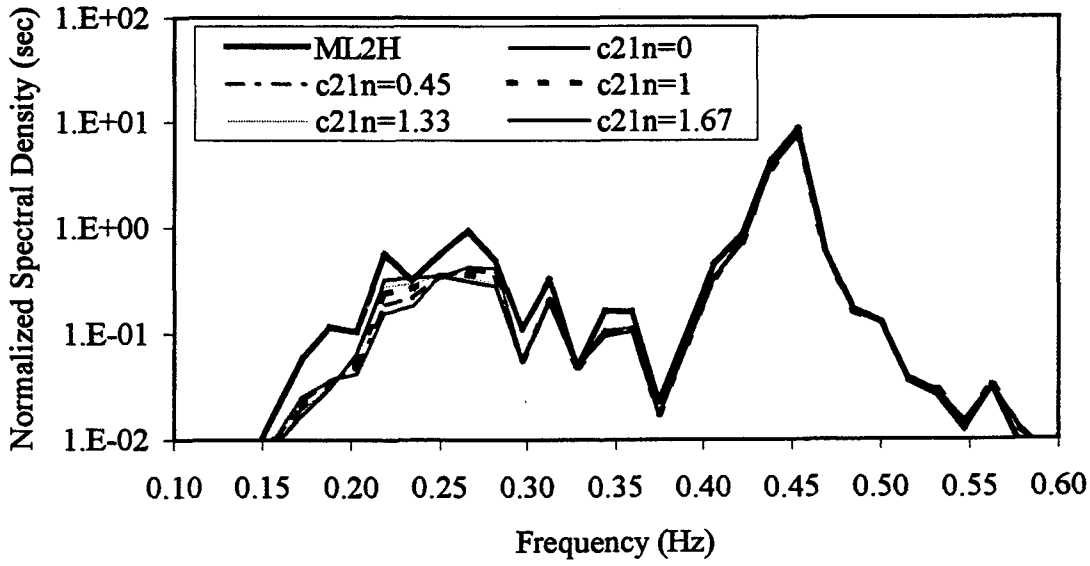

(g)

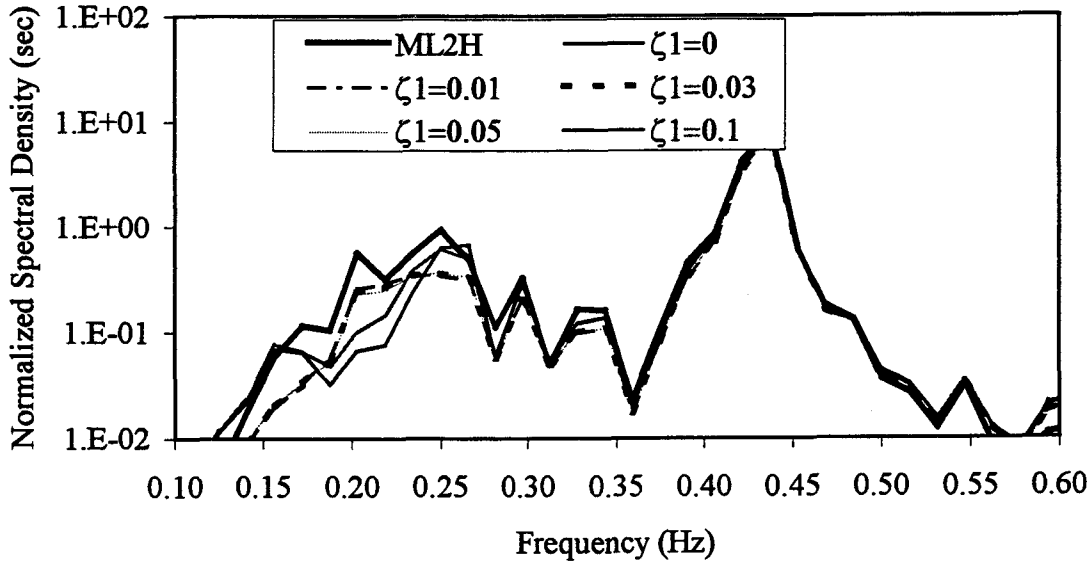

(h)

Fig.B.3 Continued

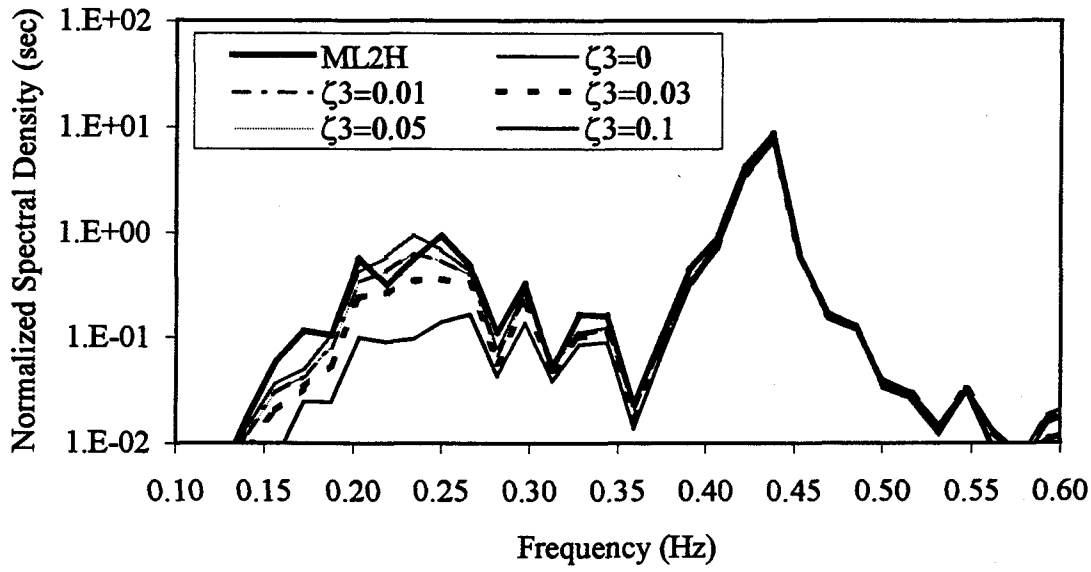

(i)

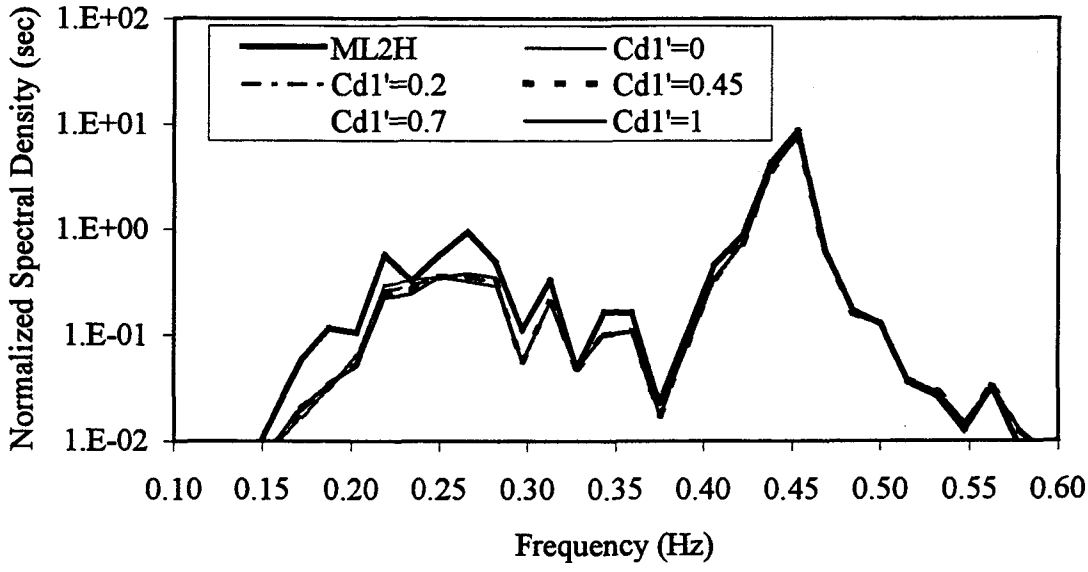

(j)

Fig.B.3 Continued

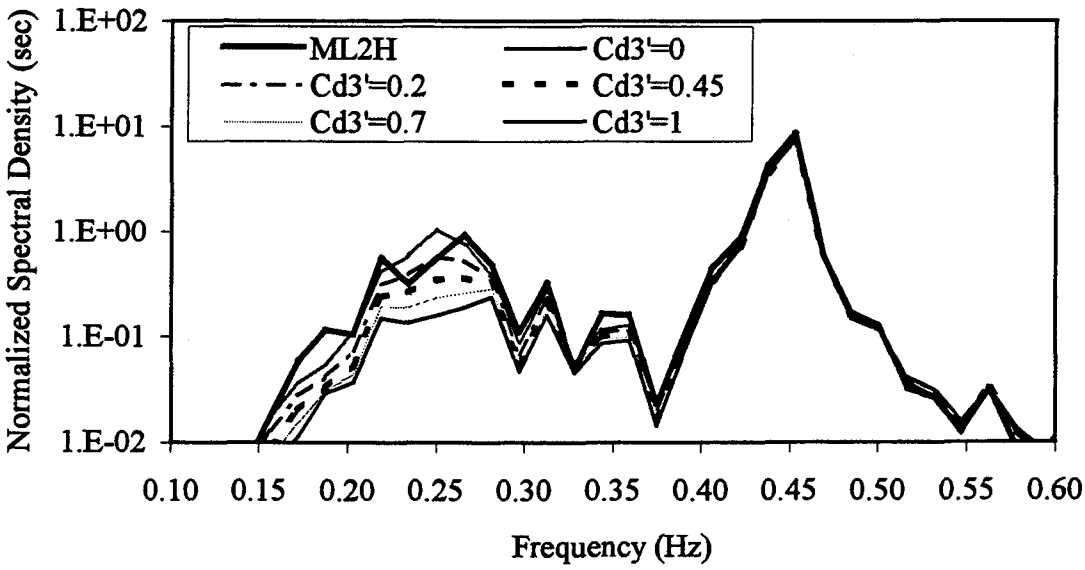

(k)

Fig.B.3 Continued

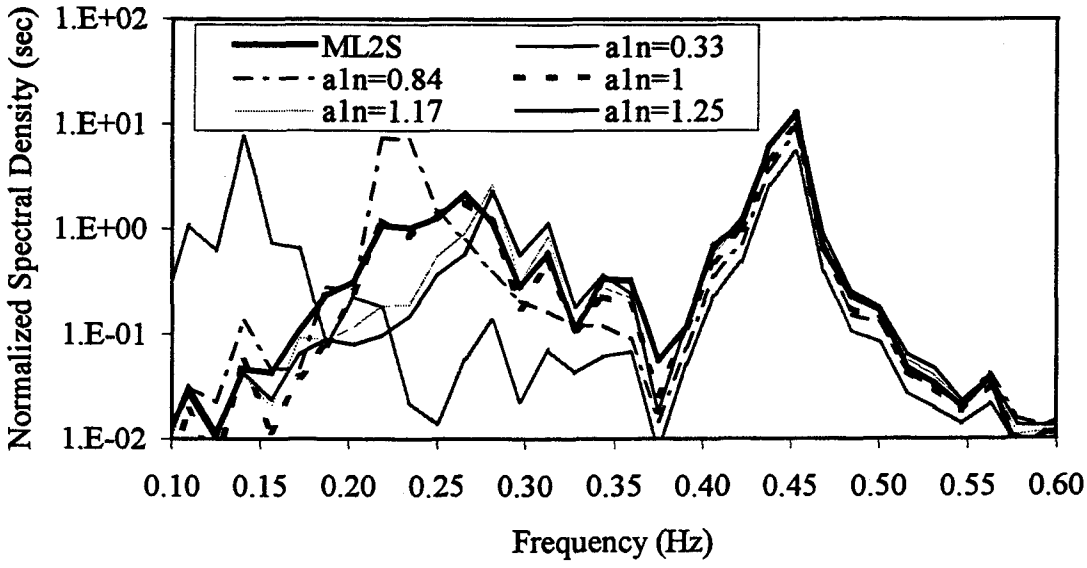

(a)

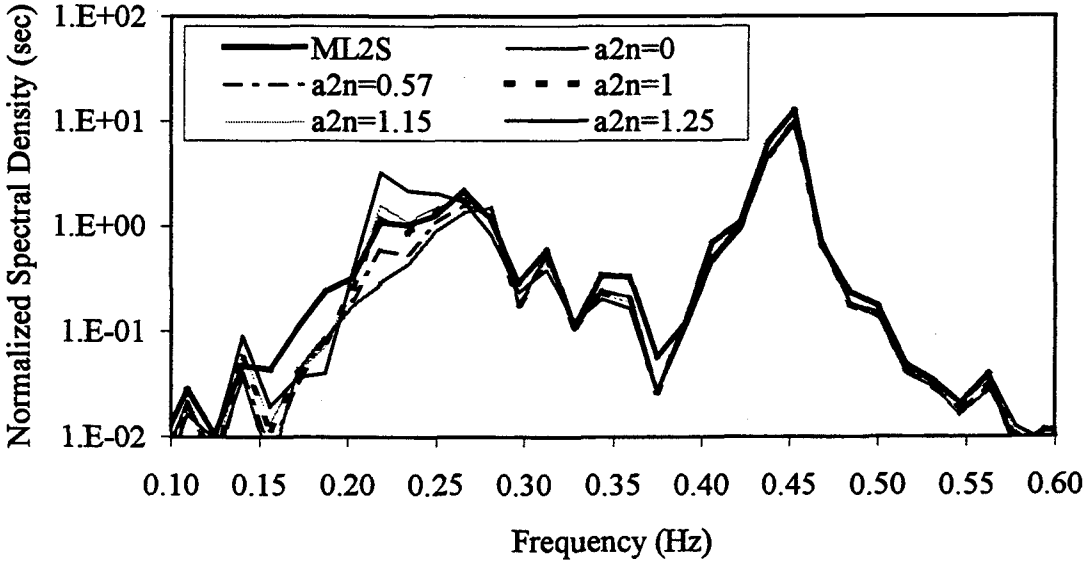

(b)

Fig.B.4 Effect of system parameters on surge response for ML2: a) a_1, b) a_2, c) a_3, d) b_1, e) b_3, f) c_{12}, g) c_{21}, h) ζ_1, i) ζ_3, j) C_{d1}', k) C_{d3}'

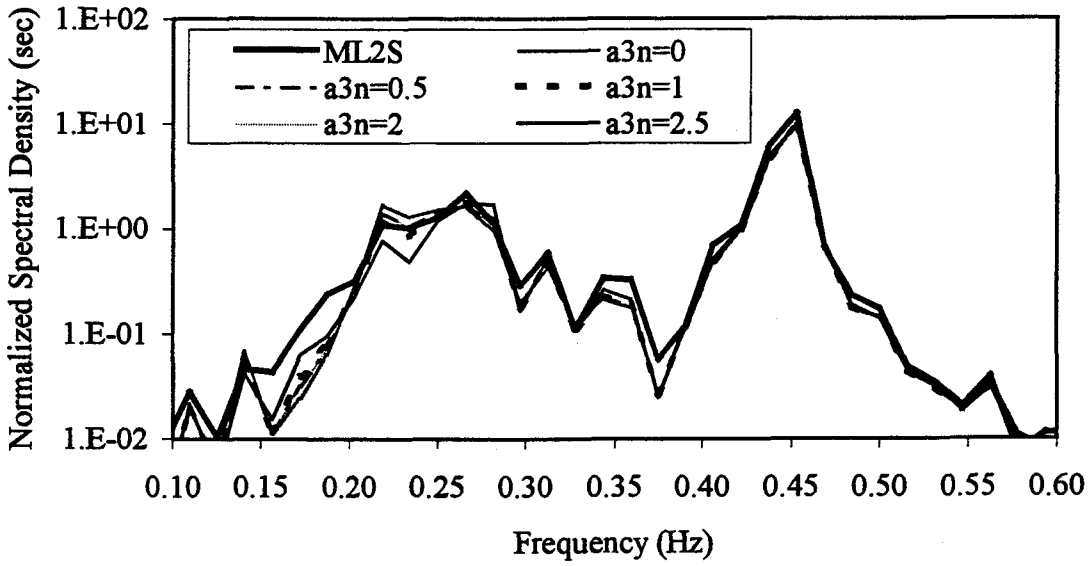

(c)

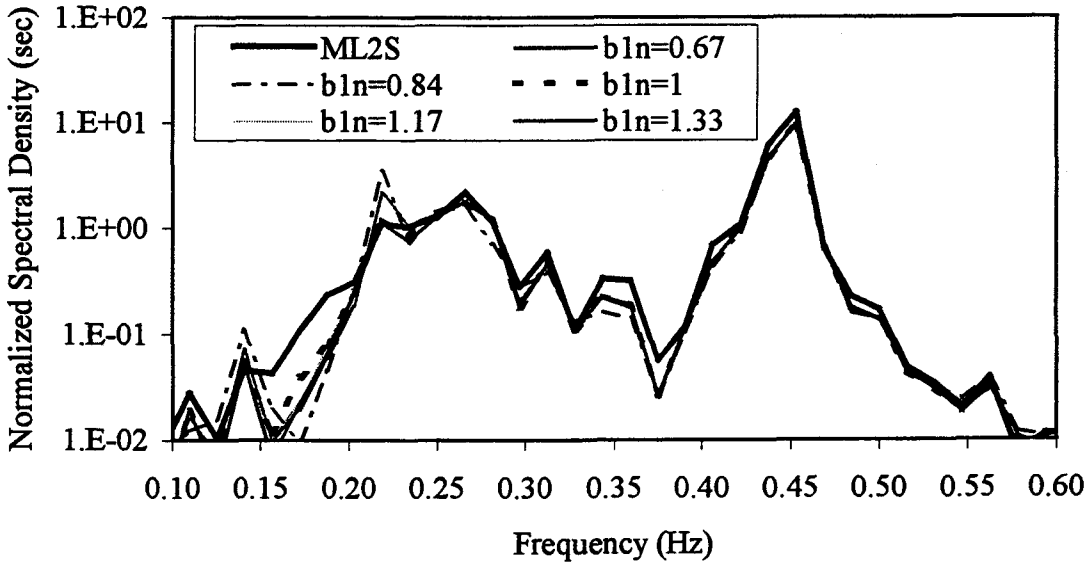

(d)

Fig.B.4 Continued

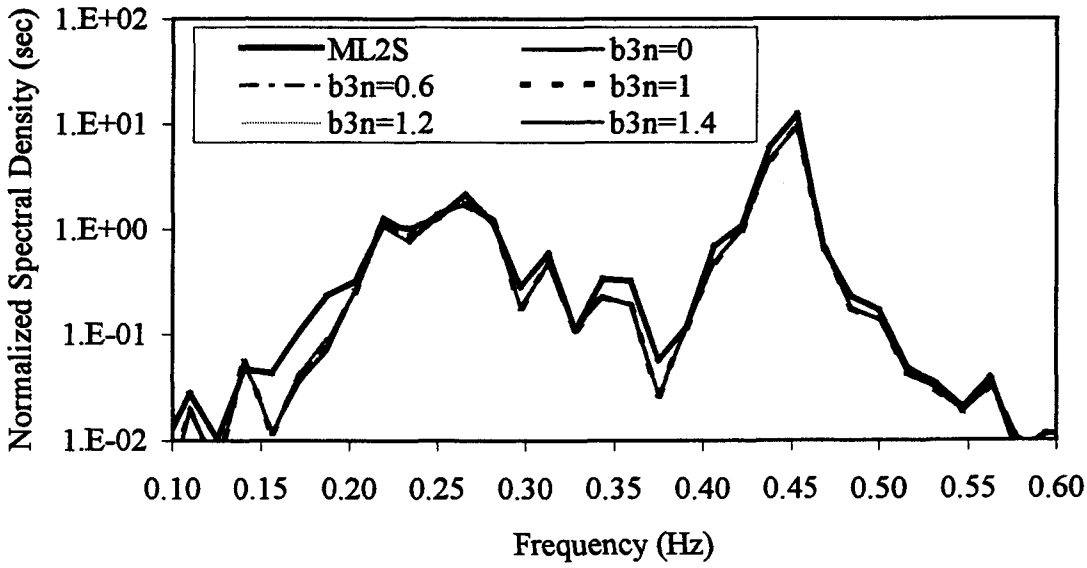

(e)

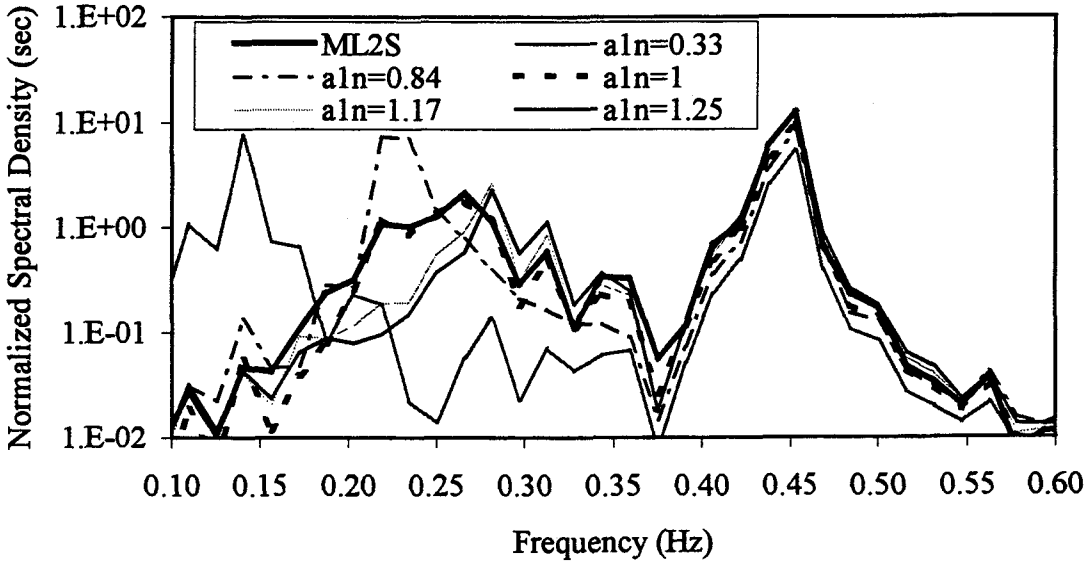

(f)

Fig.B.4 Continued

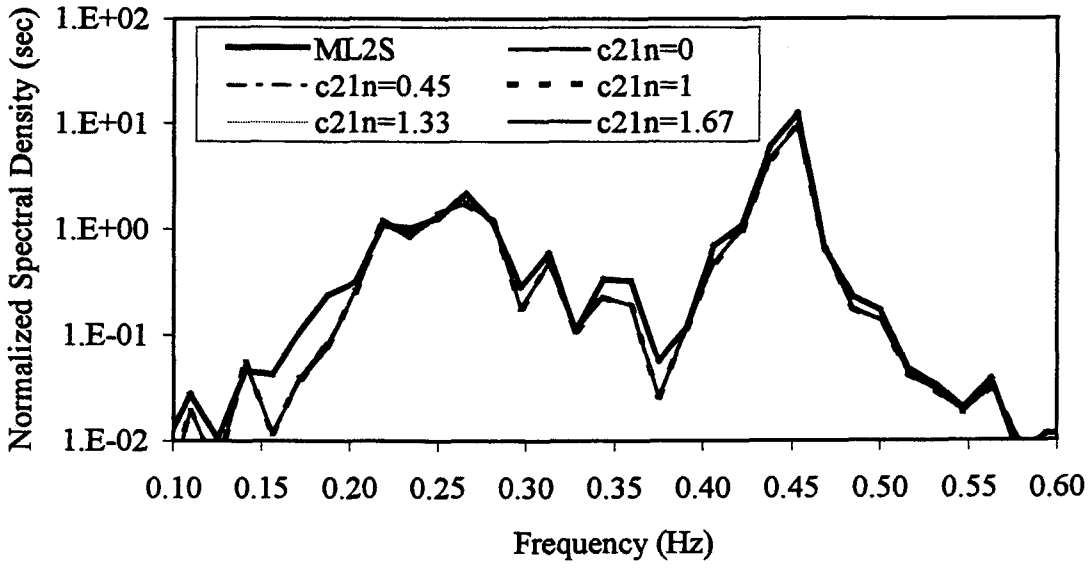

(g)

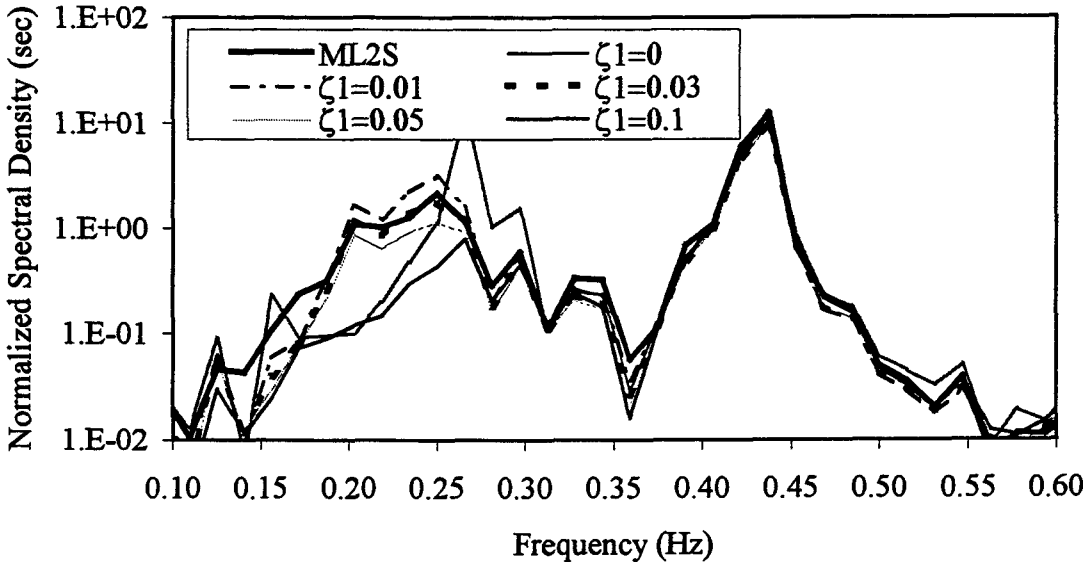

(h)

Fig.B.4 Continued

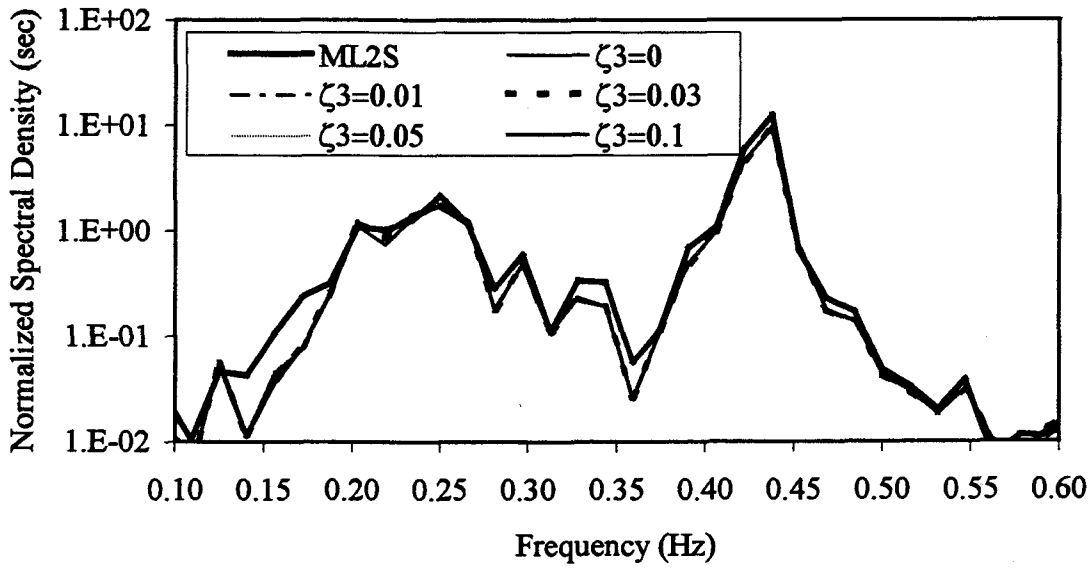

(i)

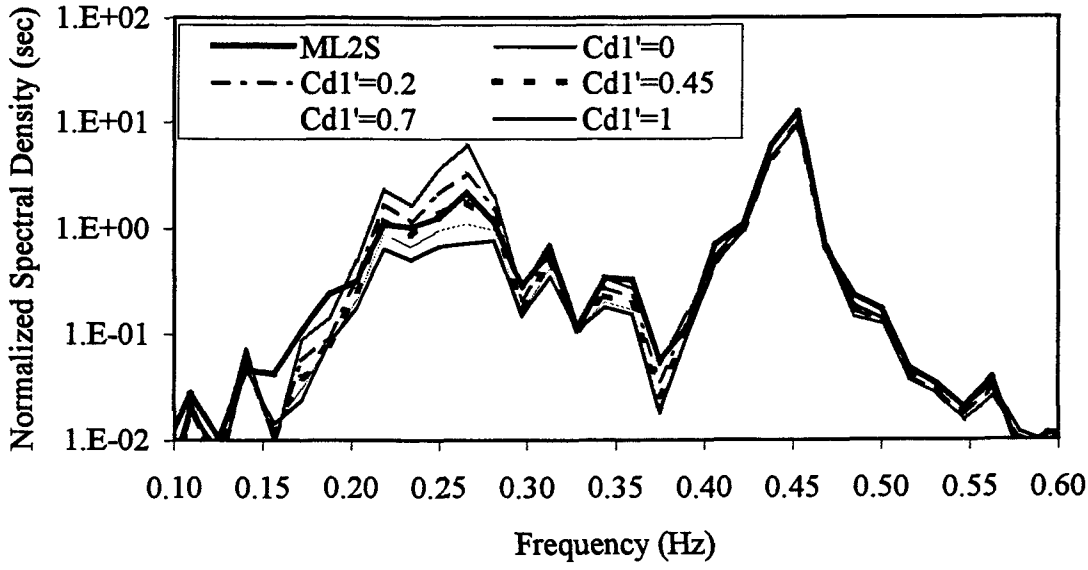

(j)

Fig.B.4 Continued

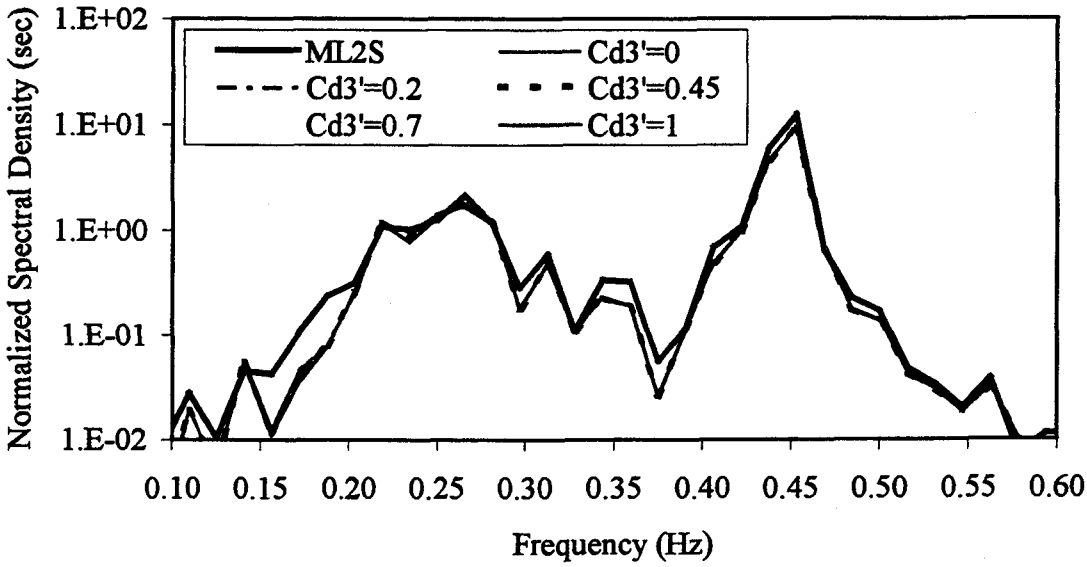

(k)

Fig.B.4 Continued

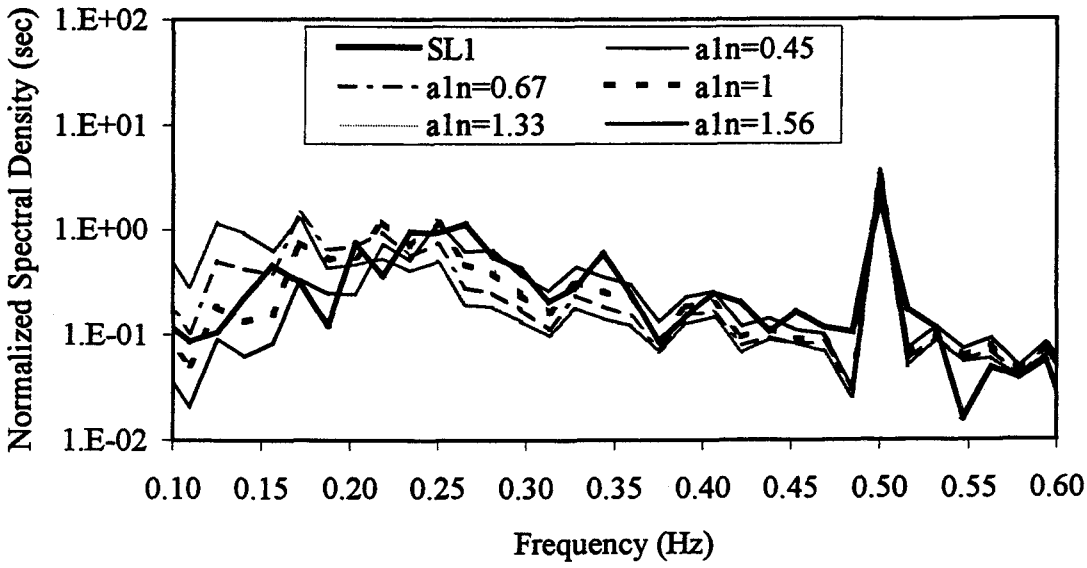

(a)

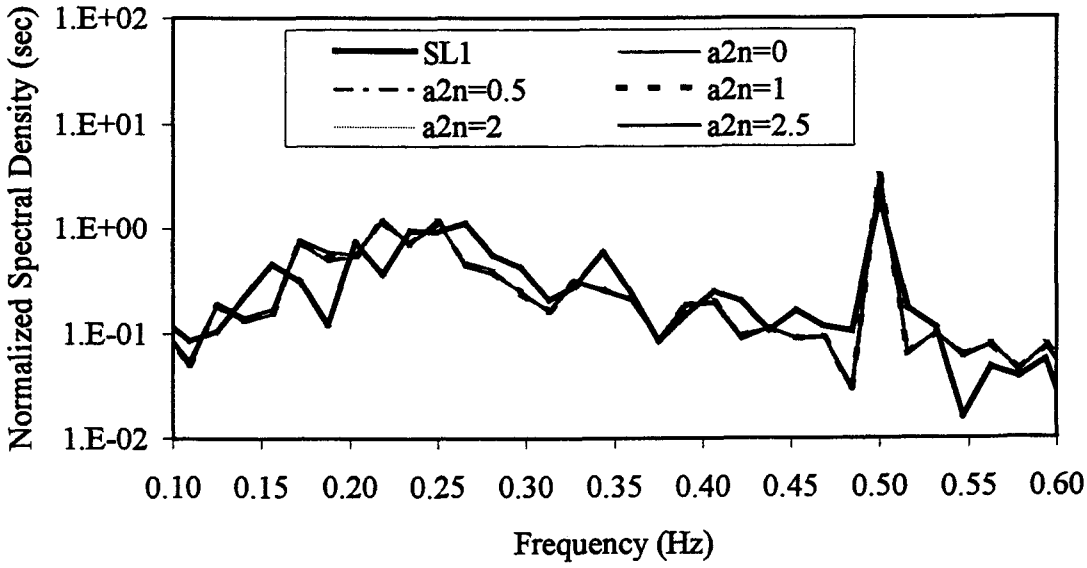

(b)

Fig.B.5 Effect of system properties on surge response for SL1: a) a_1, b) a_2, c) a_3, d) ζ_1, e) C_{d1}'

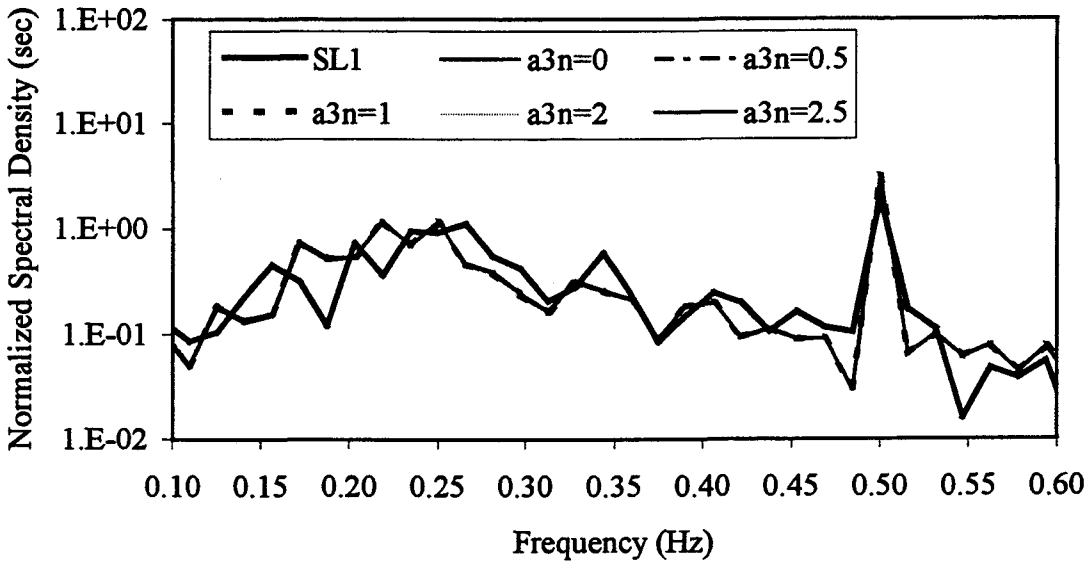

(c)

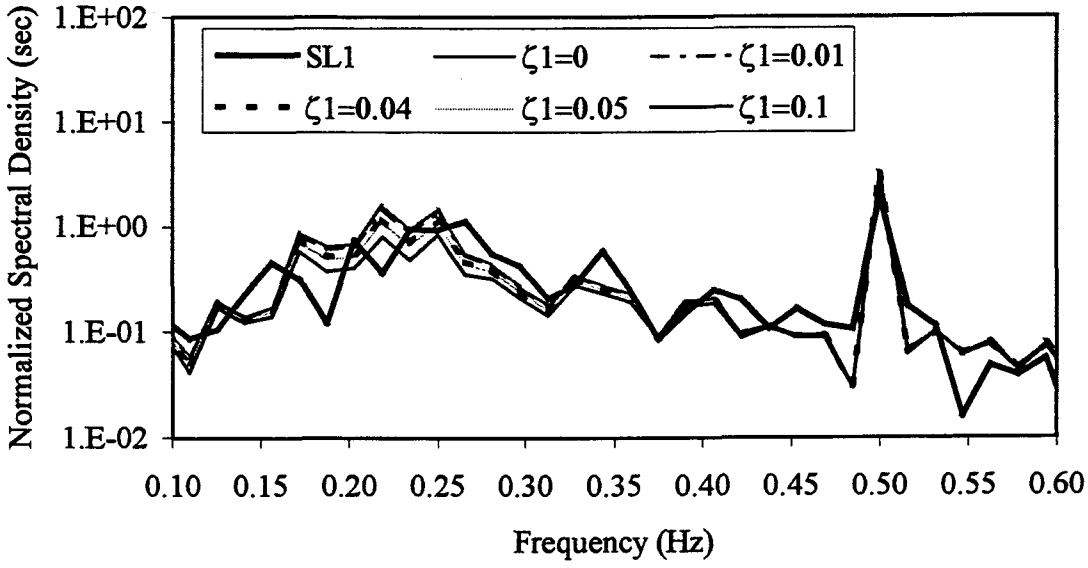

(d)

Fig.B.5 Continued

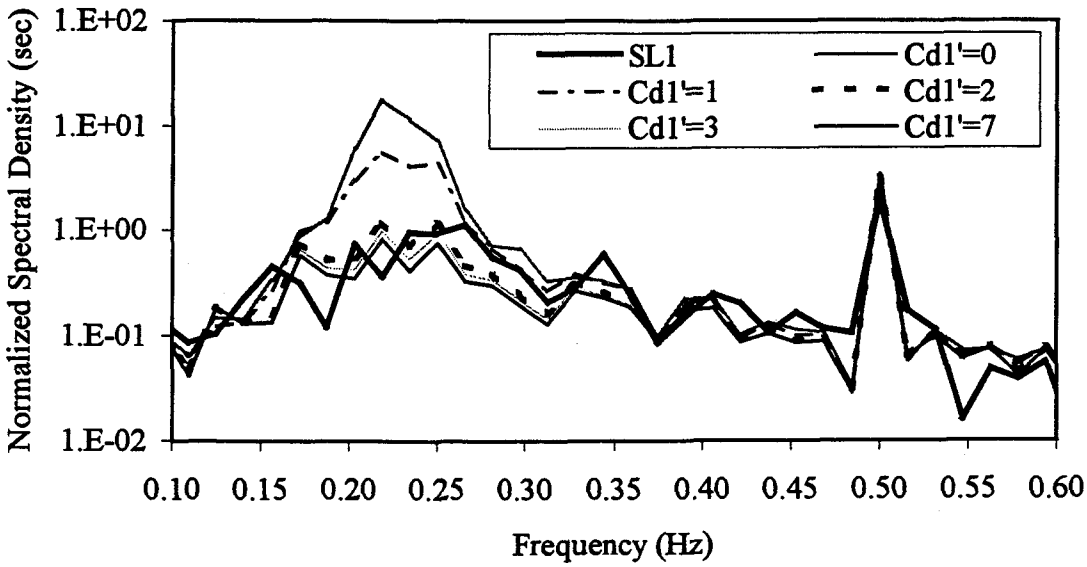

(e)

Fig.B.5 Continued

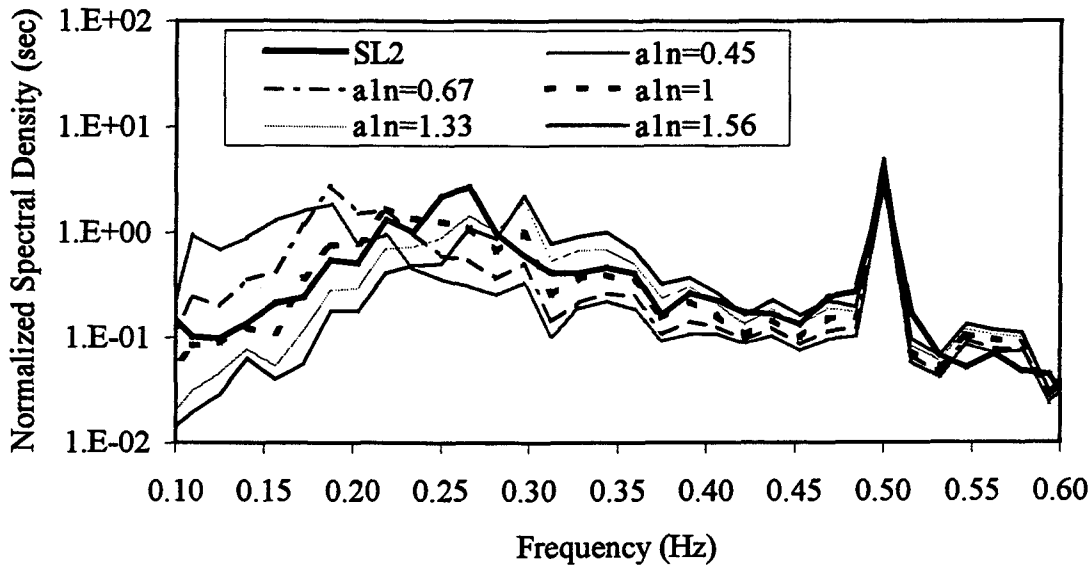

(a)

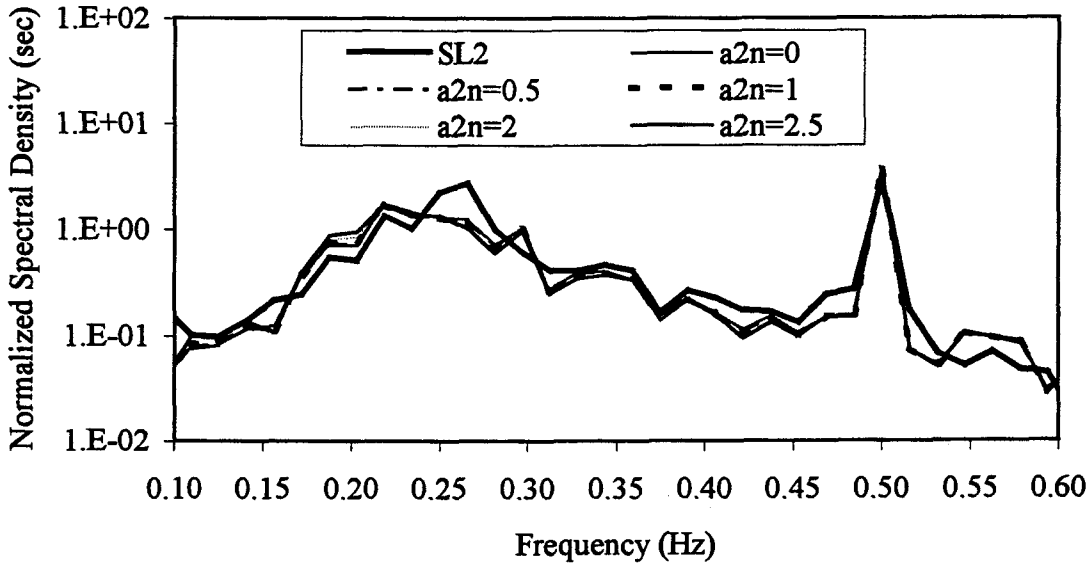

(b)

Fig.B.6 Effect of system properties on surge response for SL2: a) a_1, b) a_2, c) a_3, d) ζ_1, e) C_{d1}'

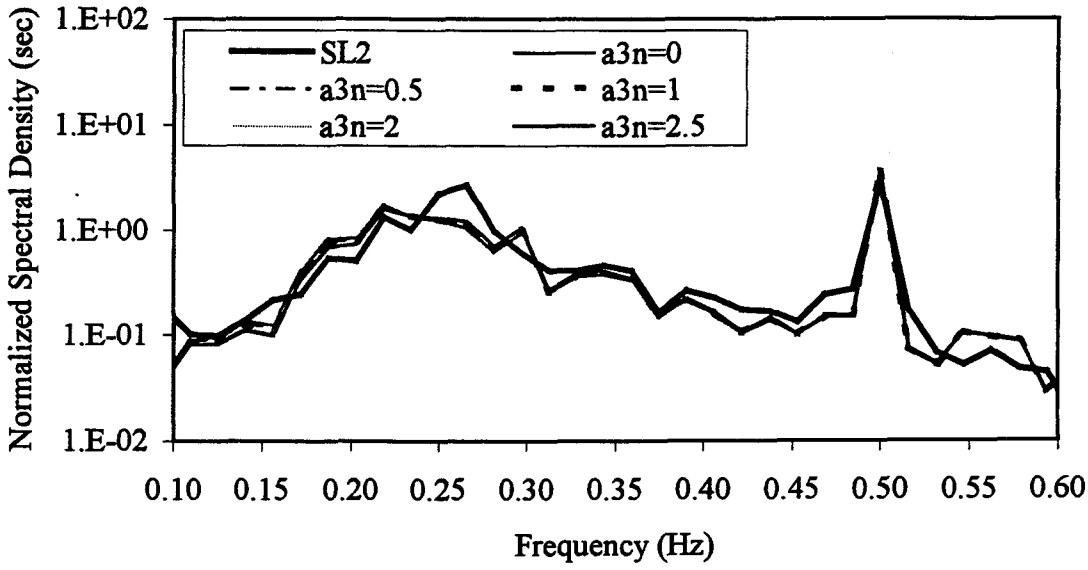

(c)

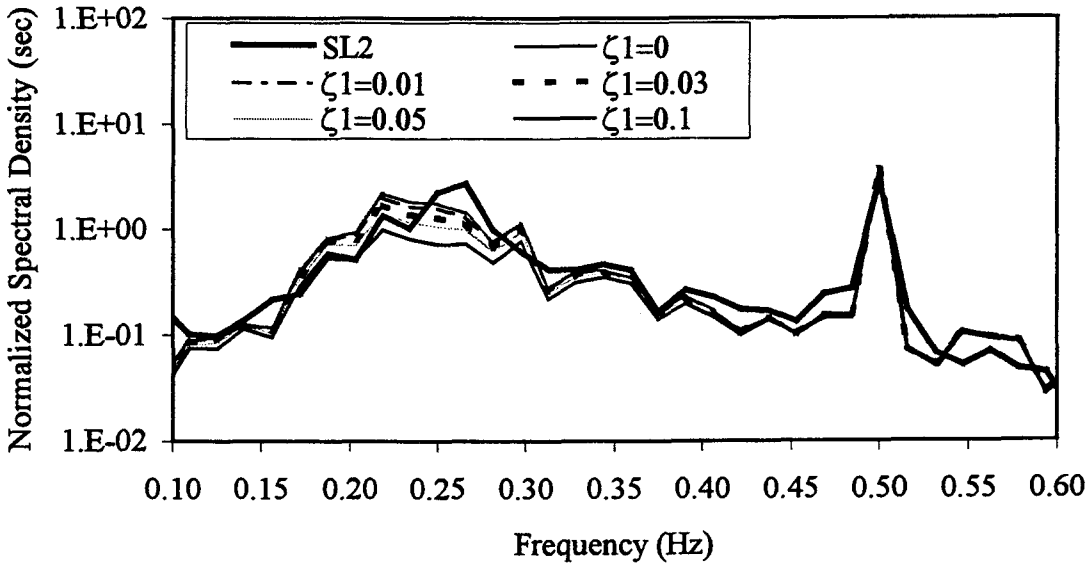

(d)

Fig.B.6 Continued

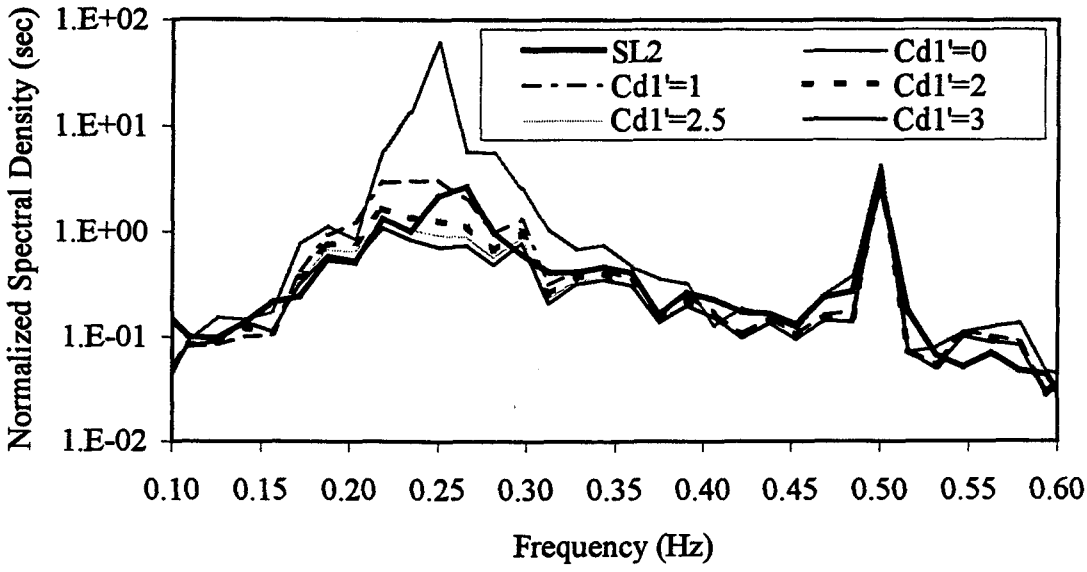

(e)

Fig.B.6 Continued

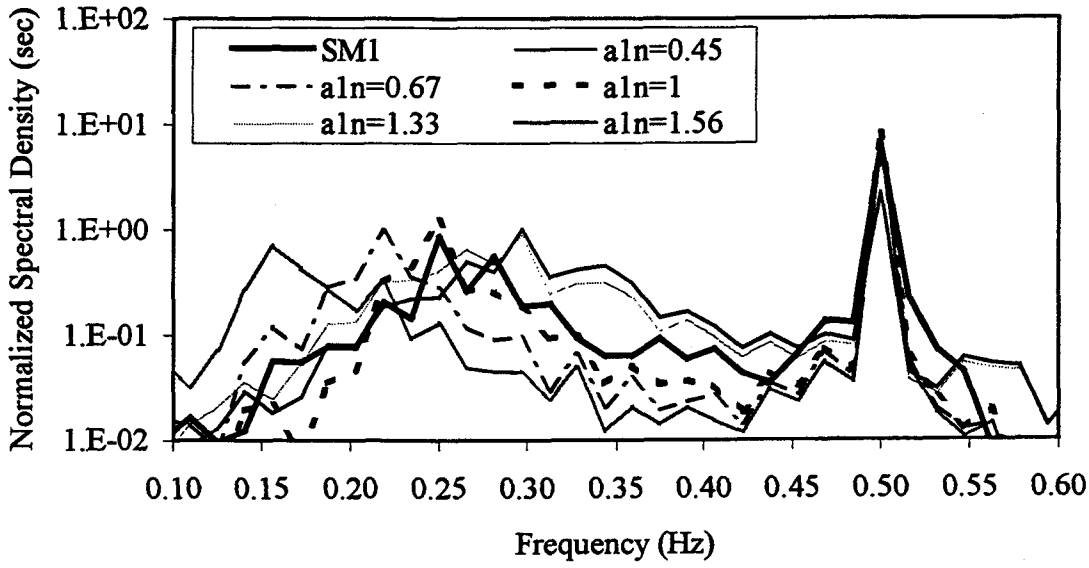

(a)

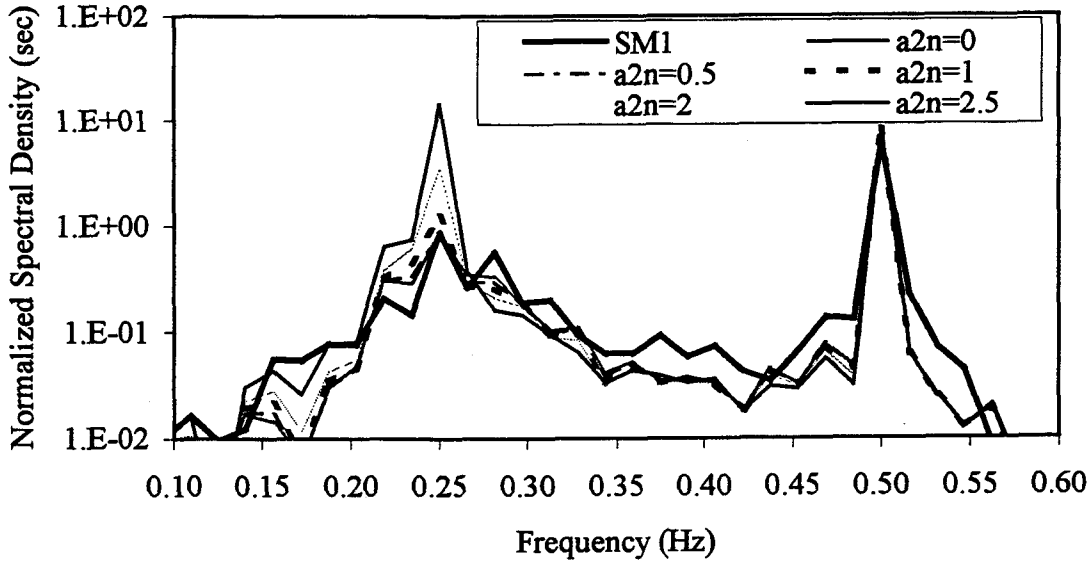

(b)

Fig.B.7 Effect of system properties on surge response for SM1: a) a_1, b) a_2, c) a_3, d) ζ_1, e) C_{d1}

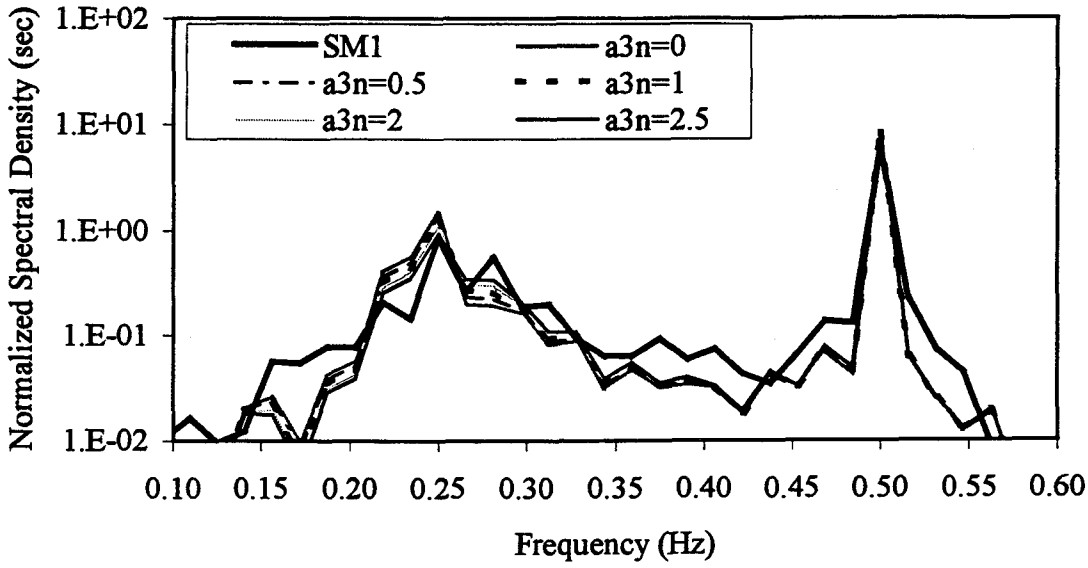

(c)

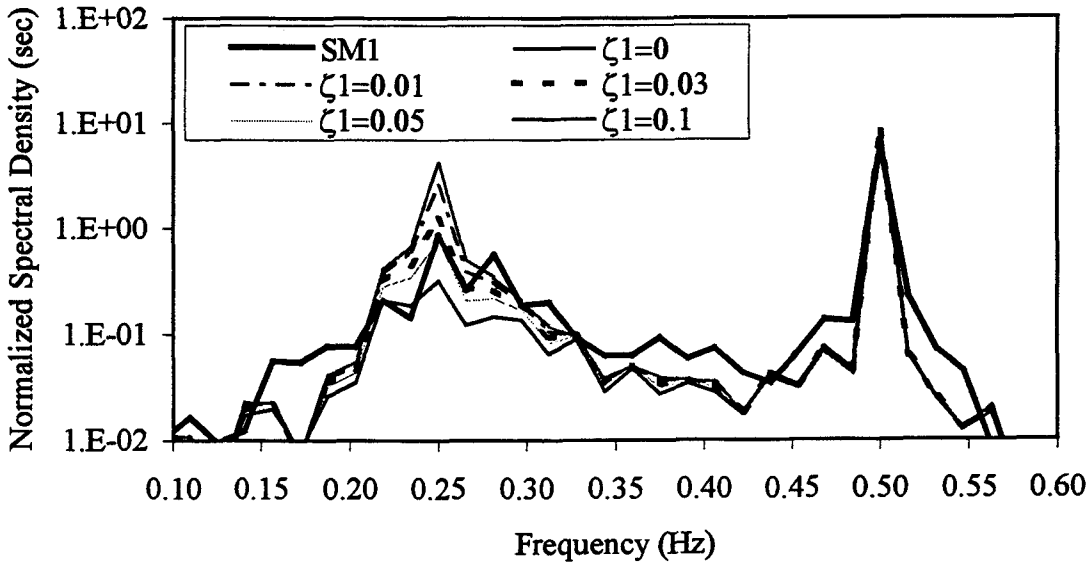

(d)

Fig.B.7 Continued

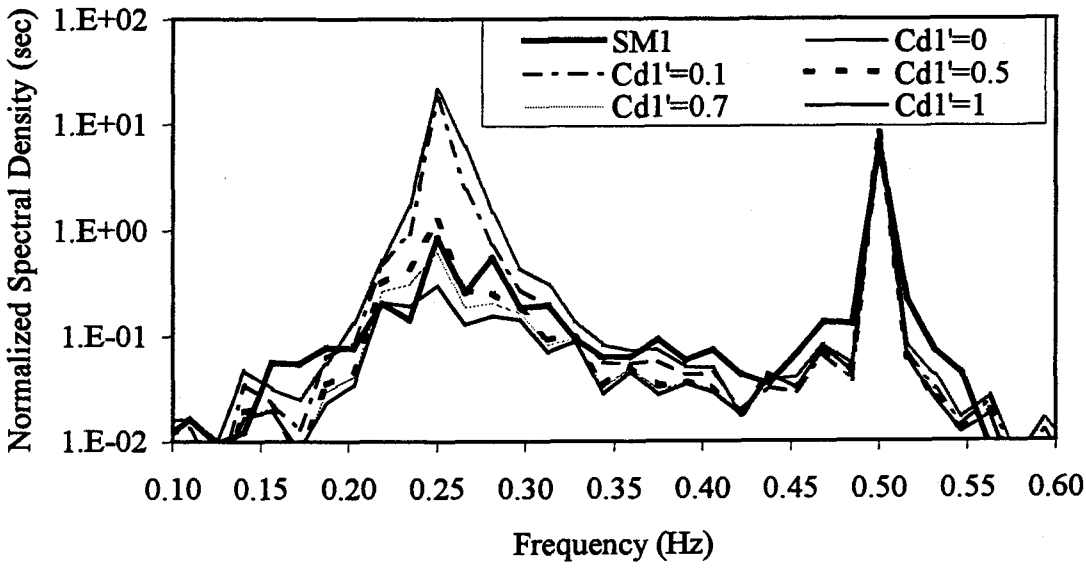

(e)

Fig.B.7 Continued

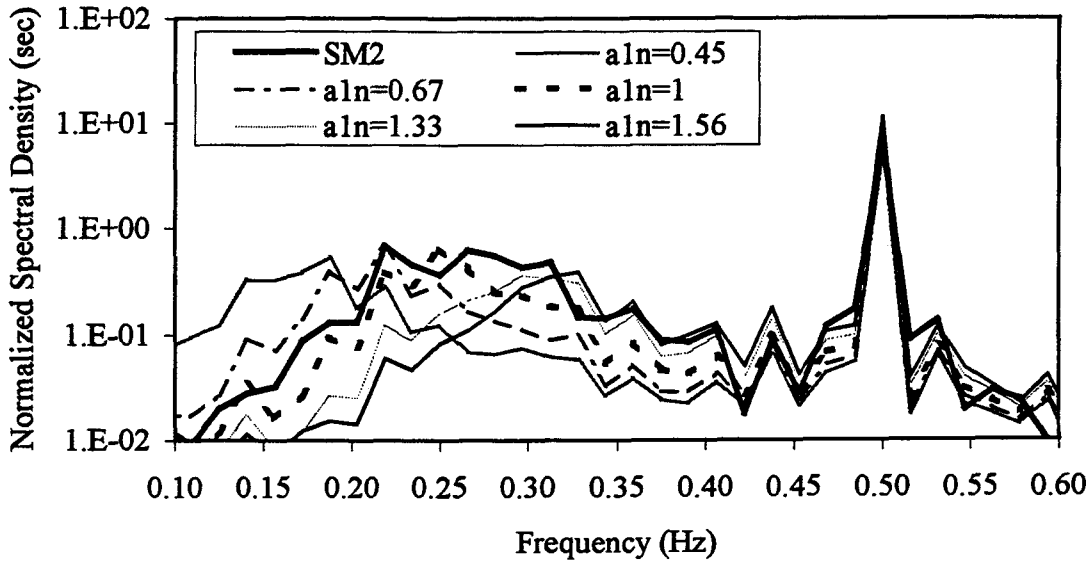

(a)

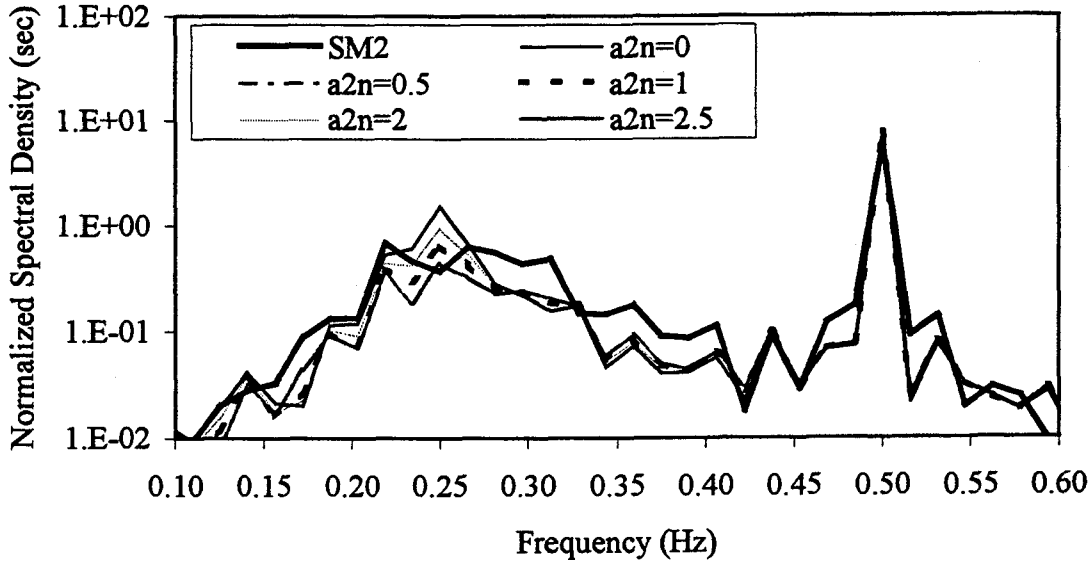

(b)

Fig.B.8 Effect of system properties on surge response for SM2: a) a_1, b) a_2, c) a_3, d) ζ_1, e) C_{d1}'

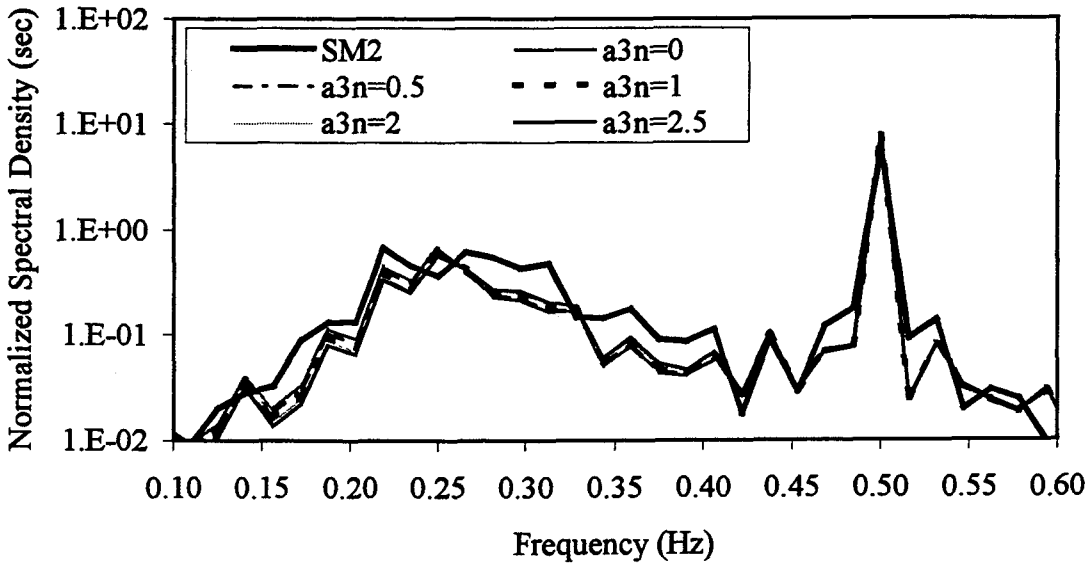

(c)

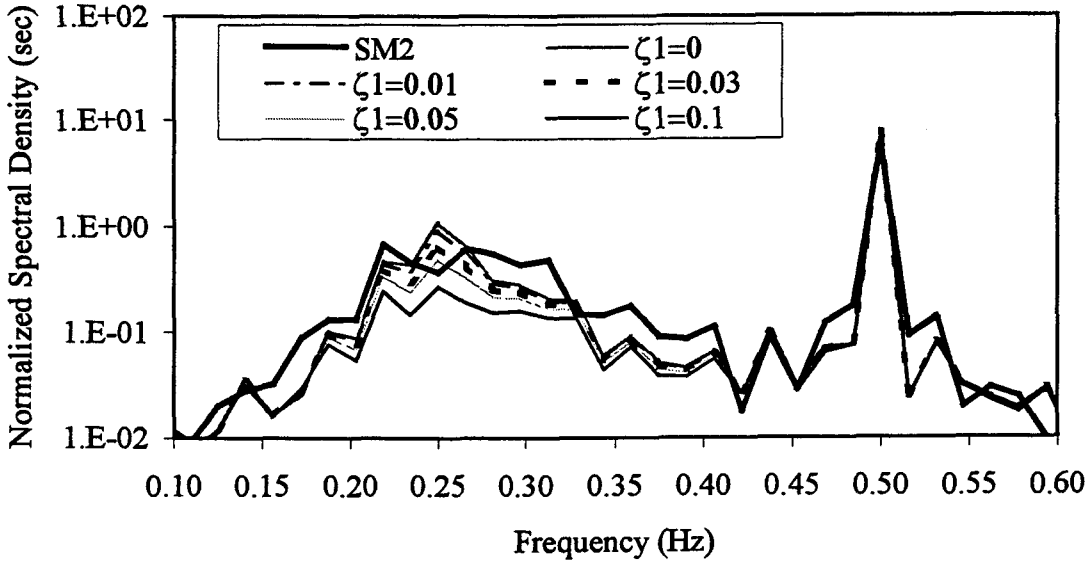

(d)

Fig.B.8 Continued

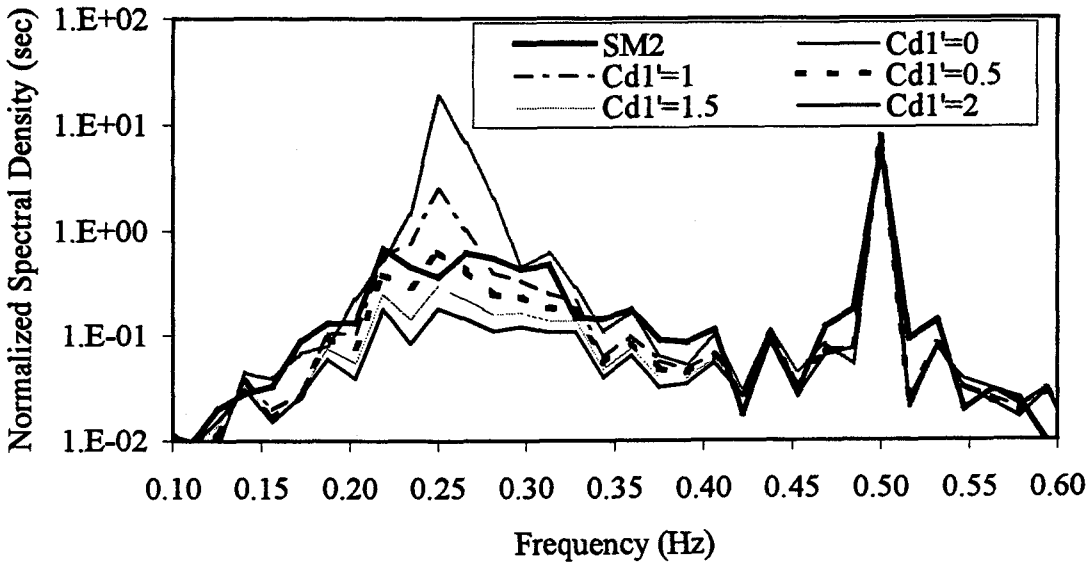

(e)

Fig.B.8 Continued

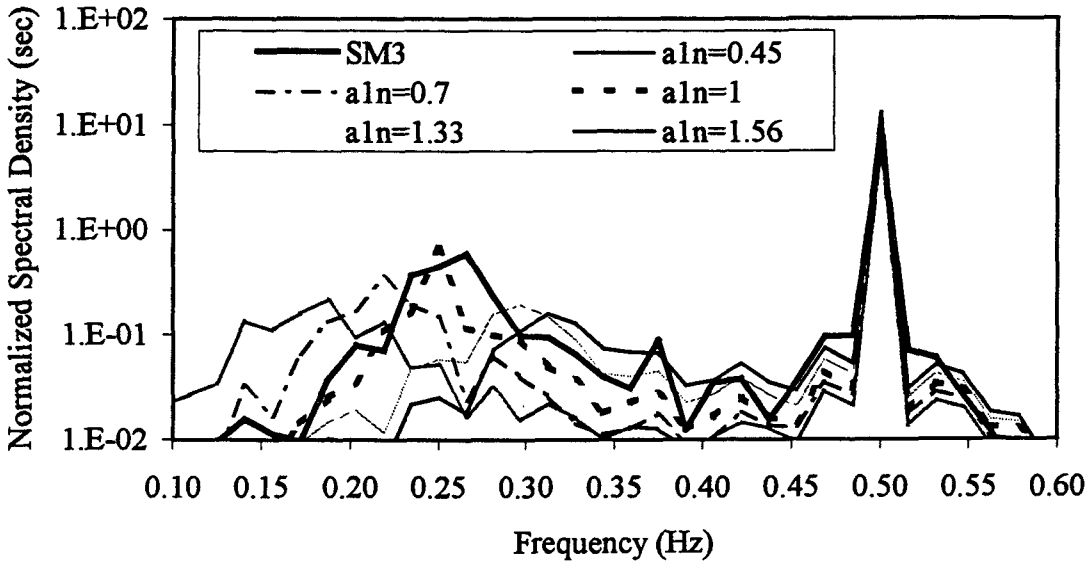

(a)

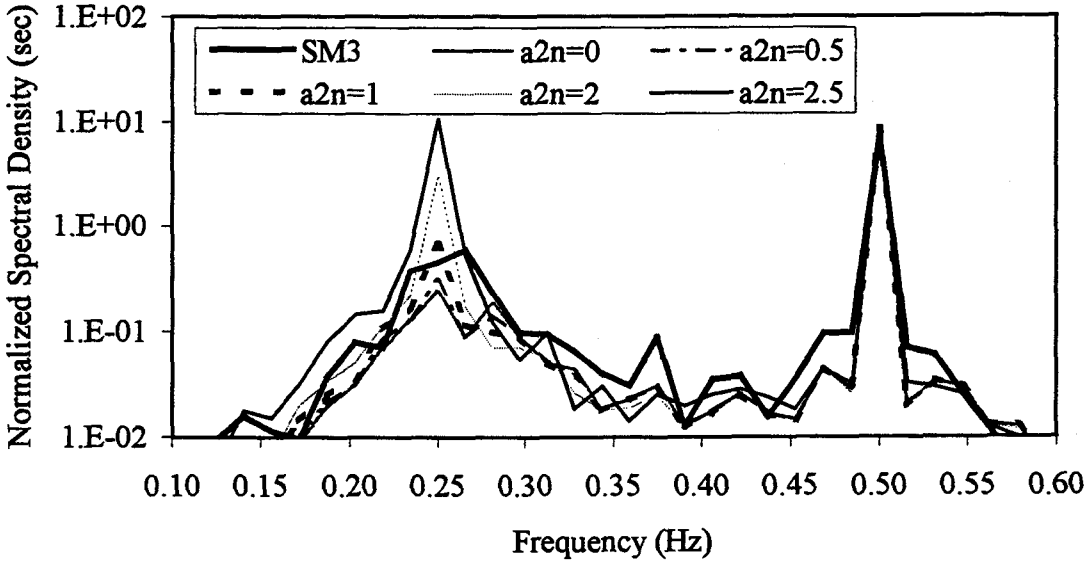

(b)

Fig.B.9 Effect of system parameters on surge response (SM3): a) a_1, b) a_2, c) a_3, d) ζ_1, e) C_{d1}'

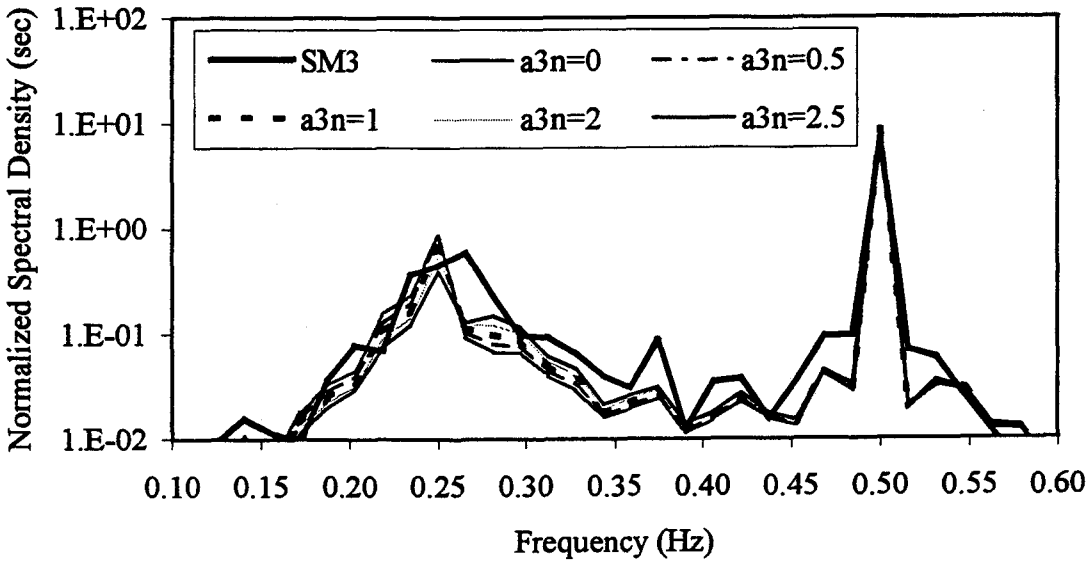

(c)

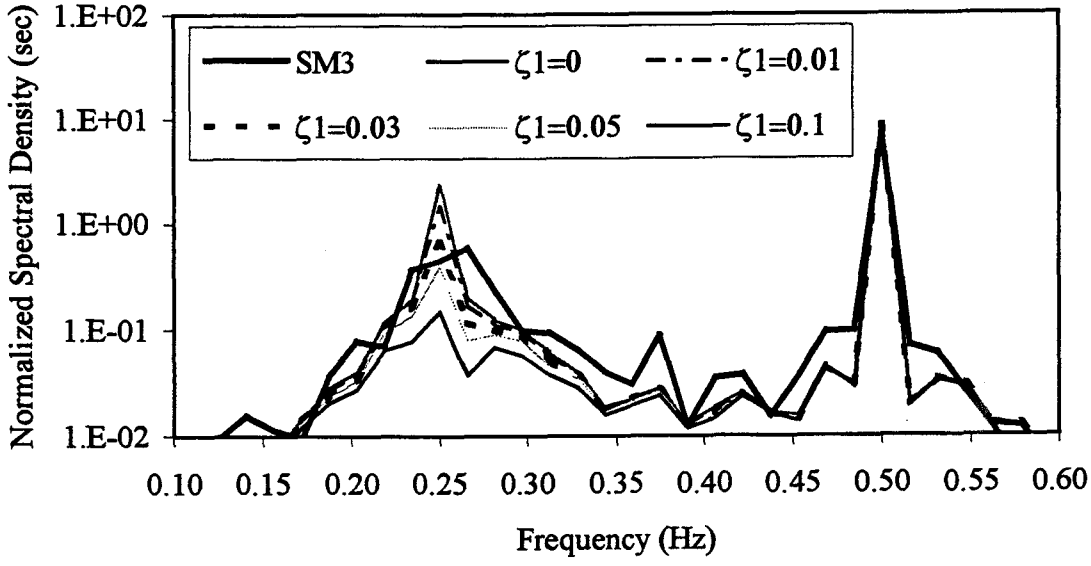

(d)

Fig.B.9 Continued

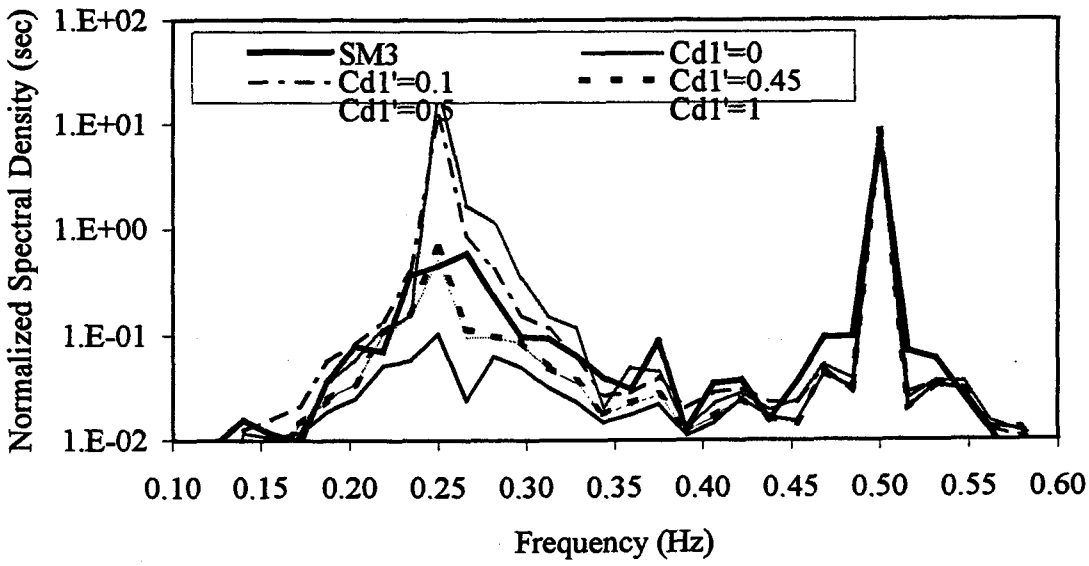

(e)

Fig.B.9 Continued

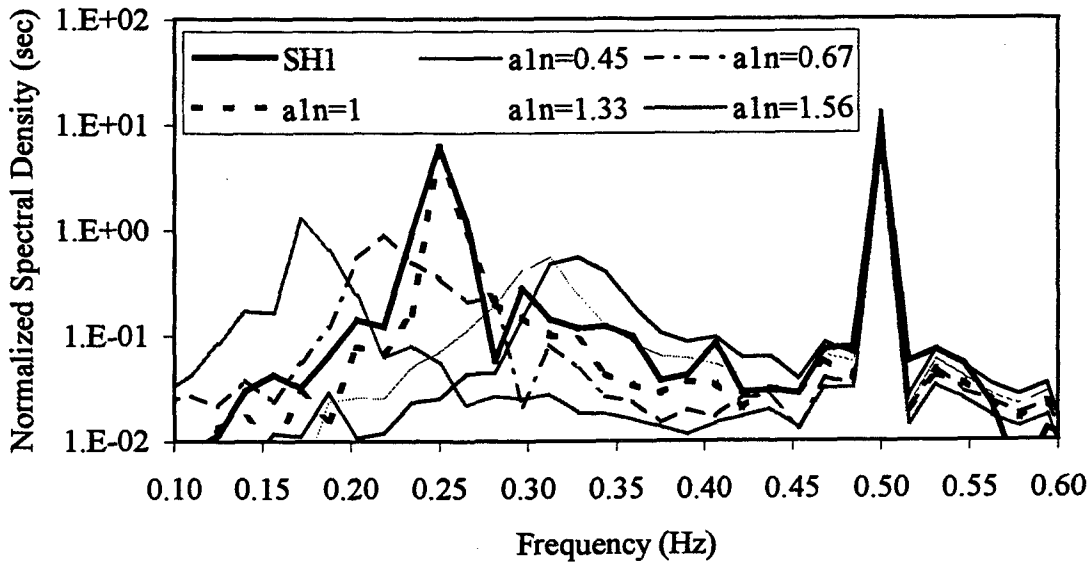

(a)

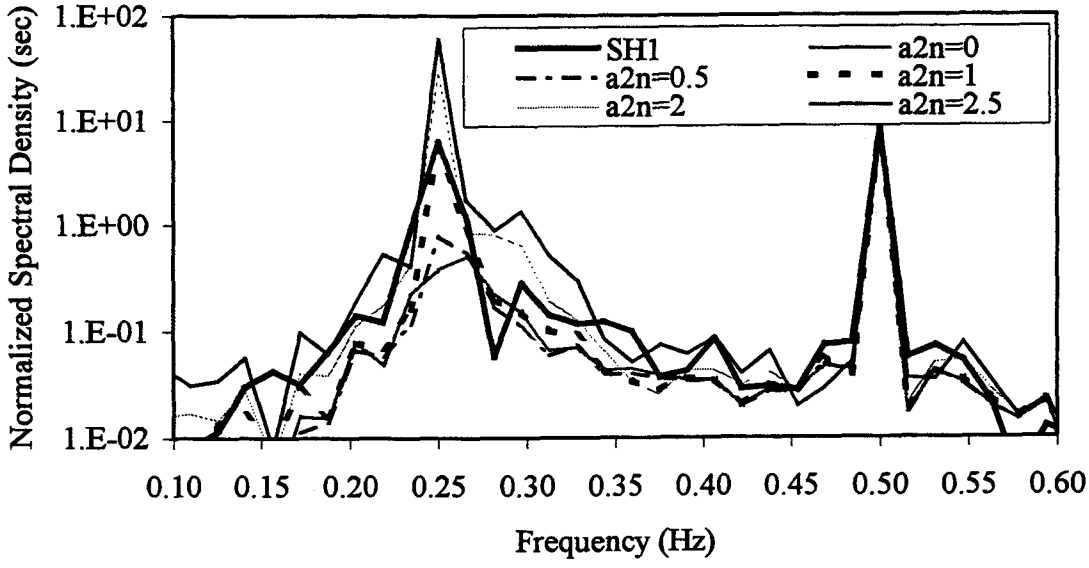

(b)

Fig.B.10 Effect of system parameters on surge response (SH1): a) a_1, b) a_2, c) a_3, d) ζ_1, e) C_{d1}'

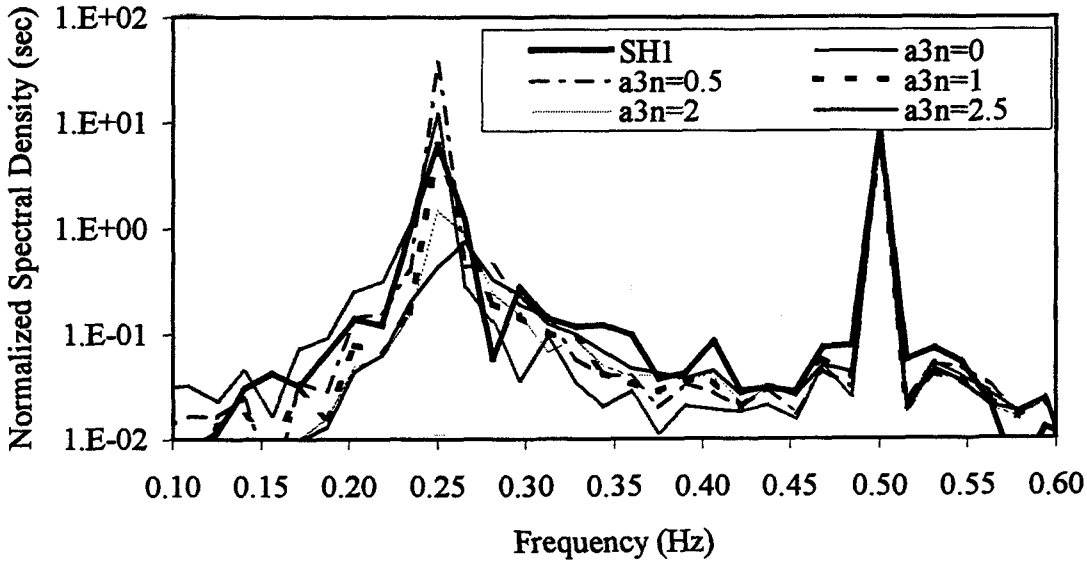

(c)

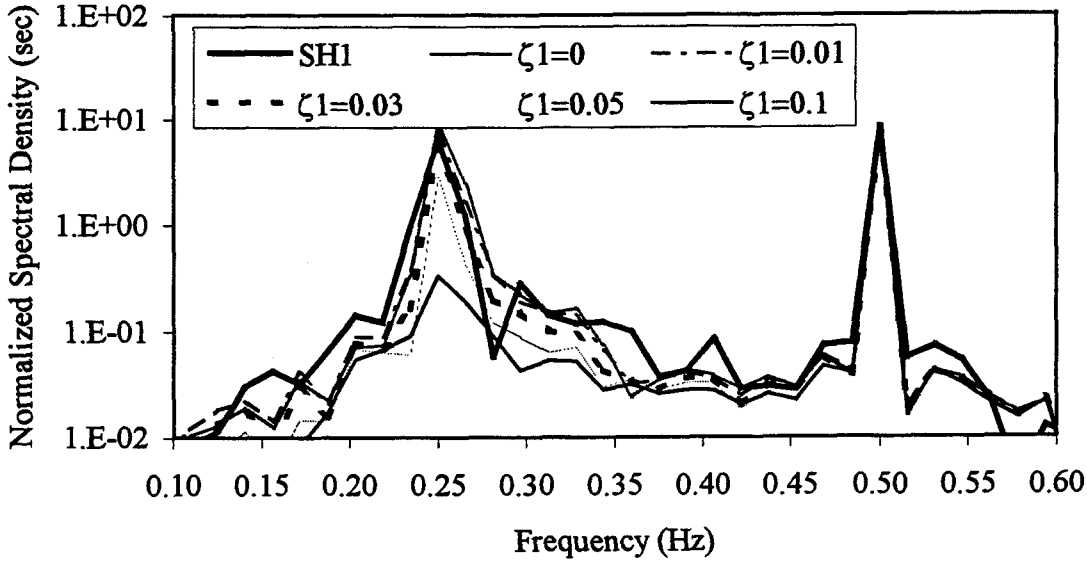

(d)

Fig.B.10 Continued

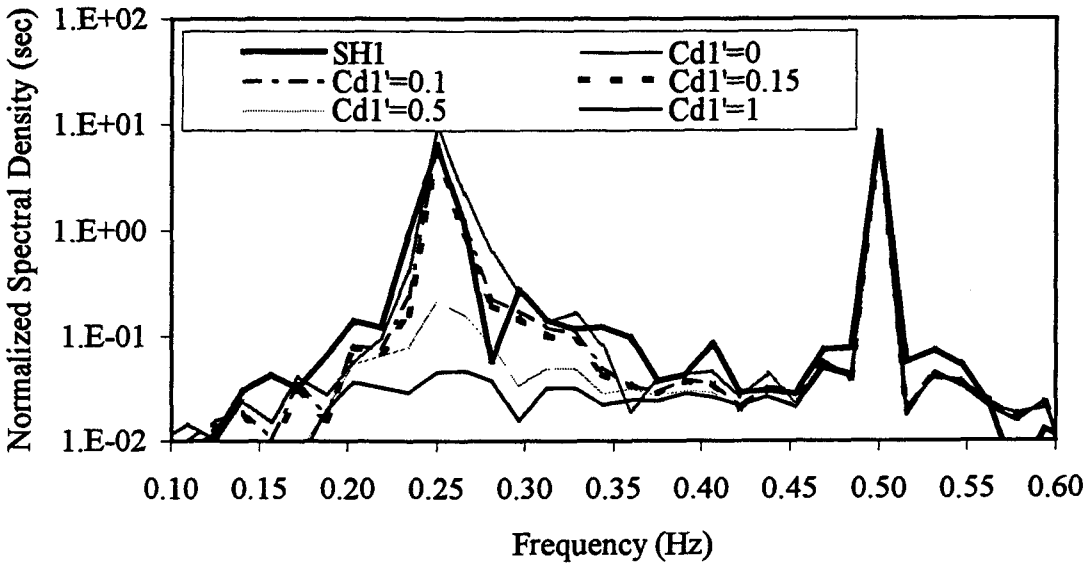

(e)

Fig.B.10 Continued

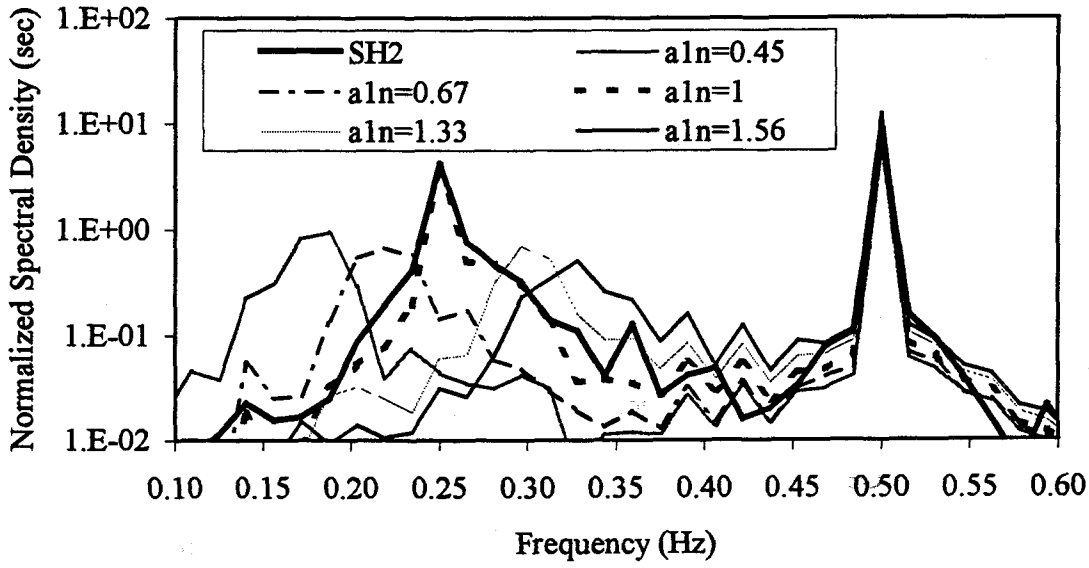

(a)

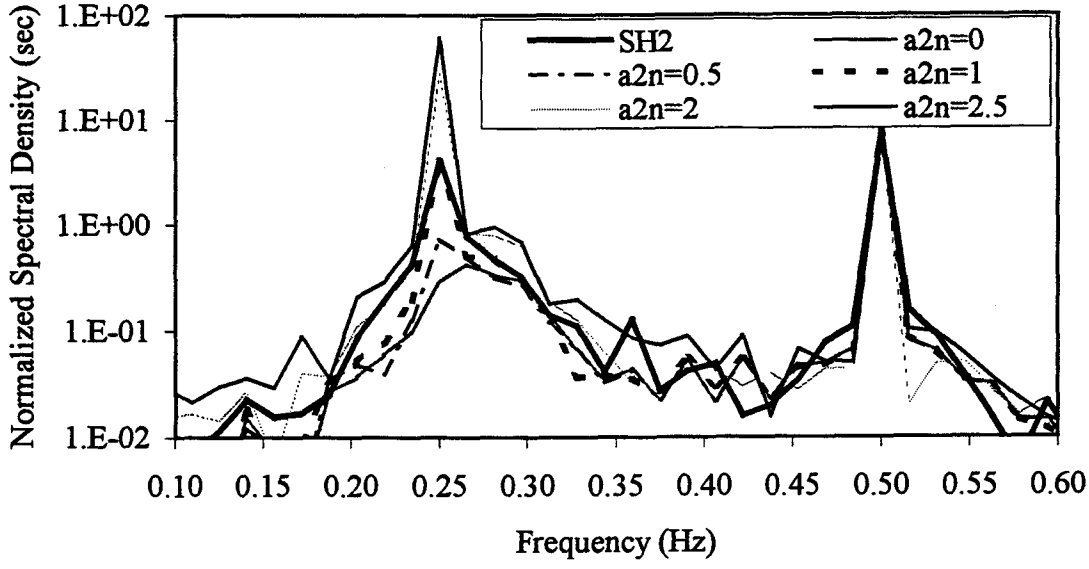

(b)

Fig.B.11 Effect of system parameters on surge response (SH2): a) a_1, b) a_2, c) a_3, d) ζ_1, e) C_{d1}'

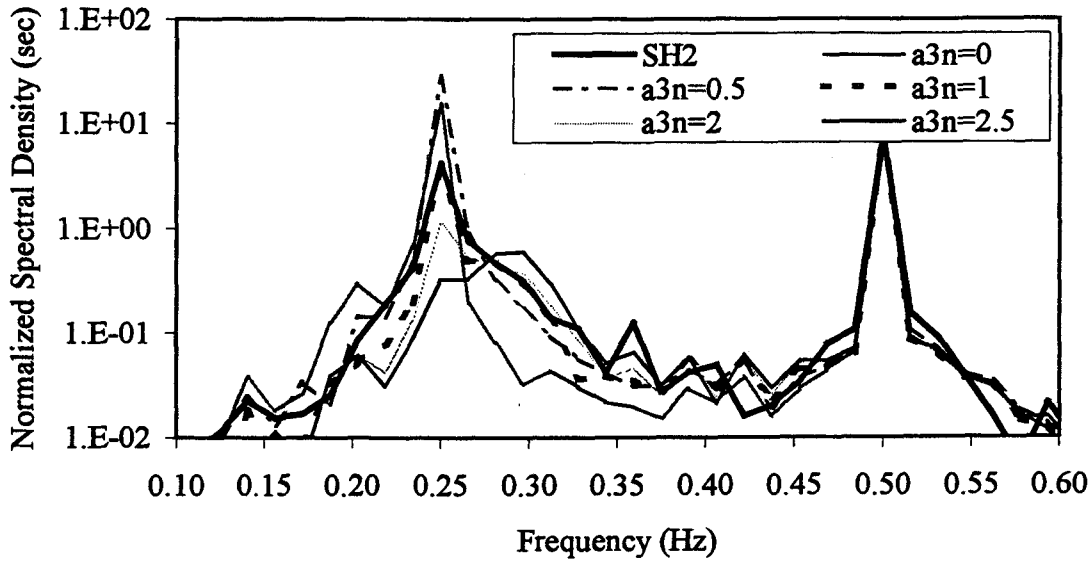

(c)

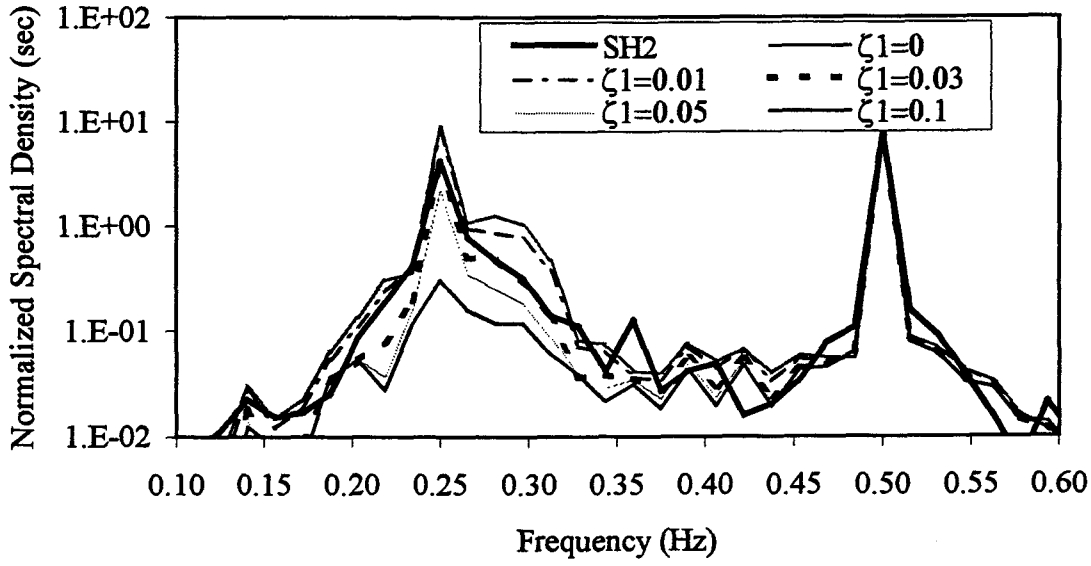

(d)

Fig.B.11 Continued

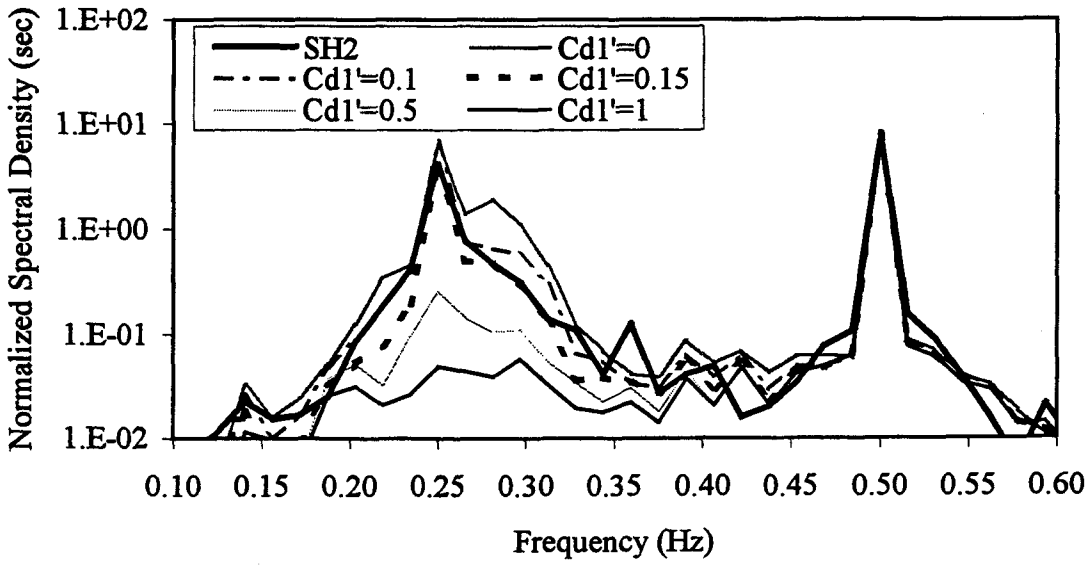

(e)

Fig.B.11 Continued

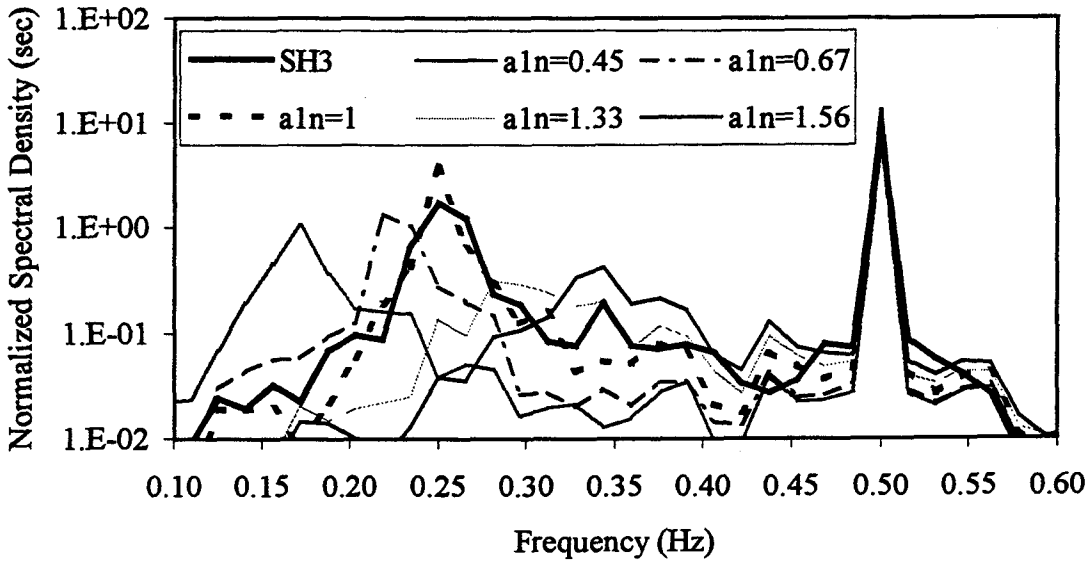

(a)

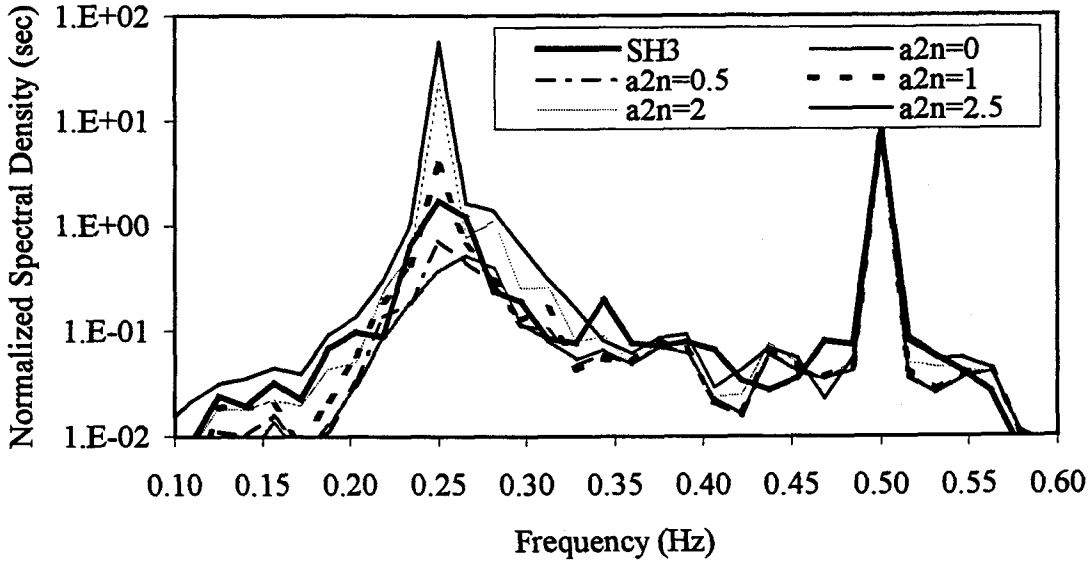

(b)

Fig.B.12 Effect of system parameters on surge response (SH3): a) a_1, b) a_2, c) a_3, d) ζ_1, e) C_{d1}'

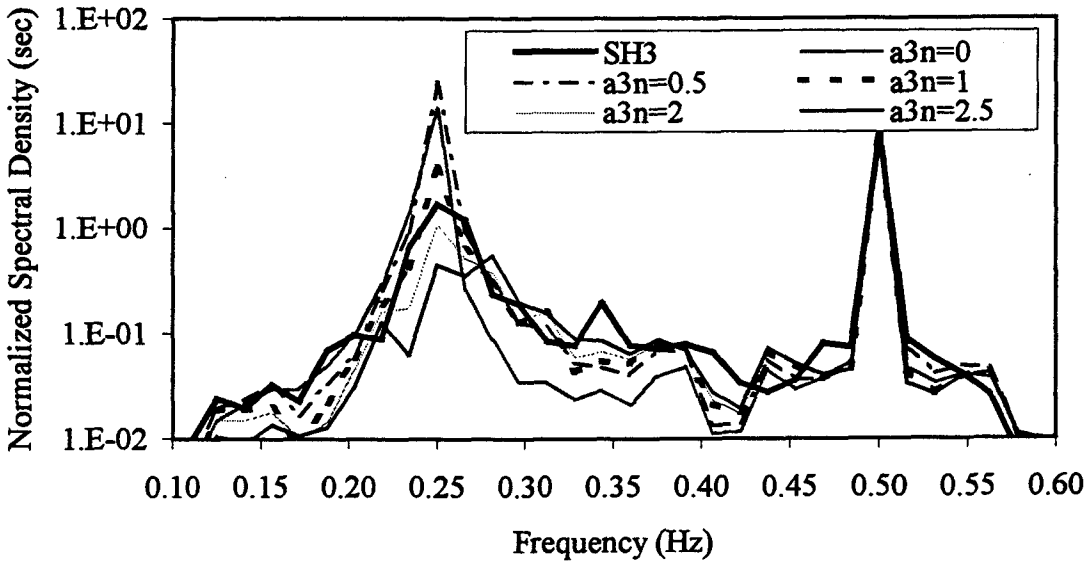

(c)

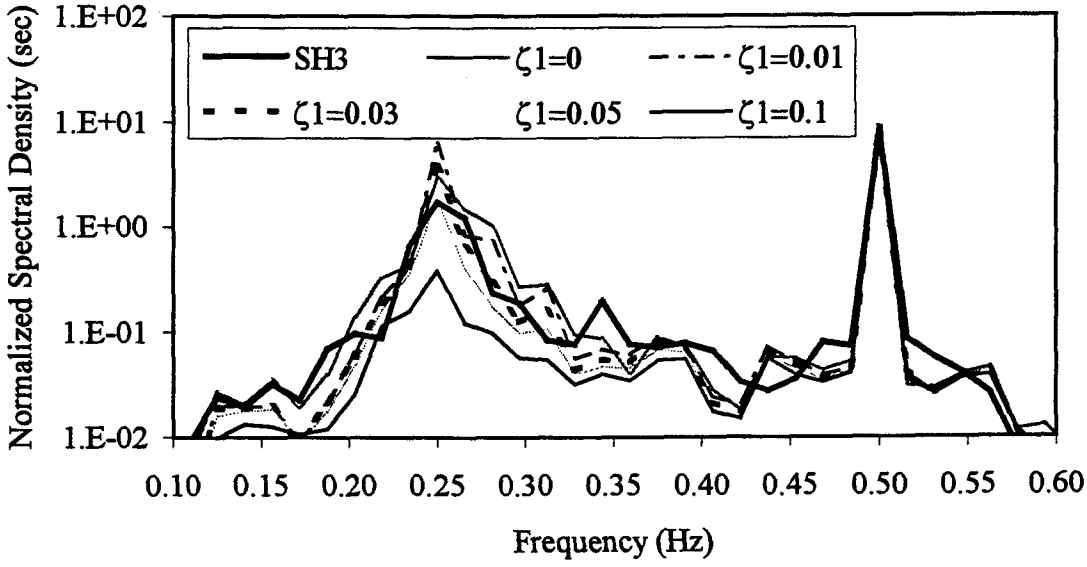

(d)

Fig.B.12 Continued

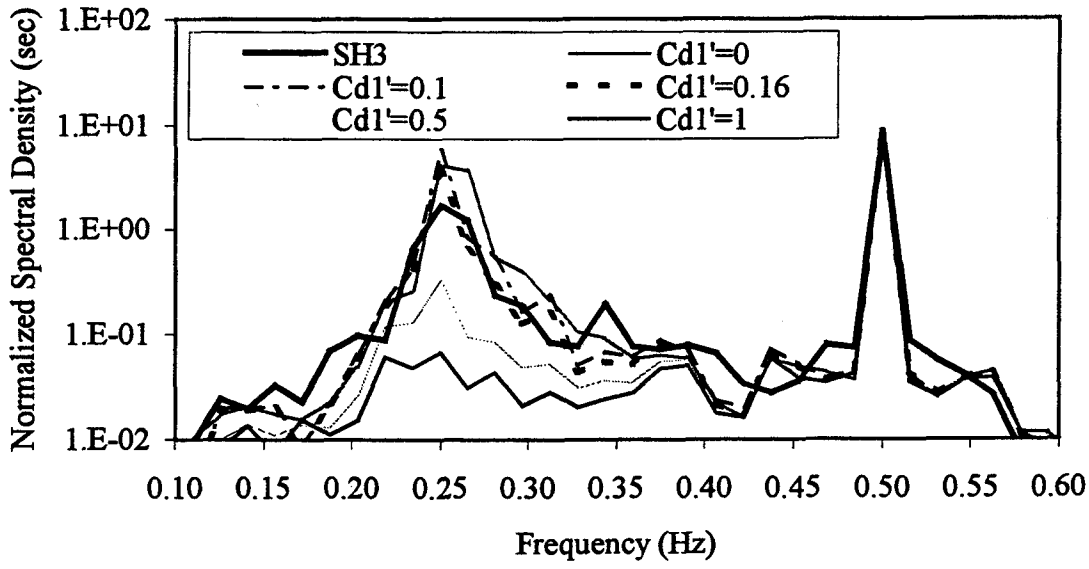

(e)

Fig.B.12 Continued

APPENDIX C

C. PROGRAM LISTING

```
%systemid.m – The program that does the parameter identification of the Nonlinear
%Structure Nonlinearly-Damped (NSND) model using the Reverse multiple-input/single-
%output (R-MI/SO) technique.

%This program loads the wave force and surge response files, calls 'misocin.m' to do the
spectral analysis and that lead to another file, 'misoain' to do the R-MI/SO application. The
results are finally plotted using plotin.m.
clear
load e14surforifm.dat %load the surge force and response
load e14heaforifm.dat %load the heave force and response
N=8192; %total number of points
dt=0.0625; %time interval
Z1=e14surforifm(1,1000:N+999);
Z1=Z1-mean(Z1);
X1=e14heaforifm(1,1000:N+999);
X1=X1-mean(X1);
X2=X1.^3;
%X3=X3-mean(X3);
X3=Z1.^2.*X1;
%X5=X5-mean(X5);
X4=e14heaforifm(2,1000:N+999);
X4=X4-mean(X4);
```

```
Y=e14heaforifm(3,1000:N+999);

Y=Y-mean(Y);

clear e12surforifm.dat

clear e12heaforifm.dat

misocin

plotin
```

```
% misocin.m
nwin=1024;nov=512;
% note that the names of the variables may be changed by editing this routine
% to accommodate the data names for your particular data set
fmax=1/(2*dt);
df=2*fmax/(nwin);
frq=[0:df:fmax];
nf=(nwin+2)/2;
p=spectrum(Y,nwin,nov)/nf;
YY=p(:,1);
XX11=zeros(size(YY));
XX12=XX11;
XX13=XX11;
XX14=XX11;
XX21=XX11;
XX22=XX11;
XX23=XX11;
XX24=XX11;
XX31=XX11;
XX32=XX11;
XX33=XX11;
XX34=XX11;
XX41=XX11;
```

```
XX42=XX11;

XX43=XX11;

XX44=XX11;

YX1=XX11;

YX2=XX11;

YX3=XX11;

YX4=XX11;

HYX1I=XX11;

HYX2I=XX11;

HYX3I=XX11;

HYX4I=XX11;

COH1=XX11;

COH2=XX11;

COH3=XX11;

COH4=XX11;

for i=1:4;

str=['p=spectrum(X' num2str(i) ',Y,nwin,nov)/nf;'];eval(str);

str=['YX' num2str(i) '= p(:,3);'];eval(str);

for j=1:4;

str=['p=spectrum(X' num2str(i) ',X' num2str(j) ',nwin,nov)/nf;'];eval(str);

str=['XX' num2str(j) num2str(i) '= p(:,3);'];eval(str);

end;

misoain;
```

```
% plotin.m
close
subplot(111)
COH5=COH1+COH2+COH3+COH4;
plot(frq',COH4)
hold;
plot(frq',COH3)
plot(frq',COH2);
plot(frq',COH5);
title('Cumulative Coherence,4 input surge motion')
set(gca,'Ylim',[0. 1]);
set(gca,'Xlim',[0.1 0.6]);
a=[frq' COH1 COH2 COH3 COH4 COH5];
clear a
pause
subplot(211),semilogy(frq',abs(HYX1I),'*',frq',abs(HYX1I));
set(gca,'Xlim',[0.1 .6]);
%set(gca,'Ylim',[0.01 100]);
ylabel('Abs(A1) ft')
xlabel('Hz')
clear a
a=[frq' abs(HYX1I) (180/pi*angle(HYX1I))];
%save linhea.dat a -ascii
```

```
title('Linear Impedance,4inp')
subplot(212),plot(frq,180/pi*angle(HYX1I),'*',frq,180/pi*angle(HYX1I))
set(gca,'Xlim',[0.1 .6]);
%set(gca,'Ylim',[-200 200]);
xlabel('Hz')
ylabel('Angle(A1) Degree')
title('Phase')
pause
clear a
a=[frq' abs(HYX2I) (180/pi*angle(HYX2I))];
%save b2heain.dat a -ascii
subplot(211),semilogy(frq,abs(HYX2I),'*',frq,abs(HYX2I));
set(gca,'Xlim',[0.1 .6]);
set(gca,'Ylim',[1e-5 1e5]);
title('Magnitude of A2(f)')
subplot(212),plot(frq,180/pi*angle(HYX2I),'*',frq,180/pi*angle(HYX2I))
title('Phase ')
set(gca,'Xlim',[0.1 .6]);
xlabel('Hz')
ylabel('Angle(A1) rad')
%title('Frequency Response: Imag(A1(f))')
pause
```

```
subplot(211),semilogy(frq,abs(HYX3I),'*',frq,abs(HYX3I));
set(gca,'Xlim',[0.1 .6]);
set(gca,'Ylim',[1e-5 1e5]);
title('Magnitude of A3(f)')
subplot(212),plot(frq,180/pi*angle(HYX3I),'*',frq,180/pi*angle(HYX3I))
title('Phase ')
set(gca,'Xlim',[0.1 .6]);
xlabel('Hz')
ylabel('Angle(A1) Degree')
clear a
a=[frq' abs(HYX3I) (180/pi*angle(HYX3I))];
%save bx2z1sur.dat a -ascii
pause

subplot(211),semilogy(frq,abs(HYX4I),'*',frq,abs(HYX4I));
set(gca,'Xlim',[0.1 .6]);
set(gca,'Ylim',[1e-5 1e5]);
title('Magnitude of A4(f)')
subplot(212),plot(frq,180/pi*angle(HYX4I),'*',frq,180/pi*angle(HYX4I))
title('Phase ')
set(gca,'Xlim',[0.1 .6]);
xlabel('Hz')
ylabel('Angle(A1) Degree')
```

```
clear a

a=[frq' abs(HYX4I) (180/pi*angle(HYX4I))];

%save bxxhea.dat a -ascii
```

```
% misocin.m
for i=1:nf
gyy=YY(i,1);
gxx(1,1)=XX11(i,1);
gxx(1,2)=XX12(i,1);
gxx(1,3)=XX13(i,1);
gxx(1,4)=XX14(i,1);
gxx(2,1)=XX21(i,1);
gxx(2,2)=XX22(i,1);
gxx(2,3)=XX23(i,1);
gxx(2,4)=XX24(i,1);
gxx(3,1)=XX31(i,1);
gxx(3,2)=XX32(i,1);
gxx(3,3)=XX33(i,1);
gxx(3,4)=XX34(i,1);
gxx(4,1)=XX41(i,1);
gxx(4,2)=XX42(i,1);
gxx(4,3)=XX43(i,1);
gxx(4,4)=XX44(i,1);
gyx(1,1)=YX1(i,1);
gyx(1,2)=YX2(i,1);
gyx(1,3)=YX3(i,1);
gyx(1,4)=YX4(i,1);
```

```
lzx=chol(gxx);

gzz=diag(diag(lzx));gzz=gzz*gzz;

lzx=inv(diag(diag(lzx)))*lzx;

lxz=lzx';

gyz=gyx*inv(lzx);

hyz=gyz*inv(gzz);

hyx=hyz*inv(lxz);

COH1(i)=abs(gyz(1,1))^2/(gzz(1,1)*gyy);

COH2(i)=abs(gyz(1,2))^2/(gzz(2,2)*gyy);

COH3(i)=abs(gyz(1,3))^2/(gzz(3,3)*gyy);

COH4(i)=abs(gyz(1,4))^2/(gzz(4,4)*gyy);

HYX1I(i)=hyx(1,1);

HYX2I(i)=hyx(1,2);

HYX3I(i)=hyx(1,3);

HYX4I(i)=hyx(1,4);

end;
```

```
% numresp.m
% The fourth order Runga kutta method to solve a second order ode
% This program uses the R-MI/SO output system parameters and generates response
%clear;flops(0);
load e12wave.dat;
e12wave=e12wave-mean(e12wave);
n1=5000;
%n1=22000;
eta=e12wave(3000:(n1+2999),1);
n=length(eta);
x1=zeros(1,n);x3=x1;t=0;h=0.0625;
t1=[0:h:(n-1)*h];
xx1=[0 0 0 0];
k11=[0 0 0 0];k21=k11;k31=k11;k41=k11;
for i=2:n-1
 xx1=xx1+(1/6)*(k11+2*k21+2*k31+k41);
 x1(i)=xx1(:,1);%disp1
 x3(i)=xx1(:,2);%disp3
 y1(i)=xx1(:,3);%vel1
 y3(i)=xx1(:,4);%vel3
etad=(eta(i+1)-eta(i-1))/(2*h);
etadd=(eta(i+1)-2*eta(i)+eta(i-1))/h^2;
 [k11]=h*funcresp(t1(i),xx1,eta(i),etad,etadd);
```

```
[k21]=h*funcresp(t1(i)+h/2,xx1+k11*(1/2),eta(i),etad,etadd);

[k31]=h*funcresp(t1(i)+h/2,xx1+k21*(1/2),eta(i),etad,etadd);

[k41]=h*funcresp(t1(i)+h,xx1+k31,eta(i),etad,etadd);

end

save numresp1.dat x1 -ascii

save numresp3.dat x3 -ascii

%funcresp.m

% This is the function to solve two second order odes using Runga kutta method.

% The main program is numresp.m

function[value]= numresp(t,x,eta,etad,etadd)

cd=.5;

cd1=0.45;cd3=.45;

ca1=.3;ca3=0.3;

cm1=1+ca1;cm3=1+ca3;

zeta1=0.03;zeta3=.03;

sb=1.5;rho=1.94;

ma1=pi/6*sb^3*rho*ca1;

ma3=pi/6*sb^3*rho*ca3;

m1=3.29+ma1;

m3=3.29+ma3;

T=2.21;% From the wave spectra info, excecuting numspec.m

%T=6.4;

w=2*pi/T;a=0.76/2;% wave height=sqrt(spectra max)
```

```
k=.256;
%k=.062;
h1=9;
s1=sb/2;db=(69.75-9)/12;s=(s1+db);
K=20 ;lc=2.73 ;d=3.98;
rho=1.94;ap1=pi*sb^2/4;ap3=pi*sb^2/4;V=pi/6*sb^3;
u1=w*cosh(k*(s+x(:,2)))/sinh(k*h1)*eta;
u3=sinh(k*(s+x(:,2)))/sinh(k*h1)*etad;
u1d=w*cosh(k*(s+x(:,2)))/sinh(k*h1)*etad;
u3d=sinh(k*(s+x(:,2)))/sinh(k*h1)*etadd;
Fx1=rho/2*cd*ap1*(u1)*abs(u1)+rho*V*cm1*u1d;
Fx3=(rho/2*cd*ap1*(u3)*abs(u3)+rho*V*cm3*u3d);
a1=14;b1=18;
a2=7;a3=6;a4=12;b2=5;b3=9;cs1=2*zeta1*sqrt(a1*m1);% best nonlinear for e12
%a2=7
cs3=2*zeta3*sqrt(b1*m3);
value(1)=x(3);
value(2)=x(4);
value(3)=1/m1*(-cs1*x(3)-a1*x(1)-a2*x(1)^2-a3*x(1)^3+a4*x(2)^2*x(1)-
pi*sb^2/4*0.5*1.94*cd1*x(3)*abs(x(3))+Fx1);
value(4)=1/m3*(-cs3*x(4)-b1*x(2)-b2*x(2)^2+b3*x(1)^2*x(2)-
pi*sb^2/4*0.5*1.94*cd3*x(4)*abs(x(4))+Fx3);
```

```
%wavemod.m
% This is the program which generates the experimental wave at every half interval,
load e12wave.dat
n=length(e12wave);
eta=e12wave(1:n,1);
for i=1:n-1;
    y(i)=(eta(i)+eta(i+1))/2;
end
for i=1:(n-1)
    x(2*i-1)=eta(i);
    x(2*i)=y(i);
 end
 x1=x';
save mode12wave.dat x1 -ascii
%wavemodre.m
% This program takes the wavemod.m output and generates output at every 1/4th interval
clear
load mode12wave.dat
n=length(mode12wave);
eta=mode12wave(1:n,1);
for i=1:n-1;
    y(i)=(eta(i)+eta(i+1))/2;
end
```

```
for i=1:(n-1)
    x(2*i-1)=eta(i);
    x(2*i)=y(i);
end
x1=x';
save fmode12wave.dat x1 -ascii
%respcon.m
load modnumresp1.dat
load modnumresp3.dat
resp1=modnumresp1(1,1:22000);
resp3=modnumresp3(1,1:22000);
n=length(resp1);
for i=1:n/2
    res11(i)=resp1(2*i-1);
    res33(i)=resp3(2*i-1);
end
for i=1:n/4
    res1(i)=res11(2*i-1);
   res3(i)=res33(2*i-1);
end
save numresp1.dat res1 -ascii
save numresp3.dat res3 –ascii
```